Universitat Autònoma de Barcelona

Unitat de Biofísica, Departament de Bioquímica i de Biologia Molecular, Centre d'Estudis en Biofísica, Facultat de Medicina

Biophysical Studies of the Tachykinin Peptides: Structural Characterization and Membrane Interactions

Arash Foroutan

2012

Biophysical Studies of the Tachykinin Peptides: Structural Characterization and Membrane Interactions

Ph.D. thesis presented by Arash Foroutan to obtain the title of doctor.

This work has been realized in the CEB-Unitat de Biofísica in the Departament of Biochemistry and Molecular Biology, Facultat de Medicina, at the Universitat Autònoma de Barcelona, under the supervision of Dr. Esteve Padrós Morell and Dr. Tzvetana Lazarova.

Read and certified by the directors.

Dr. Esteve Padrós Morell Dr. Tzvetana Lazarova

Bellaterra,
November, 2012

Abbreviations

Amino acids

Ala	alanine	Met	methionin
Cys	cysteine	Asn	asparagines
Asp	aspartic acid	Pro	proline
Glu	glutamic acid	Gln	glutamine
Phe	phenylalanine	Arg	arginine
Gly	glycine	Ser	serine
His	histidine	Thr	threonine
Ile	isoleucine	Val	valine
Lys	lysine	Trp	tryptophane
Leu	leucine	Tyr	tyrosine

General abbreviations

Å	angstrom
a.u.	arbitary unite
Aβ	amyloid beta
BSA	bovine serum albumin
BSA	bovine serum albumin
CD	circular dichroism
CMC	critical micelle concentration
CNS	central nervous system
d^2	second derivative
D_2O	deutrated water
DDM	dodecyl-maltoside
DLS	dynamic light scattering
DMPC	1,2-dimyristoyl-sn-glycero-3-phosphocholine
DMPG	1,2-dimyristoyl-sn-glycero-3-phospho-(1'-rac-glycerol)
DMSO	dimethyl sulfoxide

DPC	dodecylphosphocholine
EC	extracellular loop
Eq	equation
FPE	N-(fluorescein-5-thiocarbamyl)-1,2-dihexadecanoyl-sn-glycero-3-phosphoethanolamine
FRET	Förster resonance energy transfer
FSD	Fourier self-deconvolution
FTIR	Fourier transform infrared
FWHH	full width at half height
GPCRs	G protein coupled receptors
h	hour
HT	high tension
K_d	dissociation constant
KDa	kilodalton
LUVs	large unilamellar vesicles
MD	molecular dynamics
min	minute(s)
mL	millilitre
MLVs	multilamellar vesicles
mM	millimolar
MPs	membrane proteins
MRE	mean residue ellipticity
mW	milliwatts
NKA	neurokinin A
NKR	neurokinin receptor
NKAW	$[Trp]^6$ neurokinion A
nm	nanometer
NMR	nuclear magnetic resonance
PC	phosphatidylcholine
Phe-CN SP	[*p*-cyano Phe]^8 substance P

PNS	peripheral nervous system
POPC	1-palmitoyl-2-oleoyl-sn-glycero-3-phosphocholine
PPII	polyproline II
rpm	rotations per minute
S/N ratio	signal to noise ratio
SAXS	small angle X-ray scattering
ScyI	scyliorhinin I
SDS	sodium dodecyl sulfate
SP	substance P
SPW	$[Trp]^8$substance P
T	transmittance
TEM	transmission electron microscopy
TFA	trifluoroacetate
TFE	trifluoroethanol
ThT	thioflavin T (4-3,6dimethylbenzothiazol-2-y1)-N,N-dimethyl-aniline
TK	tachykinin
T_m	temperature phase transition
UPA	ultrafine particle analyzer
UV-Vis	ultraviolet-visible
Vol	volume
λ_{emi}	emission wavelength
λ_{exc}	excitation wavelength
λ_{max}	emission maximum
µL	microlitre
µM	micromolar

INTRODUCTION

G protein coupled receptors

G protein coupled receptors (GPCRs) are a widely distributed class of membrane proteins (MPs) responding to a variety range of ligands, which selectively activate the intracellular signaling events, mediated by membrane-anchored heterotrimeric G proteins. Genome sequencing data have revealed that approximately one out of four proteins encoded by DNA is a membrane protein. GPCRs are composed of a single polypeptide chain, which traverses the membrane seven times. GPCRs respond to diverse stimuli as hormones, neurotransmitters, nucleotides, calcium ions, odorants and light. GPCRs are involved in a wide variety of physiological processes and their proper function is vital to health. Consequently the malfunction and the specific defects of these MPs are implicated in numerous human diseases.

Despite the GPCRs pharmacological importance, the molecular mechanisms of GPCR ligand discrimination, activation and signaling are still not well understood. Revealing of the three-dimensional structure of GPCRs and their ligands is essential for understanding of their function. Elucidation of GPCRs structure, like other integral membrane proteins, is extremely difficult to determine experimentally. The major obstacles come from difficulties in protein production and purification, protein stability and homogeneity. Therefore, so far only structure of few GPCRs including rhodopsin, human β2-adrenergic receptor (ADRB2) and human adenosine A_{2A} receptor have been resolved successfully. Importantly, for many of GPCRs, so called orphan GPCRs (oGPCRs), the natural activating ligands and their (patho)physiological function are not known and identified yet. However, now it has well recognized that GPCRs might provide a path to discovering new cellular substances that are important in human physiology.

Mammalian GPCRs are grouped by amino acid sequence similarities into the three distinct families.

Family A (or rhodopsin-type receptor family) is the largest one, forming four main groups with 13 sub-branches. It is characterized by the presence of about 20 highly conserved residues, mostly localized in the transmembrane (TM) regions.

Family B (or secretin/glucagon receptor family) is characterized by the presence of a large N-terminal extracellular domain, which contains 6 well-conserved cysteine residues in addition to the about 20 highly conserved residues localized in the TM regions.

Family C (or metabotropic neurotransmitter and Ca^{2+}-sensing receptor family) is characterized by a very long N-terminal extracellular domain, which in addition to the 20 highly conserved

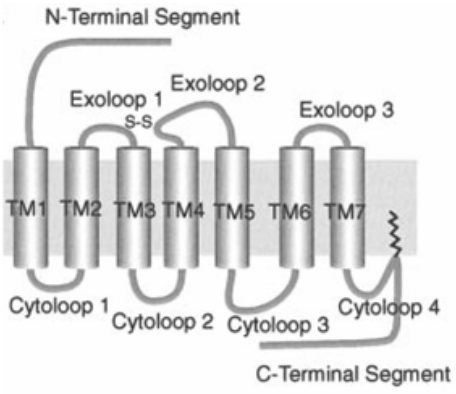

Figure 1. Schematic presentation of the general structure of GPCRs in the membrane.

residues localized in the TM regions, contains also 20 cysteine residues. Moreover, contrary to the other GPCRs families, where the ligand binding occurs either between TMs or it is mediated by both extracellular loops and the N-terminal extracellular region, in the family C the agonist binds exclusively via a large extracellular domain.

Figure 1 shows schematic structure of a GPCR in the membrane. Many of GPCRs include a conserved disulfide bridge between the first two extracellular loops, which is believed to be responsible for protein stability. A conserved GPCR signature triplet DRY motif (Asp-Arg-Tyr) found at the cytoplasmic side of TM3, is involved in G protein interaction. Recently, Rosenkilde and coworkers (2005) showed that a novel wild-type receptor, ORF74-EHV2, which lacks the Arg residue of the DRY motif, is fully functional, showing both constitutive and ligand-induced activation of G protein signaling. Flanagan (2005) believes that the conserved Arg side chain is not required for receptor function but it is important for stabilizing receptors in the inactive conformation. Glycosylation sites are found in the N-terminal extracellular domain and extracellular loop 2 of GPCRs, whereas phosphorylation and palmitoylation sites are located at the C-terminal intracellular domain and are intimately involved in receptor trafficking and signal transduction. The carboxyl terminal, the intracellular loop spanning TM5 and TM6, and the amino terminal can be counted as the most variable structures among the family of GPCRs. Amino terminal sequence of GPCRs is also quite diverse and could be relatively short (10-50 amino acids) for monoamine and peptide receptors, or much larger (350-600 amino acids) for glycoprotein hormone receptors and the glutamate family receptors.

Neurokinin receptors

NK1R, NK2R and NK3R belong to the rhodopsin-like class (class A) of GPCRs and are activated by peptides belonging to the TKs family. The similarity of the amino acid sequence between the human NKRs is 47% between NK1R and NK2R, 51% between NK1R and NK3R and 41%

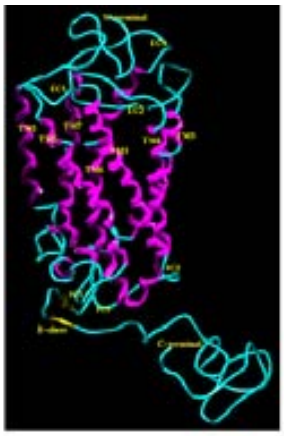

Figure 2. A 3D model of human NK1R. The transmembrane helices are shown in red and the rest of structure (ICs, ECs, N- and C-terminals) is shown in blue.

between NK2R and NK3R. The NK1R is found in the mammalian central and peripheral nervous system. The human NK1R contains 407 amino acids. Due to the diverse physiological functions of NK1Rs, including pain transmission, neurogenic inflammation, smooth muscle contraction, secretion and activation of the immune system, they have been regarded as an important drug target. Recent studies have demonstrated that truncated (tailless) NK1Rs lacking 96 amino acid residues at the C-terminal preserve some of their important functional roles. Targeting the truncated NK1Rs with pharmacologic agents might result in novel therapeutic approaches in diseases which affect the immune system, including HIV disease. So far, the attempts to crystallization of most NKRs have not been successful, possibly due to their inherent structural flexibility and the need for recombinant expression. Therefore the structural information about these receptors comes mainly from modeling studies based on Rhodopsin structure. Figure 2 shows a 3D model of human NK1R generated by homology modeling. According to this model, the C-terminal folds to form a globular structure. A beta sheet characterizes the start of the C-terminal tail. Moreover, the Asn^{23}-Phe^{25} region of the NK1R may play an important structural role in positioning or stabilizing the tertiary structure of the N-terminal. These residues are at the point where the N-terminal bends. The residues preceding Asn^{23} are projecting over the 7-TM core, whereas the residues after Phe^{25} are largely associated with the membrane (e.g. the hydrophobic residues Trp^{30}, Ile^{32}, Val^{33} and Leu^{34}) before the beginning of TM1 at Trp^{35}. The N-linked glycosylation of the N-terminal of the NK1R (Asn^{14} and Asn^{18}) may play an important role in the proposed folding of the N-terminal over the ligand in the central core of the seven TM helices. NMR studies show the presence of helical structure in second and third extracellular loop of NK1R. Conformational properties of the isolated EC2 of NK1R in 25% TFE confirm the presence of helical structures in the central portion (residues 176-182) and the C-terminal extremity (residues 190-195) of the receptor and indicating that residues 178, 179, 183 and 191-

196 are engaged in hydrogen bonds. It is worth mentioning that there is poor definition for residues 168-175 in the N-terminal extremity and residues 183-189 in the segment connecting the two helices.

The peptide Tachykinin family

Tachykinins (TKs) are characterized by the presence of the common hydrophobic C-terminal amino acid sequence Phe-X-Gly-Leu-Met-NH_2 (Table 1). They are identified as "aromatic TKs" when X is an aromatic amino acid residue (Phe or Tyr) and "aliphatic TKs" when X is beta-branched aliphatic amino acid residue (Val or Ile). There is also a different pentapeptide, a TK-like motif, at the C-terminal of two peptides, endokinin C and endokinin D. These peptides derived from preproTK PPT-C gene. It is believed that the “message” sequence comprising C terminal residues is responsible for receptor activation, whereas the divergent N-terminal segment (named as “address” sequence) provides specificity for the target receptor.

In 1931, Euler and Gaddum isolated a crude extract from equine brain and gut, named this new agent substance P, P referring to the powder obtained after the extraction procedure. However almost 40 years later, in the early 1970s, substance P was purified and identified as an undecapeptide. SP is involved in several important physiological processes including pain transmission, inflammation, blood flow, salivation and various muscle contractions. The wide range of physiological activities of SP has been accounted to the lack of selectivity for a specific receptor type. Neurokinin A (also known as substance K) and Scyliorhinin I (ScyI) are a decapeptides, respectively, found in the central and peripheral nervous system and isolated from the gut of the elasmobranch fish, Scyliorhinus canicula. SP and NKA constitute a TKs family which is generated through proteolytic cleavage of the larger precursors called preproTKs. These TKs are encoded by two homologous genes identified as preproTK A (PPT-A) and B (PPT-B). PPT-A encodes the both SP and NKA.

TKs have been found in many different species ranging from invertebrates to mammals, suggesting that the TK motif has been widely exploited throughout evolution. Mammalian TKs expression is not confined to the central nervous system (CNS) and the peripheral nervous system (PNS). There are several evidences of detection of these peptides not only in non-neuronal cells such as immune and inflammatory cells, but even in the placenta, a tissue totally devoid of nerves. Some reports proposed that TKs may facilitate the cancer cell growth, mediate the neurogenic inflammation and also their expression may change due to the infectious diseases. Immuno histochemical studies have shown that TK peptides are produced in nervous and/or gastrointestinal tissues from all classes of vertebrates. In mammals, TKs have been shown to

activities such as powerful vasodilatation, hypertensive action, and stimulation of extravascular smooth muscle and are known to be involved in variety of clinical conditions, including chronic pain, Parkinson's disease, Alzheimer's disease, depression, rheumatoid arthritis, irritable bowel syndrome and asthma.

Interaction of TKs with the NKRs

All TKs interact with all three receptor subtypes. It is proposed that SP and NKA, respectively, have more affinity to NK1 and NK2. On the other hand, homologous binding studies have demonstrated that, contrary to the generally accepted belief, NKA could bind NK1 receptor with high affinity. The 193-197 region, located at the end of the second extracellular loop of the human NK1 receptor, could be part of a common high-affinity binding domain for NKA, distinct from the SP binding site. The binding affinity of Scy I was found to be as high as that of endogenous ligands SP and NKA for NK1 and NK2, respectively. Competitive binding studies have shown that ScyI is a high-affinity agonist for both the mammalian NK1 and NK2 TK receptors and possess 50-250 times reduced affinity for NK3 receptor. The amino acid sequence and the subsequent modification of TKs residues appear to be essential for peptide function and binding to receptor. For instance, the amidation of the terminal Met appears to be the key for interaction of the peptide with the receptor. In the cells Tks are with amidated C end, as moreover it has been show that amidation it is essential for their activity. In contrary, TK-like peptides from invertebrates containing an amidated Arg at their C-terminal, are unable to activate mammalian TK receptors. The substitution of the charged Arg for the Met at C-terminal of the peptides in TKs family may have conferred a high structural mobility, increasing the possibility to fit with the different TK. The Phe^{7} residue may have an important role to address the TK ligands toward the receptors. It has been demonstrated that TKs with a neutral or basic amino acid in seventh residue have a preference for the NK1R. TKs with an acidic or a couple of acidic residues at position 7 or, 6 and 7 address the peptides toward the NK2R and NK3R. Interestingly, the extracellular loop II (EC2) has four acidic and four basic residues in the rat NK1R, three acidic and two basic residues in the NK2R, and one acidic and five basic residues in the NK3R. The couple of aromatic residues (Phe-Tyr or Phe-Phe) present at the C-terminal of the TKs provide specific binding interactions with TM domains of NK1R. Proline is a well represented residue in the natural TKs. Cascieri and coworkers (1992) suggested that all TKs having Pro at position 4 (like SP) have greatly reduced affinity for NK2R and NK3R. They have attributed this behavior to the preferred conformation of the Pro-containing peptides for the NK1R, which most likely is unfavorable for NK2R and NK3R. It has been shown that the presence of a Pro residue at position

6 causes a profound decay of biological activity of the peptide. The negative contribution of Pro^{6} has been accounted for a distorted interaction of the N-terminal sequence of the peptide with all TKRs. On the other hand, it has been shown that TKs containing a Pro residue at the position analogous to Pro^{4} of SP exhibit selectivity for NK1R versus NK2R or NK3R. The topology of NKA bound to the rat NK2R was studied using Förster Resonance Energy Transfer (FRET) and Molecular Dynamics (MD) approaches. In this model NKA residue 4 is in the vicinity of extracellular loop 2 and of the top of TM7. Residue 7 is located close to receptor residues Ile^{114}, Met^{117}, Val^{182}, Tyr^{266} and Phe^{270}. The C-terminal amino acid of NKA is more deeply buried in the receptor structure, close to residues Met^{117}, Tyr^{266}, Trp^{263}, Phe^{293} and Met^{297}.

Role of membrane in peptide-receptor interactions

The conformations of TKs' upon binging to the membrane and to their receptor is yet in debate. There is a general belief that to preserve the biologically active conformation of the neuropeptide, the membrane is exceptionally required. Moreover, several studies have shown that the membrane itself enforces a conformation of the small peptides and this may represent the biologically active conformation. Concerning SP, there is a common belief that upon binding to the membrane the peptide shifts to an active conformation before to perform its role as a neurotransmitter. Several authors proposed that the target cell surface influences the receptor to select the peptides like TKs through accumulation of the ligand at the cell membrane, induction of a specific conformation and orientation of the peptide.

However, some authors believe that lipids play no direct role in the binding of SP to its receptor but they might however play an important role for SP storage. According to Sankararamakrishnan (2006), peptide ligands can interact with their receptors in at least two ways: one is direct interaction to the extracellular loops of GPCRs from the aqueous phase, and second is by pre adsorption of flexible peptide to the target membranes in the first step, before it recognizes its receptor as the membrane-induced conformation is postulated to bind to the receptor in the second step (membrane compartments theory).

So far, the structural data of TKs mainly come from NMR and molecular dynamics (MD) studies. Usually, dimethyl sulfoxide (DMSO), SDS or TFE have been used as a mimic environment in NMR studies. For instance, several groups have investigated the binding of SP to the micelles, especially to the SDS micelles; but it is worth to stress that there are some inconsistencies in the reported conformation that is adopted by the bound peptide. For instance, Keire & Fletcher (1996) investigated the conformations adopted by SP bound to SDS and DPC micelles. They reported that SDS-bound SP most likely exhibits turn-like structures in the mid-region of the

neuropeptide instead of a well-defined helical structure. The variations in the SDS-bound conformation adopted by SP could be due to the conditions used to form the micelle. The formation of secondary structure in most resembling membrane liposomes has been object of studies, mainly for the binding of the peptide and less or only a few for structural studies. However, secondary structure characterization performed by many labs gives contradiction results, concerning the binding and the secondary structure estimation. Clearly, there is a need for additional investigations of neuropeptide-micelle and neuropeptide-model membrane interactions to help us understanding the mode of TKs-receptor interactions.

Objectives

One aim of this doctoral thesis is to study and characterize the structures and mode of the interactions with the membrane of substance P (SP), neurokinin A (NKA) and scyliorhinin I (ScyI) peptides. As ligands of the neurokinin receptors with different agonist activity, it is relevant to address the question if the cell surface plays any role on the biologically active structures of these peptides that are recognized by the receptor. The main objectives of this part of the thesis are to answer: What determines the different activity potential of these peptides? What is the active conformation of the peptides when they interact with the neurokinin receptor to transfer the signal? What is their mode of interaction with the membrane surface? Does the membrane surface affect the peptide conformation?

The other aim of this doctoral thesis relies on the study of the aggregation states of the SP, NKA and ScyI. Involvement of SP and NKA peptides in neurodegenerative diseases highlights the importance of the aggregation states of the peptides. The main objectives of this part are to answer the question, under which conditions do SP, NKA and ScyI peptides have the ability to self-associate? What kind of structure they form and which factors promote or inhibit the self assembling?

Materials and Methods

Peptides sequences and synthesis

All TK peptides and their analogues (see Table 1 of Introduction), used in the thesis, were purchased from *AnaSpec*®, Inc. (http://www.anaspec.com) and *PolyPeptide Group* (http://www.polypeptide.com/index.php). The peptides were synthesized by standard solid phase method and purified by reverse phase high-pressure liquid chromatography. All the peptides share amidated carboxy-terminal since it's required for their activity in human body. The purity of the peptides was >95% as judged by HPLC and further confirmed by mass spectrometry, as claimed by the supplier. Peptides (at about 1 mg) were stored as a lyophilized powder at -20 ºC until use. [Phe-CN]^8 SP was exceptionally stored at 4˚ C.

Peptides analogous

Mammalian TKs used in this study do not have Trp residue in their sequences (see Table 1 of Introduction), therefore for the binding studies we used analogues of TKs peptides, in which Phe^8 and Phe^6 in SP and NKA were substituted for Trp, respectively. The reason for using Trp analogues of TKs was that compared to Trp, Tyr and Phe are less sensitive to their local environment. Moreover the fluorescence characteristics (λ_{max} and fluorescence intensity) of the Trp fluorescence are very sensitive to the polarity of its environment and of the solvent, in general. This is due to the different dipole moment of the two overlapping electronic transitions of the indole side chain of Trp in polar and apolar solvents. On the other hand, fluorescence quantum yield of Trp is much higher compared to that of Tyr and Phe. Consequently, both the fluorescence intensity and emission maximum (λ_{max}) of Trp often serve to monitor folding/unfolding states of hydrophobic peptides and membrane proteins. Importantly, in case of the TKs the substitution of the Tyr or Phe with Trp does not affect the peptide molecular characteristics, such as hydrophobicity and the net charge (Table 1).

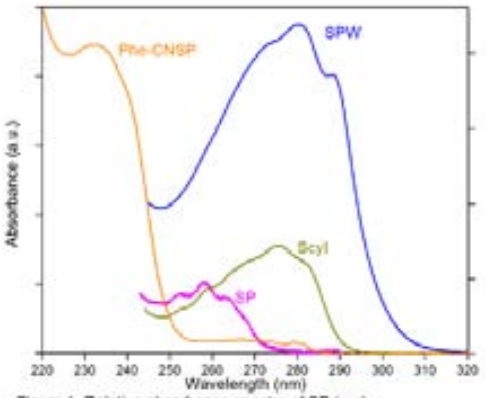

Figure 1. Relative absorbance spectra of SP (—), SPW (—), Scyl (—) and Phe-CN SP (—) in distilled water.

The other analogue of TKs used in this study was Phe-CN SP. The fluorescence quantum yield of *p*-cyano Phe is about five times more than that of phenylalanine, and unlike Tyr, *p*-cyano Phe lacks photo-induced proton transfer. Moreover, due to the small size of the C=N, it minimally perturbs the physical properties of the native peptide. On one hand, the fluorescence changes of *p*-cyano Phe upon the hydrogen binding of the C=N group with a hydrogen donor is a sensitive marker to monitor dye local environment. On the other hand, using the C=N vibration, the peptide conformations were revealed by IR spectroscopy.

Peptide stocks and concentration determination

The concentration of the peptides was determined spectrophotometrically. Prior to the measurements, the stocks solutions of the peptides were prepared by dissolving the peptide powder at about 1 mg in 150 µL distilled water. The molar extinction coefficients (in $Lmol^{-1}cm^{-1}$) of each peptide and the analogues were determined on the basis of the number of aromatic amino acid residues present in the peptides, considering molar extinction coefficient of Phe, Tyr, Trp and *p*-cyano (see Table 1 of Introduction). The absorption spectra of the peptides were recorded on UV-Vis spectrophotometer (*Varian*® *Cary3 Bio*) and peptides concentrations were calculated, given that the Beer-Lambert law. Figure 1 shows the absorption spectra of SP, SPW, ScyI and Phe-CN SP in distilled

water. The absorption spectrum of Phe-CN SP shows a strong peak at 232 nm and two weaker peaks at 268 and 280 nm.

Membrane mimetic systems

Micelles

Among the different available detergents the anionic SDS detergent was chosen because: **i).** Previous studies with TKs (SP) have shown that the neuropeptide does not incorporate in detergents, such as DDM; **ii).** The SDS micelles with a relative small size (<100 nm) and low turbidity and light scattering have been proven to be appropriate membrane mimic system for spectroscopic studies.

The stock solution of 1 M SDS was prepared in distilled water and then diluted to the desired concentrations in sub- or micellar states of SDS depending of the aim of each experiment.

Evaluation of critical micelle concentration (CMC) of SDS

The CMC of SDS was determined based on the intensities changes of some of the fluorescence emission bands of the pyrene, following the methodology. Shortly, the pyrene molecule is a condensed aromatic hydrocarbon, which has five fluorescence emission vibronic bands at 374, 379, 385, 389 and 393 nm referring to the monomer state of the dye, and one broad peak at 480 nm due to the formation of excimers (Figure 2). In polar environment, the ratio of pyrene fluorescence intensities at 385 nm (peak III) and 374 nm (peak I) is close to 0.64 (Figure 3). As the polarity of the environment decreases, the fluorescence intensity of peak III increases and the fluorescence intensity ratio of I_{385}/I_{374} get close to 1. Thus, the relative intensity of I_{385}/I_{374} can serve as an index of solvent polarity and as a marker for formation of micelles (CMC determination).

In this study, the stock solution of 1 mM pyrene was made in ethanol and the solution was kept at 4 ˚C. To determine the CMC of SDS, small aliquots of SDS were titrated into the buffer (5 mM) containing 2 μM pyrene. The measurements were performed on *PTi Photon Technology International*® spectrofluorimeter. Fluorescence emission spectra of

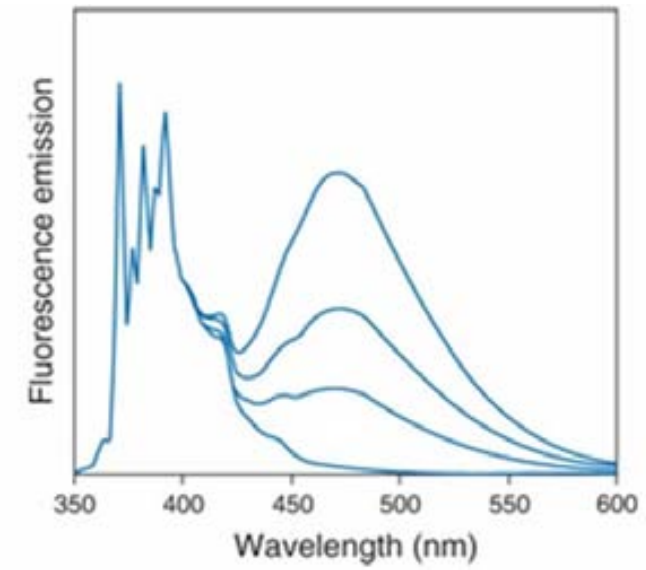

Figure 2. Schematic of excimer formation by pyrene. Upon excimer formation, the intensity of the band at about 480 nm increases.

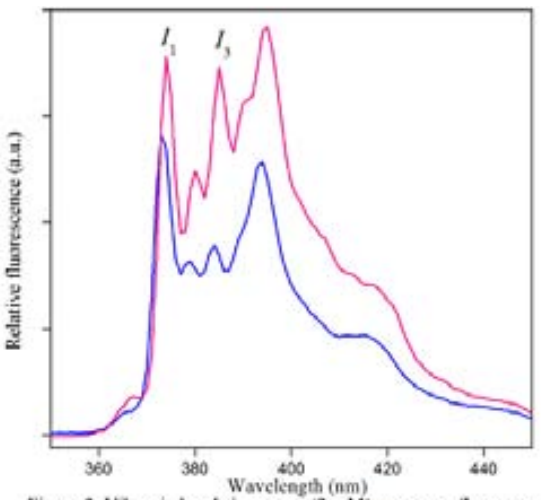

Figure 3. Vibronic bands in pyrene (2 mM) monomer fluorescence in sodium phosphate buffer alone (5 mM, pH 7.0, —) and in 10 mM SDS (—), both at pH 7.0, 22 °C. Relative intensity of I_{382}/I_{374} reflects the solvent polarity.

pyrene were recorded using λ_{max} of excitation 335 nm and the emission spectra were recorded from 350 nm to 700 nm. Usually, two emission scans were recorded and averaged. All the spectra were corrected for the dilution and light scattering by

subtracting the spectrum of the same sample but lacking the pyrene dye. The CMC of SDS was determined by plotting the ratio of the fluorescence intensities peaks I_{385}/I_{374} versus SDS concentrations. Furthermore, the CMC of SDS in the presence of each TK peptide was determined .

Large unilamellar vesicles (LUVs)

Due to the unilamellarity and appropriate radii of curvature, the LUVs serve more similarity to a biological membrane than small unilamellar vesicles and multi lamellar vesicles. Considering this fact, LUVs were used as membrane mimetic systems in this study. Both DMPC and DMPG are structurally similar to the lipid composition in the postsynaptic membranes where Neurokinin receptor and TK ligands are expressed and functioning. Therefore, LUVs prepared with these lipids mimic most closely phospholipids bilayer in vivo.

Preparation of lipids for hydration

Thin lipid films were prepared by dissolving at about 10 mg of lipid (DMPC, DMPG, or the mixture) in chloroform/methanol (2:1 vol:vol) and dried by using rotary evaporation system and a steam of dry air (Figure 4). To assure the removal of any trace of the organic solvents, the lipid film was usually kept under high vacuum over the night.

Hydration of lipid film

Depending on the purpose of the experiment, the dried lipid film was hydrated in different buffers: 3mM citrate buffer (pH 3.8), 5 mM phosphate buffer (pH 7.0) or 3 mM carbonate buffer (pH 10.7). To make the lipid suspensions well homogenized the temperature was kept above phase transition (T_m), and the suspension was vigorously vortexed at least for 30 min. The resulting multilamellar vesicles (MLVs) were freeze-thawed in liquid nitrogen for at least three cycles.

Sizing of lipid suspension

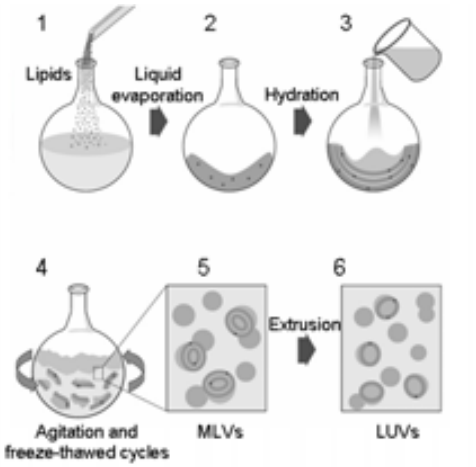

Figure 4. Schematic of LUVs preparation. Details are presented in the text.

To downsizing MLVs and obtaining large unilammelar vesicles (LUVs) the lipid dispersion was extruded through stacked polycarbonate membrane with a pore size of 100 nm using the *Avanti*® Mini-Extruder containing heating block and repeated at least for ten times to obtain LUVs. The final extrusion filled the alternate syringe to reduce the chance of contamination with the larger particles. After the extrusion, the milky appearance of the lipids became more transparent.

Liposomes were used immediately after preparation or kept at 4˚C to use later but no more than 3-4 days.

Determination of liposomes' size

In principle, freeze-thawed cycles and ten-time extrusion cycles along with the use of filters with a pore size of >100 nm results in a formation of homogenous spherical unilamellar vesicles. To determine the liposomes size distribution, dynamic light scattering (Figure 5) and transmission electron microscopy (Figure 6) were applied.

Dynamic light scattering (DLS); theory and methodology

The Brownian motion of the macromolecules in the solvent imparts randomness to the phase of the scattered light, which could interfere destructive or constructive. According

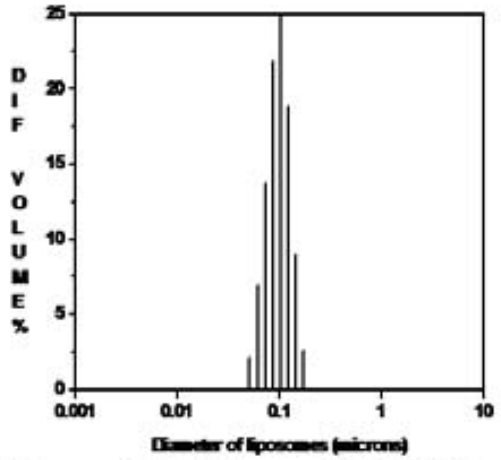

Figure 5. Representative histogram of size distribution of DMPG liposomes (1 mM, pH 7.0), made by extrusion technique using 100 nm pore size membrane.

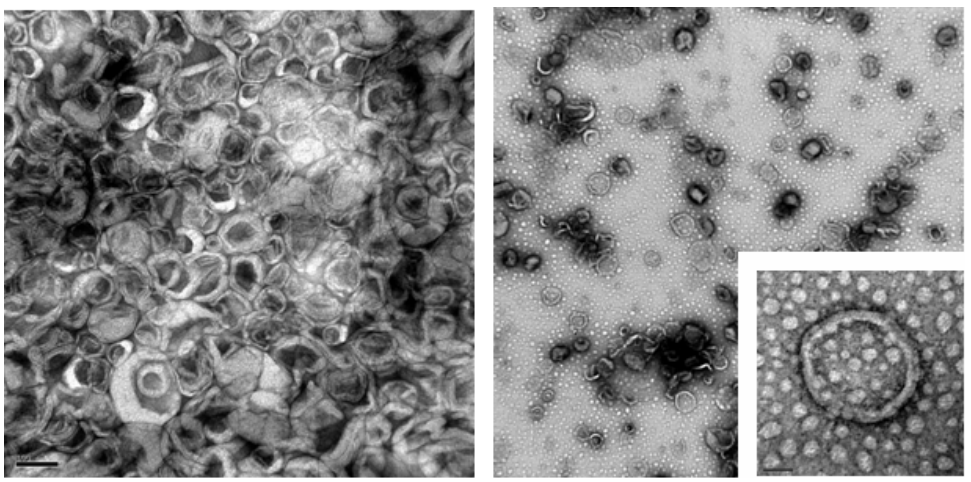

Figure 6. Electron micrograph of spherical DMPC liposomes, (A) 10mM, and (B) 5mM, at phosphate buffer pH 7.0.

to the classical light scattering theory (Rayleigh approximation), scattering of a spherical particle, smaller than the wavelength of incident light, is proportional to the λ^{-4}. Since Rayleigh theory is not valid for particles bigger than the wavelength of light, the alternative model is the theory of Mie which is valid for any particles regardless of their size. Using DLS technique, also called as photon correlation spectroscopy, the fluctuations of interfered scattered light are measured during microseconds. The

fluctuations are related to the diffusion coefficient of the molecules in the solvent. Consequently, the radius calculated is indicative of apparent size of the dynamic hydrated/solvated particles (hydrodynamic radius). Figure 7 shows the hydrodynamic radius for lysozyme compared to other radii.

Experimental scheme

The DLS was measured by *Ultrafine Particle Analyzer*® (UPA) 150 spectrometer (Microtrac, Inc., Montgomeryville, PA). The spectrometer is equipped with a diode laser having a wavelength of 780 nm and a nominal output of 3 mW of optical power. First, the signal level of LUVs was measured to find the adequate concentration of liposomes, which should be between 0.1 and 0.2. To get a satisfactory signal in the detector, the samples were diluted by the same solvents and the acquisition was performed for at least 10 min. The concentration of LUVs used in each measurement was at about 1 mM. The results from DSL measurements are presented as a distribution of volume against liposomes size

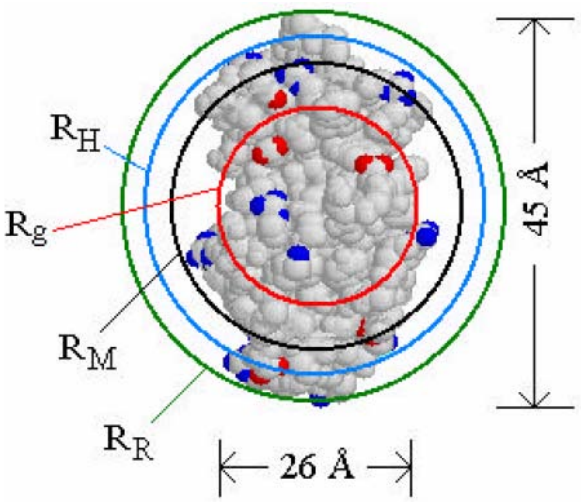

Figure 7. Comparison of hydrodynamic radius (RH) to other radii for lysozyme. Rg is radius of gyration, R_M is the equivalent radius of a sphere with the same mass and particle specific volume as lysozyme, and R_R is the radius established by rotating the protein about the geometric center.

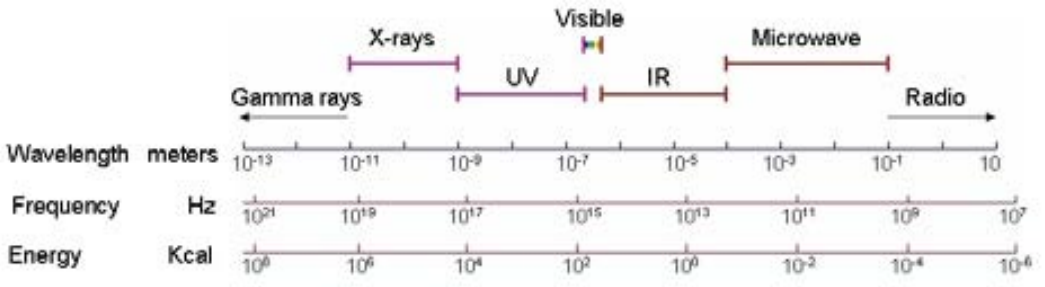

Figure 14. The electromagnetic spectrum. The relation between the wavelength, frequency and energy is illustrated.

Ultraviolet-visible (UV-vis) absorption spectrophotometry; theory and methodology

Figure 14 shows the electromagnetic spectrum. When a beam of light is passing through a substance, certain part of the radiant energy is absorbed by the substance to promote the electrons to jump to a higher energy levels. The spectrophotometer measures the intensity of the light, reaching to the detector (transmitted light or I_t) after passing through the sample and compares it to the intensity of the light before it passes through the sample (incident light or I_0). The ratio between I_t and I_0 is called the *transmittance*, and is usually expressed as a percentage (%T):

$$T = I_t / I_0 \qquad \text{(Eq. 1)}$$

$$\%T = (I_t / I_0) \times 100 \qquad \text{(Eq. 2)}$$

Mathematically, the absorbance is related to the percentage transmittance (%T) by the expression:

$$A = 2 - \log_{10}(\%T) = \log_{10}(I_0/I_t) \qquad \text{(Eq. 3)}$$

From other side, according to the Beer-Lambert equation:

$$A = \varepsilon\, b\, c \qquad \text{(Eq. 4)}$$

where, A is absorbance (no units); ε is extinction coefficient (L mol^{-1} cm^{-1}); b is optical path length (cm); and c is the concentration (mol L^{-1}). Thus, the quantitative measurement

of light absorption by the sample as a function of wavelength gives the concentration of a substance in the solution.

Experimental scheme

The absorption spectroscopy was applied to determinate the concentrations of the TK peptides and that of the fluorescent dyes, as well as to evaluate the hydrophobic-hydrophilic environment of Phe and Trp residues of peptides SPW and NKAW in the presence of micelles. The photo-physical properties of fluorescent dyes are given in Table 2. The absorption spectra of the peptides and the fluorescent dyes were recorded by using UV-visible spectrophotometer (model *Varian® Cary3 Bio*) using a 1 cm length quartz cuvette, as all experiments were done at room temperature. For all the UV-visible spectra an appropriate correction for a nonzero baseline was done.

Techniques to characterize the interactions of TK peptides with the membrane mimetic systems

Fluorescence spectroscopy experiments; theory and methodology

A fluorophore is a chemical compound (molecule or molecule's component) that can re-emit light upon light excitation. Usually the fluorophores contain several combined aromatic groups, or plane or cyclic molecules with several π bonds. Upon absorption of a photon with specific energy, the fluorophore makes so-called vertical transition to the excited electronic state. Fluorescence occurs when an excited electron returns to the lower orbital. But, not all the absorbed photons by the molecule will be emitted or in other words not all molecules present at the excited states will participate in the fluorescence process. Based on this fact, the quantum yield of a fluorescent dye is defined as:

$$\Phi_F = \frac{I_F}{I_A} \qquad \text{(Eq. 5)}$$

where, I_F is number of photons emitted , and I_A is number of photons absorbed.

Assuming very low absorption («0.05), the intensity of emitted light (I_F) at a precise emission wavelength is described by the relationship:

$$I_{F(\lambda)} = 2.3 I_0 \varepsilon_{(\lambda)} c l \Phi_F \qquad \text{(Eq. 6)}$$

where, Φ is the quantum yield, I_0 is intensity of the incident light, ε is the molar absorptivity, l is the path length of the cell, and c is the molar concentration of the fluorescent dye.

The high environmentally sensitivity of the fluorescence relates to the dye's fluorescence life time which is in the time scale of the most molecular processes. The dye's fluorescence life time is defined as an average time a fluorophore remains at excited state, which is ranging from nano to pico seconds. Generally, relative to the absorption spectrum, the emission spectrum of a fluorophore is red shifted to a longer wavelength (lower frequency or energy) (the so-called Stokes shift) due to the loss of vibrational excitation energy during excitation and emission cycle. Generally, the Stokes shift is greater in polar environments than in non-polar ones.

Spectrofluorimeter setting is arranged in a way that emitted light usually is detected at a 90° angle (Figure 8) respect to the excitation light in order to avoid the interference of the transmitted excitation light on the detector. In any case, always some stray light (light with other wavelengths than the targeted) will reach the detector. However, when measuring at 90° angle, only the light scattered by the sample will cause the stray light. Therefore, right angle setting gives better signal-to-noise ratio, and lowers the detection limit by approximately a factor 10^3.

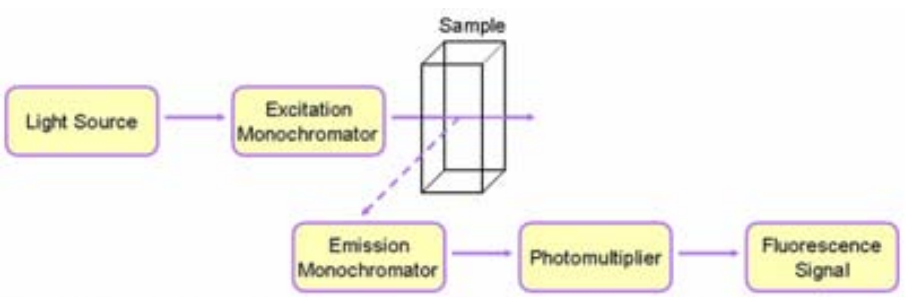

Figure 8. Schematic of a spectrofluorometer in the standard geometric arrangements. Arrows indicate light pass.

Experimental scheme

Fluorescence emission of Phe-CN; exploring the Phe residue environment

First, control experiments were done to determinate the fluorescence intensity and emission maxima of Phe-CN SP (at about 2 μM) in the presence of distilled water and different protic organics, with different dipolar character and hydrogen binding ability, like pure methanol, ethanol and TFE.

For evaluation of the environment polarity of the Phe-CN SP in sub- and micellar concentrations of SDS, the fluorescence emission spectrum of Phe-CN SP (2 μM) were collected from 260 nm to 380 nm in 5 mM sodium phosphate buffer (pH 7.0) upon titration of small aliquots of SDS (from 0 to 12 mM), setting the excitation at 232 nm.

Similar experimental scheme as in the case of micelles was applied in the experiments with LUVs, prepared at different molar ratios of DMPC/DMPG liposomes.

After performing the proper corrections for peptide dilution, the fluorescence intensities of Phe-CN residue at λ_{291} nm were plotted as a function of SDS concentrations and as a function of the mol % of DMPG in the case of the LUVs.

Fluorescence emission of tryptophan; assaying micelle saturation with mammalian TK peptide analogues and binding curve experiments

SDS micelles (20 mM) were titrated with small aliquots of SPW and NKAW peptides in a final concentration range of 0-200 μM and the fluorescence emissions of Trp were recorded from 300 to 450 nm, setting the excitation wavelength to 280 nm. All the spectra were subtracted using the corresponding background. Furthermore, the

corresponding titration curves were obtained by plotting the fluorescence intensity of Trp at 340 nm against peptide concentrations.

Fluorescence emission of tryptophan; exploring the tryptophan residue environment

The fluorescence emission spectra of SPW and NKAW were collected in aqueous solutions, in different concentrations of SDS (in sub- and micellar range usually between 0 to 25 mM, depending on the peptide) and in LUVs (with the concentration of 40 μM and 0.8 mM for SPW and NKAW, respectively) prepared with different molar ratios of DMPG/DMPC lipids. Usually, the concentration of the peptides used in SDS and LUVs experiments was 5 μM. Excitation was set at 280 nm. The changes of the fluorescence intensities and λ_{max} were plotted as a function of SDS concentrations and DMPC/DMPG mol percents in LUVs.

Assessment of surface electrostatic potential by fluorescent probe FPE; theory and mechanism

The membrane surface electrostatic potential (ψ_S) arises from the net excess electric charges at the outer surface of the membrane. Therefore, it is potential difference between the membrane surface and the bulk medium. Any interactions of charged molecules with the membrane surface would change the surface electrostatic potential. For an acidic group located on a membrane surface:

$$pKs = pKB + \psi_S \qquad \text{(Eq. 7)}$$

where, *s* and *B* indicate for surface and bulk phases, resepectively, and ψ_S is surface potential.

In this study, we used fluoresceinphosphatidylethanolamine (FPE) (see Figure 10, inset). The fluorescent probe FPE has been widely applied to monitor the binding of charged molecules to the membrane and in this work was used to explore the changes of surface potential upon eventual binding of the TKs. In general, when FPE incorporates into the

membrane, its fluorescein moiety locates on the membrane surface, precisely on the water-lipid interface, therefore, it is able to detect pH changes or charge distribution changes on the surface. According to the equation 7, some changes of the electrostatic surface potential will cause changes of the apparent pK of fluorescein's xanthene ring, as an acidic group. Consequently, protonation or deprotonation of xanthene ring affects the quantum yield of fluorescence of FPE in a manner that deprotonation causes increase of dye's fluorescence intensity.

Experimental scheme

Preparation of LUVs asymmetrically labeled with FPE

Asymmetrically FPE labeling LUVs were prepared following the published methodology. Shortly, the stock solution of FPE (5 mM) was prepared by dissolving 0.6 mg of FPE in 0.1 mL chloroform:methanol (5:1 v:v) and was kept at -20 ˚C. For labeling of 4 mM DMPG or DMPC LUVs, prepared in sodium phosphate buffer pH 8.5, we used 10 μM of FPE to give 0.25 mol % FPE of the total lipid contents. To do that, small amount of the stock solution of the FPE (2.6 μL) was added into a glass tube and the solvent was completely evaporated by purging with dry air. The FPE was then resolved in ethanol and mixed with 1.3 mL DMPG or DMPC LUVs. Importantly, the amount of ethanol should never exceed 0.1% volume parts of the total aqueous volume. Then, the mixture of FPE dyes and LUVs was incubated at 37 ˚C for 1 hour in a dark. Then, the FPE labeled LUVs were filtered by using PD10 *Sephadex*® Desalting Column (Amersham Biosciences). Prior to filtration, the gel column was calibrated by eluting 3 to 4 times (totally 25 mL) of the sodium phosphate buffer (5 mM, pH 8.5). Once the exceeding calibration buffer was removed from the column, the FPE labeled LUVs were loaded to the column. After the sample was entered completely to the packed bed, 1.2 mL of buffer was added to the column. The column was eluted by adding 3.5 mL of the same buffer. The low volumes of filtrated sample were collected in different eppendorf tubes. The presence of FPE in each of the tubes was determined spectrophotometerically by recording the absorption spectrum of FPE. Since the dye's extinction coefficient at 490

nm is pH-dependent, the absorption spectrum was recorded at pH 11 by adding a small aliquot of 2.4 mM KOH to the sample. The FPE labeled LUVs were stored at 4°C in dark for 3-4 days until the use.

Interactions with lipid bilayer

Assessing the interactions of TK peptides with membrane mimetic systems by FPE dye

The fluorescence intensity variations of FPE, incorporated into DMPG or DMPC vesicles, was monitored at a fixed wavelength of 518 nm and by setting the excitation at 496 nm and titration of the small aliquots of TKs peptides in which each aliquot was contained different concentrations of peptides. The titration of the FPE labeled LUVs with TKs was performed as following: four different samples were prepared containing the FPE labeled vesicles (at about 200µM of lipid) in sodium phosphate buffer (5 mM, pH 8.5) in each cuvette. The changes of fluorescence intensity of FPE at 518 nm was recorded and monitored until it gets to plateau. Then, small aliquot (at about 1 µL) of TKs (SP, NKA and ScyI) were added to each cuvette (considering one sample as a reference) by using Hamilton® syringe without stopping the spectrofluorimeter. At the beginning, the peptide titration was started by adding small amount of peptides (0.1 µM) and then followed by adding higher amount of peptides to the final concentration of 30 and 200 µM, in the case of DMPG and DMPC, respectively. Each addition was done when the fluorescence intensity of FPE reached to plateau. Special attention was taken to avoid the interruption of the beam line with the syringe, while peptides were adding to the cuvettes.

Processing of the binding curves

From the recorded FPE fluorescence intensity spectra, the following parameters F_0 and ΔF were determined. The F_0 (or initial fluorescence level) is the fluorescence intensity of FPE (at 518 nm) alone and before addition of peptides when it is reached to plateau. The ΔF is the difference of fluorescence intensity after each peptide addition from that of FPE

alone (F_0). Therefore, ΔF was calculated accumulatively. It should be noticed that in the cases (see p. …, Figure…) in which upon addition of peptides to the FPE labeled LUVs, the FPE fluorescence intensity was increased and then decreased to reach a plateau, we considered the maximum intensity to calculate ΔF.

The peptide-membrane binding curves were obtained by plotting the ΔF (at 518 nm) as a function of TK peptides concentrations. The binding curves were fitted to hyperbolic model by using the following equation:

$$F = \frac{F_{\max}[FP]}{K_d + [FP]} \qquad \text{(Eq. 8)}$$

where, F is the fluorescence intensity variation, F_{max} is the maximum fluorescence intensity variation, $[FP]$ is the fusion peptide concentration and K_d is the dissociation constant of the membrane binding process.

All the experiments were preformed on *PTi Photon Technology International*® spectrofluorimeter. Data processing was done by using *Felix32*® Fluorescence Analysis Software and commercial software package *Origin*® 7.0. (OriginLab Corporation, Northampton, MA).

Control experiments

Determination of FPE reconstitution into the LUVs

The accuracy of LUVs labeling with FPE was examined by recording the FPE fluorescence, given that λ_{max} of FPE reconstituted in LUVs is red shifted to about 518 nm relative to λ_{max} of free fluorescein in aqueous solutions which is about 510 nm (Figure 9).

Apparent pK of FPE in DMPG LUVs

It has been shown that increasing the bulk phase counter-ion concentration results in an acidic shift in the pK of the membrane bound FPE. Considering this fact and to achieve the maximum changes in fluorescence intensity of FPE upon addition of the peptides, the

apparent pK of FPE dye was determined in the presence of each peptide. To determine the apparent pK of FPE, the pH titration of FPE in the presence of each peptide was

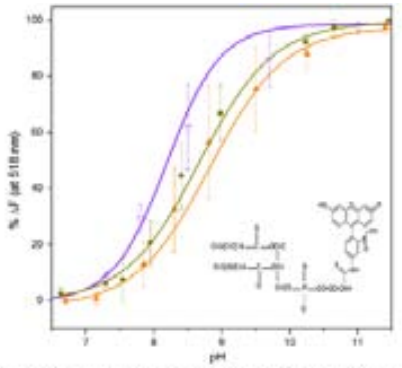

Figure 10. Determination of the apparent pK of FPE reconstituted into DMPG LUVs. The pK of FPE in the presence of the 3 μM SP(—), NKA (—) or Scyl (—) was determind by plotting the percentages of difference FPE fluorescence as a function of pH titration. Fluorescence intensity was recorded at 518 nm following excitation at 490 nm. Titration was performed in the prescence of 5mM NaCl and pH was set using 0.1 M HCl/KOH. Total lipid concentration was 24 μM.

performed as following: The stock solution of FPE labeled DMPG (at about 120 μM), containing 5 mM NaCl was made in distilled water. The samples were prepared by diluting the FPE stock to 25 μM and adding at about 3 μM of each peptide. The pH titration was performed with 0.1 M HCl/KOH and FPE fluorescence intensity was recorded at a range of pH from 6.5 to 11.5. The titration curves were obtained by plotting the percentage of difference FPE fluorescence intensities at 518 nm in the presence of each peptide as a function of pH changes (Figure 10).

Examining asymmetry and efficacy of FPE incorporation into the LUVs

The asymmetry of the incorporation of FPE into the LUVs was deduced by the addition of calcium salt and calcium ionophore A23187. The calcium ions are effectively impermeable over the time scale of the fluorescence measurements. Addition of calcium ions will cause some changes of the membrane electrostatic surface potential, which consequently will result in changes, e.g. increases of the fluorescence intensity of FPE. The resultant changes of fluorescence were taken to correspond solely to the outwardly facing FPE molecules. A23187 is a calcium ionophore serving to transfer the calcium

ions across the membrane. Thus, if some FPE has been incorporated on the inner membrane surface, after addition of the ionophore, some calcium ions will be able to

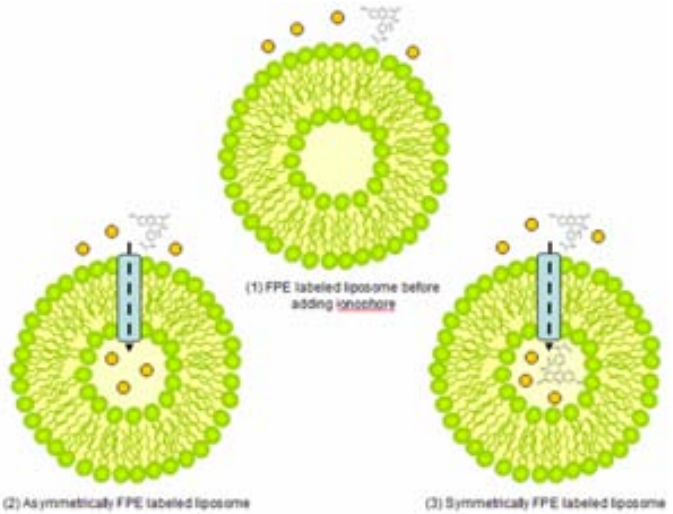

Figure 11. Schematic of symmetry in the FPE labeling liposomes evaluated by cation and ionophore. (1) In the absence of ionophores, adding of cations only changes the electrostatic potential of the outer surface of bilayer monitored by FPE molecules; (2) In asymmetrically FPE labeled liposomes and in the presence of ionophores, there is no FPE molecule in the inner bilayer to monitor the cations induced inner surface electrostatic potential changes . (3) In symmetrically FPE labeled liposomes and in the presence of ionophores, cations induced inner surface electrostatic potential changes is monitored by FPE molecules in the inner bilayer.

reach the inner membrane and FPE signal would change. The ratio of the intensity after calcium ion addition and before ionophore addition to that following the ionophore addition is deemed to present the ratio of the outside facing FPE to that facing inside. Any additional changes of fluorescence intensity indicate that some FPE has penetrated the membrane interior or has appeared on the inner leaflet of the phospholipids bilayer (Figure 11). In this study, the FPE fluorescence intensity at a constant wavelength of 518 nm was recorded following the addition of 50 μM $CaCl_2$. Once the fluorescence intensity was stabilized, A23187 ionophore was added and further changes were recorded.

Collisional quenching of Trp by brominated lipids; theory and mechanism

Collisional (also named dynamic) quenching is among the processes leading to decrease of fluorescence intensity when a fluorophore interacts with a quencher molecule.

Experimentally, the extent of reduction in either the fluorescence intensity (quantum yield) or life-time can be used to calculate the efficiency of fluorescence quenching. The decrease in quantum yield occurs because the quenching rate depopulates the excited state without fluorescence emission most probably due to the spin-orbital coupling of the excited fluorophore and quencher (Figure 12). In collisional quenching a fluorophore needs to be in close contact with quencher in a distance ranging between 3-12 Å. Thus, collisional quenching measurements are used to accurately determine the position of a fluorescent molecule in the membrane. The common quencher groups for analysis of peptide penetration into the membrane are dibromo and nitroxide derivatives. The fluorescence quenching is caused by dipole-dipole interactions between Trp and brominated lipids.

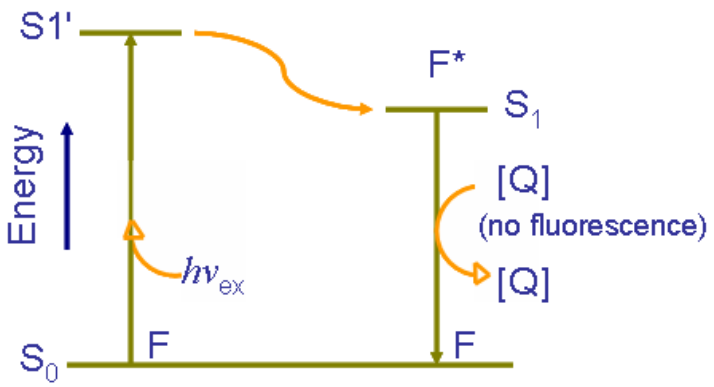

Figure 12. Jablonski diagram showing the process of dynamic quenching, where F is the fluorophore in the ground state, F* is the excited fluorophore, and Q is the quencher.

Experimental scheme

Depth-dependent fluorescence quenching of Trp by brominated-lipids

Dibromine atoms covalently attached to 6,7- and 9,10- carbon atoms of phosphatidilcholine acyl chain were used as Trp quenchers to analysis the insertion depth of mammalian TK analogues in the membrane mimetic systems. Quenching of Trp

residue in TKs peptides by brominated lipids was applied to analyze the relative location of both Trp^8 and Trp^6 residues of SP and NKA, respectively, upon membrane interaction. In this study, stocks of asymmetrically Br-PC labeled LUVs were obtained by adding 35:65 mol% Br-PC lipids to the DMPG or DMPC liposomes (total concentration of 6.2 mM) in sodium phosphate buffer (5 mM, pH 7.0) and were kept at 37°C in a dark bath for about one hour. Then, they were filtered through a PD10 *Sephadex*® desalting column (Amersham Biosciences), equilibrated with the same buffer. To determine peptides insertion into the liposomes, the Trp fluorescence emission of SPW and NKAW (4.5μM) was recorded by setting the excitation at 280 nm and in the presence of 450 μM LUVs composed of the following lipids: pure DMPC, 35:65 mol% DMPC/DMPG, 35:65 mol% Br-PC labeled DMPG and 35:65 mol% Br-PC labeled DMPC.

As a control, fluorescence emission of L-Trp amino acid (4.5 μM) was recorded in the presence of 450 μM LUVs composed of 35:65 mol% DMPC/DMPG and 35:65 mol% Br-PC labeled DMPG. The experiments were performed immediately after preparation of labeled vesicles in order to minimize the trans-bilayer exchange rate (flip-flop) of Br_2-PCs.

In all the experiments, the background corresponding to the vesicles without the peptide was also subtracted.

Penetration depth of mammalian TKs to the zwitterionic and negatively charged LUVs, determined by tryptophan-quenching

The insertion depth of the Trp residue of the mammalian TKs in the lipid bilayer was further estimated by analyzing the fluorescence quenching data with parallax method (PC) using the following equation:

where,
$$Z_{CF} = L_{C1} + \frac{-\ln(F_1 / F_2)\pi C - L_{21}{}^2}{2L_{21}} \qquad \text{(Eq. 9)}$$

Z_{CF} is the depth of the fluorophore as measured from the center of the bilayer;

L_{C1} - the distance of the center of the bilayer from the shallow quencher;

L_{21} - the difference in depth between the two quenchers;

F_1 - the fluorescence intensity in the presence of the shallow quencher;

F_2 - the fluorescence intensity in the presence of the deep quencher; and,

C - the two-dimensional quencher concentration in the plane of the membrane (molecules/Å^2).

Assuming the surface area as 70 Å^2 per lipid will give for the C as a mole fraction of quencher lipid in total lipid/70 Å^2. By X-ray diffraction, the L distances have been determined for a series of Br_2- PCs structured in POPC bilayer in the liquid-crystal phase and lately reevaluated for DMPC bilayers, because the bilayer thickness depends on the acyl chain length. According to these calculations, the thickness of DMPC bilayers in the crystal-liquid phase has been determined to be about 35.3 Å for the head-head thickness, i.e., the distance between the phosphate groups, and 25.4 Å for the hydrocarbon core region. Based on these values and assuming a uniform hydrocarbon chain packing across the bilayer, the increments per CH_2 group are equal to 0.907 Å/CH_2 in the liquid-crystal. Therefore, by using the assumptions reported by McIntosh and Holloway, the respective distances of both quenchers from the bilayer center have been estimated to be 7.7 Å for (6,7) Br_2-PC and 5.0 Å for (9,10) Br_2- PC in the liquid-crystal, respectively.

ThT fluorescent dye as a beta amyloid fibrillization probe

ThT is a cationic benzothiazole dye commonly used for identification of amyloid fibrils. Since ThT fluorescence intensity increases upon binding to amyloid fibrils, this dye is widely used to monitor beta amyloidogenesis. So far, the molecular mechanisms of ThT-amyloid binding is not well understood, however several models explaning the binding of ThT as monomeric form, micelles or through sterically binding sites in amyloid fibrils have been reported. The molecular mechanism leading to increase of ThT quantum yield is also under debate. The general idea is that the increasing of the ThT fluorescence intensity is due to the restriction of torsion oscillations and planarization of dye's fragments.

Experimental scheme

Monitoring the kinetic of the beta amyloidogenesis of TKs by ThT

Possible amyloidogenesis of NKA peptides in the presence of low concentration of SDS (4 mM) in sodium phosphate buffer (5 mM, pH 7.0) was explored by recording the fluorescence intensity of the ThT (5 μM) as a function of time at the fixed wavelength of 486 nm and setting the excitation at 425 nm. ThT fluorescence intensity was acquired for about 20 min then 80 μM of NKA was added to the sample and further changes of the fluorescence intensity were recorded. Fluorescence intensity of the ThT in the absence of peptides was recorded as a control.

Techniques to characterize secondary structures of TK peptides

Circular dichroism spectroscopy; theory and methodology

Circularly polarised light can be produced by the superposition of two linearly polarised light beams that are oscillating perpendicular to each other and propagating with a phase difference of $\pi/2$ radians (Figure 13). The resulting beam could be right or left handed. The circularly polarised light absorption depends on the orientations of transition dipole moments of the molecules. The extinction coefficients of a chiral chromophore for the left and right circularly polarized light are different ($\varepsilon_L \neq \varepsilon_R$)**.** Circular dichroism refers to the differential absorption of left and right handed circularly polarized light as a function of wavelength.

$$\Delta A = A_L - A_R \qquad \text{(Eq. 10)}$$

Yet, the data obtained from CD instruments generally is in terms of the ellipticity (θ) in degrees.

$$\theta = \frac{2.303.(A_L - A_R).180}{4\pi} = 32.98\Delta A \qquad \text{(Eq. 11)}$$

Usually, the observed CD signals are very small, and ellipticities are typically in the range of 10 mdeg. To compare the CD data of different samples, the mean residue molar

ellipticity (MRE) is usually calculated on the basis of CD intensity of the peptide according to the following equation (in deg cm^2 $dmol^{-1}$):

$$[\theta] = \frac{\theta_{obs}}{10 \times L \times c \times n} \quad \text{(Eq. 12)}$$

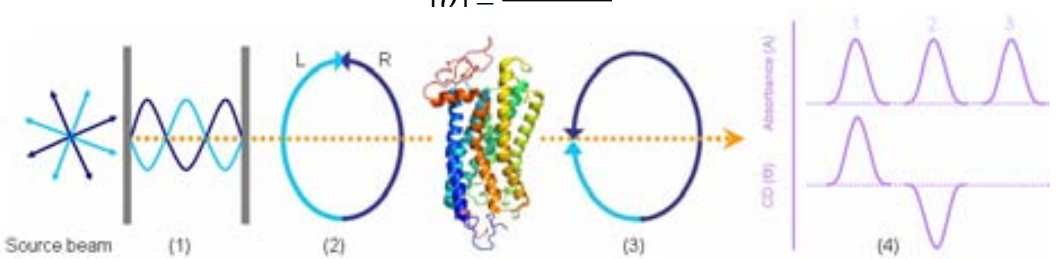

Figure 13. Schematic of CD spectroscopy.
(1) The source beam light passed the polariser filters to make the plane polarised light.
(2) Left and right circularly polarised light obtained by super position of two linearly polarised light beams with a phase difference.
(3) Differential absorption of left and right handed circularly polarized light (3).
(4) The relationship between absorption and CD spectra. Band 1 has a positive CD spectrum with L absorbed more than R; band 2 has a negative CD spectrum with R absorbed more than L; band 3 is due to an achiral chromophore.(ref.:How to study proteins by circular dichroism)

where, θ_{obs} is the observed circular dichroism (in mdeg), L is the optical path length (in cm), c is the peptide concentration (in M), and n is the number of residues.

There are two transitions in the amide chromophore which are dominated in the far-UV CD spectra and related to the peptide conformations (Figure 16). The peak around 222 nm assigned to the peptide n-π* transition, and the peaks at about 208 and 192 nm are assigned to π-π* exciton splitting polarized parallel and perpendicular to the helix axis, respectively. Consequently, the study of the CD spectra between 190 to 260 nm reveals information about the secondary structures of peptides.

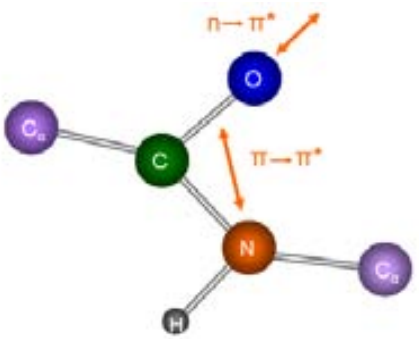

Figure 16. Diagram of a peptide bond. Arrows show the orientation of the transition dipoles.

Experimental scheme

CD data acquisition

The far-UV CD spectra (190-260 nm) of the peptides were recorded on a *Jasco*® J-715 spectropolarimeter (Tokyo, Japan). The instrument was calibrated prior to each measurement. All measurements were carried out using a 1 mm path length quartz cuvette. Each spectrum was obtained after an averaging of at least four scans or more when it was necessary to get better signal-to-noise (*S*/*N*) ratio. Dynode voltage values were simultaneously recorded with CD spectra, and only the CD spectra being in the linear range of the dynode values (generally less than 700 volts) were further considered for analysis of the data. The usual peptides' concentration used in all CD experiments was 100 μM unless otherwise mentioned. All the spectra were corrected by subtraction of the respective spectra obtained from peptide-free samples.

Analysis of CD data

The percentage of α-helix was calculated according to the method of Chen *et al*., assuming that the residue ellipticity at 222 nm is exclusively due to α-helix (in deg cm^2 $dmol^{-1}$):

$$percentage\ of\ \ \alpha - helix = [\theta]_{222} / [\theta]_{222}^{\max}\left(1 - \frac{k}{n}\right) \qquad \text{(Eq. 13)}$$

where, $[\theta]_{222}$ is the observed mean residue ellipticity at 222 nm, $[\theta]_{222}^{\max}$ is the theoretical mean residue ellipticity for a helix of infinite length (-39500 at 222 nm), *n* is the number of residues, and *k* is a wavelength-dependent constant (2.57 for 222 nm).

R_1 ($\theta_{195}/\theta_{208}$) and R_2 ($\theta_{222}/\theta_{208}$) parameters were used as a marker to determine the alpha-helical monomeric peptides and coil-coiled structures. These R_1 and R_2 parameters are independent of peptides' concentrations and have been shown to be useful in comparing

relative helicity for closely related peptides when a two-state α-helix/random-coil equilibrium exists. It has been shown that for a monomeric peptides, R_1 should be positive and R_2 less than 1, while in a coil-coiled structure, R_1 should be close to -2 and R_2 greater than 1.

Light scattering measurements by using CD dynode voltage

The high tension (HT or dynod) voltage (in volts) is applied to the photomultiplier to compensate the reduction of the light intensity during the CD measurements. Both increase in the absorption and scattering can be given by dynode voltage measured by spectropolarimeter. The higher voltage is recorded, the greater is the absorption or the scattering of the sample. Given that the Beer-Lambert law, a change in the dynode voltage can only be originated from variations in the light scattering, which depends on the particle size. Increasing of HT at a fixed wavelength of 222 nm was used as an index to monitor a possible aggregation of the peptides.

Fuorier transform infrared spectroscopy; theory and methodology

Molecules containing dipole moments may absorb the light at IR frequencies equal to the frequency of the oscillations, in which, the extinction coefficient of each vibrational group relates to the bond polarity. Two atoms of a diatomic molecule serve the simplest vibrational properties in mid-IR region (4000-1000 cm^{-1}). According to the classical mechanics (Hook's law), the vibrational frequency (ν) of a simple diatomic molecule depends on the body mass (m) and the force constant (k) as:

$$\nu = \frac{1}{2\pi c}\sqrt{\frac{k(m_1 + m_2)}{m_1 m_2}} \qquad \text{(Eq. 15)}$$

Yet, the vibration of complex molecules in mid-infrared region belongs to the both stretching along the chemical bonds and bending of bond angles. Therefore, there are 3N-6 vibrational motions for a nonlinear N-atomic molecule.

Local oscillating dipoles with similar frequency can couple and make a mixed energy level due to the resonance interactions which is sensitive to the molecular conformations

and the specific environment of chemical groups. IR spectrum of each molecule reveals a unique fingerprint of its vibrational bonds, although, the number of bands is not usually equal to the number of vibrational bonds. Bond distortions smaller than 1 pm can be detected by vibrational spectroscopy. The Fourier transform IR spectrometers are technically based on the interference pattern of two light beams with different phases, called interferogram. This is provided by an optical set, named Michelson interferometer, consists of the polychromatic IR light source, beamsplitter, laser and detector (Figure 15). When, the interferogram hits the sample, part of the energy is absorbed and some part is transmitted. Since the interferogram serves as a time domain, therefore, it will be Fourier

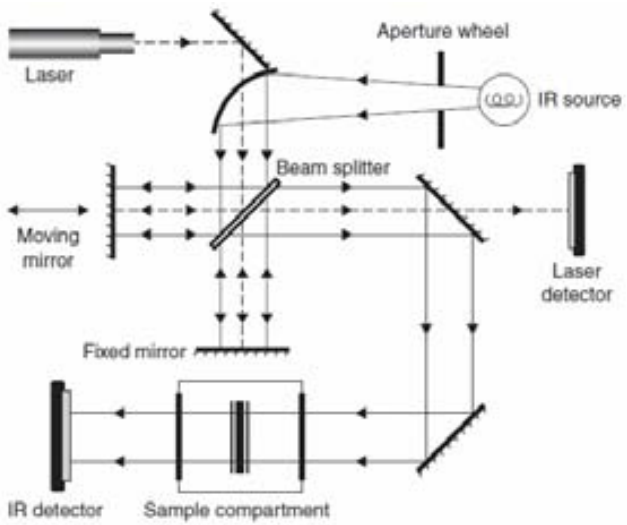

Figure 15. Optical layout of a typical FTIR spectrometer based on Michelson interferometer. The sampling position is determined precisely by laser as a reference. [ref: Fourier Transform infrared spectroscopy]

transformed to a frequency domain called single beam spectrum. The ratio between sample and reference single beam spectra gives transmittance spectrum (%T) which can be converted to absorbance by taking the negative log10 of the data points.

The absorption of peptide backbone in amide I and amide II regions

Amide I region (about 1700-1600 cm^{-1}) arises mainly from the C=O stretching vibration (near 1650 cm^{-1}) with minor contributions from the out-of-phase C-N stretching

vibration, the CCN deformation and the N-H in-plane bend. Amide II (about 1550 cm^{-1}) comes from the absorbance of the out-of-phase combination of the N-H in plane bend and the C-N stretching vibration with smaller contributions from the C=O in plane bend and the CC and N-C stretching vibrations.

Mainly, the hydrogen bonding lowers the frequency of stretching vibration, and increases the frequency of bending vibrations. The frequency of C=O stretching absorptions is strongly dependent upon the stretching of any hydrogen bonds formed and bond coupling, which make the basis for the sensitivity of FTIR spectroscopy to peptides secondary structures.

IR spectroscopy experiments in D_2O

The broad absorption band of O-H bending mode at about 1643 cm^{-1} overlaps with stretching mode of the amide groups. Although, the molar extinction coefficient of H_2O vibration bonds in mid-IR spectrum is weaker than that of peptide bonds, however, its higher absorbance comes from a very high molar concentration of water (about 55.34 M at 25˚C). Thus, IR studies of proteins and peptides in water are complicated. As a consequence, usually very short pathlength cells of 6-8 μm are needed for transmission IR measurements to prevent total IR absorption in the amide I spectral region. From other side, such a short pathlengths limit the intensities of the IR bands and the *S*/*N* ratio at a given sample concentration and relatively high protein. One way of overcoming these problems is collecting IR spectra in D_2O. According to the Eq. 15, replacing an atom with its corresponding isotopes causes a shift in the frequency of vibration. Consequently, the D_2O molar absorptivity at 1650 cm^{-1} is about 15.5 fold lower than that of H_2O. In Figure 17 the IR spectra of H_2O compared with that of D_2O.

Analysis of IR spectra by applying band narrowing techniques

More often, the FTIR spectrum is broad and consists of several overlapping bands. To identify each component band and further assignments to different peptide secondary structures, FTIR bands are subjected to a mathematically calculated Fourier self-deconvolution and second derivatives. The latter is also applied to validate deconvolved

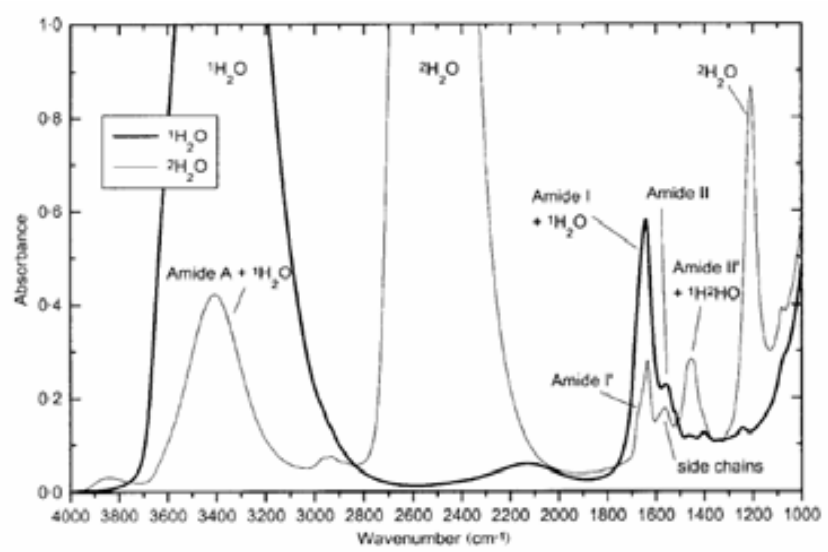

Figure 17. IR spectra of the all-b-sheet protein tendamistat in 1H2O (bold line) and 2H2O (thin line).

IR spectra. In FSD, a Lorentzian broadening of width (γ') is removed from the spectrum and the filter broadening (γ'/k) is substitute, where k is so-called narrowing factor. Further, band parameters including bandwidths and band areas are estimated by different techniques including curve fitting, which is a mathematical tool for modeling the experimental data.

Experimental scheme

Removing TFA from peptides' stocks

Synthetic peptides may contain organic ion impurities, which can give IR band. For example TFA, which is usually used in purification procedures of synthesized peptides, gives a single strong band at 1673 cm^{-1} due to the antisymmetric COO^- stretching vibration of the TFA ion. Although, TFA peak sometimes has been used as an index for internal concentration standard in FTIR spectroscopy, it is suggested to remove TFA in order to avoid its absorbance band in amide I region and its ability to bind to peptides and thus to altering peptide's conformations. Counter-ion exchange method was used to

remove TFA. 3 µL of 0.5 M HCl (final concentration of 10 mM) were added to TK peptides stocks (1mg/150µL) in H_2O and were kept at room temperature for 20 minutes. Then, the stocks were freezed by liquid nitrogen and lyophilized to get the powder. This procedure was repeated three times and finally the peptides stocks were dissolved in the 150 µL D_2O.

FTIR data acquisition and analysis

All FTIR experiments were carried out with free-TFA peptides stocks and performed in D_2O. Mid-IR spectra of the following samples were recorded: 3 mM TKs in sodium phosphate buffer (5 mM, pD 7.0) alone, and in the presence of 20 mM LUVs composed of DMPC or DMPG LUVs. In experiments with SDS micelles, IR spectra of SP peptide (2 mM) in several concentrations of SDS (2, 5, 10, and 45 mM) were recorded in sodium phosphate buffer (5 mM, pD 7.0). In all the IR experiments, small amount of the sample solutions (at about 40 µL) were placed rapidly between CaF_2 windows using path length spacer of 25 µm provided by a *Teflon*® spacer. CaF_2 windows were used mainly because of their low refractive index and mainly because they have transmitance in the range of 4000 to 1000 cm^{-1} and moderate hygroscopic character.

All the spectra were collected on a *Varian*® 7000e Fourier transform infrared spectrometer equipped with cryo-thermo bath. The IR spectra of TK peptides were acquired using attenuating filters to moderate laser intensity. In all the FTIR experiments, first 50 scans were recorded for samples and consequently 50 scans obtained from the background. Totally, 40 cycles of sample and background scanning was performed. Absorbance was automatically calculated and plotted versus wavenumber in the frequency range between 3400-1200 cm^{-1} including amide I' region using *Varian*® resolutions pro 4.0 software. Alignment and calibration were done when necessary. To minimize the atmosphere water vapor, the sample chamber was purged with dry air continuously during measurements. In all the FTIR experiments, the correct subtraction factor is achieved when the baseline got straight between 1700-1900 cm^{-1} and no sharp absorption band was seen at about 3400 cm^{-1}.

IR data processing

High signal to noise spectra lacking water vapor were chosen for further analysis and band narrowing, using *Matlab*® 5.3 (MathWorks, Inc., Natick, MA) and *Grams*® 4.01 softwares. Finally, deconvoluted and second derivative spectra compared and only absorption bands visible in both were considered to assignment.

Small angle X-ray scattering (SAXS); theory and methodology

This technique gives structural information about the overall shape and size of both crystalline and non-crystalline materials, including biological one. When SAXS is used to study biological materials, very often it is in aqueous solution, and the scattering pattern is orientation averaged. The advantage of SAXS over crystallography and NMR spectroscopy is that in former case a crystalline sample is not needed, while NMR method encounter problems with macromolecules of higher molecular mass (> 30-40 KDa). When electrons are accelerated by collimated X-rays, they emit radiation in an angle related to the initial wave direction and with the same frequency (Thomson scattering). The amplitude of the scattered wave is independent of the frequency, while the phase is shifted relative to the incident radiation. In SAXS, the elastic scattered intensity (I), with a wavelength between 0.1 to 0.2 nm, is recorded by a detector as a function of the scattering angle (typically a few degrees; see Figure 18). For a homogeneous chemical composition, the scattering intensity of a single particle varies with the square of its molecular weight. Therefore, monodispersity and high purity of samples are essential in SAXS experiments. The intensity of the scattered radiation is proportional to the contrast between the macromolecule and the bulk solvent, which rises from the difference in their electron density.

Analysis of SAXS's patterns

The scattering vector or momentum transfer (s) is defined as:

$$s = \frac{4\pi \sin\theta}{\lambda} \qquad \text{(Eq. 16)}$$

where, λ is the wavelength of incident radiation and θ is half the angle between the incident and scattered radiation.

The scattering pattern is normally expressed by intensity (I) as a function of the scattering vector:

$$I(s) = \langle I(s) \rangle_{\Omega} = \langle A(s) A^{*}(s) \rangle_{\Omega} \qquad \text{(Eq. 17)}$$

where, the scattering amplitude $A(s)$ is a Fourier transformation of the excess scattering length density, and the scattering intensity is average over all orientations (Ω).

Further, the scattering profile is Fourier transformed to obtain the interatomic distance distribution function, $P(r)$, which reveals the information concerning the shape and volume of particles. Since all particle orientations contribute equally to the signal, structural information on directionality is lost and only information on distance distributions between scattering centers (electrons or nuclei) is conserved. Since, $I(0)$ can not be distinguished from the direct beam, the Guinier analysis is a method for the extraction of the forward (or zero angle) scattering intensity $I(0)$ and the radius of gyration (R_g). These parameters also can be calculated precisely from the $P(r)$ function. The R_g is defined as the root-mean-squared distance of all elemental scattering volumes from their centre of mass weighted by their scattering densities and provides information as to the mass distribution within a particle. For a monodisperse solution of globular macromolecules the Guinier equation is defined as:

$$I(s) = I(0) \exp(-1/3 R_g^2 s^2) \qquad \text{(Eq. 18)}$$

In principle, $I(0)$ and R_g can be extracted from the Y-axis intercept and the slope of the linear region of a Guinier plot ($\ln[I(s)]$ versus s^2), respectively.

Noteworthy, aggregation state of the sample can be recognized from the linearity of the low regions (at about 0.10 nm^{-2} and lower) of Guinier plot.

Ab initio methods are widely used to model the low-resolution three dimensional shape of the macromolecules from 1D SAXS data, by minimizing the difference between the computed scattering of the model and the experimental data.

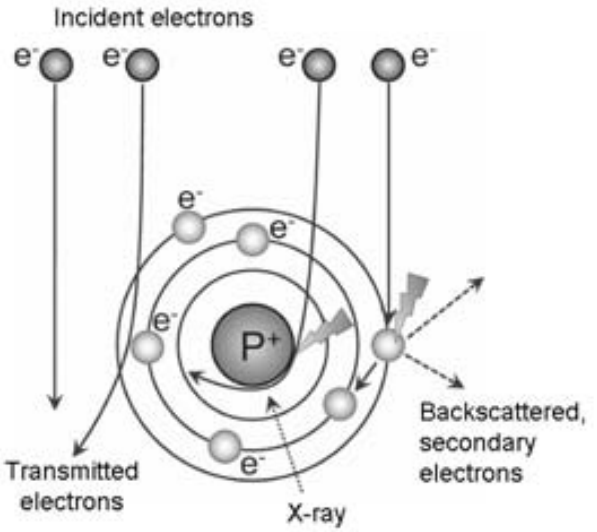

Figure 18. Schematic of consequent processes upon electron beam hits an atom

Experimental scheme

SAXS instrument calibration with BSA

Prior to sample measurements, BSA buffer was prepared as a standard solution to calibrate the SAXS instrument. BSA powder (5 mg) was placed in a tube. 1mL of Hepes buffer (50 mM, pH 7.5) was added and mixed by pipeting calmly to avoid foam formation. Then, the sample was centrifuged at 14000 rpm for 10 min (4˚C). Only the

supernatant was pipetted up into a new tube. Finally, BSA concentration was measured using the *NanoDrop*® (should be between 4-5 mg/mL).

SAXS data acquisition of NKA peptide in buffer solution

Using synchrotron beamline, SAXS patterns of different concentrations of NKA (0.6, 1.6, 3.4 and 6.7 mg/mL) in sodium phosphate buffer (5 mM, pH 7.0) were acquired to find out the optimum concentration and to check for a possible radiation damage of the peptide. The sample containing 6.7 mg/mL NKA was used for the further SAXS experiments as the optimum concentration. Experiments with NKA peptide were performed twice at different temperatures: 5, 25, 40˚C and then the sample was cooled

down to 5 ˚C. *PRIMUS*® and *GNOM*® softwares were applied to process the experimental data and further to evaluate the $P(r)$, respectively. *Ab* initio modeling was done by *DAMMIF*® software.

Transmission electron microscopy (TEM); theory and methodology

In transmission electron microscope, a stream of monochromatic electrons, produced by a filament (usually tungsten heated up to 2000-3000 ˚C), is accelerated towards the specimen with a positive electrical potential. Upon the beam hits the sample, the incident electrons may transmit the sample without scattering, or diffract without alteration of kinetic energy and velocity, or scattered inelastically due to the collision with the atomic electrons or nuclei of the matter. Schematically, the electron collision with the matter is illustrated on the Figure 19. The transmission of unscattered electrons is inversely proportional to the specimen thickness. Generally, both no scattered and elastically scattered electrons contribute to the image. Since the intrinsic contrast of the sample is

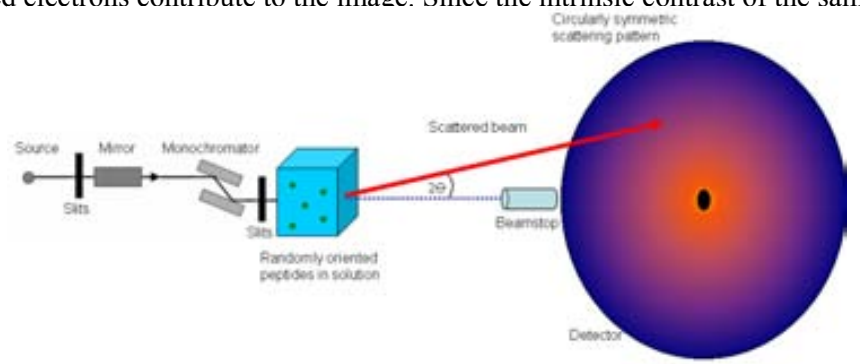

Figure 19 Schematic of a small angle X-ray scattering. Collimated X-rays accelerate the electrons of the sample causing radiation with an angle of 2θ related to the incident beam line. The direct beam is usually absorbed by a beam stop.

very low, as a rule the staining is essential. Negative staining with heavy metals is a method in which the stain binds to the background but not to the object of interest. Consequently, in negative staining the exclusion is visible. In most of the specimens, uranyl acetate gives the highest contrast. Improving the image contrast at the other level is achieved by the objective aperture in the microscope since it prevents high angle scattered electrons to reach the image plane.

The TEM practical resolution is often given by an expression:

$$d = A.C_s^{1/4}.\lambda^{3/4} \qquad \text{(Eq. 19)}$$

where, C_s is the spherical aberration coefficient of the objective lens, λ is the electron wavelength, and the constant *A* depends on the imaging.

Therefore, due to the low associated wavelength of electron (0.04-0.008 Å) the electron microscope resolution is high. The highest resolution features of the specimen are already affected at electron exposures of 10 e-/Å^2 or less. However, the attainable resolution of TEM is about 20 Å for negatively stained samples.

Experimental scheme

Preparation of specimens for TEM and obtaining the micrographs

Cooper grid supports coated by a thin, electron-transparent carbon film were used. Negative staining was done using 2% heavy metal salt uranyl acetate. Electron micrographs from different samples of the TK peptides in buffer alone, or at different concentrations of SDS and also in DMPG or DMPC LUVs at neutral pH were collected either after immediately preparation of the samples or after incubation at room temperature for different hours.

Carbon grids were fixed on the surface of a Petri dish covered by a piece of *Parafilm*®. Usually, a small drop (10 µL) of each sample was deposited on the grid and waited to settle down for two minutes. Then, the rest of sample was removed from the grid very gently and carefully. Next, a small drop (10 µL) of 2% uranyl acetate negative stain was placed on the grid. After one minute, this drop was also blotted dry and the grid replaced on a single tilt holder to check the sample by microscope.

The TEM models *JEOL*® 1400 and *Hitachi*® 7000 were used to obtain micrographs. Uranyl acetate is toxic and should be kept at 4 ˚C in dark.

Table 1. Theoretical net charges of TK peptides at different pH.□

TKs	theoretical net charges*			
	pH 3.8	pH 7.0	pH 8.5	pH 10.7
Substance P (SP)	+3	+3	+2.5	+1.6
Neurokinin A (NKA)	+2.6	+1	+0.5	-0.45
Scyliorinin I (ScyI)	+2.6	+2	+1.5	-0.7

*Theoretical net charges derived from the Henderson-Hasselbalch equation.

Table 2. The absorption photo-physical properties of applied fluorescent dyes.

Fluorescent dye	Abs λ_{max} (nm)	Extinction coefficient ($M^{-1}cm^{-1}$)	Solvent
Pyrene	335[a]	54 000	methanol
ThT	412	36 000	H_2O (recrystallized)
FPE	490[b]	36 400	ethanol

[a] pyrene has eight absorption peaks at 232, 242, 252, 260, 272, 308, 320 and 335 nm

[b] and 465 nm

RESULTS AND DISCUSSION

PART I

CHARACTERIZATION OF THE TK PEPTIDES INTERACTIONS WITH MEMBRANE MIMETIC SYSTEMS

In this chapter of the thesis, we studied the mode of interactions (binding, insertion and topology of the peptides into bilayer) of the TK peptides with the membrane mimetic systems. To get insight into the structural details of these interactions, we applied the following fluorescence approaches:

First, we used two fluorophores: the natural Trp and unnatural Phe-CN amino acids as environment sensitive probes. These fluorescence dyes exhibit strong changes in their dipole moments upon electronic excitation. Thus these molecules can provide direct information for their molecular environment through measuring their fluorescence characteristics (wavelength maximum, fluorescence intensity, and/or fluorescence life-time). Second, we used two external probes: i) the membrane potential-sensitive probe fluorescein phosphatidylethanolamine (FPE) to characterize the peptide binding and the possible insertion into the membrane bilayer; and, ii) brominated lipids (6,7 and 9,10) lipids to evaluate depth of the insertion of the peptide (the topology of the Trp residue) into the membrane bilayer.

Control experiments

3.1.1. Determination of critical micelle concentration (CMC) of SDS

As we have explained in Materials and Methods the measuring the intensity of pyrene fluorescence peaks has been shown to be very sensitive method for determining the CMC of SDS. The fluorescence emission spectra of pyrene in buffer (pH 7.0) and in the presence of different concentrations of SDS are shown in Figure 1. In addition to the five characteristics monomer vibration peaks (see Material and Methods section), the pyrene spectra reveals some shoulders at 364 nm and also in the range between 400 and 450 nm,

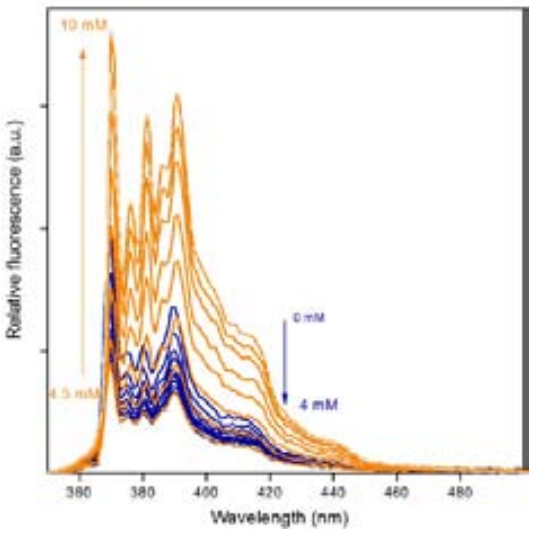

Figure 3.1 Fluorescence emission spectra of monomeric pyrene (0.5 mM) in the presence of sodium phosphate buffer (5 mM, pH 7.0) alone and as a function of SDS titration from 0 to 10 mM. Excitation was set at 335 nm and temperature was 25 °C.
No excimer emission were detected at about 480 nm.
Arrows indicate for SDS concentrations.

with less intensity compared to that of the main vibration peaks. Importantly, no emission bands were observed between 460 to 500 nm, assigned to the excimer formation of pyrene, which ruled out some possible interactions between pyrene-pyrene molecules in the samples. The pyrene emission spectra (Figure 1) show also that the way, in which the intensities of the dye change depends on the concentration of the surfactant. Two different patterns can be distinguished with SDS titrations. First, between 0 and 4.5 mM of SDS, the fluorescence intensities of pyrene (360-450 nm) decreased with increases of SDS concentration. In contrary, titration of the pyrene with SDS at concentrations above 5 mM causes an increase of the pyrene fluorescence, accompanied with a small shift of the all peaks to a longer wavelength.

The CMC of SDS in buffer was determined by plotting the ratio of the fluorescence ntensities of the I_{385}/I_{374} pyrene peaks as a function of the SDS concentrations (Figure 2, red curve). Below 4 mM of SDS, the I_{385}/I_{374} ratio is close to 0.63, while increases of the SDS concentration from 4 to 8 mM, results in an increase of the I_{385}/I_{374} ratio to about 0.97.

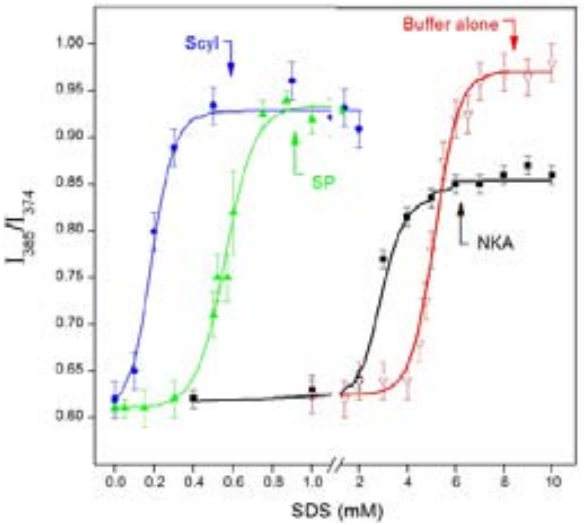

Figure 3.2 Determination of the CMC of SDS.
Plot of the fluorescence intensities ratios of the third and the first vibronic peaks (I_{385}/I_{374}) of 2 mM pyrene in sodium phosphate buffer alone (5 mM, pH 7.0, ▽); and in the presence of 25 mM NKA (■), 25 mM SP (▲) and 80 mM ScyI (●) as a function of increasing concentrations of SDS. Continuous lines indicate global fits to the data using nonlinear least squares program (commercial software package Origin). The fitting of the data gives sigmoid curves in all cases. Arrows indicate the CMC.

In the range below 4 mM, SDS molecules mainly exist as monomers. Most likely the pyrene and SDS monomers molecules are not associated and remain solubilized in the aqueous phase, thus giving a ratio around 0.64, very similar to that previously measured in water (around 0.64). Above some critical concentration CMC (which is usually in small concentration range) the SDS molecules associate to give micelles. Due to its hydrophobic nature, the pyrene molecules associate with the SDS molecules penetrating deeply in the hydrophobic region of formed micelles and cause an increase of the I_{385}/I_{374} ratio. Moreover, the I_{385}/I_{374} values do not show any appreciable changes at SDS concentrations above 8 mM. Above the CMC of SDS, this association is saturated and become the predominant when all pyrene molecules are solubilized inside the SDS micelles. The pyrene-SDS associates are in equilibrium giving a I_{385}/I_{374} ratio around 1.

From this plot, we determined a CMC of about 9 mM for SDS in sodium phosphate buffer (5 mM, pH 7.0), in keeping with published values (Chatterjee, A. et al. 2001.Fuguet, Elisabet. et al. 2005.Thévenot, Caroline. et al. 2005).

3.1.2. Effect of TK peptides on the CMC of SDS

It is well known that the CMC of SDS is a complex parameter, depending on a number of factors, such as ionic strength, pH and temperature (Fuguet, Elisabet. et al. 2005.Hassan, P.A, et al. 2002.Inayathullah, N. Mohammed. et al. 2003). Taking into account that all the TKs are cationic peptides (e.g. carry a net positive charge at neutral pH, see Materials and Methods, we seek to evaluate whether and how TKs would affect the CMC of SDS. For this reason, we performed the same type of titration experiments of the pyrene with SDS, but in the presence of each of the TKs peptides. Therefore, the fluorescence emission spectra of the pyrene upon SDS titration were recorded separately in the presence of SP, NKA and ScyI peptides. Then, the ratios of the fluorescence intensity of the I_{385}/I_{374} pyrene monomers peaks were plotted as a function of SDS concentration (Figure 2). The obtained curves for the ratio of I_{385}/I_{374} intensities of the pyrene in the presence of TKs as a function of the SDS follow the same sigmoid patterns as the curve obtained in buffer alone. However, in the presence of the TKs the curves are shifted to a lower SDS concentration. Moreover, each TK peptide affects the pyrene intensities in a different way. In the presence of ScyI peptide, the I_{385}/I_{374} ratio increases most rapidly (from 0.62 to 0.93) by the addition of the lowest SDS concentrations (below 0.5 mM), and the I_{385}/I_{374} reaches a steady values at about 0.5 mM of the SDS. In the presence of SP, the I_{385}/I_{374} ratio of pyrene keeps nearly constant (at about 0.61) below 0.4 mM of SDS and increases to about 0.94 in the range of 0.4 to 0.9 mM SDS. In the presence of NKA and up to 2 mM of SDS, the I_{385}/I_{374} ratio is about 0.61. It increases to about 0.85 when SDS concentration rises up to about 6 mM, and finally I_{385}/I_{374} ratio keeps invariable above 7 mM of SDS.

From the fitting of the data plots, were determined the apparent CMC of SDS in the presence of TKs: NKA, SP and ScyI as about 6, 0.9 and 0.5 mM, respectively. These data show clearly that the CMC of SDS is strongly affected by the three TK peptides, but not in the same degree. ScyI shows the strongest effect, decreasing at about 10 fold CMC of the SDS, followed by SP (at about 9 fold) and NKA for (1.8 fold). From other side the measured values for CMC of SDS in the presence of the peptides show that there is not

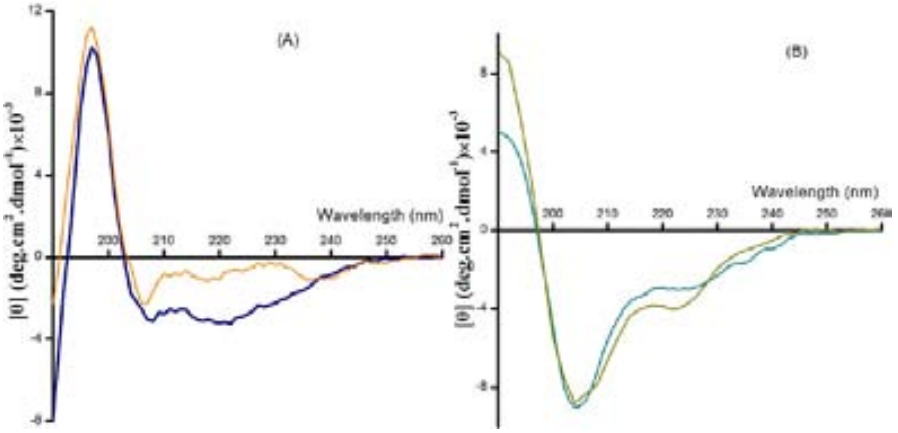

Figure 3.3. CD spectra of (A) SP (——) and SPW (——); and (B) NKA (——) and NKAW (——) in DMPG LUVs. In all cases, the peptide:LUVs ratio was 1:100. The buffer was sodium phosphate (5 mM, pH 7.0). All the spectra were collected immediately after preparation of samples. Temperature was set at 22 °C.

correlation between the net charge of the peptide and the value for the CMC, since (see the Materials and Methods) ScyI has the strongest effect, but not the highest positive net charge at pH 8.5. These findings imply for the complex mechanism of micelization of SDS as shown previously.

3.1.3. Secondary structural characterization of TK analogues, SPW and NKAW

As we have already described in Material and Methods section, the TKs do not contain Trp residue in their sequences. Thus, we engineered SPW and NKAW analogues, in which Phe^{8} and Phe^{6} were substituted for Trp, respectively. Before performing the binding experiments, we did some control experiments to check whether the residue substitution changes somehow the secondary structural conformations of the TKs in studied systems. Figure 3 represents the comparison of NKA with NKAW, and SP with SPW CD spectra in liposomes. The overall CD spectra of the peptides and their analogues are similar, indicating that Trp residue substitution do not impair the overall conformation of the peptides into membrane mimetic systems.

3.1.4. Characterization of the mammalian TK peptides interactions with the micelles

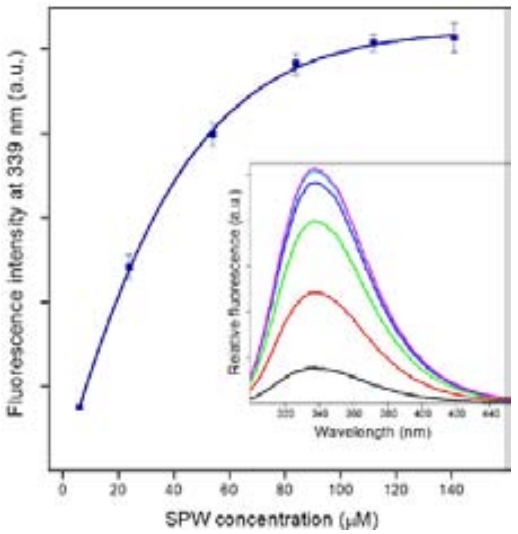

Figure 3.4. Titration curve obtained by plotting the Trp fluorescence intensity of SPW at λ_{339} as a function of the peptide concentration. Inset. Fluorescence spectra of different concentrations of SPW: 6 (—), 24 (—), 54 (—), 84 (—), 112 (—), and 141 μM (—) in the presence of SDS (20 mM) and sodium phosphate buffer (5 mM, pH 7.0), recorded at 25 °C. In all the cases, λ_{exc} was set at 280 nm. The data points were polynomial fitted, giving a hyperbolic curve.

The Trp fluorescence emission maximum (λ_{max}) and the quantum yields of the Trp fluorescence are very sensitive to the microenvironment (see Materials and Methods section). A blue shift (movement to a shorter wavelength) of the emission maximum accompanied by an increase in the quantum yield is generally observed when the Trp residue is transferred from medium of high polarity to a medium of low polarity. These properties of the Trp were explored to get a description of the location/environment of mammalian TKs' Trp residue in the membrane mimetic systems.

3.1.5 Titration of SDS micelles with mammalian TKs

The Trp emission spectra of mammalian TK peptides were recorded upon the titration of SDS micelles (20 mM highly above the CMC) with SPW (Figure 4, inset) and NKAW (Figure 5, inset) peptides in. An enhancement of the Trp fluorescence intensity was observed with an increase of the peptide concentrations from 6 to about 160 μM, but with no detectible changes of the λ_{max} of the fluorophore. The plot of Trp fluorescence intensities at the λ_{max} of 339 nm for SPW and at 334 nm for NKAW, as a function of the TK peptides concentrations is presented in Figure 4 and 5. The titration curves show a

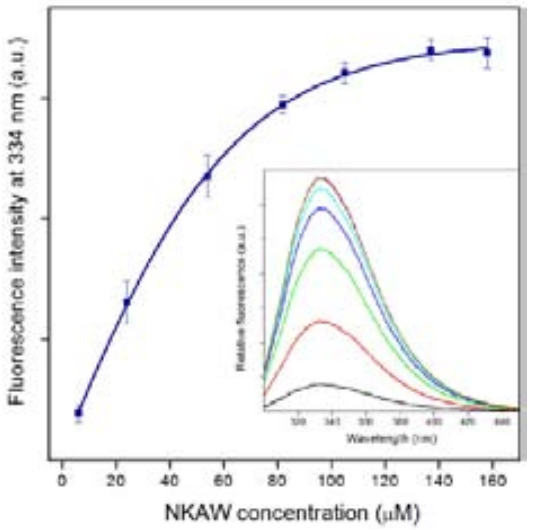

Figure 3.5. Titration curve obtained by plotting the Trp fluorescence intensity of NKAW at λ_{334} as a function of different peptide concentrations. Inset. Fluorescence spectra of different concentrations of NKAW: 6 (—), 24 (—), 54 (—), 82 (—), 105 (—), 137 (—), and 158 μM (—) in the presence of SDS (20 mM) and sodium phosphate buffer (5 mM, pH 7.0), recorded at 25 °C. λ_{exc} was set at 280 nm. The data points were polynomial fitted, giving a hyperbolic curve.

rapid increase of the Trp intensity by adding low concentrations of peptides (up to about 60 μM). At higher concentrations of peptides, the fluorescence intensities still increased, but the changes were not appreciable significant and finally above 80 μM SPW and 100 μM NKAW peptides concentrations λ_{max} values reached a plateau.

3.1.6 Interactions of the mammalian TK peptides with SDS surfactant. Evaluation of the TK peptides-SDS interactions by Trp fluorescence intensity

Figure 6 and 7 (insets) show the Trp emission spectra of SPW and NKAW peptides upon titration with SDS (below and above CMC, see also Figure 2). It is well seen that two fluorescence parameters of the Trp emission spectra, intensity and λ_{max}, undergo changes with SDS. To get more insight into these changes, Trp fluorescence intensities were plotted at two wavelengths (350 and 339 nm for SPW, and 350 and 334 nm for NKAW) against SDS concentrations (Figure 6 and 7). The reason of plotting the intensities at two different wavelengths was because of λ_{max} changes upon the titration with SDS,

Figure 3.6

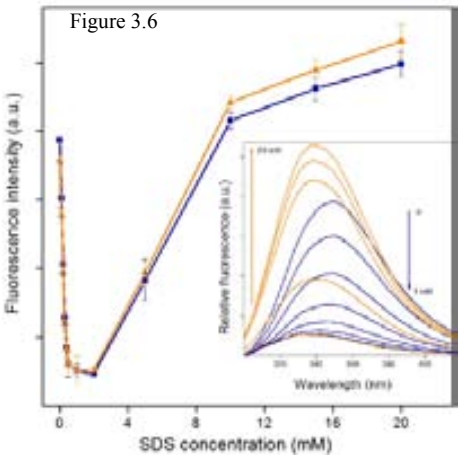

Figure 3.7

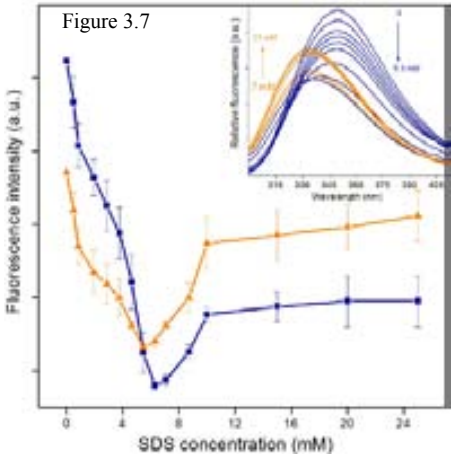

Figure 3.6. Plot of the fluorescence intensities of SPW at 350 nm (■) and 339 nm (▲) as a function of the SDS concentrations. Inset. Fluorescence spectra of SPW (5 μM) in sodium phosphate buffer (5 mM, pH 7.0) and in different concentrations of SDS: 0.1, 0.2 ,0.3, 0.4, 0.5, 1, 2, 5, 10, 15 and 20 mM (arrows). In all cases, λ_{exc} was set at 280 nm. Temperature was set at 25 °C.

Figure 3.7. Plot of the fluorescence intensities of NKAW at 350 nm (■) and 334 nm (▲) as a function of the SDS concentrations. Inset. Fluorescence spectra of NKAW (5 μM) in sodium phosphate buffer (5 mM, pH 7.0) alone and in different concentrations of SDS: 0.5, 0.8, 2, 3, 4, 4.6, 5.5, 6, 7, 9, 10, 15, 20 and 25 mM. λ_{exc} was set at 280 nm and all the spectra were collected at 25 °C.

indicating for a displacement of Trp in a different polarity environments. In SPW, the titration with up to 1 mM SDS, very near to its CMC caused a decrease of Trp fluorescence at both wavelengths, compared to that in the absence of SDS. However, above CMC (1 mM SDS), an apparent increase of the intensities was recorded. Similarly in NKAW, increase of the SDS concentration up to CMC (about 6 mM SDS) caused a decrease of the intensities of the Trp fluorescence at both wavelengths, while, above this concentration fluorescence intensities increases.

These data show clearly that the changes in Trp fluorescence intensity correlate closely with the formation of SDS micelles in the solution. Thus, in both SPW and NKAW, before the formation the SDS micelles the intensity of Trp fluorescence decreases with SDS concentration up to some threshold value, which closely reflects the CMC of SDS in the peptides. At that points Trp intensities reach to a minimum value. Once yet the SDS reaches this critical concentration, the Trp intensity starts to increases with SDS.

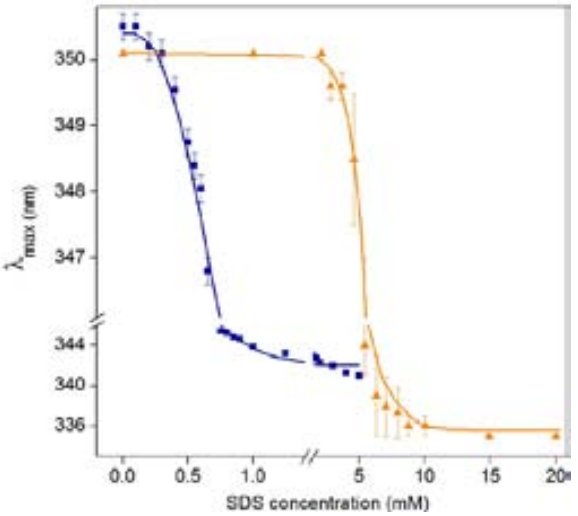

Figure 3.8. Plot of the fluorescence emission λ_{max} of SPW (■) and NKAW (▲) as a function of various SDS concentrations. Concentration of peptides was 5 μM and λ_{exc} was set at 280 nm. The buffer was sodium phosphate (5 mM, pH 7.0). All the spectra were collected at 25 °C. The data points for both SPW and NKAW peptides were fitted and the continued lines represent the best fit as a reverse-sigmoids.

3.1.7. Interactions of the mammalian TK peptides with SDS surfactant. Evaluation of the TK peptides-SDS interactions by studying fluorescence emission maximum (λ_{max}) of Trp residue

Figure 8 shows the plot of λ_{max} of Trp against SDS concentrations (below and above CMC). As can be seen from the plot, below 0.1 mM of SDS, λ_{max} is at about 350 nm. Further titration with the SDS (up to 1 mM) caused a significant steep blue shift of λ_{max} to about 342 nm. Above this SDS concentration λ_{max} was not affected significantly. The λ_{max} of Trp of the NKAW follows different behavior with the SDS titration. λ_{max} was at 350 nm in the absence of SDS and at concentrations of SDS below 2 mM. A significant blue shift of λ_{max} to a lower wavelength (334 nm) was reached with SDS concentration at about 6 mM. In general, the maximum blue shift of Trp λ_{max} in NKAW is about 9 nm over than that of SPW.

Summarizing we can conclude that the significant blue shift of the λ_{max} from 350 nm (in absence of SDS) to 342 nm and 334 nm for SPW and NKAW in presence of SDS micelles strongly indicates for the insertion of the some peptide segment including Trp residue into hydrophobic core of the micelles. From other side the detected changes of both: λ_{max} and fluorescence intensity before the micelle formation imply that the peptides

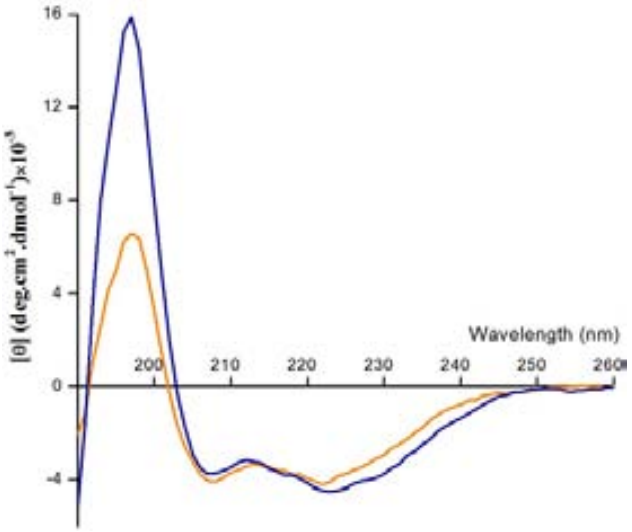

Figure 3.9. CD spectra of Phe-CN SP (80 μM) in 12 mM SDS (—), and SP (80 μM) in 10 mM SDS (—). The buffer was sodium phosphate (5 mM, pH 7.0). All the spectra were collected immediately after sample preparation. Temperature was set at 22 °C.

also interact with the SDS monomers. The blue shift of λ_{max} with an increases of the SDS monomers concentrations suggests for some movement of Trp side chain to more unpolar environment, while the decreases of fluorescence intensity reflects the quenching of the Trp fluorescence. In fact, the rule for the changes of the quantum yield is not always followed strictly. In some cases even Trp maximum showing movement to hydrophobic environment the quantum yield (intensity) decreases instead to increase. Quenching of the Trp intensity before formation of micelles may due to to quenching from acceptor (Muino, P. L. and P. R. Callis 2009) charged Lys and Arg side chains, placed near toTrp residue and known as Trp quenchers (Chen, Y., Barkley, M.D 1998). Indeed a structural information for the peptides in the same conditions is needed to perform deeper analysis of these observations and we will discuss them again lately in the thesis (see chapter 2)

3.1.8. Characterization of SP-micelles interactions by Phe-CN fluorescence

Complementary to characterize the location of the Phe^8 of SP in membrane bilayer and in SDS micelles, we used Phe-CN SP in which Phe^8 was labeled with CN group. Prior to the fluorescence studies, two control experiments were performed:

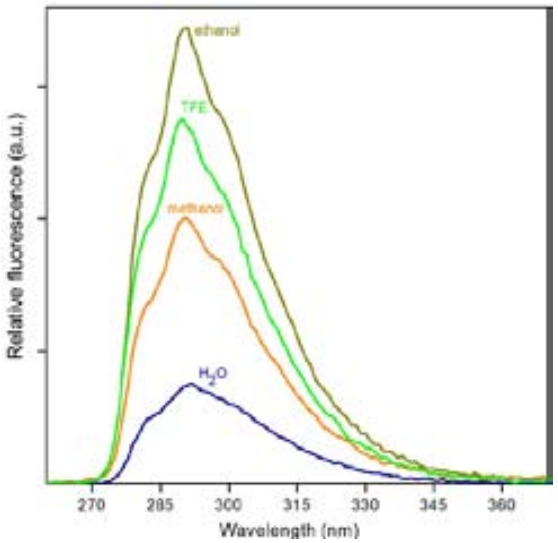

Figure 3.10. Fluorescence spectra of Phe-CN SP (2 μM) in H_2O (—), methanol (—), TFE (—), and ethanol (—). In all the cases, λ_{exc} was set at 232 nm. Temperature was set at 25 °C.

1). As a new peptide was studied, CD experiments were performed to find out whether the introduced CN group to Phe[8] would change the secondary structures of the SP peptide in membrane mimetic systems. Figure 9 shows CD spectra of the SP and Phe-CN SP in the presence of micelles. Two negative bands at about 208 and 222 nm and a positive peak at about 198 nm indicate for a dominant alpha helical structure of peptides in micelles. The similarity of the spectra indicates the absence of significant structural changes induced by the presence of the label.

2). As a control, the fluorescence spectra of Phe-CN SP in the presence of H_2O and a series of protic solvents (a molecule containing a hydrogen atom bound to an oxygen or a nitrogen) ethanol, methanol and TFE were recorded to understand how the environmental factors such as hydrogen binding and polarity affects fluorescence properties of the Phe-CN SP. In all these media, Phe-CN SP fluorescence spectra show a peak at about 291 nm with two shoulders at about 284 and 298 nm (Figure 10). Table 1 shows the solvatochromic parameters of the H_2O, ethanol, methanol and TFE. Other than TFE, in the rest of solvents (H_2O, ethanol and methanol), the fluorescence intensity of Phe-CN SP is related to the solvent's polarity, since a polarity increase causes a decrease of the Phe-CN fluorescence intensity. Although the hydrogen bonding donating ability (α) of TFE is

Table 1. Solvatochromic properties of the solvents used in Phe-CN SP experiments. The parameters are adopted from

solvent	π	β	α
water	1.09	0.18	1.17
methanol	0.60	0.62	0.93
ethanol	0.54	0.77	0.83
TFE	0.73	0.00	1.51

π: dipolarity/polarizability; β: hydrogen binding accepting ability; α: hydrogen binding donating ability

higher than that of other solvents used here (Table 1), the fluorescence of Phe-CN SP in the presence of TFE is higher than that in distilled water and bulk methanol. This might relate to variation in the Phe-CN hydrogen binding caused by the structural changes of the peptide in different environments (Bowie, J. U. .Taskent-Sezgin, H. et al. 2009). These data show some discrepancy with Gai´s data (Serrano, A. L. et al.)However, it is important to stress that the both experiments are performed not in the same conditions. In case of the Gai work was measured the fluorescence of only Phe-CN group, while in our case we measured the analog of SP, including Phe-CN group in the sequence. Therefore the different intensity trends in these solvents recoded by us suggest strongly that polarity is not basic factor defining the fluorescence intensity changes, but include other also crucial factors like hydrogen bonding. We believe that in our experiment the role of the Phe-CN SP peptide itself on the fluorescence intensity of the Phe-CN should not be neglected. The hydrogen bonding of the Phe-CN with peptide side chains (Taskent-Sezgin, H. et al. 2009.Taskent-Sezgin, H. et al.) may cause an increase of the intensity of the Phe-CN group and should be considered.

Next to this control, we performed SDS titration. Up to about 1 mM SDS, fluorescence intensity of Phe-CN decreased, as at concentration close to CMC (1 mM SDS), the intensity of Phe-CN is the lowest. But above CMC of SDS an increase of the intensity is observed (Figure 11) and at about 6 mM SDS no significant changes of the Phe-CN fluorescence were detected. Figure 12 displays the plot of Phe-CN SP fluorescence intensities (at λ_{291}) as a function of SDS concentrations. From the plot is clearly seen that fluorescence intensity changes of Phe-CN in presence of SDS follow the same trend as

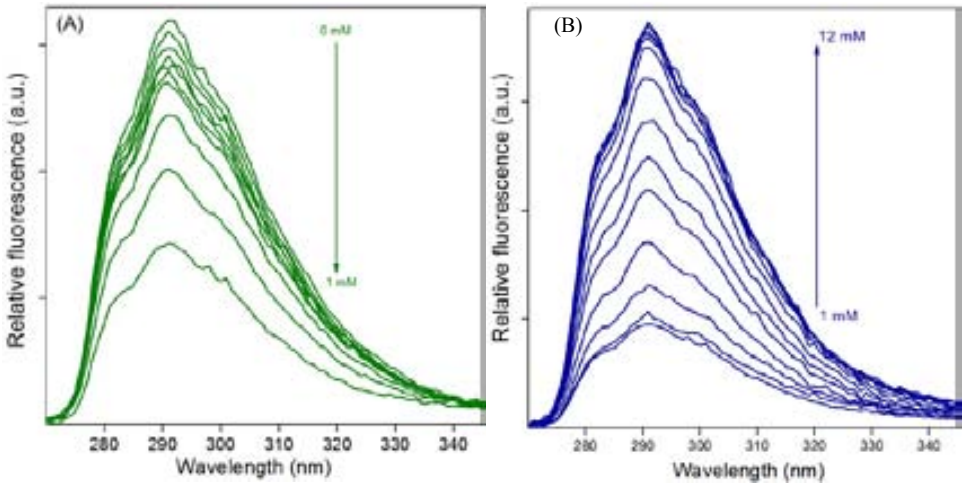

Figure 3.11. Fluorescence emission spectra of Phe-CN SP (2 μM) as a function of the SDS titration: (A) 0 to 1 mM; and (B) 1 to 12 mM. λ_{exc} was set at 232 nm. The buffer was sodium phosphate (5 mM, pH 7.0). Temperature was set at 25 °C.

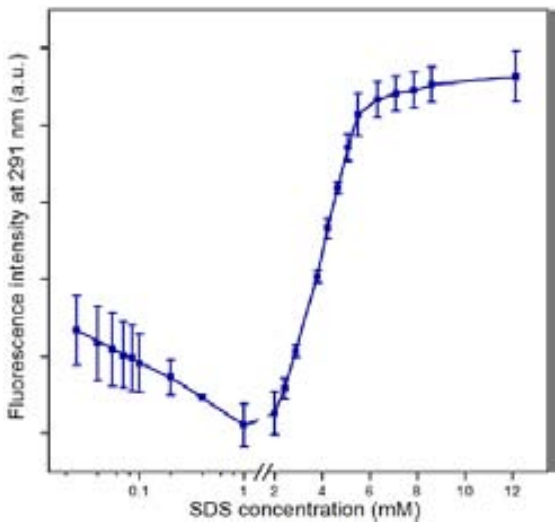

Figure 3.12. Plot of the fluorescence intensity changes of Phe-CN SP (2 μM) at 291 nm as a function of various SDS concentrations. λ_{exc} was set at 232 nm. The buffer was sodium phosphate (5 mM, pH 7.0) and temperature was set at 25 °C. The dependence of the Phe-CN fluorescence on SDS follows a sigmoidal pattern.

that observed for the Trp residue. In contrary to the data for λ_{max} of Trp, the λ_{max} of Phe-CN SP did not show any changes with SDS concentration (with maximum measured at 291 nm, as in water). These data strongly implies that Phe-CN can serve as a precise

marker for detecting and monitoring polarity changes in near environment of the group by only measuring its fluorescence intensity.

Role of the membrane surface charges on mammalian TKs interactions with LUVs

Experiments using the Trp fluorescence

3.1.9. Binding affinity of the mammalian TKs to the negatively charged LUVs

The titrations of SPW and NKAW with DMPG LUVs in buffer (pH 7.0) show a blue shift of the λ_{max} (Figure 13 and 14, insets) and changes in fluorescence intensities. Usually Trp emission spectra are composed and represent the contributions of all Trp molecules being into different environment. That why the emission spectra of the peptide vary with respect to λ_{max} and intensity showing different spectral shapes and maxima.

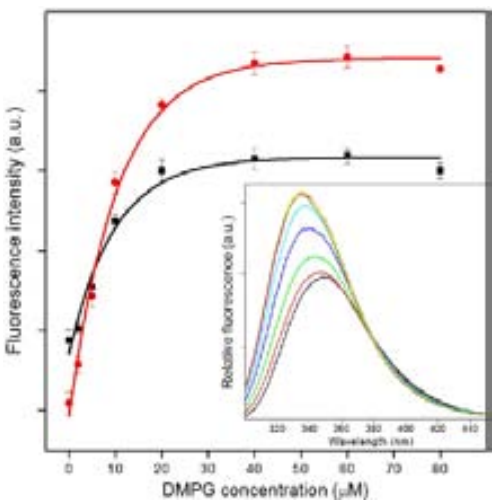

Figure 3.13. Titration curves obtained by plotting the Trp fluorescence intensity of SPW at λ_{350} (■) and λ_{335} (●) as a function of the DMPG concentration. Inset. Fluorescence spectra of SPW (5 μM) as a function of DMPG titration: 0 (—), 2 (—), 5 (—), 10 (—), 20 (—), 40 (—), 60 (—) and 80 μM (—). λ_{exc} was set at 280 nm. The buffer was sodium phosphate (5 mM, pH 7.0) and all the spectra were recorded at 25 °C.

Upon titration with DMPG LUVs, we observe distinct shifts of the emission maxima and two main different groups of emission spectra with significantly different emission peak maxima can be identified. The peak maxima at 335 nm reflect for relatively nonpolar

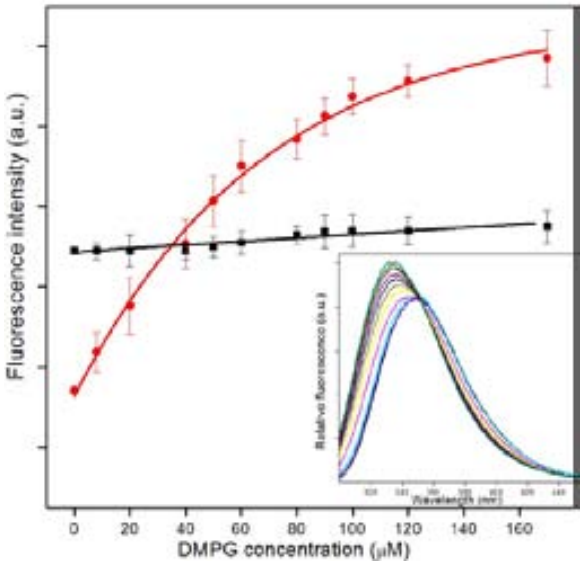

Figure 3.14. Titration curves obtained by plotting the Trp fluorescence intensities of NKAW at λ_{350} (■) and λ_{335} (●) as a function of the DMPG concentration. Inset. Fluorescence spectra of NKAW (5 μM) as a function of DMPG titration: 0 (——), 8 (——), 20 (——), 40 (——), 50 (——), 60 (——), 80 (——), 90 (——), 100 (——), 120 (——) and 170 μM (——). λ_{exc} was set at 280 nm.

The buffer was sodium phosphate (5 mM, pH 7.0) and all the spectra were collected at 25 °C.

environment of the Trp chromophore inside the membrane bilayer, while λ_{max} at 350 nm represent Trp at the membrane surface surrounded by polar water molecules.To quantify peptide-membrane interaction we follow the fluorescence intensities at dual-wavelengths of 350 nm and 335 nm for both the SPW (Figure 13) and NKAW (Figure 14). Up to about 6:1 mol:mol DMPG:SPW ratio Trp fluorescence intensity increases at both wavelengths, as further titration with LUVs did not changed significantly the intensity. Titration of NKAW with DMPG shows that intensity changes followed at I_{335} are more significantly than at I_{350}. Both curves cross at 10 μM and 40 μM DMPG for SPW and NKAW respectively, suggesting that the transition from fully exposed to inserted Trp molecules occurs differently. The solid curves represent the best fits of the data and K_d (the parameter should coincide with the fraction of peptide bound versus unbound).

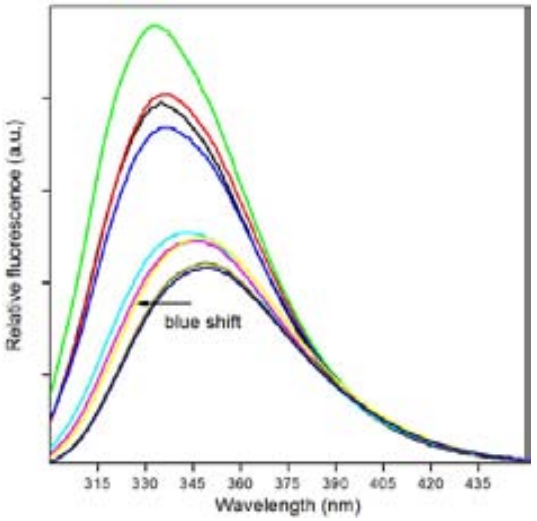

Figure 3.15. Fluorescence spectra of SPW (5 μM) in DMPC/DMPG mixtures (40 μM) as a function of different molar percentages of DMPG: 0% (—), 4% (—), 10% (—), 15% (—), 30% (—), 50% (—), 60% (—), 80% (—) and 100% (—). λ_{exc} was set at 280 nm. The buffer was sodium phosphate (5 mM, pH 7.0) and all the spectra were collected at 25 °C.

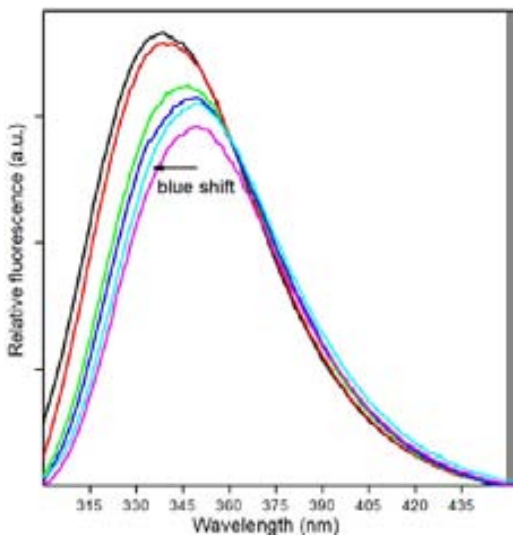

Figure 3.16. Fluorescence spectra of NKAW (5 μM) in DMPC/DMPG mixtures (0.7 mM) as a function of different molar percentages of DMPG: 0% (—), 30% (—), 50% (—), 60% (—), 80% (—), and 100% (—). λ_{exc} was set at 280 nm. The buffer was sodium phosphate (5 mM, pH 7.0) and all the spectra were collected at 25 °C.

3.1.10. TKs interactions with zwitterionic and negatively charged LUVs

The interactions of the TKs with liposomes, composed of mixture of pure DMPC and DMPG lipids were studied by exploring the changes of Trp λ_{max} of SPW (Figure 15) and NKAW (Figure 16) peptides. In the presence of zwitterionic LUVs, Trp emission spectra of SPW and NKAW exhibit a peak at about 350 nm. This maximum implies that the Trp residues of the two TKs face completely hydrophilic environment. In the presence of negatively charged LUVs, the λ_{max} of SPW and NKAW is significantly blue shifted with λ_{max} at about 333 and 338 nm, respectively, which strongly suggest a movement of the Trp residues to a hydrophobic environment. Furthermore, in the presence of negatively charged LUVs, the fluorescence intensity of Trp at λ_{max}, for both SPW and NKAW peptides, is higher than that in zwitterionic LUVs.

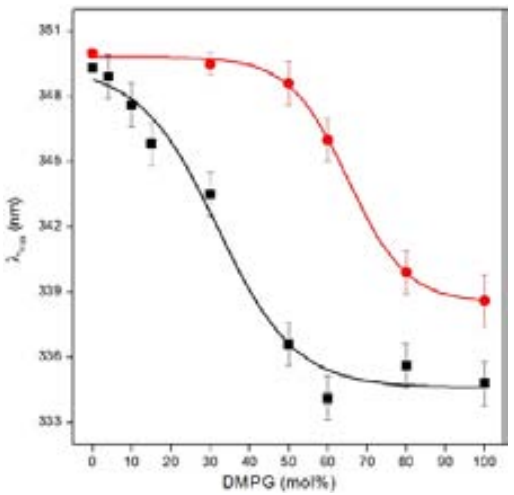

Figure 3.17. Black curve is the plot of the fluorescence emission λ_{max} of SPW in 40 μM DMPC/DMPG mixtures as a function of different percentages of DMPG: 0%, 4%, 10%, 15%, 30%, 50%, 60%, 80% and 100% (mol:mol). Red curve is the plot of the fluorescence emission λ_{max} of NKAW in 0.8 mM DMPC/DMPG mixtures as a function of different percentages of DMPG: 0%, 30%, 50%, 60%, 80%, and 100% (mol:mol). λ_{exc} was set at 280 nm. Concentration of peptides was 5 μM.
The buffer was sodium phosphate (5 mM, pH 7.0), and temperature was at 25 °C.

3.1.11. TKs interactions with LUVs composed of the mixed zwitterionic and negatively charged lipids

To study the role of electrostatic interactions of TKs with membrane surface, Trp emission spectra of SPW (Figure 15) and NKAW (Figure 16) were studied in the

presence of LUVs containing different molar ratios of DMPC/DMPG lipids. In both peptides, increase of the mol fraction of DMPG in the LUVs caused an increase of the Trp fluorescence intensity, while in the NKAW, these changes are more significant in the low mol fraction of DMPG (between 30-50 %). On the other hand, the λ_{max} undergo a significant blue shift with increasing the mol fraction of DMPG in LUVs (Figure 17). In low mol fraction of DMPG (below about 5%), λ_{max} is at about 350 nm while further increase of DMPG (to about 45 mol%) causes a blue shift of λ_{max} to about 336 nm. In NKAW, λ_{max} is at 350 nm up to about 50 mol% of DMPG, while increase of the DMPG lipid to about 80 mol% causes a blue shift of λ_{max} to about 339 nm. Moreover, the plots reveal that λ_{max} get to the steady values above about 50 mol% and 80 mol% of DMPG, for SPW and NKAW, respectively.

These data show that the electrostatic interactions are important for the peptide insertions into bilayer. The λ_{max} of Trp at about 350 nm in DMPC implies that the Trp side chain faces hydrophilic environment, thus at least a peptide segment including Trp residue is not inserted inside into bilayer. The blue shift of Trp maximum with increases of the negative charge density at the membrane surface by higher DMPG molarities present into mixed DMPG/DMPC liposomes, further supports the importance of the electrostatic peptides-membrane interactions for the anchoring of the peptides and it insertion into bilayer. As the data reveal that a maximum insertion of SPW and NKAW peptides is reached at 50 mol% and 80 mol% fractions of DMPG, into mixed DMPG/DMPC liposomes. Moreover, these data also revel that for the insertion of NKAW peptide inside the bilayer needs higher negative charge density of bilayer surface then SPW. Summarizing the data the electrostatic peptides-membrane interactions assist the anchoring of the TKs on the membrane surface, thus endorsing the insertion into bilayer core.

Experiments using the fluorescence of Phe-CN

3.1.12. Phe-CN SP interactions with negatively charged LUVs

The fluorescence emission of Phe-CN SP in negatively charged LUVs shows higher intensity than in the presence of buffer at pH 7.0 (Figure 18). Moreover, λ_{max} shows a

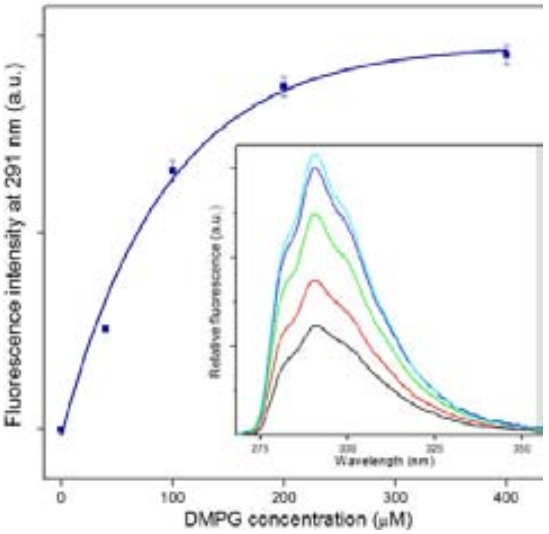

Figure 3.18. Binding curve of Phe-CN SP peptide to the negatively charged LUVs, obtained by plotting of the fluorescence intensity of Phe-CN SP (2 μM) at 291 nm as a function of various concentrations of DMPG LUVs: 0 (—), 40 (—), 100 (—), 200 (—), and 400 μM (—). In all the cases, λ_{exc} was set at 232 nm. The buffer was sodium phosphate (5 mM, pH 7.0). All the spectra were collected at 25 °C. Fitting gives a hyperbolic curve.

small blue shift in the DMPG LUVs. As the molar ratio of the LUVs:Phe-CN SP increased, the fluorescence emission of Phe-CN increases in a hyperbolic curve behavior. These data are consistent with the SDS experiment as the titration with SDS above it CMC causes increases of Phe-CN SP fluorescence intensity.

3.1.13. Phe-CN SP interactions with LUVs composed of the mixed zwitterionic and negatively charged lipids

Comparison of the Phe-CN emission intensities mixtures of pure DMPC and DMPG LUVs (Figure 19, inset) reveals two main trends. First, in any DMPC/DMPG ratios of LUVs, λ_{max} did not change and kept at about 291 nm. Second, increase of the DMPG mol fractions results an increase of the Phe-CN SP fluorescence intensity, following a hyperbolic behavior (Figure 19).

3.1.14. Characterization of the TK peptides interactions with LUVs by electrostatic surface potential changes

Negatively charged LUVs

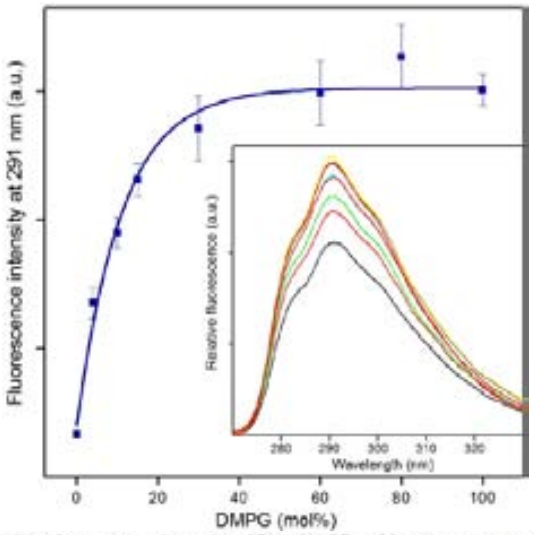

Figure 3.19. Plot of the fluorescence intensity of Phe-CN SP at 291 nm and corresponding fluorescence spectra (inset) in 0.4 mM DMPG/DMPC mixtures as a function of different percentages of DMPG: 0% (—), 4% (—), 10% (—), 15% (—), 30% (—), 60% (—), 80% (—), and 100% (mol:mol,—). In all the cases, λ_{exc} was set at 232 nm. The peptide concentration was 2 μM and buffer was sodium phosphate (5 mM, pH 7.0). Temperature was set at 25 °C. Fitting was made by first order exponential decay using commercial software package Origin. The binding curve shows hyperbolic model.

SP. The FPE fluorescence intensity variation upon SP titration of FPE labeled negatively charged LUVs is shown in Figure 20 (panel A and B). Panel A indicates the experiment in which the initial ratio of LUVs:SP (mol:mol), in the first addition of peptide, was about 1500, while in panel B, the experiment starting with initial ratio of LUVs:SP about 500 is presented (see the Figure 20 legend). In general, the titration with SP up to about 20 μM caused an increase of the FPE fluorescence intensity, regardless of the initial molar ratio of LUVs to the peptide.

1). Observations related to the experiment with higher initial ratio of liposomes to peptide (Figure 20, panel A) are as the followings: i). After the titration with relatively low concentrations of SP, in the range below about 5 μM (shown by arrows), FPE fluorescence intensity increases very rapidly (less than few seconds) then it reaches to a constant value; ii). Further titrations of SP caused more increase of the FPE fluorescence intensity, while, after some peptide additions the fluorescence intensity first increases rapidly and then decreases to a constant level. It should be mentioned that in different experiment repetitions, increasing and consequent decreasing of the intensity occurred in different concentrations of peptide.

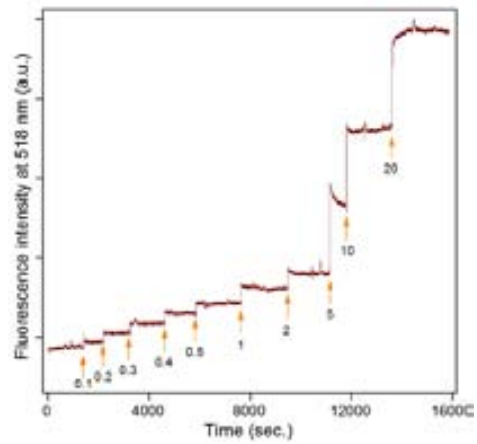

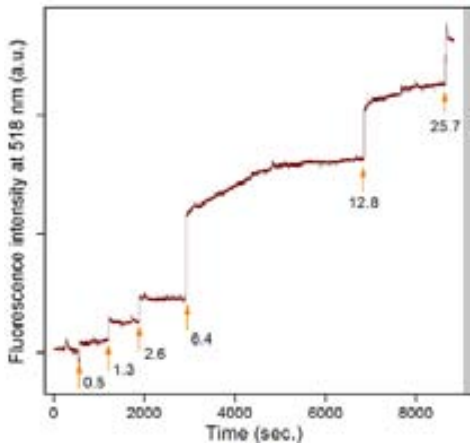

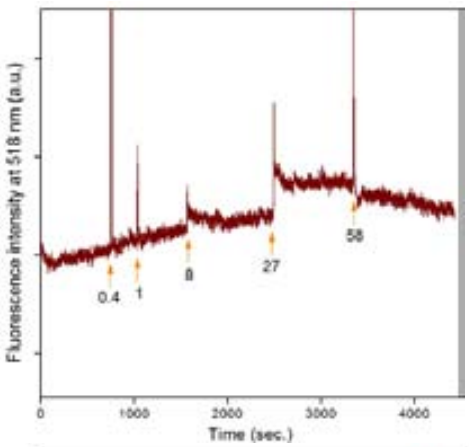

Figure 3.20, panel A. Time course studies of the TKs interactions with the negatively charged LUVs. The fluorescence intensity changes of FPE (at 518 nm) was monitored upon titration of (A) SP; (B) NKA; and (C) Scyl to the FPE labelled DMPG vesicles as a function of time. The lipid concentration was 150 μM. λ_{exc} was set at 496 nm. The buffer was sodium phosphate (5 mM, pH 8.5) and temperature was set at 25 °C. Arrows indicate the time at each titration and numbers correspond to the concentration of peptides (μM).

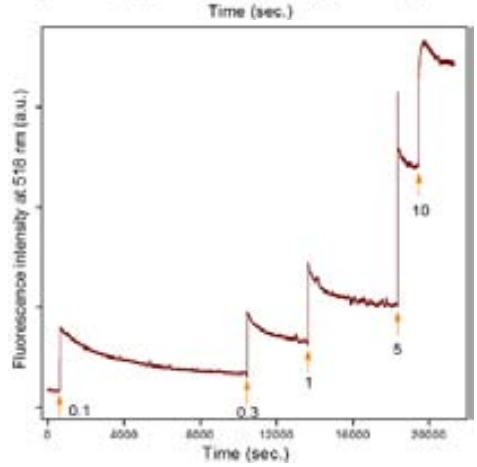

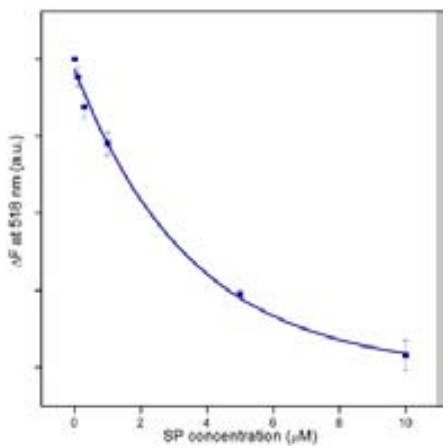

Figure 3.20, panel B. Time course studies of the SP interactions with negatively charged LUVs. Fluorescence intensity changes of FPE (at 518 nm) after titration of SP to the FPE labelled DMPG LUVs was monitored as a function of the time. The lipid concentration was 50 μM. λ_{exc} was set at 496 nm. The buffer was sodium phosphate(5 mM, pH 8.5) and temperature was set at 25 °C. Arrows indicate the time at each titration and numbers correspond to the concentration of the SP (μM).

Figure 3.21. Insertion curve of SP into the FPE labeled DMPG LUVs obtained by plotting the amplitudes of fluorescence intensity changes of FPE (at 518 nm) upon titration of SP. Lipid concentration was 50 μM and λ_{exc} was set at 496 nm. The buffer was sodium phosphate (5 mM, pH 8.5) and temperature was set at 25 °C. The amplitude of fluorescence variation was measured when the trace shown in Figure 3.20, panel B reached to a plateau. Fitting was made by the first order exponential decay using commercial software package Origin.

This experiment was used to study the binding affinity of the SP to negatively charged LUVs (Figure 24) and determination of K_d.

2). In the experiment with the lower initial ratio of liposomes to peptide (Figure 20, panel B), the FPE intensity changes rapidly after the titration of SP (from around 0.1 to 5 μM), however it decays slowly and in a variable time span between about 20 to 160 minutes. By this experiment, we obtained the SP insertion curve to the negatively charged LUVs (Figure 21). The plot of ΔF as a function of different SP concentrations shows that as the SP concentration was increased, the ΔF was decreased in which ΔF changes were bigger in lower concentrations of peptide.

NKA. Slight increase of the FPE fluorescence intensity to a constant level occurred suddenly, just a few seconds after titration of NKA (up to about 27 μM) to the FPE labeled negatively charged LUVs (Figure 22). Increase of the NKA concentration to about 58 μM caused a slight decrease of the FPE fluorescence intensity.

ScyI. Titration of ScyI (to about 26 μM) to the FPE labeled negatively charged LUVs caused an increase of the FPE fluorescence intensity (Figure 23). After titration of a small aliquots of the ScyI (below about 6 μM) and before the next titration, FPE fluorescence intensity increased just for a few seconds and then was stabilized immediately. Although, additional titration of ScyI (above about 6 μM) caused some increase of the FPE fluorescence intensity, yet these changes occurred slowly (in contrast to the beginning of titration) in a time of several minutes (Figure 23).

In regards to these findings the fooling conclusions can be presented: the interaction of TKs with negatively membrane mimetic systems occurs at two steps. First the TKs bind to the surface of the membrane and subsequently they insert into the hydrophobic core.

In low peptides:LUVs ratio, we detected mainly the binding which might due to low signal of inserted fraction of the peptide

At higher of peptide:LUVs ratios, a decrease of the FPE signal imply for peptide insertion .These data coloborate with the Trp experiments, representing the binding and insertion of mammalian TKs to negatively charged LUVs.

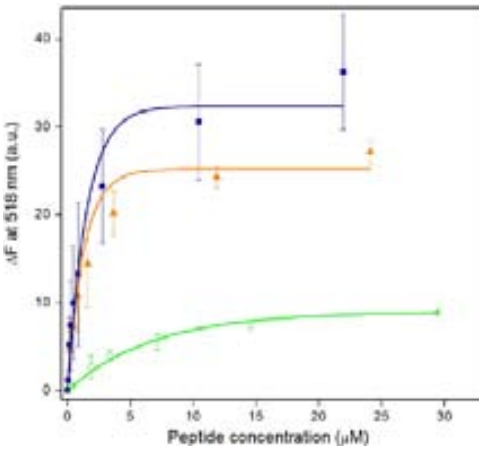

Figure 3.22. Binding curves of SP (■), ScyI (▲) and NKA (●) to the FPE labelled DMPG LUVs obtained by plotting the amplitudes of fluorescence intensity variations of FPE at 518 nm as a function of TKs concentrations. Lipid concentration was 150 μM and λ_{exc} was set at 496 nm. The buffer was sodium phosphate (5 mM, pH 8.5) and temperature was set at 25 °C. The amplitudes of fluorescence variation were measured when the traces shown in Figure 3.21 reached to a plateau. Fitting was made by the first order exponential decay using commercial software package Origin. All the binding curves are hyperbolic.

3.1.15. Binding affinity of the TK peptides to negatively charged LUVs; determination of K_d

The plot of ΔF as a function of different TKs concentrations, obtained by titration of FPE labeled negatively charged LUVs, is presented in Figure 24. Summarizing the data from these experiments, the following observations can be made: **i).** The overall changes of ΔF was positive for all the TKs; **ii).** In the lower concentrations of TKs, ΔF was changed more significantly, while, higher peptide concentrations caused only small changes of ΔF; **iii).** The hyperbolic behavior of the binding curves indicate no cooperativity upon the interaction of the TK peptides to negatively charged LUVs (Moreno, M. R. et al. 2007); **iiv).** The maximum ΔF at which the TKs binding curves reach to a plateau is in an order of SP>ScyI>NKA; **v).** The K_d of TK peptides to the negatively charged LUVs calculated on the basis of the affinity binding curves are 0.8±0.02, 0.9±0.03 and 4.5±0.3 (μM) for SP, ScyI and NKA, respectively.

These data show the relation between the affinities of the TKs to negatively charged LUVs with their net charges, as the net charges of peptide increases the binding affinity is also increases.

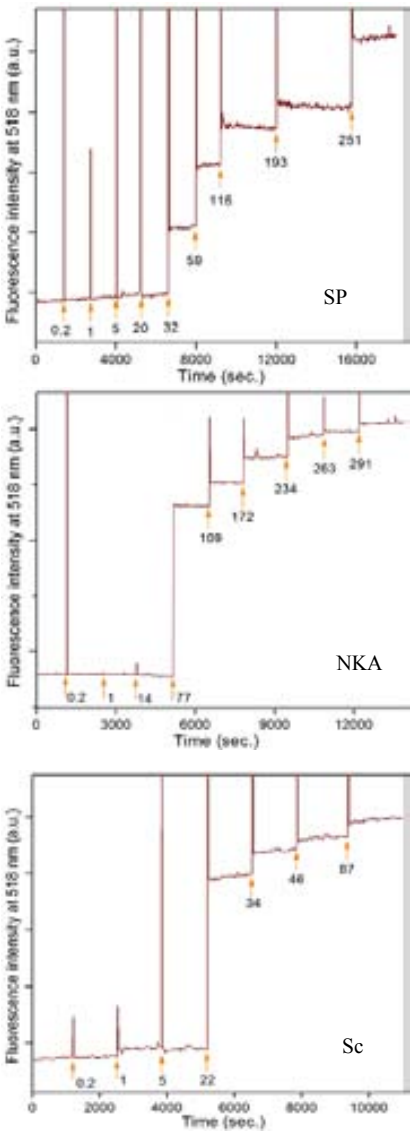

Figure 3.23. Time course studies of the TKs interactions with zwitterionic LUVs. Fluorescence intensity changes of FPE (at 518 nm) upon titration of (A) SP; (B) NKA; and (C) ScyI to the FPE labelled DMPC liposomes were monitored as a function of the time. The lipid concentration was 50 μM. λ_{exc} was set at 496 nm. The buffer was sodium phosphate (5 mM, pH 8.5) and temperature was set at 25 °C. Arrows indicate the time at each titration and numbers correspond to the concentration of peptides (μM).

II) Zwitterionic LUVs. In general, the fluorescence intensity of FPE was increased after titration with a small aliquots of TK peptides (up to about 251, 290 and 87 μM of SP, NKA and ScyI, respectively) to FPE labeled DMPC LUVs (Figures 25-27). FPE intensity changes occurred very rapidly in a few seconds (about 10-20 sec.) after TKs titrations. In

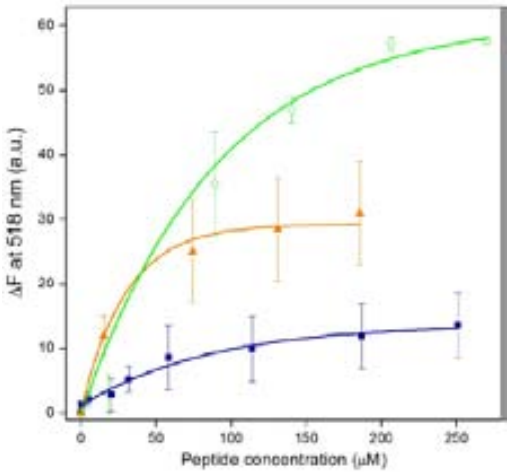

Figure 3.24. Binding curves of SP (•), ScyI (▲) and NKA (○) to the FPE labelled DMPG LUVs; obtained by plotting the changes of FPE fluorescence intensity at 518 nm as a function of TKs concentrations. Lipid concentration was 50 μM and λ_{exc} was set at 496 nm. The buffer was sodium phosphate (5 mM, pH 8.5) and the temperature was set at 25 °C. The amplitude of fluorescence variation was measured when the traces shown in Figure 3.23. reached to a plateau. Fitting was made by first order exponential decay using commercial software package Origin. All the binding curves are hyperbolic.

contrast to the FPE experiments in the presence of negatively charged LUVs, no decay of the FPE fluorescence was detected when the zwitterionic LUVs were titrated with peptides. These data show that TKs are not free in the solution and some peptide segment bind to zwitterionic surface, however further insertion into the hydrophobic core do not take part. These finding are consistent with the Trp fluorescence studies. Comparing the FPE and Trp experiments we belive that most likely binding to zwitterionic membrane surface is through N-terminal part of the peptides and Trp segment is not involved in binding.

3.1.16. Binding affinity of the TK peptides to zwitterionic LUVs

The binding curves of the TK peptides to the zwitterionic LUVs (Figure 28) show that: **i).** All the binding curves of TKs follow a hyperbolic profile, suggesting no cooperative interactions of the peptides with the membrane; **ii).** ΔF changes were always positive in the used concentration range of the TKs; **iii).** The maximum ΔF in which the TKs binding curves reached to a plateau are in following order of NKA, ScyI and SP; **iiv).** The

calculated K_d from the binding curves for the TK peptides in zwitterionic LUVs gives 38.0±0.4, 20.6±0.3 and 57.31±0.7 (μM) for SP, ScyI and NKA, respectively.

In conclusion, the affinities of the TKs to zwitterionic membrane are not related to the peptides' net charge. Moreover, the TKs affinities to zwitterionic membrane are much lower (about 13-47 times, depending on the peptide) than those to negatively charged membrane.

3.1.17. Study of the mammalian TKs insertion into the lipid bilayer by Trp residue quenching

Next to distinguish between TK peptides insertion into lipid vesicles and binding to the lipid surface, we applied the quenching of the Trp fluorescence by brominated lipids, using PC lipids brominated at two different positions along the acyl chain (6,7 and 9,10 Br_2-PCs). Since both the SP and NKA peptides lack the intrinsic Trp in their sequences, we applied this approach to the TKs analogues, NKAW and SPW. As have been already described in this thesis, the substitution of Phe for Trp did not perturb significantly the secondary structure of the peptides as seen by CD data (Figure 3). We chose Br_2-PCs as a suitable collisional quenchers of Trp fluorescence because they act over a short distance (see Materials and Methods) and are thought to perturb the lipid bilayer minimally (Zhao, H. and P. K. Kinnunen 2002). A collisonal quenching between the Trp fluorophore and brominated phospholipids leads to a distance-dependent decrease in the fluorescence signal in which it can readily be observed by using steady-state fluorescence (Bolen, E. J. and P. W. Holloway 1990).

3.1.18. Mammalian TKs insertion to the negatively charged LUVs

The Trp fluorescence of SPW and NKAW peptides in the LUVs composed of either (6,7) Br_2-PC or (9,10) Br_2-PC and DMPG lipids were quenched related to that in the presence of DMPC/DMPG LUVs (Figure 29). In both peptides, and compared to the Trp fluorescence of the TKs in the control liposomes (only composed of DMPC/DMPG), the Trp fluorescence quenched more effectively from (6,7) bromine atoms placed closer to the polar head groups in (6,7) Br_2-PC/DMPG liposomes than from the bromide atoms, which located near in the middle of the hydrocarbon tail (9,10) Br_2. Moreover the

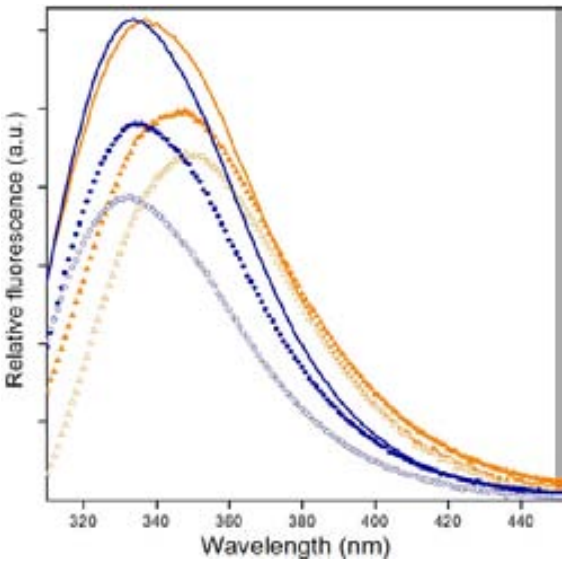

Figure 3.25. Collisional quenching of Trp by brominated lipids.
Fluorescence emission spectra of SPW in the presence of 35:65 mol%: DMPC:DMPG (—); (6,7) Br_2-PC:DMPG (▫); and (9,10) Br_2-PC:DMPG (●) LUVs.
Fluorescence emission spectra of NKAW in the presence of 35:65 mol%: DMPC:DMPG (—); (6,7) Br_2-PC:DMPG (△); and (9,10) Br_2-PC:DMPG (▲) LUVs. The concentrations of peptides and total lipids were 4.5 and 450 μM, respectively. All the spectra were recorded in sodium phosphate buffer (5 mM, pH 7.0), at 25 °C. The λ_{max} was set at 280 nm. The spectra of NKAW were normalized to that of SPW in DMPC/DMPG liposomes.

fluorescence of Trp residue of SPW was more quenched by the two bromine lipids than that of NKAW.

In regards to DMPC/DMPG LUVs, the Trp λ_{max} of SPW undergoes a blue shift of about 3 nm in the presence of (6,7) Br-PC/DMPG LUVs, while λ_{max} did not show any shift in the presence of the LUVs composed of (9,10) Br-PC/DMPG (Figure 29). In NKAW, the Trp λ_{max} undergoes a red shift of about 9 and 13 nm in the presence of (9,10) Br_2-PC/DMPG and (6,7) Br_2-PC/DMPG, respectively.

Prior to perform fluorescence quenching experiments and as a control, the fluorescence of L-Trp was recorded in the presence of Br_2-PC/DMPG and DMPC/DMPG LUVs (Figure 30). The fluorescence intensity of L-Trp was not changed neither in the presence of (6,7) nor (9,10) Br_2-PC/DMPG LUVs, compared to that in DMPC/DMPG LUVs. In all these control experiments, the Trp λ_{max} was at about 350 nm.

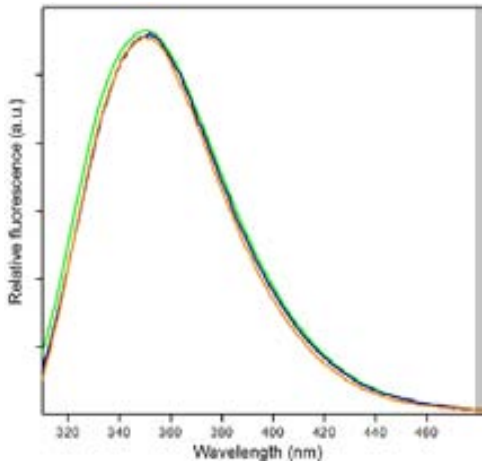

Figure 3. 26. Fluorescence emission spectra of L-Trp in the presence of 35:65 mol%: DMPC:DMPG (—); (6,7)Br_2-PC:DMPC (—); and (9,10)Br_2-PC:DMPC (—) LUVs. The concentrations of Trp and total lipids were 4.5 and 450 μM, respectively. All the spectra were recorded in sodium phosphate buffer (5 mM, pH 7.0) at 25 °C. The λ_{exc} was set at 280 nm.

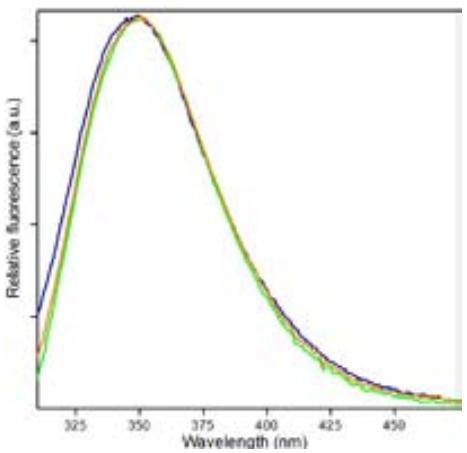

Figure 3.27. Fluorescence emission spectra of SPW in the presence of pure DMPC (—); 35:65 mol% (6,7)Br_2-PC:DMPC (—); and (9,10)Br_2-PC:DMPC (—) LUVs. The concentrations of peptide and total lipids were 4.5 and 450 μM, respectively. All the spectra were recorded in sodium phosphate buffer (5 mM, pH 7.0) at 25 °C. The λ_{exc} was set at 280 nm.

Since quenching is distance dependent, fluorescence quenching data obtained from LUVs composed of lipids brominated at two different depths were further used to estimate the depth of membrane penetration using parallax method. In regard to the fluorescence quenching data and applying the Eq. 9, we determined the Z_{cw} (the depth of Trp residue as measured from the center of the bilayer) for NKAW and SPW as 7.8 and 9.1 Å,

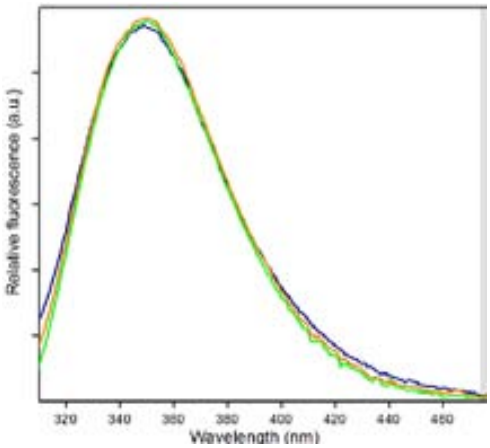

Figure 3.28. Fluorescence emission spectra of NKAW in the presence of pure DMPC (—); 35:65 mol% (6,7)Br_2-PC:DMPC (—); and (9,10)Br_2-PC:DMPC (—) LUVs. The concentrations of peptide and total lipids were 4.5 and 450 μM, respectively. All the spectra were recorded in sodium phosphate buffer (5 mM, pH 7.0) at 25 °C. The λ_{exc} was set at 280 nm.

respectively (Figure 33), assuming that the lipid motions (such as transverse fluctuations, lateral diffusion, wobbling) and the alteration of bromide position by the presence of the peptides are negligible.

3.1.19. Mammalian TKs insertion to the zwitterionic LUVs

For both SPW (Figure 31) and NKAW (Figure 32) peptides, fluorescence emission of Trp was not quenched in the presence of Br_2-PC/DMPC LUVs compare to that in pure DMPC LUVs, as in all these cases, λ_{max} was at about 350 nm.

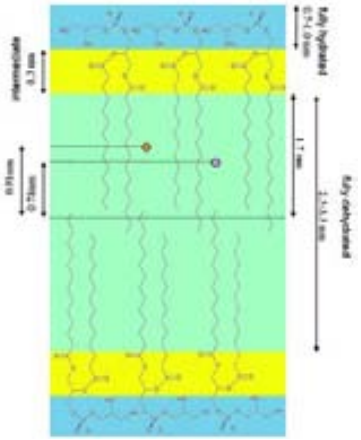

Figure 3.29. Schematic model reflects our hypothesis about the insertion depths of Trp residue of SPW (orange) and NKAW (violet) to the vesicles. The Trp distances are from the center of bilayers.

Bolen, E. J. and P. W. Holloway. 1990. Quenching of tryptophan fluorescence by brominated phospholipid. *Biochemistry* 29 (41):9638-9643.

Bowie, J. U. Membrane protein folding: how important are hydrogen bonds? *Curr Opin Struct Biol* 21 (1):42-49.

Chatterjee, A. et al. . 2001. Thermodynamics of Micelle Formation of Ionic Surfactants: A Critical Assessment for Sodium Dodecyl Sulfate, Cetyl Pyridinium Chloride and Dioctyl Sulfosuccinate (Na Salt) by Microcalorimetric, Conductometric, and Tensiometric Measurements. *J. Phys. Chem.* 105:12823-12831.

Chen, Y., Barkley, M.D. 1998. Toward understanding tryptophan fluorescence in proteins. *Biochemistry* 37:9976.

Fuguet, Elisabet. et al. . 2005. Critical micelle concentration of surfactants in aqueous buffered and unbuffered systems. *Analytica Chimica Acta* 548:95- 100.

Hassan, P.A, et al. . 2002. Microstructural changes in SDS micelles induced by hydrotropic salt. *Langmuir* 18:2543-2548.

Inayathullah, N. Mohammed. et al. . 2003. Effect of osmolyte on the micellization of SDS at different temperatures. *Langmuir* 19:9545-9547.

Moreno, M. R., J. Guillen, A. J. Perez-Berna, D. Amoros, A. I. Gomez, A. Bernabeu and J. Villalain. 2007. Characterization of the interaction of two peptides from the N terminus of the NHR domain of HIV-1 gp41 with phospholipid membranes. *Biochemistry* 46 (37):10572-10584.

Muino, P. L. and P. R. Callis. 2009. Solvent effects on the fluorescence quenching of tryptophan by amides via electron transfer. Experimental and computational studies. *J Phys Chem B* 113 (9):2572-2577.

Serrano, A. L., T. Troxler, M. J. Tucker and F. Gai. Photophysics of a fluorescent non-natural amino acid: p-Cyanophenylalanine. *Chem Phys Lett* 487 (4-6):303-306.

Taskent-Sezgin, H., J. Chung, V. Patsalo, S. J. Miyake-Stoner, A. M. Miller, S. H. Brewer, R. A. Mehl, D. F. Green, D. P. Raleigh and I. Carrico. 2009. Interpretation of p-cyanophenylalanine fluorescence in proteins in terms of solvent exposure and contribution of side-chain quenchers: a combined fluorescence, IR and molecular dynamics study. *Biochemistry* 48 (38):9040-9046.

Taskent-Sezgin, H., P. Marek, R. Thomas, D. Goldberg, J. Chung, I. Carrico and D. P. Raleigh. Modulation of p-cyanophenylalanine fluorescence by amino acid side chains and rational design of fluorescence probes of alpha-helix formation. *Biochemistry* 49 (29):6290-6295.

Thévenot, Caroline. et al. . 2005. Aggregation number and critical micellar concentration of surfactant determined by time-dependent static light

scattering (TDSLS) and conductivity. *Colloids and Surfaces A Physicochemical and Engineering Aspects* 252:105-111.

Zhao, H. and P. K. Kinnunen. 2002. Binding of the antimicrobial peptide temporin L to liposomes assessed by Trp fluorescence. *J Biol Chem* 277 (28):25170-25177.

RESULTS AND DISCUSSION

PART II

CHARACTERIZATION OF THE SECONDARY STRUCTURES OF TKs

In this chapter, we characterized the role of different factors (such as environment, peptides net charges and membrane surface charges) on the secondary structures of TK peptides and their analogues in non aggregated, monomer state (for a reference see transmission electron microscopy data, Tables 1-4, part III Results and Discussion). Moreover, we estimated the different secondary structural components of SP, such as unordered, alpha helical and extended polyproline (PPII) conformation, in different membrane mimetic environments.

3.2.1. TKs' conformations in aqueous solutions; identification of the polyproline II (PPII) conformation

The CD spectra of TKs in aqueous solutions (at 5 ˚C) contain a weak positive peak at about 222 nm and a strong negative peak at about 196 nm (Figure 1, panel A). Moreover, the CD spectra of TKs display a weak negative band at about 238, 230 and 239 nm for SP, NKA and ScyI respectively. The spectral features of these spectra resemble unordered or PPII conformation or might arise from the superposition of PPII, unordered (Rucker, A. L. and T. P. Creamer 2002) and beta turns presence. Because of the spectral similarity of the random coil and PPII structures (Shi, Zhengshuang. et al. 2006), we analyzed the CD spectra of TKs in aqueous solutions at various temperatures, as a relevant approach (Bochicchio, B. and A. M. Tamburro 2002.Woody, R. W. 2009), to discern between unordered and PPII conformations (Figure 1, panel B). For all the TK peptides, increases of the temperature from 5 to 80 ˚C caused a significant decrease of the negative band at about 198 nm, and the positive band at about 222 nm. For all the TKs, variation of the CD spectra upon the heating is completely reversible, by cooling down the temperature from 80 to 5 ˚C. An isoelliptic point at about 210, 206 and 205 nm for SP, NKA and ScyI respectively is clearly seen, indicative for a two-state unordered-PPII

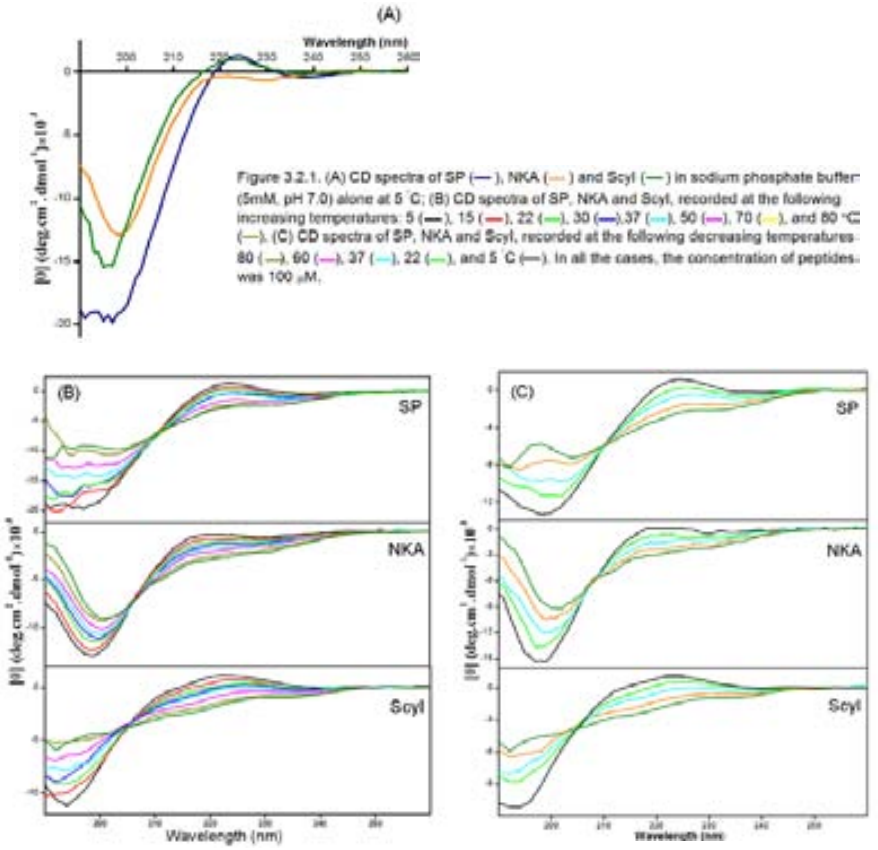

Figure 3.2.1. (A) CD spectra of SP (—), NKA (—) and ScyI (—) in sodium phosphate buffer (5mM, pH 7.0) alone at 5 ˚C; (B) CD spectra of SP, NKA and ScyI, recorded at the following increasing temperatures: 5 (—), 15 (—), 22 (—), 30 (—),37 (—), 50 (—), 70 (—), and 80 ˚C (—). (C) CD spectra of SP, NKA and ScyI, recorded at the following decreasing temperatures: 80 (—), 60 (—), 37 (—), 22 (—), and 5 ˚C (—). In all the cases, the concentration of peptides was 100 μM.

structural equilibrium. Isoelliptic point (also named isosbestic or isodichroic point) is a term applied for a fixed wavelength of a set of spectra in which the absorptions of all the components are equal, and consequently, addressing the equilibration of the components' concentrations.

The histograms of difference CD molar ellipticities (Δ[θ], see Figure 2 legend) at 222 and 197 nm as a function of increasing (Figure 2, left panel) and decreasing temperatures (Figure 2, right panel), obtained for the TK peptides in aqueous solutions, show that:

a). Upon increasing the temperature to 70 ˚C, the $\Delta[\theta]_{222}$ and $\Delta[\theta]_{197}$ are strongest for SP, and smallest for NKA (Figure 2, left panel).

b). Upon cooling down the temperature from 80 to 5 ˚C (Figure 2, right panel), the Δ[θ] of SP (at both 222 and 197 nm) is higher than that of NKA and ScyI. The $\Delta[\theta]_{222}$ of NKA and ScyI are very similar and $\Delta[\theta]_{197}$ of NKA is higher than that of ScyI.

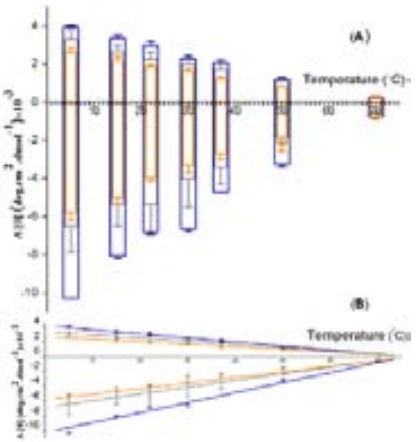

Figure 3.2.2. (A) Histogram and (B) plot of the difference CD molar ellipticities ($\Delta[\theta]$) of SP (—), NKA (—), and ScyI (—) in phosphate buffer (5 mM, pH 7.0) as a function of decreasing temperatures. CD intensities at 222 nm (positive values) and 197 nm (negative values) at each temperature were subtracted from those at 80 °C, assuming that the secondary structure of peptides is completely unordered at 80 °C. In all the cases, the concentration of peptides was 100 μM.

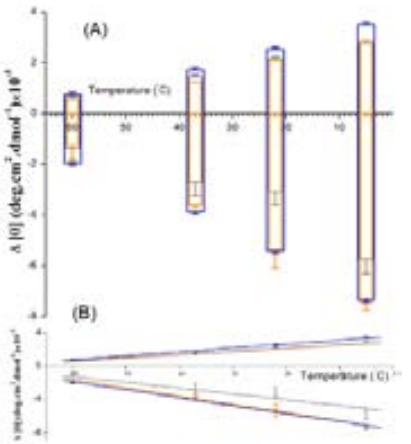

Figure 3.2.3. (A) Histogram and (B) plot of the difference CD molar ellipticities ($\Delta[\theta]$) of SP (—), NKA (—), and ScyI (—) in phosphate buffer (5 mM, pH 7.0) as a function of increasing temperatures. CD intensities at 222 nm (positive values) and 197 nm (negative values) at each temperature were subtracted from those at 80 °C, assuming that the secondary structure of peptides is completely unordered at 80 °C. In all the cases, the concentration of peptides was 100 μM.

The plots of the $\Delta[\theta]$ indicate that in all cases, the PPII structure is reversible upon cooling the temperature. Moreover, the temperature trend of (Figure 2 plot B) reveals, that the formation and the disruption of PPII is a non-cooperative process. These findings further support the presence of PPII conformational in TKs in aqueous solutions. It is known that PPII conformation is deficient of intermolecular hydrogen bonding, but can make intermolecular hydrogen bonds with the solvent (Bienkiewicz, E. A. et al. 2000).

3.2.2. Determination of the PPII fraction of TKs in aqueous solution

There are various models to calculate the PPII fraction of TKs (Bienkiewicz, E. A. et al. 2000.Kelly, M. A. et al. 2001). We used the model of Creamer *et. al*, as described in Materials and Methods. The positive band at 220 nm, assignable to n-π* electronic transition, was used to determine quantitatively the PPII fraction of TKs. The calculated values for PPII contents in the TKs in aqueous solution as a function of the temperature are presented in Table 2. The data show that at 5 ˚C , the temperature at which PPII presence is highest, it constitutes at about 50% of total structural conformations of the peptides.

3.2.3. TKs' conformations in TFE; intrinsic propensity of TKs to adopt helical structure

TFE is known to induce helical structure in peptides by providing a low dielectric environment around the peptides that favors the formation of intra-hydrogen bindingwithout disruption of the hydrophobic interactions (Jaravine, V. A. et al. 2001.Roccatano, D. et al. 2002).

To determine the intrinsic helical propensity of the TKs, we carried out experiments in the presence of different mixtures of TFE/H_2O (v:v). In the case of SP (Figure 3), below 15% TFE, the CD spectra exhibit a strong negative peak around 196 nm, a weak negative band at about 237 nm, and a weak positive band at about 222 nm, representative of PPII structure. As the concentration of TFE was increased, the intensities of the positive and strong negative band decreased, while the intensity of the negative band at about 237 nm slightly increased. Above 30% TFE, SP CD spectra show a positive band at about 196 nm and two negative peaks at about 208 and 222 nm, indicating the dominant alpha helical structure of peptide, in which the intensity of the peak at 208 nm is higher than that of 222 nm. Moreover, the isoelliptic point at about 212 nm indicates for a two state structural transition of peptide.

In the presence of different mixtures of TFE/H_2O, CD spectral features of NKA undergo smaller changes than in case of SP (Figure 4). The overall features of the CD spectrum in

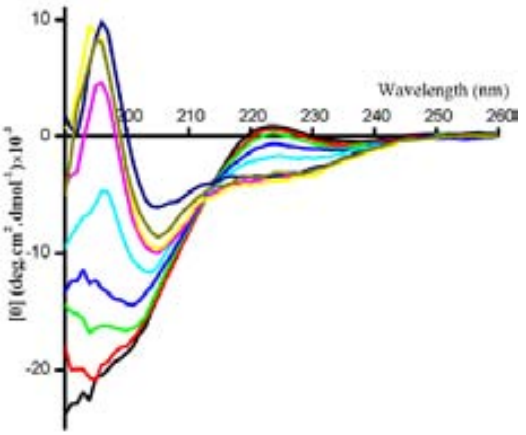

Figure 3.2.4. CD spectra of 100 μM SP in various percentages of TFE/H_2O mixtures (v:v). The spectra were collected in distilled water (—) and in 5% (—), 10% (—), 15% (—), 20% (—), 30% (—), 40% (—), 70% (—), and 100% (—) TFE. All the spectra were collected immediately after preparation of samples at 22 °C.

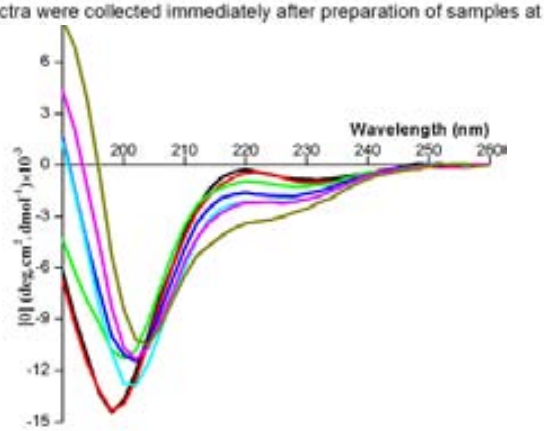

Figure 3.2.5. CD spectra of 100 μM NKA in various percentages of TFE/H_2O mixtures (v:v). The spectra were collected in distilled water (—) and in 5% (—), 15% (—), 30% (—), 40% (—), 70% (—), and 100% (—) TFE. All the spectra were recorded immediately after preparation of samples at 22 °C.

the presence of 5% TFE are very similar to that in H_2O, while in 15% TFE, the shoulder at 220 nm disappears and the intensity of negative peak at 198 nm decreases. In 30% TFE and above, the positive ellipticity about 191 nm indicates for a band in which its peak is few nm lower than the range of the measured wavelength. Moreover, as the TFE percentages increases, the strong negative peak shifts about 4 nm to a lower wavelength, and the intensity of the peak at 222 nm increases.

The CD spectrum of ScyI in the presence of 5% TFE shows a weak shoulder around 225 nm and a strong negative band at about 193 nm (Figure 5), indicating PPII secondary

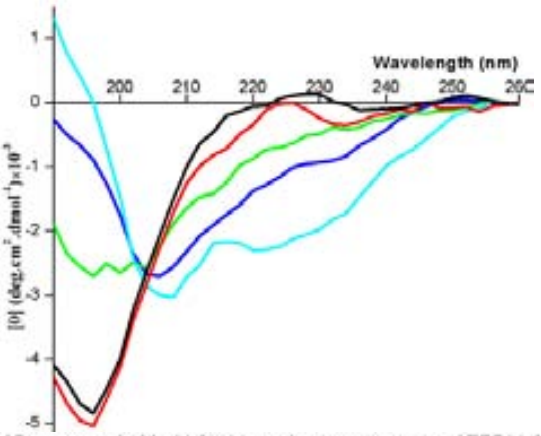

Figure 3.2.6. CD spectra of 100 μM ScyI in various percentages of TFE/H_2O mixtures (v:v). The spectra were collected in distilled water (—) and in 5% (—), 20% (—), 50% (—), and 100% (—) TFE. All the spectra were recorded immediately after preparation of samples at 22 °C.

structure. By increasing the TFE to 50%, the shoulder at 225 nm disappeared and the negative peak shift to about 205 nm. CD spectrum of the ScyI in pure TFE indicates two negative peaks at about 207 and 222 nm. Moreover, the positive CD ellipticity below 196 nm indicates for a peak slightly below the measured wavelength. Based on this experiment, ScyI peptides adopt alpha helix as a dominant secondary structure in TFE. The CD spectra indicate an isoelliptic point at about 204 nm.

3.2.4. Study of the secondary structures of TK peptides in the presence of SDS

i). SP. In the absence and in low (0.2 mM) SDS concentration, below CMC, CD spectra of SP indicate a strong negative peak at about 195 nm and a small positive peak at about 222 nm (Figure 6A), indicative for a PPII structure. A further increase of SDS (between 0.8 and 1.3 mM) results in a decrease and blue shift of the negative peak and appearance of a broad and variable positive peak in the range of 205-213 nm. A shift of the CD spectral bands to a longer or lower wavelengths has been attributed to differences between secondary and tertiary amides of PPII and/or contribution of other structures (Woody, R. W. 2009). To examine the shape diversities of the CD spectra in SDS concentrations close to CMC, we calculated the CD difference spectrum (Figure 6, inset). In all cases, the difference spectra obtained by subtracting the CD spectrum of SP in the

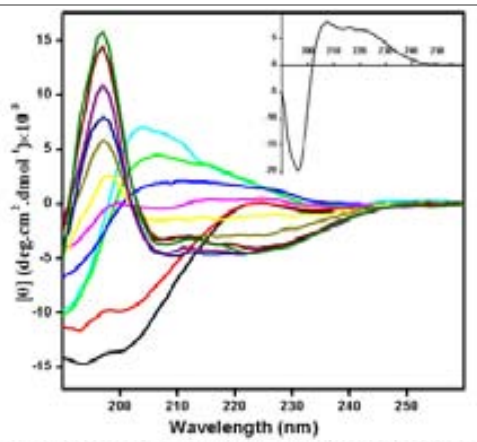

Figure 3.2.7. CD spectra of SP (80 μM) in various concentrations of SDS: 0 (—), 0.2 (—), 0.8 (—), 1 (—), 1.2 (—), 1.3 (—), 1.4 (—), 1.5 (—), 1.6 (—), 3 (—), 8 (—) and 10 mM SDS (—). The buffer was sodium phosphate (5 mM, pH 7.0). All the spectra were collected immediately after preparation of samples at 22 °C. Inset. Difference CD spectrum calculated by subtraction of the spectrum of SP (80 μM) in 10 mM SDS from that in 0.8 mM SDS.

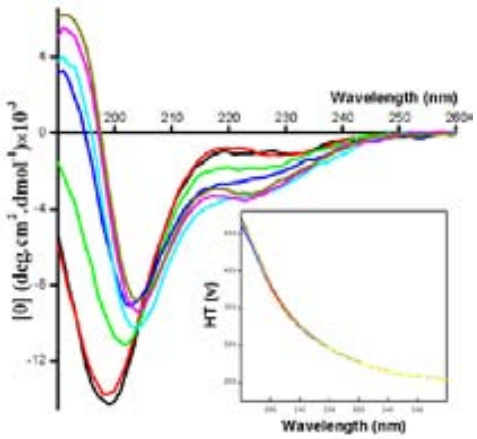

Figure 3.2.8. CD spectra of NKA (80 μM), recorded upon SDS titration: 0 (—), 0.8 (—), 2.5 (—), 3 (—), 4 (—), 6 (—), and 8 mM SDS (—). The buffer was sodium phosphate (5 mM, pH 7.0). All the spectra were collected immediately after preparation of samples at 22 °C; Inset. Plot of the CD HT voltages presented as a function of wavelength, corresponding to the CD spectra.

presence of 10 mM SDS (highly above CMC) from those measured in lower SDS concentrations (close to CMC) exhibit a negative band below 200 nm and a positive one at about 217 nm indicative of PPII structure.

These findings imply that in the presence of SDS, below and near the CMC, SP forms complex secondary conformations of largely PPII admixed with alpha helical. Moreover, the enhancement of these bands with an increase of SDS concentration strongly suggests a rise of the fractional population of SP residues involved in PPII structure formation.

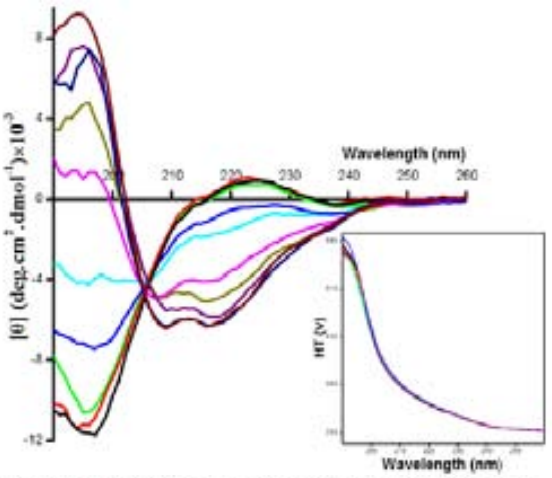

Figure 3.2.9. CD spectra of Scyl (80 μM), recorded upon SDS titration: 0 (—), 0.1 (—), 0.2 (—), 0.3 (—), 0.4 (—), 0.6 (—), 0.8 (—), 1.5 (—), 3 (—), and 8 mM SDS (—). The buffer was sodium phosphate (5 mM, pH 7.0). All the spectra were collected immediately after preparation of samples at 22 °C; Inset. Plot of the CD HT voltages presented as a function of wavelength, corresponding to the CD spectra.

Above 1.4 mM SDS (above CMC) CD spectra show a positive peak at about 197 nm and two negative peaks at about 208 and 222 nm, indicative for alpha helical structure of peptide. Increases of the SDS concentration from 1.4 to 10 mM causes an increase of the intensity of the positive band at 197 nm, while, the intensities of the two other bands at 208 and 222 nm increase only in SDS concentration range from 1.4 to 1.6 mM and further increasing of the SDS concentration results only in a minor variations of the bands magnitude, indicating that the SDS-dependent folding of SP is completed. Above 1.6 mM SDS, the intensities of the bands at 208 and 222 nm are almost equal (R_2=1).

ii). NKA. The CD spectra of NKA in different SDS concentrations show different features than those of SP. In the range between 0 and 0.8 mM SDS, the CD spectra of NKA display a strong negative peak at about 199 nm, a negative band at 233 nm, and a shoulder around 222 nm, indicative of PPII structure of peptides (Figure 8A). By increasing of the SDS concentration to 2.5 mM, the intensity of the strong negative band decreases and undergoes a red shift to about 202 nm. Moreover, the shoulder at 222 nm disappears. In the range of 3 to 8 mM SDS, a positive peak about 191 nm appears and the negative peak undergoes a red shift which in 8 mM SDS is at about 204 nm. Furthermore, a negative band appears at about 220 nm. These spectra suggest for a superposition of the

spectra corresponding to unordered and alpha helical structures. Above 4 mM SDS, the intensities of 208 and 222 nm bands did not change significantly. Moreover, the plot of HT voltages at 222 nm against different SDS concentrations did not change significantly, suggesting the absence of aggregation (Figure 8, inset).

iii). ScyI. Below 0.2 mM SDS (which is below CMC), the CD spectra of ScyI contain a strong negative peak around 195 nm, a weak positive band at about 222 nm, and a weak negative band at about 238 nm, representing a dominant PPII structure for the peptide (Figure 10A). By increasing of the SDS concentration to 0.4 mM (close but still below CMC), the intensity of the strong negative band at 195 nm decreases, the shoulder disappears and the intensity of the band at 238 nm increases. In 0.6 mM SDS and above (above CMC), the CD spectra show a positive band around 195 nm and two negative peaks at about 209 and 217 nm (characteristic of dominant alpha helical structure) in which their intensities increase slightly as the SDS concentration increases. In SDS concentrations above 0.8 mM, the intensities of the bands at 209 and 217 nm are almost equal (R_2=1). CD spectra of ScyI in different concentrations of SDS show an isoelliptic point at about 206 nm.

In the presence of ScyI, the plot of HT voltages at 222 nm against different SDS concentrations did not change significantly, implying for the absence of aggregation (Figure 10, inset).

In conclusion, in SDS monomers, PPII helical structure is the most populated conformation in all the TKs, while upon formation of micelles, they undergo a structural transition to dominant α-helical structure.

Role of the membrane surface charges on secondary structures of the TK peptides

3.2.5. TKs' conformations in zwitterionic LUVs

The CD spectra of TK peptides in zwitterionic LUVs (at 22 ˚C) display the same features as in aqueous solutions seen by a strong negative peak at about 200 nm and a shoulder around 222 nm (Figures 11A). For all the TKs, increase of the temperature from 5 to 80

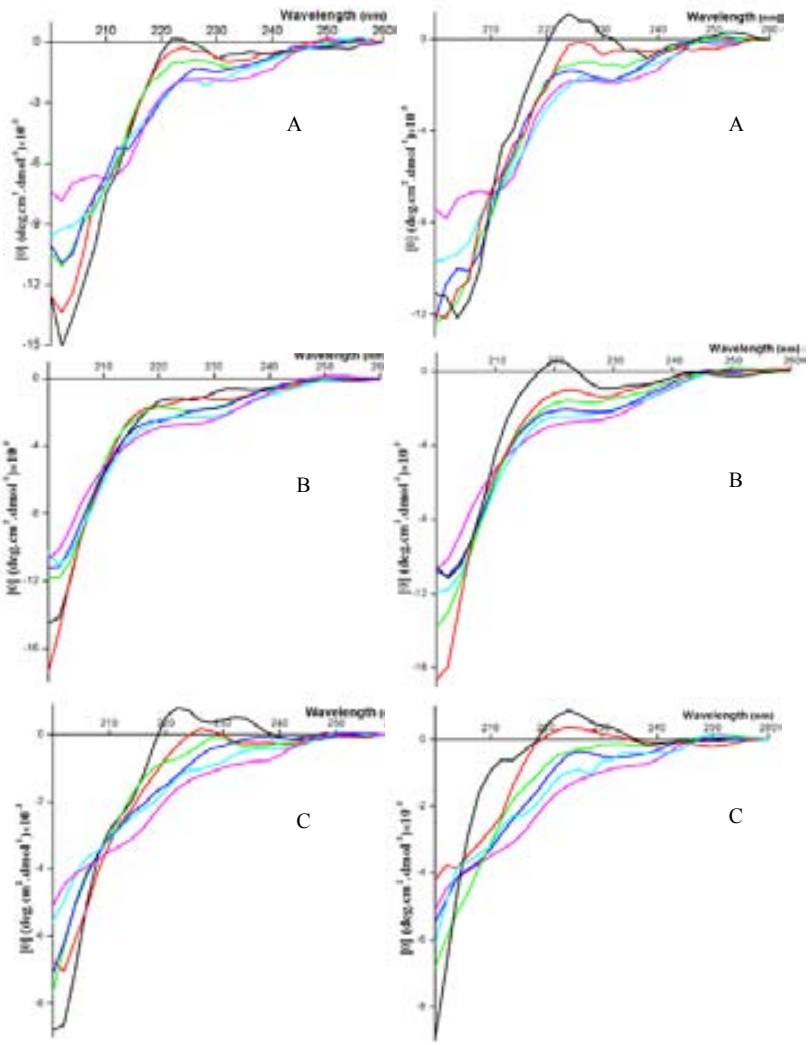

Figure 3.2.10. Left panel: CD spectra of (A) SP; (B) NKA; and (C) Scyl, recorded at the following increasing temperatures: 15 (—), 22 (—), 37 (—), 50 (—), 60 (—), and 70 °C (—).
Right panel: CD spectra of SP (A), NKA (B); and Scyl (C), recorded at the following decreasing temperatures: 70 (—), 60 (—), 50 (—), 37 (—), 22 (—), and 15 °C (—).
In all the cases, concentrations of peptides and lipids were 60 μM and 6 mM, respectively. The buffer was sodium phosphate (5 mM, pH 7.0).
All the samples were incubated for a few min to reach a thermal equilibration then spectra were recorded immediately.

°C causes a decrease of the both bands (Figure 11B). In zwitterionic LUVs, the CD spectra of all the TK peptides at different temperatures are reversible. The CD spectra of SP recorded at increasing the temperature indicate an isoelliptic point at about 207 nm

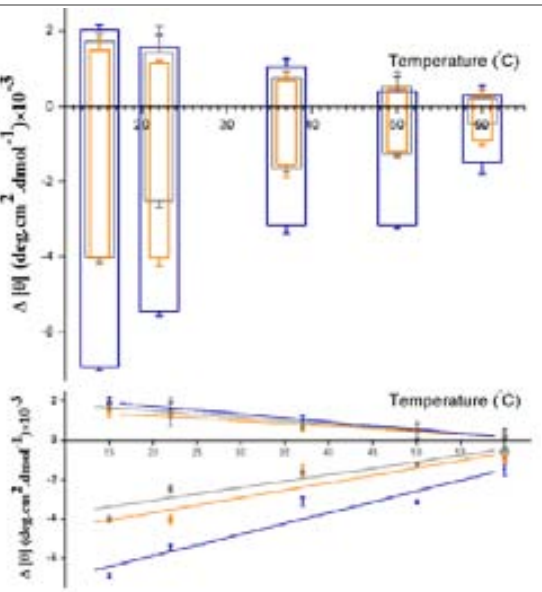

Figure 3.2.11. (A) Histogram and (B) plot of the difference CD molar ellipticities ($\Delta[\theta]$) of SP (—), NKA (—), and Scyl (—) in DMPC LUVs (6 mM) as a function of increasing temperatures.
CD intensities at 222 nm (positive values) and 197 nm (negative values) at each temperature were subtracted from those at 60 °C, assuming that the secondary structure of peptides is completely unordered at 60 °C.
In all the cases, the concentration of peptides was 60 μM.

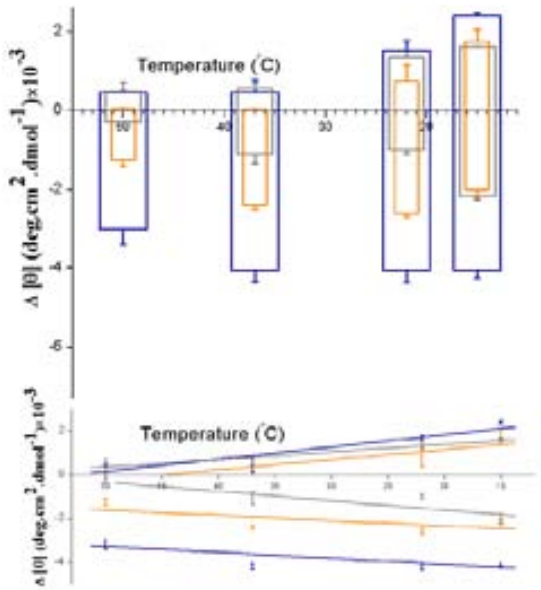

Figure 3.2.12. (A) Histogram and (B) plot of the difference CD molar ellipticities ($\Delta[\theta]$) of SP (—), NKA (—), and Scyl (—) in DMPC LUVs (6 mM) as a function of decreasing temperatures.
CD intensities at 222 nm (positive values) and 197 nm (negative values) at each temperature were subtracted from those at 60 °C, assuming that the secondary structure of peptides is completely unordered at 60 °C.
In all the cases, the concentration of peptides was 60 μM.

while for those recorded at decreasing the temperature is at about 212 nm, implying of two-state conformational equilibration.

The histograms of difference CD molar ellipticities ($\Delta[\theta]$) at 222 and 202 nm as a function of increasing and decreasing temperatures, obtained for the TK peptides in DMPC LUVs, are shown in Figure 12. Regardless of the heating or cooling, the histograms reveal that:

a). The $\Delta[\theta]$ at both 202 and 222 nm are strongest in SP than those of the other peptides.

b). The value of $\Delta[\theta]_{222}$ in case of ScyI is slightly stronger or equal to that of NKA.

c). In contrast to $\Delta[\theta]_{222}$, the value of $\Delta[\theta]_{202}$ in NKA is stronger or equal to that of ScyI.

In conclusion, in the presence of zwitterionic LUVs, the formation of PPII structure is reversible process with temperature changes. Moreover for all the TKsPPII formation and disruption occurs in non-cooperative manner, like in the aqueous solutions

3.2.6. TKs' conformations in LUVs composed of the mixed zwitterionic and negatively charged lipids

a). SP. Compared to the zwitterionic LUVs, the CD spectra of SP undergo significant changes as the mol percentage of DMPG increases in the mixture of the DMPC/DMPG (mol/mol) LUVs (Figure 13). The presence of DMPG up to 25 mol% of the mixed DMPG/DMPC liposomes causes a decrease of the band intensity at 196 nm, concomitantly with a red shift of the band to 205-208 nm. Moreover, the small positive shoulder at about 222 nm disappears, and a negative band appears at about 220 nm. In 40 mol% DMPG, the CD spectra show a helical structure with a positive band at 196 nm and two negative bands at 208 and 222 nm. As the DMPG increases to above 40 mol%, the intensity of the positive band increases, while the intensities of the negative peaks decrease. It is worth mentioning that the intensities of the bands at 208 and 222 nm are almost equal (R_2=1).

In a search to identify the structural origin of these spectral changes, we calculated the difference spectra by subtracting the CD spectrum of SP in pure DMPG, with dominant alpha helical structure from those in DMPG/DMPC vesicles. The difference spectra

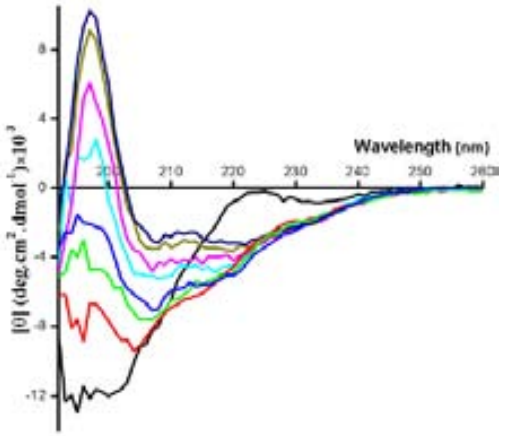

Figure 3.2.13. CD spectra of 100 μM SP in 10 mM DMPC/DMPG LUVs, prepared at different molar ratios: pure DMPC (—), 10% DMPG (—), 15% DMPG (—), 25% DMPG (—), 40% DMPG (—), 50% DMPG (—), 75% DMPG (—), and pure DMPG (—). All the spectra were collected immediately after preparation of samples at 22 °C. The buffer was sodium phosphate (5 mM, pH 7.0).

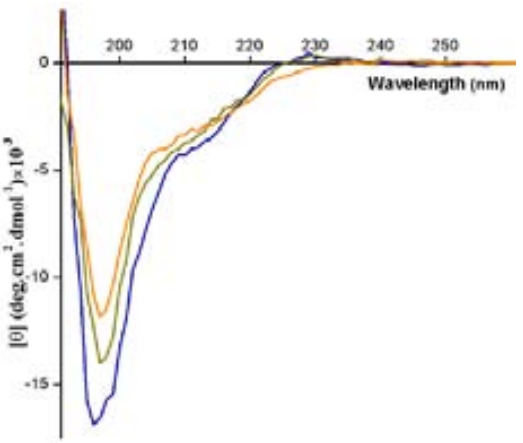

Figure 3.2.14. Difference CD spectra calculated by subtraction of the spectrum of 100 μM SP in 10 mM pure DMPG LUVs from that in 10 mM DMPC/DMPG LUVs with 10 (—), 15 (—), and 25 (—) mol% of DMPG (pH 7.0).

display a strong negative peak at about 195 nm and a small positive peak at about 225 nm (Figure 14), representative of a PPII structure. In addition, the intensities of the negative and positive bands decrease as the DMPG percentage increases.

b). NKA. In the case of NKA, as the DMPG increases to 40 mol% of DMPC/DMPG LUVs, the intensity of the shoulder at about 222 nm decreases (Figure 15). Moreover, the strong negative band at about 199 nm undergoes a red shift to about 203 nm. In pure DMPG LUVs, the CD spectrum of NKA contains two negative peaks at 204 and 222 nm,

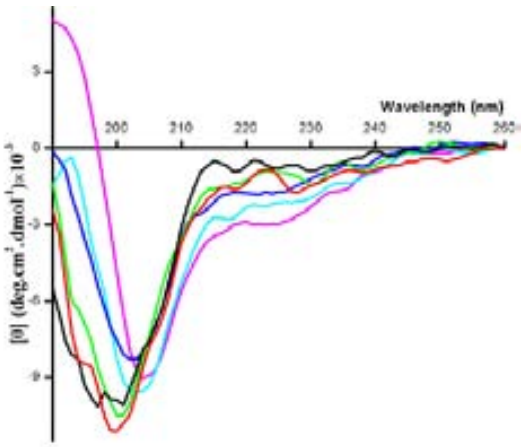

Figure 3.2.15. CD spectra of 60 μM NKA in 6 mM DMPC/DMPG LUVs, prepared at various molar ratios: pure DMPC (—), 10% DMPG (—), 15% DMPG (—), 25% DMPG (—), 40% DMPG (—), and pure DMPG (—). The buffer was sodium phosphate (5 mM, pH 7.0). All the spectra were collected at 22 °C, immediately after preparation of samples.

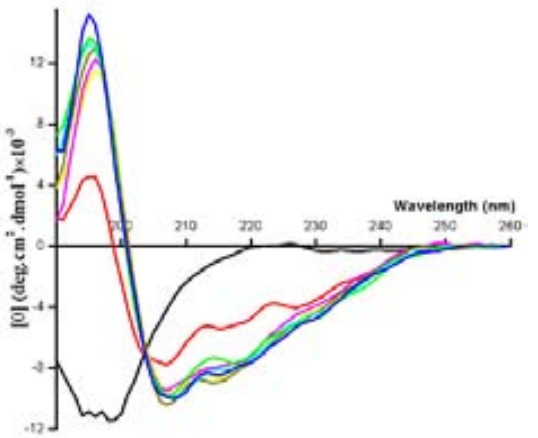

Figure 3.2.16. CD spectra of 60 μM ScyI in 6 mM DMPC/DMPG LUVs, prepared at various molar ratios: pure DMPC (—), 10% DMPG (—), 15% DMPG (—), 25% DMPG (—), 40% DMPG (—), 50% DMPG (—), 75% DMPG (—), and pure DMPG (—). All the spectra were collected immediately after preparation of samples at 22 °C. The buffer was sodium phosphate (5 mM, pH 7.0).

as the intensity of peak at 204 nm is about three times stronger than the peak at 222 nm. Moreover, the positive ellipiticity below 196 nm indicates for a positive peak which is slightly below the measured wavelength range.

c). ScyI. Compared to zwitterionic LUVs, even a low amount of DMPG (10 mol%) in the mixture of DMPC/DMPG LUVs, results in a significant changes of the CD spectral features of the ScyI peptide (Figure 16). In 10 mol% DMPG, the CD spectra show a

positive peak at about 198 nm, and three negative bands at 206, 217, and 227 nm, suggesting a dominant alpha helical structure. Further increases of DMPG to 15 mol% causes an increase of the band intensities at 206 and 217 nm, while the peak at 227 nm disappears, which are the characteristics of a typical spectrum of an alpha helix. The intensity of the negative band at 206 nm is slightly more than that at 217 nm. The CD spectra did not change significantly above 15 mol% of DMPG. Moreover, the spectral changes go through isoelliptic point implying a two-state structural equilibration.

These data demonstrate clearly that the alpha helical fold of TKs strongly depends on the relative amount of anionic DMPG in the vesicles, since zwitterionic DMPC alone did not induce any alpha helix formation. Moreover, conformational preference for the alpha helical structure in mixed DMPG/DMPC liposomes reflects the favorable electrostatic interaction of the SP with the headgroups of the lipid matrix.

3.2.7. Analysis of the secondary structures of SP, evaluated by the CD experiments

The method of Chen's and co-workers (Chen, Y. H. et al. 1972) has been widely used for quantitative evaluation of the alpha helical content of peptides, and in particular, it has been employed in previous CD studies of SP (Williams, R. W. and J. L. Weaver 1990). The CD spectra of SP recorded in TFE solvent, SDS micelles, or DMPG and mixed DMPG/DMPC liposomes are distinct from the spectral signatures for unordered or beta sheet conformations. They represent clearly alpha helical conformation, and applying Chen's equation.

Using the method of Chen *et al*., we determined the alpha helical content of SP in the presence of membrane mimetic systems (Table 1). These calculations show that:

a). The alpha helical content of SP varies depending on the environment of the peptide, suggesting genuine differences in the intrinsic helical propensity of SP in different membrane mimic systems. **b).** In negatively charged LUVs and in micelles, the alpha helical content of SP is slightly higher at pH 10.7 compare to that at pH 7.0.

c). The R_1 ($\theta_{195}/\theta_{208}$) parameter, in all studied cases, is negative, while R_2 ($\theta_{222}/\theta_{208}$) is positive and close to 1 in SDS micelles and in DMPG liposomes. Furthermore, in 70% (v:v) TFE/H_2O mixture, R_2 value is much less than 1.

In conclusion, the calculated MRE values are in good agreement with a 10-30% alpha helical content of SP, previously estimated by CD and Raman spectroscopy measurements (Williams, R. W. and J. L. Weaver 1990). From the other side, however, the relatively low MRE values obtained by us and others stress the presence of other conformations being overlooked by Chen's method. We should keep in mind that in any CD spectrum the signal from the alpha helical structure usually predominates over the beta turn and unordered ones (Yang, J. T. et al. 1986), resulting in an inability to distinguish between very short helical segments and β-turns. Additionally, any inaccuracy in the determination of peptide concentration could also add some error in estimation of the mean residue ellipticity (Greenfield, Norma J. 2004). Altogether, these considerations reinforce our assumption that the CD spectra of SP most likely represent a superposition of different local conformations, dominated by the most visible and best predicted by CD spectroscopy, the alpha helical conformation.

3.2.8. Role of the peptides net charge on the secondary structures of TKs

I). Aqueous solutions. The overall features of the CD spectra of TK peptides at different pH, from acidic to alkaline, are very similar, although, the intensities of the bands may show minor changes (Figure 17-19). In buffer solutions at pH of 3.8, 7.0 and 10.7, the CD spectra of SP, NKA and ScyI show a strong negative peak at about 195, 199, and 193 nm, respectively. CD spectra of SP and NKA indicate a weak negative band at about 235 and 230 nm, respectively. Moreover, the CD spectra of TKs have a shoulder in which in the case of SP and ScyI is around 224 nm, and for NKA is at about 220 nm.

These data show that in aqueous at various pH the TKs have a dominantly PPII helical structure.

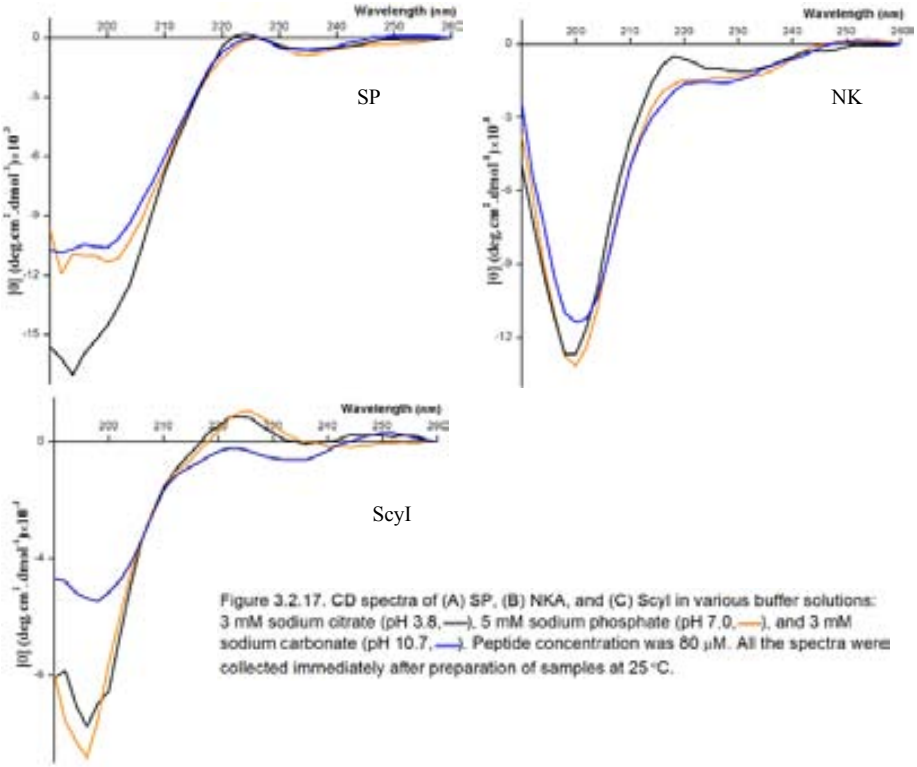

Figure 3.2.17. CD spectra of (A) SP, (B) NKA, and (C) ScyI in various buffer solutions: 3 mM sodium citrate (pH 3.8, —), 5 mM sodium phosphate (pH 7.0, —), and 3 mM sodium carbonate (pH 10.7, —). Peptide concentration was 80 μM. All the spectra were collected immediately after preparation of samples at 25 °C.

II). Micelles. The CD spectra of the TK peptides in SDS (20 mM), highly above CMC, were recorded at various pH of 3.8, 7.0, and 10.7. Prior to that and to evaluate a some possible effect of the pH on the micelle formation of SDS, the fluorescence spectra of the pyrene were recorded at various pH of 3.8, 7.0 and 10.7 in the presence of 20 mM SDS (Figure 20). In all these cases, the ratio of I_{385}/I_{374} vibronic bands was about 0.83, thus discarding any pH effect on the SDS micelles formation.

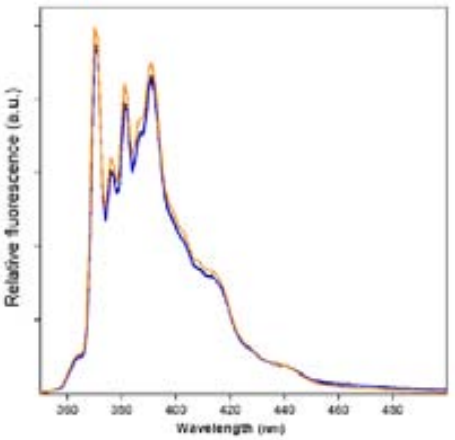

Figure 3.2.16. Fluorescence emission spectra of monomeric pyrene (2 μM) in the presence of 20 mM SDS at various buffer solutions: 3 mM sodium citrate (pH 3.8,——), 5 mM sodium phosphate (pH 7.0,——), and 3 mM sodium carbonate (pH 10.7,——). λ_{exc} was set at 335 nm. All the spectra were recorded immediately after preparation of samples at 25 °C. No emission of excimer was detected (about 480 nm).

i). SP. In the presence of micelles at pH 3.8, the CD spectrum of SP exhibits a helical structure, with a positive band at about 198 nm and two negative peaks at about 208 and 222 nm (Figure 21). Change of the pH from acidic (3.8) to alkaline (10.7) had a small effect on the negative peak intensities of the SP CD spectra, while caused an intensity increases. In all the pH, the intensities of the negative peaks were almost equal (R_2=1).

ii). NKA. In contrast to SP, the CD spectrum of NKA in 20 mM SDS at pH 3.8 presents a strong negative peak at about 201 nm, a negative band at about 230 nm and a weak shoulder at about 217 nm (Figure 22). By changing the pH from acidic (3.8) to alkaline (10.7), a positive peak at about 192 nm appears and the intensity of the band at 217 nm

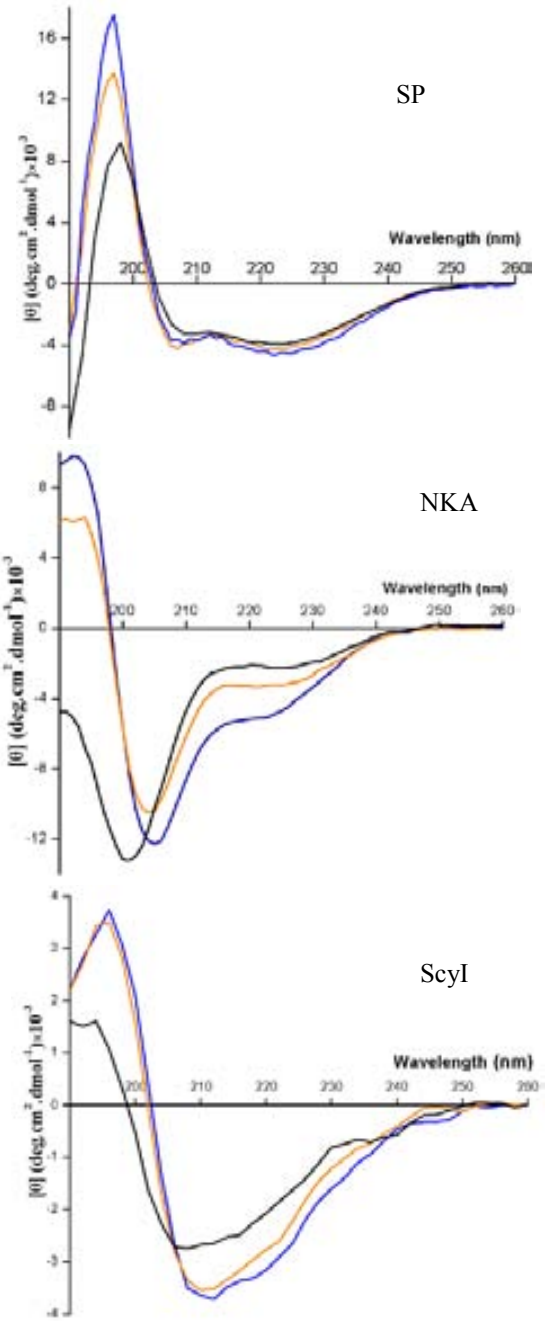

Figure 3.2.19. CD spectra of (A) SP (100 μM), (B) NKA (80 μM), and (C) ScyI (80 μM) in SDS (20 mM) at various buffer solutions: 3 mM sodium citrate (pH 3.8, ——), 5 mM sodium phosphate (pH 7.0, ——), and 3 mM sodium carbonate (pH 10.7, ——). All the spectra were collected immediately after preparation of samples at 22 °C.

increases. Moreover, intensity of the strong negative peak decreases and undergoes a red shift to 205 nm.

To get more knowledge about these findings, we performed the following complementary experiments.

a). The CD spectrum of NKA in micelles at pH 3.8 (Figure 22) shows a high similarity to the CD spectra of NKA in aqueous solution at low temperatures (see Figure 1). Since the peptide adopts PPII structure in these conditions, we examined whether increases of the temperature would induce some changes in the CD spectrum of NKA in the presence of micelles with acidic pH. As presented in Figure 23, increase of the temperature up to 85 ˚C caused minor changes of the CD spectrum of NKA, compared to the spectral changes observed upon PPII to unordered structural transitions by heating (see Figure 1). This finding indicates dominant unordered structure of NKA in micelles at pH 3.8.

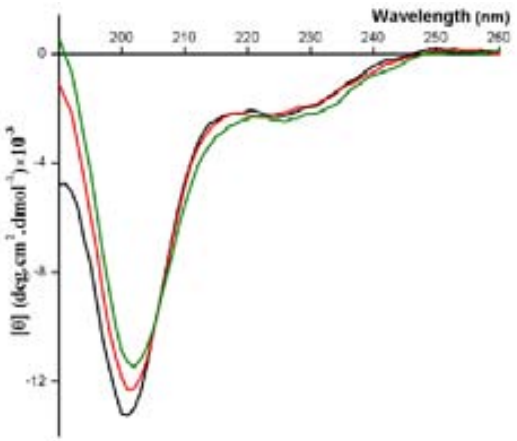

Figure 3.2.20. CD spectra of NKA (80 μM) in SDS (20 mM) at buffer pH 3.8 (3 mM sodium citrate) and various temperatures: 10 (—), 37 (—), and 85 ˚C (—). All the spectra were recorded immediately after preparation of samples.

b). To get some knowledge about the Trp environment, we analyzed the Trp fluorescence spectra of NKAW in SDS (20 mM) at various pH of 3.8, 7.0 and 10.7 (Figure 24). Comparison of the spectra show that changes of the pH from acidic to alkaline, caused an increases of the fluorescence intensity about 1.6 times, accompanied by about 2 nm red shifts of the Trp λ_{max}. These data indicate that, although, the Trp environment is mainly

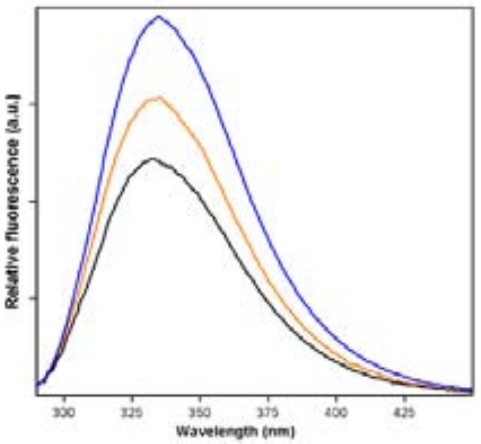

Figure 3.2.21. Fluorescence spectra of NKAW (5 μM) in the presence of 20 mM SDS and at various buffer solutions: 3 mM sodium citrate (pH 3.8,——), 5 mM sodium phosphate (pH 7.0,——), and 3 mM sodium carbonate (pH 10.7,——). All the spectra were collected immediately after preparation of samples at 25 °C.

hydrophobic in all the pH values, while, there is a clear quenching of the Trp fluorescence in the acidic pH.

c). To check whether the substitution of Phe[6] residue for Trp impairs the secondary structures of NKA, we recorded the CD spectra of NKAW in SDS micelles at pH 3.8, 7.0 and 10.7 (Figure 25). The CD spectra contain two negative peaks at about 220 nm and 204 nm. Moreover, the positive CD ellipticities below about 195 nm indicate for a peak slightly below the recorded wavelength.

The overall features of spectra at pH 7.0 and 10.7 are highly similar to those of NKA (see Figure 23), while the spectra of NKA and NKAW are different at pH 3.8.

iii). ScyI. Similarly to SP , the CD spectrum of ScyI in 20 mM SDS at pH 3.8 shows alpha helical structure with a positive peak at about 192 nm and two negative peaks at about 207 and 217 nm (Figure 26). In neutral (7.0) and alkaline (10.7) pH, the peak intensities increase and undergo a red shift of about 3 nm. Moreover, the intensity of the negative peak at about 220 nm is slightly lower ($R_2 = 0.78$) than that at 210 nm.

In conclusion, pH has no significant effect on the alpha helical content of SP and ScyI, while causes a structural changes in NKA in the presence of micelles.

Since the secondary structures of NKA and NKAW are similar only above pH 7.0, the resulting Trp fluorescence data at pH 7.0 and 10.7 apply for both peptides, showing the

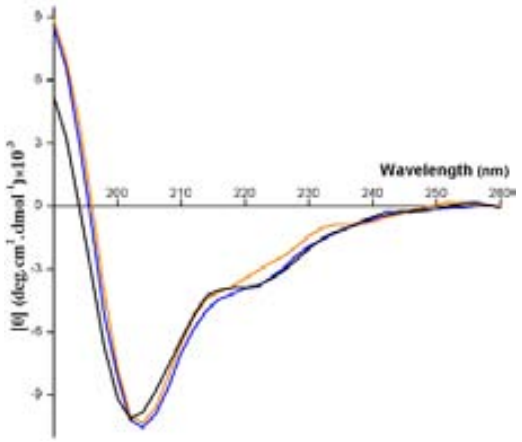

Figure 3.2.22. CD spectra of NKAW (80 μM) in SDS (20 mM) at various buffer solutions: 3 mM sodium citrate (pH 3.8,——), 5 mM sodium phosphate (pH 7.0,——), and 3 mM sodium carbonate (pH 10.7,——). All the spectra were recorded immediately after preparation of samples at 25 °C.

hydrophobic environment of Trp in both cases. At pH 3.8, due to the structural changes, the Trp fluorescence data of NKAW is not applicable for NKA.

Complementary characterization of the secondary structures of mammalian TK peptides analogues

SPW, Phe-CN SP and NKAW peptides were applied to study the interactions of TKs with the membrane mimetic systems by using fluorescence spectroscopy (part I of the Results and Discussions). As a control, we characterized the secondary structures of these peptides.

3.2.9. Aqueous solutions

a). [Trp]^{8}SP (SPW). In aqueous solutions with low temperature (15 ˚C) , the CD spectrum of SPW show a strong negative band around 199 nm, a weak negative band at about 237 nm, and a weak positive band at about 226 nm (Figure 27A). To discern whether this spectrum indicate for unordered or PPII secondary structures, we performed CD experiments in various temperatures. Increases of the temperature, up to 85˚C , caused a decrease of the negative band and a shift to about 202 nm. Moreover, the intensity of the positive band decreases as the temperature increases. Similar to SP (see Figure 1), temperature induced changes of CD spectra of SPW, suggests for the PPII structure as dominant conformation of peptide in aqueous solutions. Cooling down the

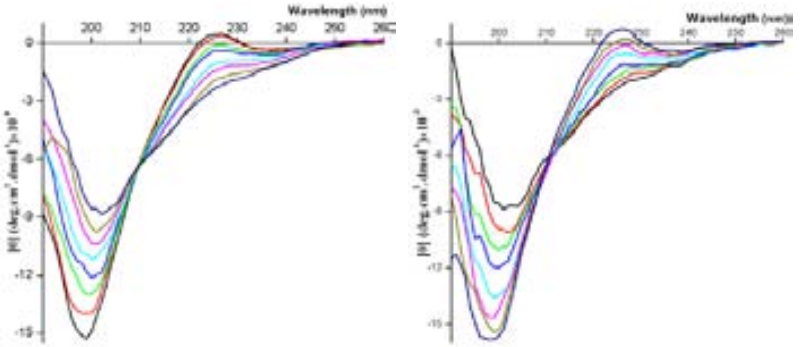

Figure 3.2.23.(A) CD spectra of SPW (100 μM) in sodium phosphate buffer (5 mM, pH 7.0), recorded at the following increasing temperatures: 15 (—), 22 (—), 30 (—), 37 (—), 50 (—), 60 (—), 70 (—), and 85 ˚C (—).
(B) CD spectra of SPW (100 μM) in sodium phosphate buffer (5 mM, pH 7.0), recorded at the following decreasing temperatures: 85 (—), 70 (—), 60 (—), 50 (—), 37 (—), 30 (—), 22 (—), and 15 ˚C (—).

temperature to 15˚C, caused an increase of the negative and positive bands, to the same intensities as the starting temperature of 15˚C, and shift of the negative band to about 198 nm (Figure 27B). Moreover, the negative band at about 226 nm appeared again upon cooling down the temperature. CD spectra of SPW at various temperatures show an isoelliptic point at about 210 nm, indicating for a two-state structural transition of peptide.

b). Phe^{8}-CN SP. Similar to SP, the CD spectrum of Phe-CN SP in aqueous solutions contains a negative peak at about 197 nm, a shoulder at about 224 nm and a weak positive band at 240 nm (Figure 28). Increase of the temperature (up to 60 ˚C) caused a decrease of the negative band and disappearing of the shoulder, in which is the representative of dominant PPII secondary structure. The CD spectra of Phe-CN SP show complete reversibility upon cooling down the temperature to 15 ˚C. The CD spectra indicate an isoelliptic point around 211 nm.

c). [Trp]^{6}Neurokinin A (NKAW). In aqueous solutions, the CD spectrum of NKAW has two negative bands at about 199 and 230 nm, and a weak shoulder around 220 nm (Figure 29A). As the temperature increases the intensity of the negative band at 199 nm decreases, while, the intensity of the band at about 230 nm increases and the shoulder at 220 nm disappears. Like NKA in the same conditions, these data are indicative for the PPII structure of NKAW in aqueous solutions. Upon cooling down the temperature to 5

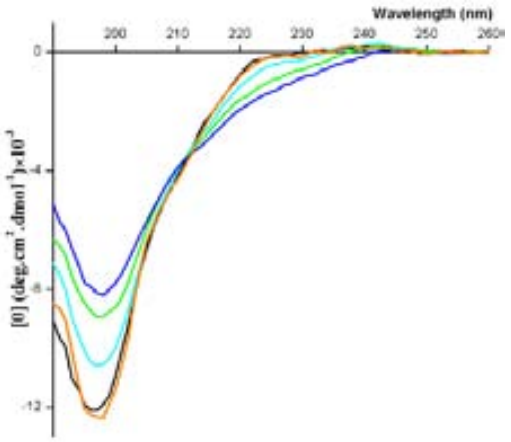

Figure 3.2.24. CD spectra of Phe-CN SP (100 μM) in distilled water, recorded at the following increasing temperatures: 15 (—), 30 (—), 45 (—), 60 (—); and cooling down to 15 °C (—).

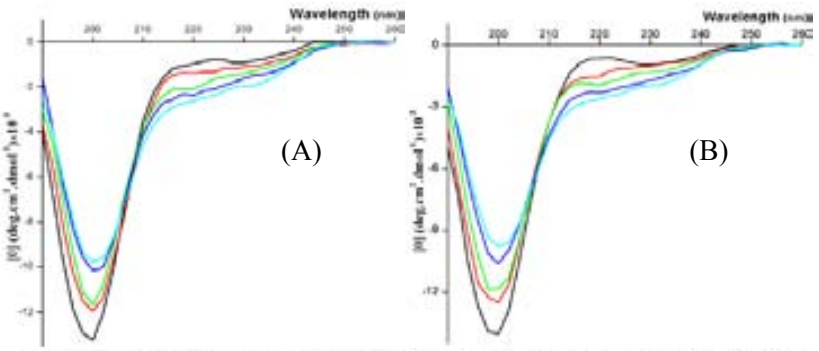

Figure 3.2.25. (A) CD spectra of NKAW (100 μM) in sodium phosphate buffer (5 mM, pH 7.0) recorded at the following increasing temperatures: 5 (—), 22 (—), 37 (—), 60 (—), and 80 °C (—).

(B) CD spectra of NKAW (100 μM) in sodium phosphate buffer (5 mM, pH 7.0), recorded at the following decreasing temperatures: 80 (—), 60 (—), 37 (—), 22 (—), and 5 °C (—).

°C, the intensity of the negative band at 199 nm increases, while the intensity of the band at 230 nm decreases and the shoulder at 220 nm appears, which shows the complete reversibility of the peptide's secondary structure (Figure 29B). The CD spectra show an isoelliptic point at about 207 nm, indicative of a two-state structural changes of peptide.

3.2.10. Hydrophobic environment

a). SPW. In the absence of SDS, the CD spectrum of SPW shows a positive band at 226 nm, and a strong negative band around 199 nm (Figure 30A). Upon addition of 0.4 mM

SDS, a weak positive peak appeared at about 242 nm and both the positive and negative bands undergo a blue shift about 7 nm. Further titration of SDS caused more blue shifts of the peaks, in which in the presence of 1.4 mM SDS, the positive band is at about 206 nm and the negative ellipticity below about 197 nm indicates for a peak slightly lower than recorded wavelengths. Moreover, the intensity of the bands increased as the SDS concentration increased. However, the intensity of the negative band, in all cases, is about 2-2.5 times more than that of positive peak. We calculated the CD difference spectra by subtracting the CD spectrum of SPW in the presence of 10 mM SDS (highly above CMC) from that in 1.4 mM SDS (Figure 30A, inset). The CD difference spectrum is a representative of PPII structure. Similar to SP, in 10 mM SDS micelles, the CD spectrum shows a positive peak around 196 nm and two negative peaks at 206 and 222 nm (Figure 30B), which are typical characteristics of an alpha helical structure. For SPW in micelles (Figure 30), the intensity of the peak at 208 nm is more than that in 222 nm (R_2=0.59), while in SP is about one.

b). Phe-CN SP. In low concentration of SDS (0.2 mM), the CD spectrum of Phe-CN SP has a weak shoulder around 226 nm, a weak positive band at 240 nm, and a negative band at about 196 nm with less intensity compared to that in buffer (Figure 31), suggesting dominant PPII structure of peptide. In the presence of 0.4 mM SDS, the CD spectrum indicates two positive bands at about 239 nm and 218 nm. Moreover, the negative ellipticities below about 206 nm indicate for a negative peak slightly lower than the collected wavelengths. Further increase of the SDS to 1 mM caused an increase of the intensities of the positive and negative bands, and the blue shift of the positive peak to about 208 nm. Noteworthy, the intensity of the negative band is about 2-3 times more than that of the positive peak at 208-218 nm. The difference CD spectrum obtained by subtraction of CD spectrum of Phe-CN SP in 12 mM SDS (highly above CMC) from that in 1 mM SDS, is a representative of PPII structure (Figure 31, inset). In 2 mM SDS, the CD spectrum shows two negative peaks at 207 and 222 nm and a positive band at 197 nm, indicative of the alpha helical structure of peptide. Increase of the SDS concentration to 12 mM only caused an increase of the negative and positive bands. Similar to that of SP, the R_2 value is about one.

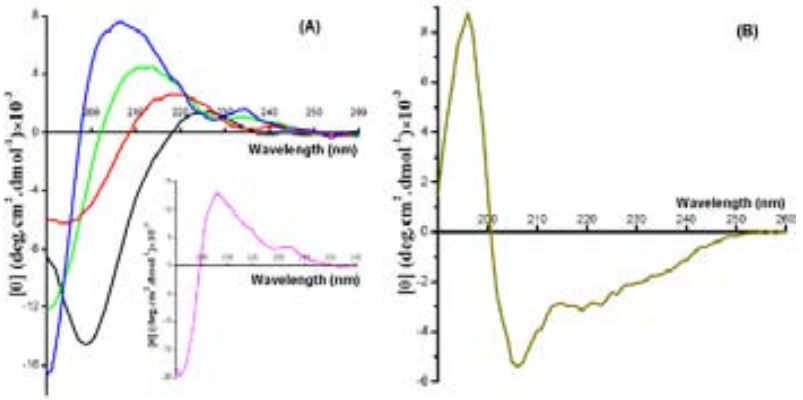

Figure 3.2.26. CD spectra of SPW (100 μM) in various concentrations of SDS: (A) 0 (—), 0.4 (—), 0.6 (—), 1.4 mM SDS (—), and (B) 10 mM SDS (—). The buffer was sodium phosphate (5 mM, pH 7.0). Inset. Dfference CD spectrum calculated by subtraction of the spectrum of SPW (100 μM) in 10 mM SDS from that in 1.4 mM SDS. All the spectra were collected immediately after preparation of samples at 22 °C.

c). NKAW. In general, the CD spectrum of NKAW in micelles (Figure 32) has similar characteristics to that of NKA, indicating a positive band at about 192 nm and two negative bands at about 203 and 220 nm, while, the CD spectrum between 225 and 240 nm is about 2.4 times less intense in NKAW than NKA. Like NKA, the CD spectrum of NKAW implies for a superposition of the spectra representative of unordered and alpha helical secondary structures of peptide.

3.2.11. Zwitterionic and negatively charged LUVs

a). SPW. Similarly to SP in DMPC LUVs, the CD spectrum of SPW has a strong negative band at 198 nm, a shoulder at about 226 nm (Figure 33), characteristics of dominant PPII structure. In the DMPC/DMPG LUVs mixtures composed of 10 mol% DMPG, the negative peak shifts to 203 nm. Further increase of DMPG (to 25 mol%), caused more red shift of the strong negative peak to 206 nm and decreases of its intensity. Moreover, the CD spectra show low positive ellipticity below 195 nm. Above 40 mol% DMPG, CD spectrum represents dominant alpha helical structure of peptide, indicated by two negative peaks at 206 and 220 nm, and a positive band at 197 nm. Increase of the mol fractions of DMPG to above 40 mol% causes an increase of the positive band and a decrease of the negative peaks at 206 and 222 nm. It is worth mentioning that, in contrast

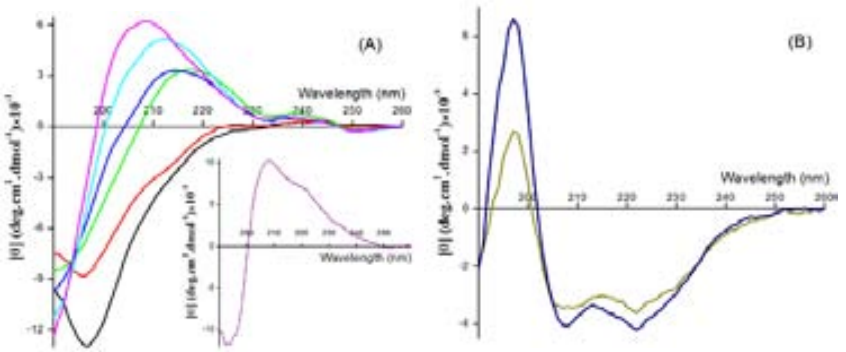

Figure 3.2.27 CD spectra of Phe-CN SP (80 μM) in various concentrations of SDS: (A) 0 (—), 0.2 (—), 0.4 (—), 0.6 (—), 0.8 (—), 1 mM SDS (—), and (B) 2 (—), and 12 mM SDS (—). Inset. Difference CD spectrum calculated by subtraction of the spectrum of Phe-CN (80 μM) in 12 mM SDS from that in 1 mM SDS. All the spectra were collected immediately after preparation of samples. The buffer was sodium phosphate (5 mM, pH 7.0) and the temperature was set at 22 °C.

to DMPC, a weak negative band appears at about 237 nm in the presence of LUVs composed of DMPC and DMPG.

b). Phe-CN SP. The CD spectrum of Phe-CN SP in DMPC LUVs shows a strong negative peak at 197 nm and a shoulder at 222 nm (Figure 34), the similar characteristics as the CD spectrum of SP in the same condition. Small mol fraction of DMPG (4 mol%) in the LUVs composed of the mixed DMPC and DMPG, caused a decrease of the intensity of the strong negative peak at 198 nm and the shoulder disappears. By increasing of DMPG to 10 mol%, the intensity of the negative peak at 197 nm decreases and undergoes a red shift to 203 nm, while the intensity of the negative band at 225 nm did not change significantly. Above 25 mol% DMPG, a positive peak at 197 nm and two negative peaks at 207 and 224 nm appear (indicative of dominant alpha helical structure of the peptide) and R_2 is about 1. The CD spectra show an isoelliptic point at about 216 nm.

c). NKAW. In DMPC LUVs, the CD spectrum of NKAW has similar features with that of NKA and reproduces well the characteristic features of a stable PPII helix (Figure 35). In contrast to NKA in which small mol fractions of DMPG (up to 25 mol%) in the DMPC/DMPG LUVs caused some changes of CD spectra (see Figure 15), while in the case of NKAW, increase of the mol fractions of DMPG up to 30 mol% of the LUVs, did not change the CD spectrum of the peptide compared to that in DMPC LUVs (Figure 35).

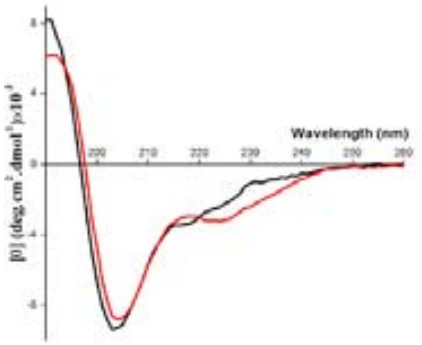

Figure 3.2.28. CD spectra of NKAW (—), and NKA (—), respectively, in 12 and 8 mM SDS. Concentration of peptides was 80 μM. The buffer was sodium phosphate (5 mM, pH 7.0). Both the spectra were recorded immediately after preparation of samples at 22 °C.

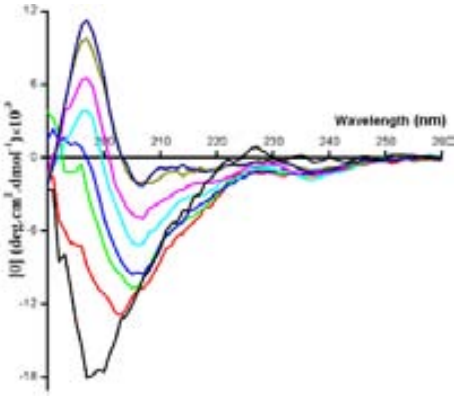

Figure 3.2.29. CD spectra of 60 μM SPW in DMPC/DMPG LUVs (6 mM), prepared at various molar ratios: pure DMPC (—), 10% DMPG (—), 15% DMPG (—), 25% DMPG (—), 40% DMPG (—), 50% DMPG (—), 75% DMPG (—), and pure DMPG (—). All the spectra were collected at 22 °C. The buffer was sodium phosphate (5 mM, pH 7.0).

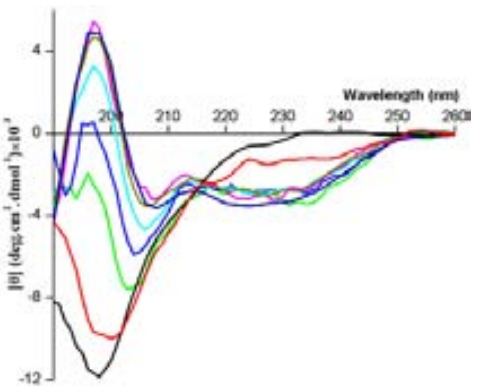

Figure 3.2.30. CD spectra of 60 μM Phe-CN SP in DMPC/DMPG LUVs (6 mM), prepared at various molar ratios: pure DMPC (—), 4% DMPG (—), 10% DMPG (—), 15% DMPG (—), 25% DMPG (—), 65% DMPG (—), 85% DMPG (—), and pure DMPG (—). All the spectra were collected immediately after preparation of samples, at 22 °C. The buffer was sodium phosphate (5 mM, pH 7.0).

In 50 mol% DMPG, the CD spectrum of NKAW has two negative peaks at 204 and 221 nm, a weak shoulder at about 235 nm, and a positive band around 191 nm (Figure 35) and further increasing of DMPG caused no significant changes of the spectra. The atypical characteristics of the CD spectra of NKAW in above 50 mol% DMPG suggest for a superposition of the spectra representative of unordered and alpha helical secondary structures.

In conclusion, in spite of some insignificant changes, the dominant secondary structures of all TKs' analogues in aqueous solution, micelles and LUVs (at pH 7.0) were very similar to those of TKs.

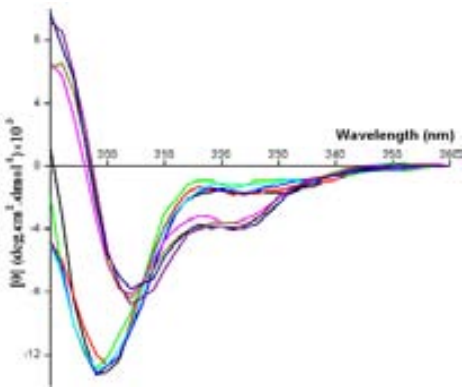

Figure 3.2.31. CD spectra of 60 μM NKAW in DMPC/DMPG LUVs (6 mM), prepared at various molar ratios: pure DMPC (—), 4% DMPG (—), 10% DMPG (—), 15% DMPG (—), 30% DMPG (—), 50% DMPG (—), 60% DMPG (—), 80% DMPG (—), and pure DMPG (—). All the spectra were collected immediately after preparation of samples at 22 °C. The buffer was sodium phosphate (5 mM, pH 7.0).

3.2.12. Small angle X-ray scattering (SAXS) patterns of the overall shape of NKA peptides in aqueous solutions

The overall dimensions of the NKA peptide in aqueous solutions were studied by SAXS patterns at different temperatures. The SAXS curves of NKA as a function of temperature show that as the temperature increases (from 5 to 40 ˚C), the intensity of the scattering decreases (Figure 36). Furthermore, the intensity of the scattering is reversible by cooling down the temperature from 40 to 5˚C. In all the measured temperatures, the SAXS curves represent a plateau at low angles ($s < 0.5$ nm^{-1}) indicating for the absence of

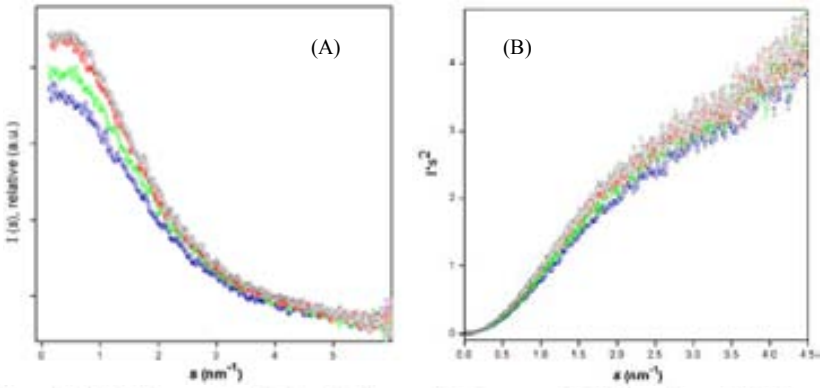

Figure 3.2.32. Temperature-induced changes in the ensemble dimensions of NKA, studied by SAXS. (A) Plot of the absolute intensities of the scattering for NKA (2 mM) in sodium phosphate buffer (5 mM, pH 7.0) against the momentum transfer and as a function of different temperatures: 5°C (○), 25°C (○), 40°C (○), and cooling down to 5°C (○). The scattering pattern below 0.1 nm^{-1} is not presented due to the presence of the primary beam.

(B) Overall SAXS profiles represented as Kratky plots of NKA (2 mM) in sodium phosphate buffer (5 mM, pH 7.0) at increasing temperatures: 5°C (○), 25°C (○), 40°C (○); and cooling down to 5°C (○).

aggregation and inter-particle interactions (Jacques, D. A. and J. Trewhella). The average R_g was determined as 0.71±1% nm. Figure 37 shows that at 5 and 25˚C, the distance distribution function consists of two broad peaks at about 0.4 and 1.2 nm, the peak at about 0.4 nm being more intense compared to that in 1.2 nm. At 40˚C, a small peak at about 2.2 nm appears and the width of the main peaks gets narrower. Cooling down the temperature to 5 ˚C caused the band widening of the main peaks and the band at 2.2 nm appears as a shoulder. The $P(r)$ plot characteristics indicate for a two-domain geometric shapes. Considering the $P(r)$ when it returns to zero at large values of r, D_{max} was determined as about 2.4 nm. The Kratky plots were used to study the peptide folded/unfolded states upon heating. The overall features of Kratky plots at different temperatures are very similar (Figure 38) and show a continuous increase of I^*s^2 with s, as a remarkable characteristic of unordered structures (Mertens, H. D. and D. I. Svergun), but on the other hand, they lack a plateau over the specific range of momentum transfer (s), as normally observed experimentally in unfolded proteins. Moreover, the increases of the temperature from 5 to 40C, caused a shift of the Kratky plots to a higher s. The temperature induced changes in Kratky plots are reversible upon cooling down the temperature to 5 ˚C. Using SAXS patterns, we applied DAMMIF software to obtain *Ab*

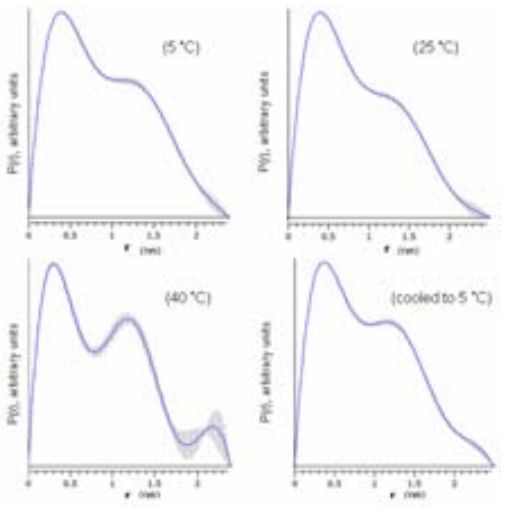

Figure 3.2.32. (C) Distance distribution functions of NKA (2 mM) in sodium phosphate buffer (5 mM, pH 7.0) and at increasing temperatures: 5, 25, 40 ˚C; and cooling down to 5 ˚C.

initio models of an overall shape of the peptide (see Materials and Methods). At all temperatures, the *Ab* initio models show a side-tailed dumbbell shape (Figure 39).

In conclusion, although the atypical Kratky plots of NKA in aqueous solution are mostly indicative of unordered structures while they imply for the presence of non-dominant conformations. This is consistent with two-domain geometric shape of the peptide revealed by P(r) plots.

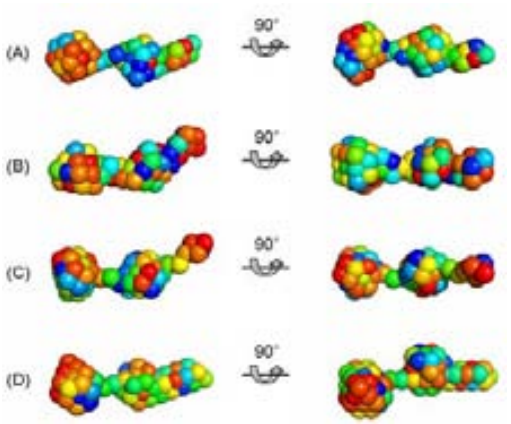

Figure…*Ab initio* shape reconstructions, calculated from the SAXS scattering profiles of NKA (2 mM) in sodium phosphate buffer (5 mM, pH 7.0) at various increasing temperatures: (A) 5C, (B) 25 ˚C, (C) 40

Table 1. Evaluation of the alpha helical content of SP in different membrane mimetic environments.

		DMPG Liposomes		SDS micelles		
	70% TFE/water (v/v)	**pH 7.0**	**pH 10.7**	**pH 7.0**	**pH 10.7**	**40:60 mol% DMPG:DMPC[b]**
α-helix %	10.50±1.4	11.5±1.0	13.5±1.5	13.3±0.8	15.3±0.02	16.7±1.4
R_1[a]	-1.05±0.12	-2.5±0.5	-2.84±0.4	-4.09±0.8	-4.50±0.02	-0.56±0.04
R_2[a]	0.41±0.02	0.90±0.2	1.00±0.02	1.15±0.2	1.20±0.02	0.86±0.04

[a] $R_1=\theta_{195}/\theta_{208}$ and $R_2=\theta_{222}/\theta_{208}$ (see Materials and Methods)

[b] at pH 7.0.

Table 2. PPII helical contents of TKs peptides in aqueous solution and as a function of increasing temperature.

temperature (˚C)	%PPII content		
	SP	**NKA**	**ScyI**
5	52.44	41.88	51.31
15	49.13	38.92	46.64
22	45.82	35.86	43.84
30	40.87	33.81	42.91
37	40.60	31.77	41.04
50	32.60	28.70	36.36
70	25.98	25.63	32.63
80	24.33	22.56	29.83

Bienkiewicz, E. A., A. Moon Woody and R. W. Woody. 2000. Conformation of the RNA polymerase II C-terminal domain: circular dichroism of long and short fragments. *J Mol Biol* 297 (1):119-133.

Bochicchio, B. and A. M. Tamburro. 2002. Polyproline II structure in proteins: identification by chiroptical spectroscopies, stability, and functions. *Chirality* 14 (10):782-792.

Chen, Y. H., J. T. Yang and H. M. Martinez. 1972. Determination of the secondary structures of proteins by circular dichroism and optical rotatory dispersion. *Biochemistry* 11 (22):4120-4131.

Greenfield, Norma J. 2004. Analysis of circular dichroism data. *METHODS IN ENZYMOLOGY* 383:282-317.

Jacques, D. A. and J. Trewhella. Small-angle scattering for structural biology--expanding the frontier while avoiding the pitfalls. *Protein Sci* 19 (4):642-657.

Jaravine, V. A., A. T. Alexandrescu and S. Grzesiek. 2001. Observation of the closing of individual hydrogen bonds during TFE-induced helix formation in a peptide. *Protein Sci* 10 (5):943-950.

Kelly, M. A., B. W. Chellgren, A. L. Rucker, J. M. Troutman, M. G. Fried, A. F. Miller and T. P. Creamer. 2001. Host-guest study of left-handed polyproline II helix formation. *Biochemistry* 40 (48):14376-14383.

Mertens, H. D. and D. I. Svergun. Structural characterization of proteins and complexes using small-angle X-ray solution scattering. *J Struct Biol* 172 (1):128-141.

Roccatano, D., G. Colombo, M. Fioroni and A. E. Mark. 2002. Mechanism by which 2,2,2-trifluoroethanol/water mixtures stabilize secondary-structure formation in peptides: a molecular dynamics study. *Proc Natl Acad Sci U S A* 99 (19):12179-12184.

Rucker, A. L. and T. P. Creamer. 2002. Polyproline II helical structure in protein unfolded states: lysine peptides revisited. *Protein Sci* 11 (4):980-985.

Shi, Zhengshuang. et al. . 2006. Conformation of the Backbone in Unfolded Proteins. *Chem. Rev.* 106:1877-1897.

Williams, R. W. and J. L. Weaver. 1990. Secondary structure of substance P bound to liposomes in organic solvents and in solution from Raman and CD spectroscopy. *J Biol Chem* 265 (5):2505-2513.

Woody, R. W. 2009. Circular dichroism spectrum of peptides in the poly(Pro)II conformation. *J Am Chem Soc* 131 (23):8234-8245.

Yang, J. T., C. S. Wu and H. M. Martinez. 1986. Calculation of protein conformation from circular dichroism. *Methods Enzymol* 130:208-269.

RESULTS AND DISCUSSION

PART III

Study of the fibrillar state of the TK peptides

The questions we addressed in this chapter are: Do the TKs have ability to self-associate in aggregates and importantly do these aggregates form fibrillar structures? Secondly, do the fibrils have an amyloid structure?

Numerous previous studies have led to the conclusion that various factors can promote or inhibit the formation of fibrils in peptides *in vitro*. Among these different factors, the concentration, the ionic strength, and solutions composition (Gorbenko, G. P. and P. K. Kinnunen 2006) are considered as basic factors. Therefore we initially focused on the concentration and on the solution composition. TKs were incubated under a range of different solution conditions, as the varied solution parameters included: aqueous, liposomes and surfactants, known to affect or induce amyloid fibril formation in other protein/peptides systems.

Next to find out whether TKs self-associate in aggregates in above conditions and more importantly to find out whether these aggregates have fibrillar ultrastructural morphology we examined the samples by transmission electron microscopy (TEM).

A summary of all conditions examined is presented in Table 1-4 and the morphologies of the formed structures are shown on Figures 1-5 and 9.

In aqueous solutions as jugged by TEM, at a concentration of 3 mM, TKs show formation of fibrils immediately after sample preparation (Figure 1). However, at a half concentration (1.5 mM), no fibrils were detected. At even lower concentrations in the μM range (at about 100 μM) no formation of any aggregate was detected even for overnight incubation (Table 1-3, Figure 1).

Analysis of TEM micrographs reveals the presence of various fibrillar morphologies. For example for SP, there are both: long twisted fibrils and straight single filaments in a width of about 15 nm, while in NKA and ScyI, fibrils are only single-straight with a width of about 9 and 12 nm, respectively, which are characteristics of the amyloid-like fibrils. In any of the TKs, no branched fibrils were detected (see Figure 1).

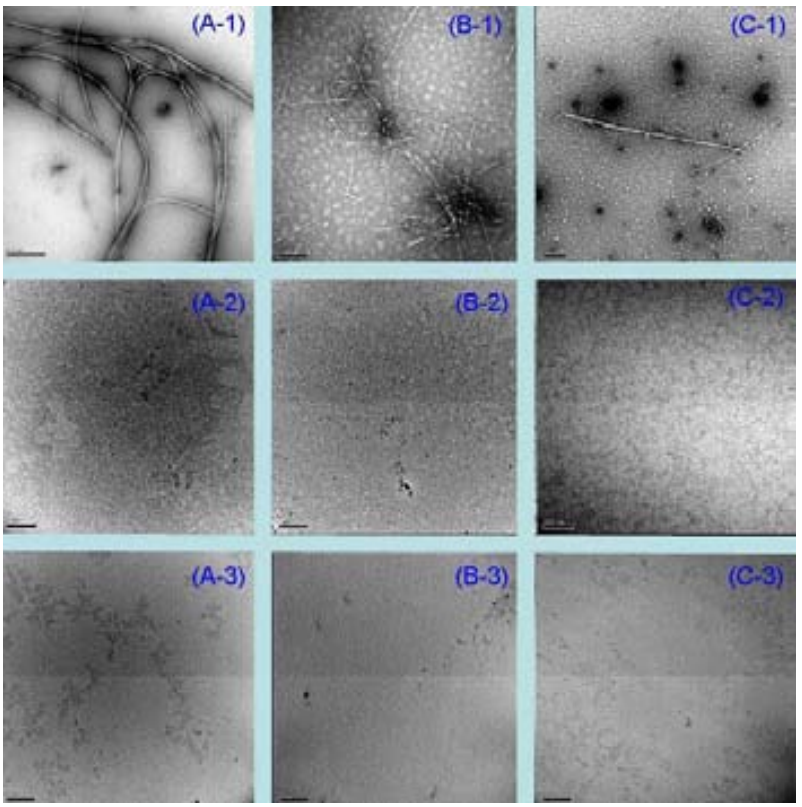

Figure 3.3.1. Morphology of the fibrils formed by TKs. TEM images of the negatively stained:
3mM (A-1) SP, (B-1) NKA, and (C-1) ScyI;
1.5mM (A-2) SP, (B-2) NKA, and (C-2) ScyI;
100 µM (A-3) SP, (B-3) NKA, and (C-3) ScyI;
in buffer (5 mM sodium phosphate, pH 7.0), without performing agitation. Non of the samples
were incubated before preparation of the microscopy grids. Fibrils of SP consist of several long
twisted filaments, while those of NKA and ScyI are short straight ribbons.

From TEM micrographs of TKs incubated in the presence of LUVs two main species can be distinguished:

i). In DMPG, at high concentration (above 1.5 mM) of TKs, the fibrils were formed immediately (Figure 2).

All the TKs fibrils are straight, and some fibrils in ScyI may be twisted (in a width of about 21 nm), while in SP and NKA because of their huge amount, some of the fibrils overlaid and the width of each single strand can not be evaluated. It is worth mentioning that although the amount of the fibrils in SP and NKA in each grid seems higher than that of ScyI, further complementary techniques are required to determine exactly the fibrils production.

ii). When the concentration was 0.75 mM, SP formed fibrils in DMPG immediately, but no fibrils were detected in DMPC for any of the TKs (Figure 2).

In SP, a huge amount of straight fibrils are stuck together like a "*hank*". Due to the presence of several sticking filaments, the detection of each single strand (and subsequently its width) was not possible.

Incubation of the TKs in low concentration (100 μM) with the anionic surfactant SDS at concentrations highly above CMC does not initiate neither favor (even on overnight incubation time) the formation of aggregates or fibrils (Figure 3). In contrary the incubation with the surfactant at 2 mM TKs results in an immediate formation of fibrils (Figure 3).

In the presence of 10 mM SDS, fibrils of SP are straight in a width of about 22 nm with two or more single strands stacked each other. In NKA different morphologies were detected as some fibrils consist of several straight bundles, sticking each other side by side in a width of about 19-25 nm; while other fibrils consist of several filaments twisted each other in a form like "*hank*", in which single strands can not be detected. In the case of ScyI, single straight fibrils are about 20 nm width. They look separate (not sticked), and no twisting were detected.

Interestingly the incubation of the TKs in a low concentration range (80-100 μM, depending on the peptide) in SDS solutions at concentrations close to CMC 1 mM (for SP), and 4 mM (for NKA) causes the formation of fibrils. In SP fibrils form after overnight incubation (Figure 4), while for NKA they form immediately or in a few

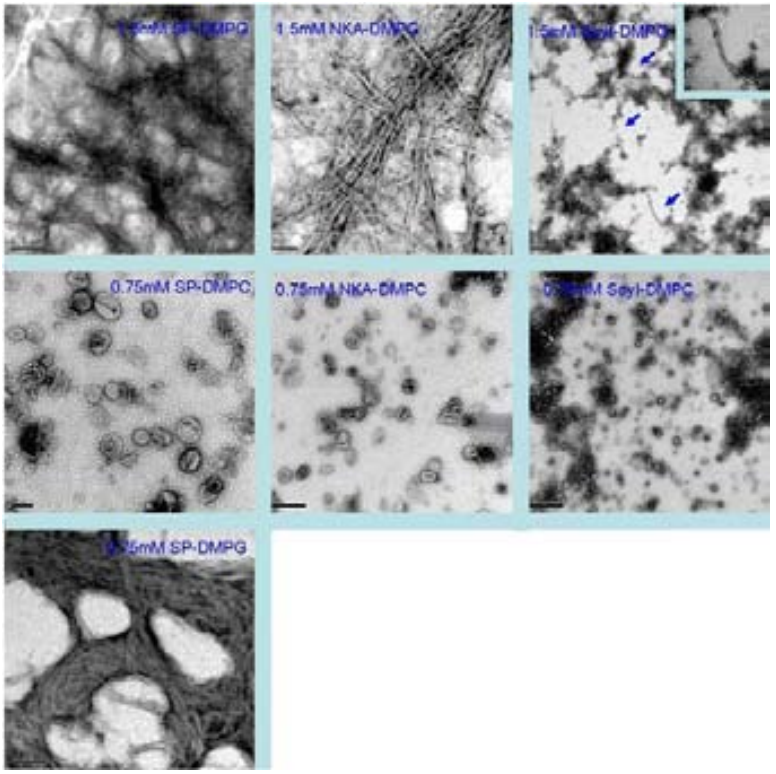

Figure 3.3.2 Negatively stained TEM images of the TKs in DMPG and DMPC vesicles.
In all the cases, electron micrographs were obtained immediately after samples preparation. The buffer was sodium phosphate (5 mM, pH 7.0). Arrows indicate for fibrils. Electron micrograph image in inset shows the fibrils of Scy I at higher resolution.

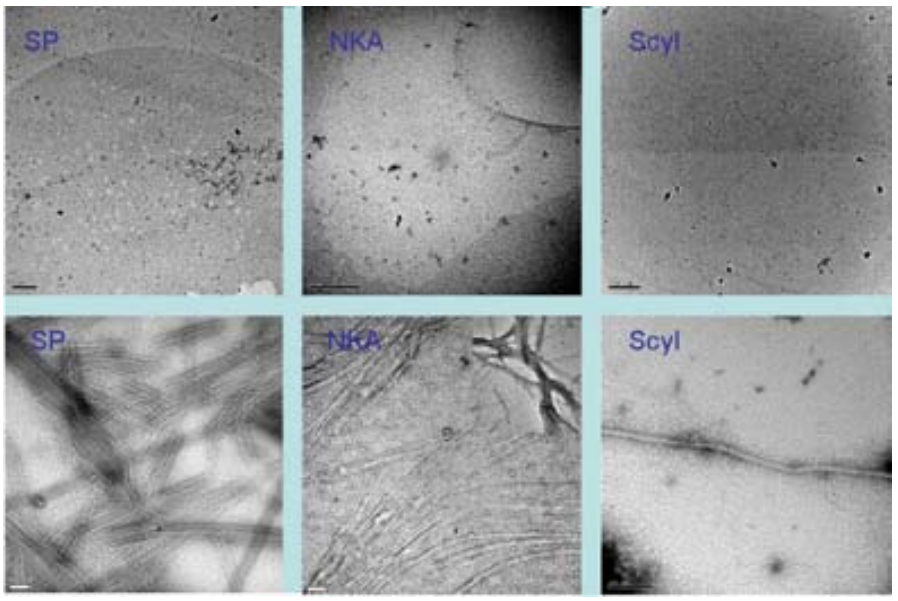

Figure 3.3.3 Negatively stained TEM images of the TKs in 10 mM SDS. Upper panel shows TKs in 100 μM. Lower panel shows TKs in 2 mM.
In all the cases, electron micrographs were obtained immediately after samples preparation. The buffer was sodium phosphate (5 mM, pH 7.0). Electron micrograph image in inset shows the polymorphic fibrils of NKA.

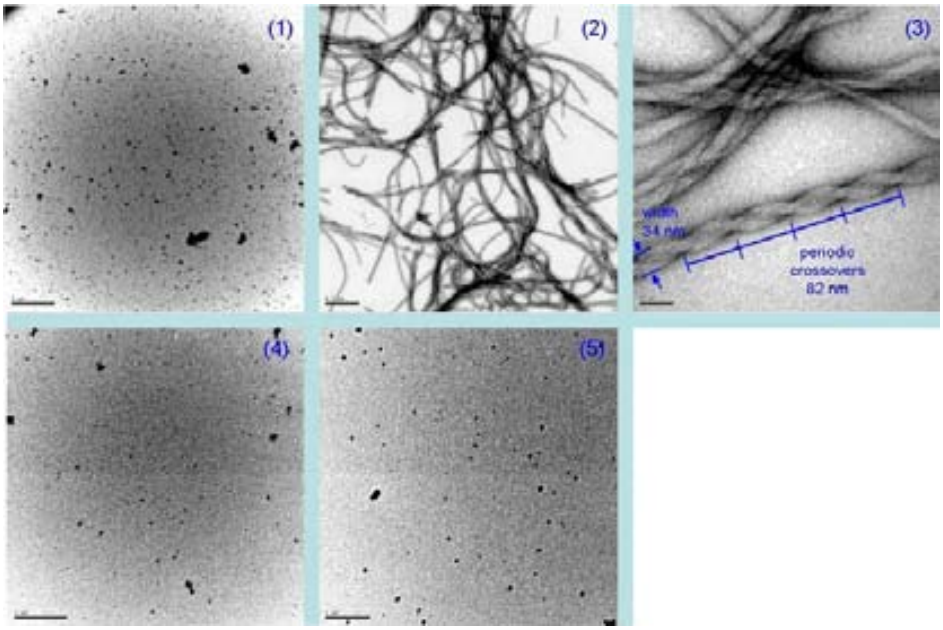

Figure 3.3.4. Morphology of the SP fibrils in the presence of the SDS (1 mM, close to CMC). No fibrils were detected by TEM immediately after sample preparation (1), while fibrils formed after incubation for overnight at room temperature with no agitation (2 and 3). Fibrils of SP show polymorphism (straight and twisted ribbons). Peptide concentration was 100 µM.
No fibrils were detected by TEM immediately and after over night incubation of SPW (4 and 5).

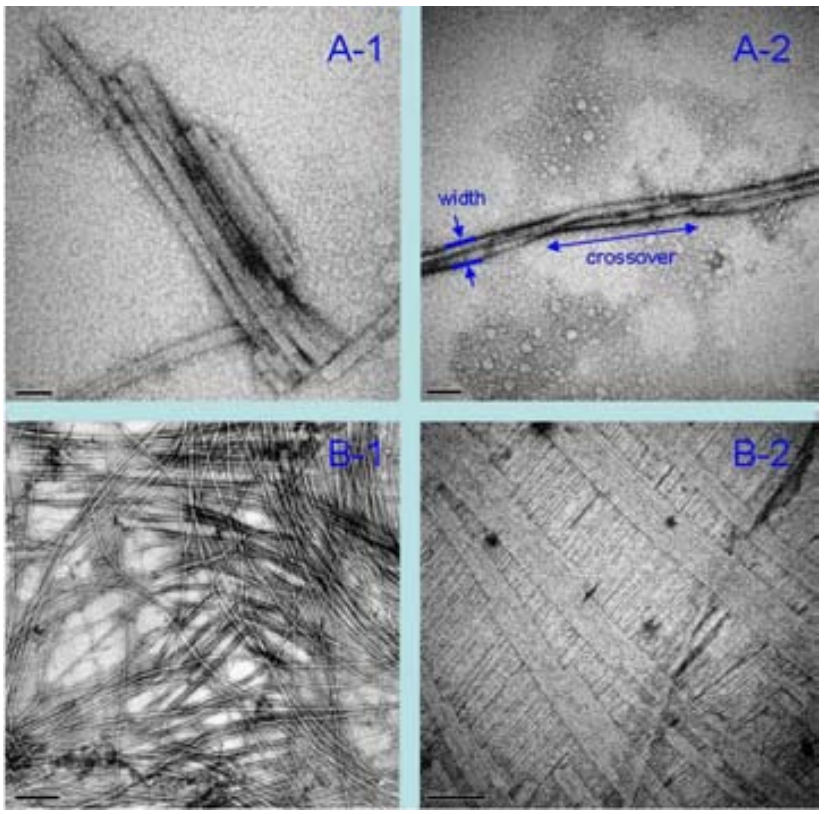

Figure 3.3.5. Polymorphism of the amyloid fibrils of NKA observed by TEM. Negatively stained electron micrograph images of the NKA (80 µM) in the SDS (4 mM) incubated for 24 h at room temperature: upper panel with agitation, and lower panel with no agitation.
A-1: short-length fibrillar clumps aligned laterally
A-2: periodically twisted ribbon with two or more protofilaments. Arrows indicate for crossover distance about 400 nm and width of about 65 nm.
B-1: long straight ribbons
B-2: flat ribbons of laterally aligned protofilaments parallel to the axis of the fibrils.

minutes. The resulting fibrils were polymorphic, twisting around each other or straight, with heterogeneity (details are indicated in Figure 5).

3.3.1. Structural characterization of TKs by FTIR

As is known, the CD is a powerful spectroscopic method to characterize secondary structures of peptides/proteins, although it is mostly sensitive to the alpha and beta structures.

In addition, some CD spectra present superposition of different structural conformations. In superimposed CD spectra, beta sheet structures can be masked due to the smaller molar extinction coefficients for beta structures relative to alpha helical structures.

On the other hand, FTIR spectroscopy has the advantage to detect distinctly the presence of different secondary components; moreover the aggregation is not obstacle like in CD. IR spectroscopy is weaker in the prediction of alpha helical structure but superior in the estimation of the beta sheet content of proteins. Therefore, CD and FTIR are two complementary techniques in the study of the secondary structure of peptides and proteins.

To characterize the secondary structural components and conformational transitions of the TKs peptides, the FTIR spectra were recorded in amide I' and amide II' in D_2O solutions in the equivalent conditions as the TEM (Figure 6 and 7). The IR spectra were analyzed in amide I' (D_2O) wavenumber range (1700 cm^{-1} to 1600 cm^{-1}), which arises primarily from stretching vibrations of main-chain carbonyl groups.

3.3.2. TKs secondary structures in aqueous solution

In aqueous solution the IR absorption spectra of the TK peptides are similar having a broad amide I' band with a maximum at about 1643-1647 cm^{-1} (Figure 6), attributed to an unordered structure , as the maximum of the band remains essentially unchanged within ±3 cm^{-1}.

To resolve the overlapping secondary components and to identify the "hidden" bands in the amide I' range we performed second derivative (SD) and Fourier deconvolution (FD) analysis (Figure 6, for FD parameters, see the legend). For SP peptide, apart from the main band centered at 1643 cm^{-1}, FD and SD resolved a low intense band at 1672 cm^{-1} ,which can be attributed to beta turns structure, and a shoulder at 1611 cm^{-1}, which most likely arise from beta sheet and/or side chain vibration of Arg residue (Barth, Andreas and Christian Zscherp 2002). FD and SD spectra of NKA did not show any additional band apart from the major absorption band at 1644 cm^{-1}. FD and SD spectra of ScyI displays the main band centered at 1645 cm^{-1}, and a shoulder at about 1628 cm^{-1} and a peak at 1611 cm^{-1}. Both bands can be assigned to the extended beta sheet structure; however it cannot be ruled out that the side chain vibration of Asp residue also may contribute to the small intensity peak resolved at 1611 cm^{-1}.

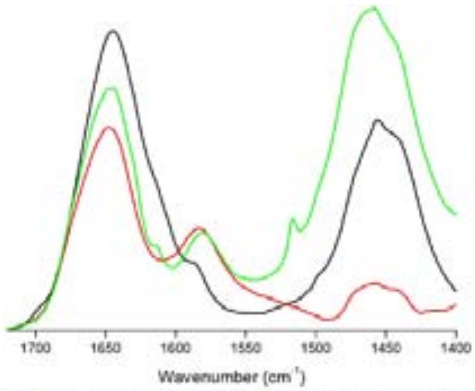

Figure 3.3.6. The amide I' and amide II' regions of the main FTIR spectra of 1.5 mM SP (—); NKA (—); and Scyl (—) in buffer (5 mM sodium phosphate, pD 7.0) at 15 °C. The TFA was removed from the peptides stocks. Samples were just incubated for 5 min at each temperature before collecting the spectra

Figure 3.3.7. The Fourier deconvolution (—) and second derivitives (—) of the main FTIR spectra of 1.5 mM (A) SP; (B) NKA; and (C) Scyl in buffer (5 mM sodium phosphate, pD 7.0) at 15 °C. The TFA was removed from the peptides stocks. Samples were just incubated for 5 min at each temperature before collecting the spectra. FD parameters were: K=1.5, FWHH=14 Lorentsian

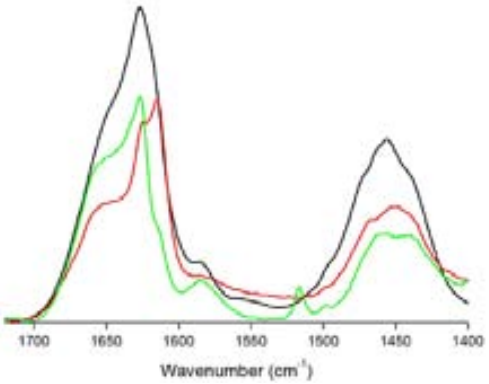

Figure 3.3.8. The amide I' and amide II' regions of the main FTIR spectra of 3 mM SP (—); NKA (—); and ScyI (—) in 20 mM DMPG LUVs. The buffer was 5 mM sodium phosphate (pD 7.0) . The TFA was removed from the peptides stocks. Samples were just incubated for 5 min at each temperature before collecting the spectra.

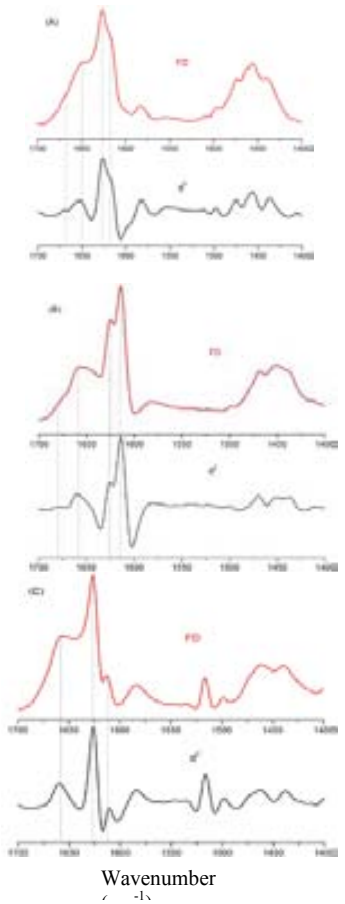

Figure 3.3.9. The Fourier deconvolution (—) and second derivitives (—) of the main FTIR spectra of 3 mM (A) SP; (B) NKA; and (C) ScyI in 20 mM DMPG LUVs. The buffer was 5 mM sodium phosphate (pD 7.0). The TFA was removed from the peptides stocks. Samples were just incubated for 5 min at each temperature before collecting the spectra. FD parameters were: K=1.5, FWHH=14 Lorentsian

Summarizing we can conclude that the major and intense band at 1643-48 cm^{-1} indicates for dominantly presence of the unordered structure of TKs in aqueous solutions, however it cannot be discarded the presence of other "hidden" secondary components which contribute to the intensity of this broad band.

3.3.3. *TKs secondary structures in phospholipid bilayers*

Figure 7 represents the IR absorption spectra of the TK peptides in the presence of the DMPG LUVs. SP and ScyI in DMPG produce IR absorption spectra with a narrower amide I' band and most intense band at 1626 cm^{-1}, while in NKA, IR absorption spectra the intensity of the band at 1611 cm^{-1} is more intense than the band at 1627 cm^{-1}.

The SD sand FD spectra of amide I' and II' of the SP reveals bands at 1625 cm^{-1}, 1670 cm^{1}, 1650 cm^{-1} and at 1584 cm^{-1}. The most intense band at 1625 cm^{-1} can be attributed to beta sheet component, while the band at 1670 cm^{-1} represent beta turn structural component (Juszczyk, P. et al. 2009). Assignment of the peak resolved at 1650 cm^{-1} can be attributed to helical or unordered structures (see below).

Using FD and SD analysis of NKA, the IR absorption spectra determine peaks at 1658, 1627 and 1615 cm^{-1} in amide I' and an small peak at 1584 cm^{-1} in amide II'. The peak at 1627 cm^{-1} can be assigned to beta sheet component, the broad peak at 1658 cm^{-1} can be attributed to helical structural component or unordered, while the peak at 1615 cm^{-1} can be assigned to that the beta strands, which may also have infrared bands at wavenumbers below 1620 cm^{-1}. In NKA, similarly to SP, beta sheet remains the dominant conformational arrangement with the presence of both parallel (at 1627 cm^{-1}) and antiparallel (at 1615 cm^{-1}) beta sheet components.

In ScyI, amide I' resolved peaks by FD and SD are placed at 1660 cm^{-1}, 1625 cm^{-1} and 1611 cm^{-1} in amide I' and at 1584 cm^{-1} and 1516 cm^{-1} in amide II'. Similarly to SP and NKA strong intense peak at 1625 cm^{-1} implies that beta sheet remains the dominant conformational motive and following the above assignment, the broad peak at 1660 cm^{-1} was assigned to unordered or helical segments.

Summarizing: in the three TK peptides, SD and FD analysis resolve a most significant beta sheet presence. The second strong band in the three peptides resolved by SD and FD is the band 1650 cm^{-1}; although there are controversial assignments of this band to helical

or unordered structures, we believe it indicates the presence of α helical structure in the peptides.

The vibration bands observed below 1628 cm^{-1} (at 1610-1628 cm^{-1}) usually are assigned to intermolecular hydrogen bonded extended beta sheets chains (Barth, Andreas and Christian Zscherp 2002). From the other side, care must be taken in interpreting the peaks at 1618-1620 cm^{-1} due to the contribution of vibration of some residues' side chains. Thus, the low wavenumber vibration at 1615 cm^{-1} (for NKA) and 1611 cm^{-1} (for SP and ScyI) indicates for beta sheets, however the relatively high intensity of these bands (especially in NKA) may reflect the contribution of the side chain vibrations of Arg for SP, His for NKA, and Tyr for ScyI (Barth, Andreas and Christian Zscherp 2002).

In all the TK peptides and in both solutions and DMPG, in the amide II (which is localized near 1550 cm^{-1} and reflects the presence of unexchanged amide hydrogens) a band at about 1584 cm^{-1} is resolved, which is most likely due to an overlap of vibrations from side chains of Asp, $\nu_{as}(COO^-)$; and Arg, $\nu_{as}(CN3H5^+)$ (Barth, Andreas and Christian Zscherp 2002).

Finally, the band at 1515 cm^{-1} in ScyI can be assigned to Tyr ring vibration.

Considering the TEM and FTIR experiments, the results reveal that fibrillogenesis of the peptides occurs by conformational changes of the TKs after addition of the DMPG LUVs, with an increase of the β sheet content of the peptides and decreased helical contributions. The structural information from the CD spectra is in agreement with the FTIR results.

3.3.4. Effect of SDS on the formation of fibrils and structural transitions in SP and its analogue SPW. Conformational switch between dominant PPII to beta sheet conformations

i). Fibrillization of SP. Time course studies of SP (100 μM) by TEM in the presence of SDS at concentration highly above CMC (10 mM) reveals no fibril formation for one week incubation at room temperature (see Table 1). In contrast, the equivalent sample, but in lower concentration of SDS, close to CMC (1 mM), shows the formation of fibrils after incubation overnight (Figure 4). The resulting fibrils were polymorphic, twisting around each other or straight. Twisted fibrils have a width of about 34 nm, consisting with the presence of several single strands. The crossovers are about 82 nm (see Figure 4, legend).

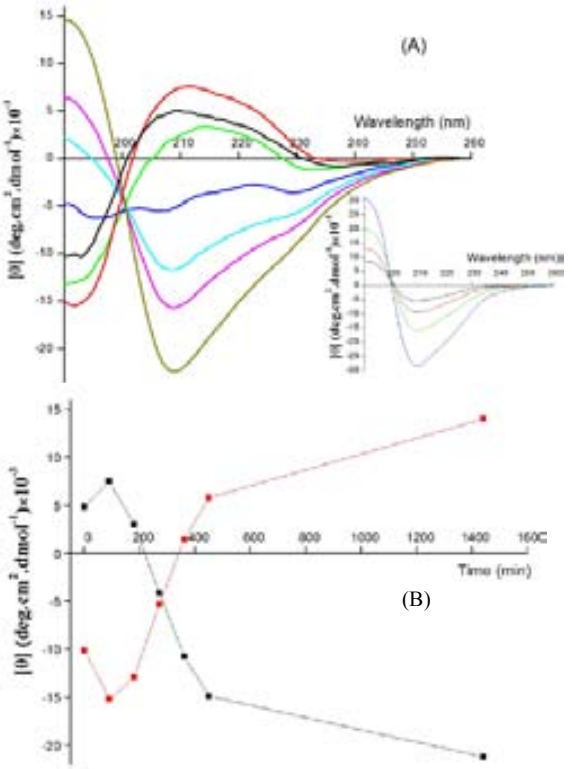

Figure 3.3.10. (A) CD spectra of 100 μM SP in 1 mM SDS, recorded: immediately after sample preparation (—); and after: 90 min (—); 180 min (—); 270 min (—); 360 min (—); 450 min (—); and overnight (—). The buffer was 5 mM sodium phosphate (pH 7.0), and the temperature was set at 15 C. Inset. Difference spectra of equivalent samples with (A); calculated by subtracting of the CD spectra after 90 (—), 270 (—), 360 (—) and 450 (—) min from that after overnight.
(B) Plot of the CD ellipticities of spectra in (A) at 210 nm (—) and 192 nm (—) as a function of the time

To characterize the conformational changes of SP during the incubation time, the CD spectra of the corresponding samples as in TEM were recorded (Figure 8). The initial CD spectrum of SP in 1 mM SDS at zero incubation time shows a broad positive band at about 215 nm and a negative band at about 192 nm and is consistent with a prior aggregation state. As we already demonstrated in part II of this thesis, the CD spectrum related to this sample indicates for a mixture of PPII and α helical structures (see page..., Figure…). Consistent with a monomeric state of the peptide as seen by the CD experiments, no fibrillar state was detected by TEM (see Table 1 and Figure 9). Throughout an incubation time up to 180 min, only the intensities of the peaks slightly decrease but the overall features of the spectra stay very similar (Figure 8). However at 270 min incubation time the CD spectrum undergoes significant changes, seen by the appearance of three negative

bands at about 196, 206 and 230 nm, suggesting for a superposition of different secondary components and intermediate structures. A further incubation to 360 min results in further changes as revealed by the appearance of a positive peak at about 191 nm and two distinct negative peaks at about 206 nm and 230 nm. Moreover the peak at 206 nm is about twice more intense than that of 230 nm. There is an isoelliptic point at about 200 nm, implying for a two-state structural transition. Over night incubation of sample only causes an increase of the intensities of the spectral bands, but overall spectrum features remain the same. From the other side the overall features of some of CD spectra recorded throughout different incubation time strongly suggest for superposition of different secondary structural components.

To understand more about these structural transitions, we calculated some difference CD spectra (Figure 8, inset), by subtracting the spectra recorded at different times from that with overnight incubation. The difference spectra show a negative band at about 210 nm and a positive peak at about 192 nm, suggesting for a β sheet structure, which increases by time. Considering both TEM and CD data, an increase of the β sheet content of the peptide with time occurred coherently with the fibrils formation.

ii). There are various beliefs about the possible roles of the aromatic residues in amyloid fibrillogenesis , on the fibrils morphology and the rate of fibrils formation. All TKs contain Phe residues (see Materials and Methods, Table 1). Moreover in SP the $Phe^{8}Phe^{9}$ form a motif. In regard to this, we wonder if the Phe-Phe motif in the SP would have some impact on the fibrillization process. As we have explained in the part II of the Results and Discussion, in order to study the interactions of the TKs with the membrane, we used SPW and NKAW analogues, in which Phe^{7} or Phe^{6} were substituted for Trp, respectively. As was detected by TEM we found that in contrast to SP, which forms fibrils in high concentration (3 mM) in aqueous solution (Figure 1), no fibrils are formed in SPW in the same condition as SP of (see Table 1). Moreover, an incubation of low concentration of SPW (100 μM) in 1 mM SDS (close to CMC) did not show any fibrils even after about three months (see Table 1 and Figure). This finding is also in contrast to the fibril formation of the SP in equivalent condition (compared to Figure 4).

To understand the possible conformational changes of SPW in the SDS, the CD spectra of the peptide in equivalent conditions as TEM experiments were recorded (Figure 10). CD

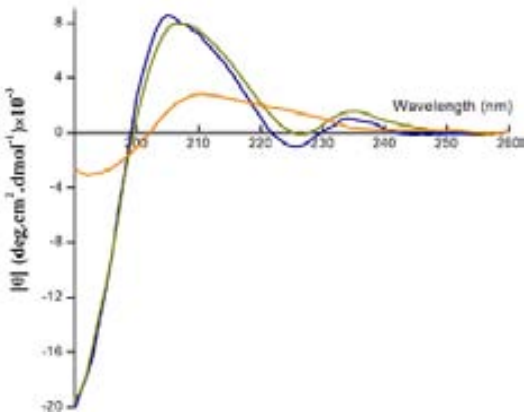

Figure 3.3.11. CD spectra of 100 μM SPW in SDS (1 mM), recorded immediately after preparation of sample (—), after overnight (—), and after 3 months (—).

spectrum of the peptide immediately after sample preparation shows two positive bands at about 207 nm and 235 nm, and a strong negative band at about 191 nm. This spectrum suggests for a dominant contribution of the PPII extended structure. The origin of the second positive band at 235 nm is more difficult for an assignment. Interestingly this peak is not seen in the corresponding spectrum of SP, and most likely is to assign it to aromatic Trp side chain. This has been suggested from studies of contribution of the Trp residues to CD spectra, which have demonstrated that peaks due to the aromatic side chain are usually at 230 nm. Incubation for about 24 hours did not cause significant changes of the spectrum. After a long incubation time of about three months, CD spectrum was recorded again and we observed mainly the decrease of the intensities of the positive and negative bands accompanied with wideness of the positive band. These findings clearly show that the substitution of Phe^8 for Trp^8 in SP completely abolishes the switch from PPII to beta sheet structure; as well it abolishes the formation of the fibrils. These finding are the first report about significance of the Phe^8 for structural conformational switch and fibrillization process in SP. Moreover, they demonstrate that nearly identical peptides have drastically different amyloid propensities, likely as previously reported for amyloidogenic peptide from human amylin, NFGAILSS, and its variants where Phe is substituted with Tyr and Trp and recently reported for Aβ16-22.

The crucial effect of the Phe[8] substituted Trp on the fibril formation of SP is highlighted when considering the fact that both substituted amino acids are aromatic and the peptide still has an intrinsic aromatic Phe[6] residue.

3.3.5. *Polymorphism within the amyloid fibrils of NKA*

It has been shown previously that an stirring during the incubation of some amyloid peptides can be critical for the morphology of the formed fibrils. To test these observations on NKA peptide we incubated NKA for 24 hours with and without stirring.

The electron micrograph images obtained from the NKA peptides (80 μM) in SDS (4 mM) incubated with strong stirring and with no stirring for 24 hours show clearly polymorphic fibrils within these samples (Figure 5, for details see the legend), indicating that formation of the polymorphic fibrils is independent of stirring in this case.

To understand whether stirring causes structural variations of peptides, we studied the CD spectra of the equivalent samples as the TEM. The CD spectrum of the sample with stirring has a minimum at about 221 nm and a positive band at 192 nm, suggesting the beta sheet structure as dominant conformation (Figure 11). In contrast, the spectrum of the sample with no stirring show overlap of the bands, as it has a negative peak at 202 nm and a shoulder at about 214 nm. Moreover, the ellipticity below about 192 nm is slightly positive indicating for a band slightly below the recorded wavelengths. Importantly for the samples incubated with the stirring we observed a strong increase of the HT voltages of these samples, compared to that of not incubated and no agitated, showing clearly that the sample aggregates due to the fibrils formation (Figure 11, inset, see the TEM). Although the CD spectra undergo some changes after incubation for about 4 months (compared to those which recorded after 24 hours), the overall features of the spectra remain completely different, (see Figure 11 and 12). After incubation for about 4 months, CD spectra of both samples show strong decreases in the amplitude of the signal as virtually the spectrum of the sample with stirring shows more significant conformational changes than the sample with no stirring. The CD spectrum of agitated sample shows appearance of a negative peak at 228 nm and a positive peak at 204 nm, suggesting for a beta turn conformation. This transition from dominant beta sheet to beta turn conformation strongly implies for polymorphism of formed fibrils. On the other hand, the CD spectrum

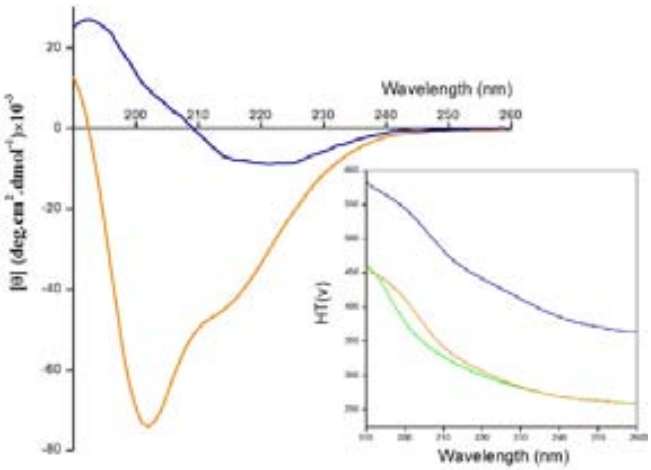

Figure 3.3.12. CD spectra of 80 μM NKA in 4 mM SDS recorded after incubation for 24 hours at room temperature with stirring (⟷) and with no stirring (—). Inset. Plots of the CD HT voltages as a function of wavelengths corresponding to the CD spectra of NKA. The green curve (control) is the HT plot of the same sample but with no incubation time. The buffer was sodium phosphate (5 mM, pH 7.0).

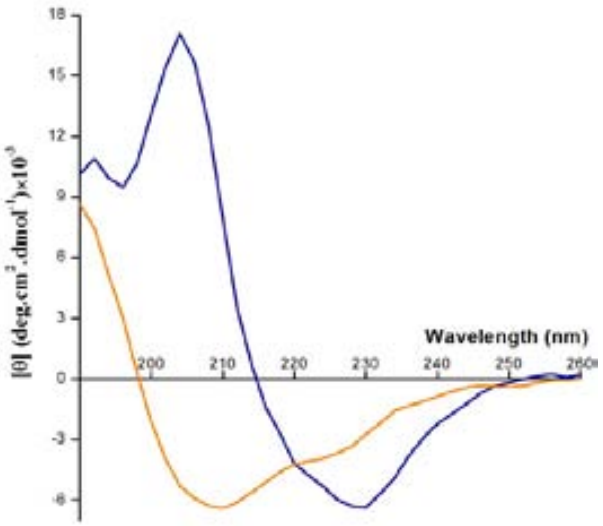

Figure 3.3.13. CD spectra of 80 μM NKA in 4 mM SDS incubated for 4 months with different initial preparation processes. Blue spectrum corresponds to the sample incubated at room temperature whith agitation for 24 hours, while the orange is related to that with no agitation. After 24 hours, both the samples were kept at room temperature with no agitation until the spectra were recorded. The buffer was 5 mM sodium phosphate (pH 7.0).

of the sample with no stirring reveals a similar overall feature (a negative peak at about 210 nm, a shoulder at about 225 nm and the positive band below 198 nm), but with less intensities.

Using the fluorescence spectroscopy, ThT assay was applied in the same condition as TEM to monitor the formation of beta sheet amyloid fibrils. Increase of the ThT fluorescence at 486 nm was observed in both agitated and no agitated samples (Figure 13).

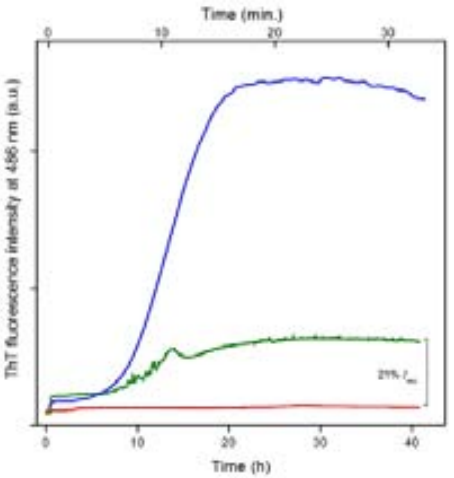

Figure 3.3.14. Time course studies of NKA (80 mM) fibrillization in the presence of low concentration of SDS (4 mM), using ThT (5 mM) fluorescence assay. The red curve correspond to the control: ThT alone in SDS (4 mM) with stirring. The blue and green curves, respectively, present the ThT fluorescence changes in the presence of NKA and SDS with stirring and with no stirring.
In all the cases, excitation was set to 425 nm and intensities were recorded at 486 nm.
Temperature was at 22 °C.

The ThT intensity was increased after about 4 min and 7 hours for agitated and no agitated samples, respectively, and reflects much decrease of the lag time in the presence of the stirring. Changes of the ThT intensity in the case of stirring occurred very fast (in about 12 min), while for no agitated sample it was much slower (about 14 hours), showing the necessity of the longer time for amyloid fibril elongation in the absence of stirring. Moreover, increase of the ThT intensity was about 5 times more in the case of agitated sample than that of no agitated, which may be related to the higher amount of beta sheet amyloid fibrils due to the stirring.

3.3.6. Conformational transition of TKs in SDS micelles detected by CD. Peptide dilution experiments

As we have discussed in part II of Results and Discussion, in SDS micelles SP and ScyI in low concentrations (about 100 μM) form dominantly helical conformation, while in the case of NKA this conformation is partially helical structure (mixture of helical and unordered structures).

However, the CD spectra of TKs in high concentrations (between 2-3 mM depending on peptide) in SDS micelles (highly above CMC at about 20 mM) show a negative peak at about 229 nm, suggesting presence of a beta sheet conformation (Figure 14-16).

In case of SP, decrease of the peptide concentration to 2 mM caused a blue shift of the negative band to 224 nm (Figure 14). Further decreases of the concentration to 1 mM caused a dramatically change of the spectrum as a positive peak appear at 198 nm, and two negative peaks at 208 nm and 224 nm, representative of alpha helical structure. More dilution of the peptide only caused small changes of the band intensity.

In the case of NKA, the dilution of peptide concentration to 0.75 mM caused a blue shift of negative band and a small positive band appeared (Figure 15). Further dilution of the peptide caused some spectral changes as in 98 μM a positive peak at 198 nm and two negative bands at about 207 nm and 226 nm appeared, suggesting for a helical conformation.

In case of ScyI the dilution of the peptide to 1.25 mM dramatically changes the overall features of the spectrum, as a positive band appeared at 210 nm and a negative band get more intense at about 225 nm (Figure 16). Further dilution of the peptide caused shifts of the spectral bands to a lower wavelengths in the spectra, as in 156 μM peptide the spectrum has a broad negative band at about 225 nm and a positive band at 205 nm, implying some superposition of spectral bands.

In all cases, the CD HT voltages curves show a decrease of the HT voltage signal with the peptide dilution, indicating changes in the size of the particles in samples (Figures 14-16, insets).

Altogether these data imply that upon increases of the peptide concentration above some threshold range (depending of the peptide) TKs undergo conformational transitions from dominant helical (in low concentration) to beta sheets (in high concentration) structures and these transitions are reversible. Obviously at some level of the TKs peptide concentration in SDS micelles solution, a competition between the interaction of the monomer peptides with SDS micelles and it self-association exists. This process results in the formation of peptide aggregates visibly detected by the increase of the HT voltage. At the present, these conformational transitions can be only related to aggregation phenomena. To identify the morphology of these aggregates further TEM assays is

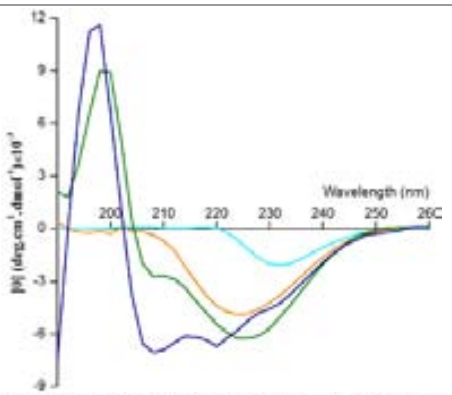

Figure 3.3.15. CD spectra of SP dillutions: 2 mM (—), 0.5 mM (—), 0.1 mM (—), and 0.05 mM (—); in the presence of 20 mM SDS. The buffer was sodium phosphate (5 mM, pH 7.0). The spectra were recorded immediately after samples preparation, with no stirring, at 22 °C.

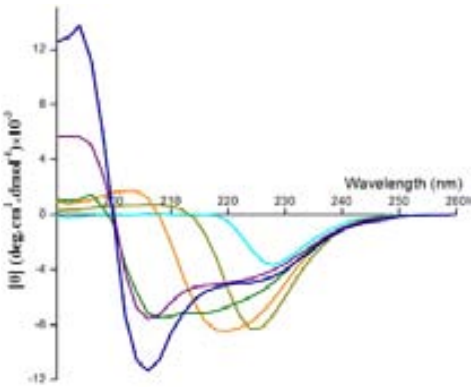

Figure 3.3.16. CD spectra of NKA dillutions: 3 mM (—), 1.5 mM (—), 0.75 mM (—), 0.375 mM (—), 0.187 mM (—), and 0.094 mM (—); in the presence of 20 mM SDS. The buffer was sodium phosphate (5 mM, pH 7.0). All the spectra were recorded immediately after samples preparation, with no stirring at 22 °C.

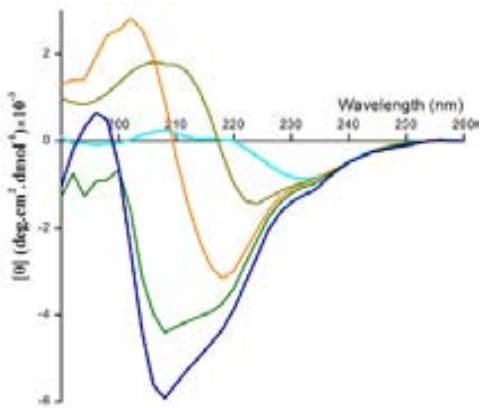

Figure 3.3.17. CD spectra of Scyl dillutions: 2.5 mM (—), 1.25 mM (—), 0.625 mM (—), 0.312 mM (—), and 0.156 mM (—); in the presence of 20 mM SDS. The buffer was sodium phosphate (5 mM, pH 7.0). All the spectra were recorded immediately after samples preparation, with no stirring, at 22 °C.

required. Furthermore at the present, we can not address these observations to stability of the morphological fibrillization in these samples.

3.3.7. *Effects of the pH on amyloidogenesis of NKA and NKAW*

CD measurements of the TKs in SDS micelles at different pH have shown that only NKA peptide undergo structural changes on pH. To get some information on how the pH affects the fibrillization of NKA we study the time course amyloidogenesis of NKA at different pH by ThT fluorescence and CD spectroscopy.

NKA

At acidic pH (3.8), CD spectrum of 80 µM NKA in 4 mM SDS micelles (immediately recorded after preparation of sample) has a shoulder at about 218 nm and a negative band at about 200 nm, implying for the dominant PPII structure of peptide (Figure 17A). After an incubation of the sample for 75 min with strong stirring, the CD spectrum shows a negative peak at about 220 nm and a positive band at about 199 nm, suggesting for the formation of some beta sheet structure (Figure 17A). Equivalent experiment with ThT shows that immediately after addition of low concentration of NKA (80 µM), the intensity of ThT at 486 nm increases significantly, indicating formation of amyloid fibrils (Figure 18). After about 75 min the intensity of ThT did not change significantly. These findings demonstrate clearly that the spectral transition from a PPII to beta sheet conformation correlates with the formation of the amyloid fibrils.

At neutral pH (7.0), the CD spectrum of 80 µM NKA in 4 mM SDS (recorded immediately after preparation of sample) indicates intermediate structure of PPII transition to partially alpha helix Figure 17B (see also part II of Results and Discussion, Figure…). The CD spectrum of this sample after incubation for about 30 min with strong stirring shows a strong positive band at about 208 nm and a weak negative peak at about 236 nm (Figure 17B). Moreover the negative ellipticity slightly below 195 nm indicates for a negative peak slightly below the recorded wavelengths. Altogether, these spectral features suggest that this spectrum may relate to the presence of some beta turn structures formation. ThT experiment in the same condition as CD shows that at pH 7.0, the intensity of ThT increased few min after the addition of NKA in a sigmoidal shape and the signal

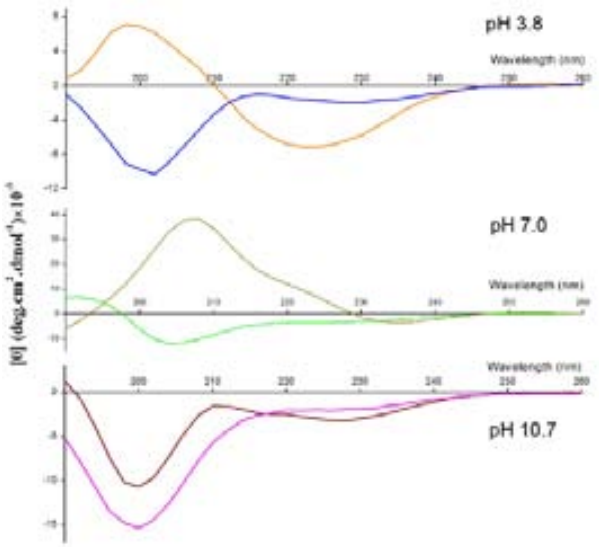

Figure 3.3.18. CD spectra of NKA (80 μM) in SDS (4 mM) and at different pH recorded immediately (——, ——, ——) and after incubation for 14 h with strong stirring (——, ——, ——). All the spectra were recorded at 25 °C.

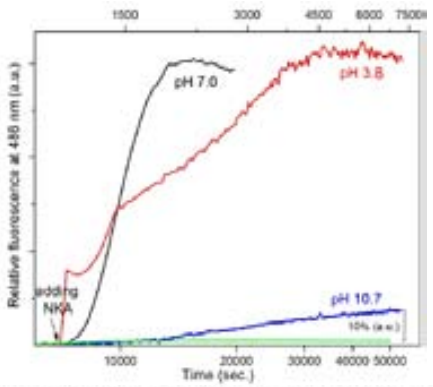

Figure 3.3.19. Time course studies of NKA (80 μM) fibrillization in the presence of low concentration of SDS (4 mM), using ThT (5 μM) fluorescence assay. The black, red and blue curves, respectively, present the ThT fluorescence changes at pH 7.0, 3.8 and 10.7. The green curve correspond to the control: ThT alone in SDS (4 mM) with stirring. Upper time course belongs to pH 3.8 and 10.7; and lower time course belong to pH 10.7. In all the cases, excitation was set to 425 nm and intensities were recorded at 486 nm. Temperature was at 22 °C.

reaches to a plateau after about 30 min, which represents the formation of amyloid fibrils (Figure 18).

At alkaline pH 10.7, the CD spectrum of NKA (80 μM) in 4 mM SDS, recorded immediately after preparation of the sample, has a shoulder at about 215 nm and a negative peak at about 200 nm, implying for a dominant PPII structure of peptide (Figure 17C). After the incubation of the sample for about 14 h no significant changes were seen in the spectrum, although a small decrease of the intensity of the negative peak occurred

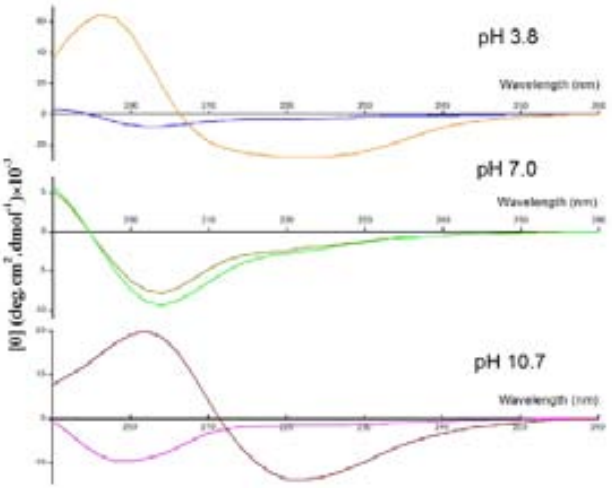

Figure 3.3.20. CD spectra of NKAW (80 μM) in SDS (4 mM) and at different pH recorded immediately (——, ——, ——) and after overnight incubation with strong stirring (——, ——, ——). All the spectra were recorded at 25 °C.

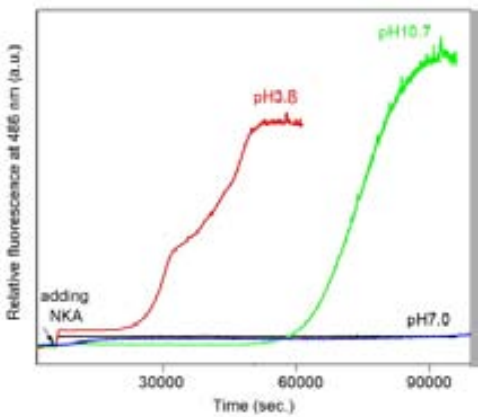

Figure 3.3.21. Time course studies of NKAW (80 μM) fibrillization in the presence of low concentration of SDS (4 mM), using ThT (5 μM) fluorescence assay. The black, red and green curves, respectively, present the ThT fluorescence changes at pH 7.0, 3.8 and 10.7. The blue curve correspond to the control: ThT alone in SDS (4 mM) with stirring. In all the cases, excitation was set to 425 nm and intensities were recorded at 486 nm. Temperature was at 22 °C.

(Figure 17C). ThT experiment of the equivalent sample shows a small (10% compare to similar conditions but at pH 3.8 and 7.0) increase of the ThT intensity after addition of peptide (Figure 18). Compare to pH 3.8 and 7.0, ThT assay indicate for a few amyloid formation of the peptide at pH 10.7 after incubation.

NKAW

At acidic pH (3.8), the CD spectrum of the NKAW (80 μM) in SDS (4 mM) (immediately recorded after sample preparation) shows two negative peaks at about 220 nm and 205 nm, and positive ellipticity below about 195 nm (Figure 19A). The spectrum suggests an overlapping of spectra, most probably related to the intermediate structures of PPII and alpha helical. Atypical CD spectrum of incubated sample (after overnight, with stirring) indicates a broad negative band at about 220 nm and a positive peak at about 198 nm (Figure 19A). The ThT assay of the equivalent sample (Figure 20) shows no changes of the intensity for about 6 h after addition of peptide (lag time). Then, the intensity increases for about 8 h (elongation time) and reaches to a plateau. ThT assay indicates formation of the amyloid fibrils for NKAW at pH 3.8.

At neutral pH (7.0), overall features of the CD spectrum of the NKAW, immediately recorded after preparation of sample, is very similar to that at pH 3.8, containing two negative peaks at about 205 nm and 220 nm and positive ellipticity below about 195 nm (Figure 19B). However in contrast to acidic pH (3.8), the CD spectrum of the NKAW at pH 7.0 did not change significantly after overnight incubation (Figure 19B). ThT assay of the equivalent sample implies no formation of the amyloid fibrils, since ThT intensity did not change compared to the control (Figure 20).

At alkaline pH (10.7), the CD spectrum of NKAW, immediately recorded after preparation of sample in low concentration of SDS (below CMC) has a shoulder at about 220 nm and a negative band at about 198 nm, suggesting for a PPII structure of the peptides (Figure 19C). The CD spectrum of the sample after overnight incubation with strong stirring shows a negative peak at about 220 nm and a positive peak at about 204 nm, suggesting for a beta sheet structure of peptides (Figure 19C). ThT assay of equivalent sample (Figure 20) indicate no changes of the ThT intensity in about 15 h after addition of the peptide (lag time). Then, intensity increases following a sigmoidal shape and after about 10 h (elongation time) reaches to a plateau. ThT assay reveals the formation of the amyloid fibrils in this case.

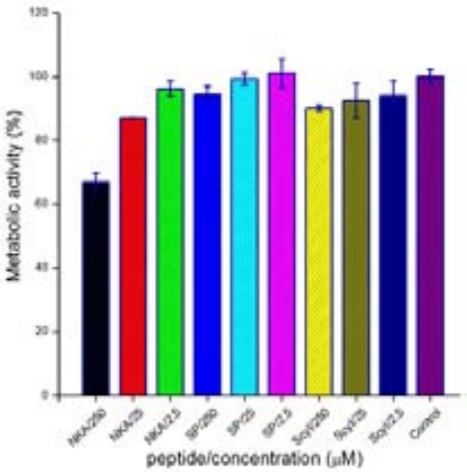

Figure 3.3.22. Metabolic activity of the PC12 cell lines after the treatment with the TKs for 24 hours. Cell metabolic activity was measured by MTT assay. TK peptides in various concentrations (2.5, 25 and 250 μM) were added to the cells dissolved in water. The control corresponds to the metabolic activity of the cells in the absence of TKs. 96 well plates were used and 20000 cel./well were seeded. Error bars are standard errors.

3.3.9. Effects of the TKs on the cell metabolic activity

MTT test was applied to study the effects of the TKs on the metabolic activity of PC12 cells. TKs were added at a concentrations of 2.5, 25 and 250 μM to the cells and incubated for 24 h (Figure 21). The results indicate that in the presence of 2.5 to 250 μM SP and ScyI, metabolic activity of the cells did not change significantly after 24 h. Similarly, incubation of 2.5 NKA with the cells did not change the metabolic activity of the cells while in contrast, 25 and 250 μM of NKA was toxic for the cells and caused a decrease of about 30±4% of the cells' metabolic activities.

Table 1. Summary of the fibrillar state of SP in the conditions studied in this research.

Media	**Peptide concentrations**	**Incubation period[b]**	Fibril formation
buffer[a]	80 μM	one week	-
buffer[a]	100 μM	immediately	-
10 mM SDS[a]	100 μM	one week	-
20 mM SDS	100 μM	one week	-
0.75 mM DMPC	1.5 mM	immediately	-
buffer[a]	3 mM	immediately	+
1 mM SDS	2 mM	immediately	+
10 mM SDS	2 mM	immediately	+
10 mM DMPG	1.5 mM	immediately	+
5 mM DMPG	0.75 mM	immediately	+

[a] phosphate buffer (5mM, pH 7.0)
[b] at the room-temperature

Table 2. Summary of the fibrillar state of NKA in the conditions studied in this research.

Media	**Peptide concentrations**	**Incubation period[b]**	Fibril formation
buffer[a]	80μM	overnight	-
buffer[a]	2mM	immediately	-
10mM SDS	100μM	immediately	-
20mM SDS	100μM	overnight	-
0.75 mM DMPC	1.5 mM	immediately	-
buffer[a]	3mM	immediately	+
4mM SDS	80μM	immediately[c]	+
4mM SDS	80μM	overnight	+
10mM SDS	2mM	immediately	+
10mM DMPG	1.5mM	immediately	+

[a] sodium phosphate buffer (5mM, pH 7.0)
[b] at the room-temperature

[c] In this condition, the amount of fibrils observed in each grid was much less compare to the other conditions of fibrillar states of the peptide.

Table 3. Summary of the fibrillar state of ScyI in the conditions studied in this research.

Media	**Peptide concentrations**	**Incubation period**[b]	Fibril formation
buffer[a]	80μM	overnight	-
8mM SDS	80μM	immediately	-
8mM SDS	80μM	overnight	-
20mM SDS	100μM	immediately	-
20mM SDS	100μM	overnight	-
0.75 mM DMPC	1.5 mM	immediately	-
buffer[a]	3mM	immediately	+
8mM SDS	80μM	after one week	+
10mM SDS	2mM	immediately	+
10mM DMPG	1.5mM	immediately	+
5mM DMPG	0.75mM	overnight	+

[a] sodium phosphate buffer (5mM, pH 7.0)
[b] at the room-temperature

Table 4. Comparison of the fibrillar state of SP and SPW in 1 mM SDS[a]. In all cases, peptide concentration was 100μM.

peptide	**Incubation period**[b]	Fibril formation
SP	immediately	-
SP	overnight	+
SPW	immediately	-
SPW	overnight	-

[a] in sodium phosphate buffer (5mM, pH 7.0)
[b] at the room-temperature

Barth, Andreas and Christian Zscherp. 2002. What vibrations tell us about the proteins. *Quarterly Reviews of Biophysics* 35 (4):369.

Gorbenko, G. P. and P. K. Kinnunen. 2006. The role of lipid-protein interactions in amyloid-type protein fibril formation. *Chem Phys Lipids* 141 (1-2):72-82.

Juszczyk, P., A. S. Kolodziejczyk and Z. Grzonka. 2009. FTIR spectroscopic studies on aggregation process of the beta-amyloid 11-28 fragment and its variants. *J Pept Sci* 15 (1):23-29.

GENERAL DISCUSSION

Tachykinins are ligands for Neurokinin (NK) receptors belonging to the G-protein coupled receptor (GPCRs) family. By binding to the NK receptors they transfer numerous signals between the cells of an organism. Defects in ligand-receptor interactions have been shown to affect inter- and intra-cellular signaling process and are considered as one of the main reasons for many human diseases. In this line, knowledge about molecular mechanism of ligand- receptor interactions is basic for understanding how these proteins perform their function.

One of the basic questions in studying molecular mechanism of the mechanism of ligand-receptor interactions relates to the role of the cell surface. Like the other members of GPCRs family, the NK receptors, as membrane proteins are imbedded into membrane by 7 trans-membrane domains, connected by EC and CP loops segments floating above the membrane surface. Moreover the cell surface is the place where the signal comes from and further is transferred to the receptor.

According to the membrane-compartment theory, the target cell surface has an important role in the biological activity of TKs by increasing the peptide concentration at the membrane surface and by inducing preferred conformations and orientations. Other authors, however, believe that membrane surface is not directly involved into the binding of TKs to its receptor, but is only a place for the neuropeptide storage. Both theories most likely cooperate in catalyzing ligand-receptor interactions .

Studies of ligands and neuropeptides in membrane mimic systems have been proposed to adopt conformations that are relevant for receptor recognition, and that might more closely resemble the receptor-bound state. Furthermore it has been shown that membrane mimetic systems are quite capable of inducing structures in small neuropeptides, which may hold some biological relevance. Moreover, mimicking the conformations of other bound ligands in membrane mimic environment has been proven to be a successful approach for drug designs of inhibitors.

Therefore, the study of conformations and binding properties of the TKs in membrane mimetic systems is a relevant approach for understanding the factors which govern these

conformations, in particular what is the role of the membrane bilayer for adopting different conformations.

The TKs share common C-terminal segment, considered as a "address" segment and differ in their N-segment, so called the "message" segment. The idea of a message-address model for the tachykinins and their receptors is attractive in ligand-receptor recognition process, but the assumption that the ligands are selective for the receptors based solely on their primary sequence is oversimplified. The conformation factor is a critical aspect essential for understanding why homology peptides have different activities as agonists for NK receptors.

In this research we investigated the TKs peptides at two levels: in non aggregate monomeric state and in self-associated fiblilar state. In normal physiological conditions, TKs concentration in the body has been estimated to be relatively low, about 10 μM for SP (Choo, L. P. et al. 1994). However in some neurodegenerative diseases, over expression and increase of SP and NKA content has been found. Therefore knowledge about self-aggregation ability, the morphology of the aggregates and their structure as well as the factors that promote or inhibit the self assembling is an important factor when considering the role of TKs in neurodegenerative diseases. Applying FTIR and CD spectroscopy, we understood that TKs in some special conditions adopt beta sheet structure. This finding raises the question about the origin of this structure. By using electron transmission microscopy, we found a formation of fibrils in the same conditions as we observed beta sheet structure.

In respect to the mentioned levels of TKs, we discuss our data and compare them with previously published data.

Considering TKs as ligands of the NK GPCR receptors

Identification of the polyproline II (PPII) conformation in Tachykinins

Previous studies on SP, NKA and ScyI have reported structural data, basically based on spectroscopic and MD data (Dike, A. and S. M. Cowsik 2005.Prabhu, A. et al. 2005.Qi, X. F. et al. 2000.Williams, R. W. and J. L. Weaver 1990). However, in these reports, whatever solutions or membrane mimic systems the peptides had been studied, the PPII extended structure was not reported as conformational segment of the TKs. In fact, CD spectra of SP in aqueous solutions and in zwitterionic lysophosphatidylcholine micelles in the show spectral features very similar to those reported here, but the authors assigned them to the random coil structures (Chassaing, G. et al. 1986.Seelig, A. et al. 1996.Woolley, G. A. and C. M. Deber 1987.Wu, C. S. et al. 1982).

In this thesis we presented solid experimental evidences that PPII extended helical structure forms in the TKs and moreover is a predominant structural conformation of the peptides in solutions, sub-micellar concentrations of SDS and DMPC vesicles.

Both unordered and PPII structures share very similar spectral features, but they differ into their properties .The PPII structure lacks intermolecular hydrogen bonds, which make it flexible, but it can form intermolecular hydrogen bonds with the solution or other peptide protein. Having into mind that the PPII structure conformation is temperature dependent, we have performed CD experiments to distinguish it from unordered. Based on CD data analysis we have demonstrated that the formation and stabilization of the spectral form observed in the TKs in solutions at sub-micellar concentrations of SDS and DMPC vesicles is a temperature-dependent reversible process. The PPII conformation of TKs occurs as a dominant conformation in these conditions as in aqueous solutions at 5 ˚C was estimated to be 50% of overall secondary structure of the peptides. Moreover both the formation and disruption of PPII conformation in aqueous solutions is a non-cooperative process, indicating that the conformation is deficient of intramolecular hydrogen bonds, which further strengths its assignment. Formation of PPII structure in aqueous suggest that its formation might depend on the primary sequence properties. However PPII conformation was identified as a conformational motif of TKs also in SDS in concentrations below CMC of the surfactant and in zwitterionic DMPC. From the other side, binding studies of the peptides (Trp fluorescence, Figures X, Y; and FPE experiments, Figure…) have revealed interaction and binding of the TKs. Although the

binding experiments do not give direct evidence on which residues are involved into binding in all conditions where CD spectra reported a dominant PPII conformation in the TKs, the fluorescence experiments demonstrated that Trp side chain faces the hydrophilic environment, thus ruling out that the peptide segments of SPW or NKAW including Trp, partition into the hydrophobic core of the micelle. These data are consistent with previous data reporting that peptide segments forming PPII conformation were well exposed to the solvent (Rucker, A. L. and T. P. Creamer 2002). Altogether these data can be interpreted in the light that the electrostatic interactions between the peptide and negatively charged SDS monomers or zwiterionic DMPC might stabilize it formation. This interpretation is consistent with the hypothesis of Arunkumar and coworkers (1997) about an important role of the electrostatic interactions in stabilization of the PPII helical structure.

On the basis of our CD and fluorescence data we found that the interaction between TKs and the membrane mimetics and formation of stable secondary conformations strongly depends on peptide environment. It is worth comparing the fluorescence with CD data, reporting the conformation of SP and NKA in these conditions. While in aqueous solutions, sub-micellar concentrations of SDS and DMPC liposomes the extended PPII helical structure appears to be the most preferred and dominant conformation for SP and NKA, in SDS micelles and DMPG liposomes the alpha helical conformation is stabilized and appears as the dominant conformation for SP. We found that in the process of conformation switch between PPII and unordered in non membrane mimic systems to helical structure in micelles and liposomes, the membrane surface charge density is an important factor not only for the formation but for its stabilization and the amount of helical component. As the CD data demonstrate, an increase of DMPC percentage in DMPG/DMPC liposomes leads to a decrease of helicity of TKs; in pure DMPC liposomes the extended PPII helical structure appears to be the most preferred and dominant conformation. This indicates that hydrophobic interactions between the peptides and the zwitterionic DMPC liposomes are not sufficient to promote alpha helical conformation even though DMPC has the same hydrophobic potential, 12-carbon hydrophobic tail, as DMPG. On the contrary, the negatively charged SDS micelles and

DMPG liposomes are able to induce alpha helical folding of TKs. CD spectra of TKs in SDS surfactant below the CMC represent mainly the extended PPII helical conformation. Sub-micellar SDS is a mixed solvent system, providing a partially organic (low dielectric) and a partially aqueous environment.

With increase of SDS concentration the dominant presence of PPII conformation is lost, and when SDS concentration reaches the CMC, the secondary structure of TKs is dominated by the alpha helical conformation. These findings point out that electrostatic interactions between membrane-mimetic and the charged residues of SP are essential prerequisites for efficient alpha helical fold. The electrostatic interactions between peptides and negatively charged lipids have been proposed as driving forces for binding of some peptides to membranes (Bordag, N. and S. Keller.Lazarova, T. et al. 2004).

Factors governing the secondary structures of Tachykinin peptides

Hydrophobic environment

To determine the TKs conformation(s) in a membrane-mimetic environment, we first analyzed the CD spectra of the peptides in the presence of SDS micelles, a system widely used in previously structural studies of membrane active peptides (Lazarova, T. et al. 2004).

Micellar systems have been used extensively in spectroscopic studies of peptide-membrane interaction as membrane mimics and their ability to induce conformations in neuropeptides that are biologically relevant have been studied. Among them, SDS micelles have been widely adopted to study peptide- and protein-lipid interactions.

In the presence of SDS micelles (pH 7.0), the CD spectra of SP and ScyI indicate dominant alpha helical conformation, and the CD spectrum of NKA shows a mixture of alpha and unordered structures. The structural transition from extended PPII helical structure in aqueous solutions to alpha helical in SDS micelles raises the question of how the peptide environment controls and stabilizes these two different conformations. To address this question, we recorded CD spectra of TKs in SDS solutions below and above the CMC. On the other hand, we determined the CMC of SDS in the presence of SP,

NKA and ScyI, respectively, as 0.9, 7 and 0.6 mM. In the presence of the SDS monomers, TKs are in PPII structures while upon micelles formation the dominant secondary structure is alpha helical. On the other hand, in aqueous solution λ_{max} is at about 350 nm, indicates that Trp is totally exposed to the media solution. Upon micelles formation, λ_{max} undergo a significant blue shift to about 339 and 334 nm, respectively, for SPW and NKAW, point out the insertion of Trp side chain into the hydrophobic core of this membrane mimetic. This is in agreement with NMR studies reporting the insertion of Phe residue of SP into the micelles (Beard, D. J. et al. 2007). Based on thermodynamic considerations, CD and Infrared spectroscopy, Schwyzer (1986) proposed an alpha helical conformation of the residues Pro^4 to Met^{11}, while there are some reports indicating the helical content of SP in the region from Pro^4 to Phe^8. Qi and coworkers (2000) used CD, NMR and molecular modeling to study SP conformation. They show that SP is capable of adopting a helical structure involving in particularly, residues Phe^7 to Met^{11}. NMR studies indicate that replacement of Phe^8 in SP by Tyr alters the helical conformation of the peptide to beta turn in lipid bilayers, while two-dimensional NMR and restrained simulated annealing calculations indicate that there is not major difference in the structures of SP and [Tyr^8]SP in zwitterionic and negatively charged micellar media.

Based on NMR studies, it is shown that in SDS micelles, NKA adopts helical structure from residues 6 to 9 with an extended N-terminus (Chandrashekar, I. R. and S. M. Cowsik 2003.Whitehead, T. L. et al. 1998). Other report indicates the extended conformation of NKA in aqueous solution while it has a helical conformation in the central core and the C-terminal region (Asp^4-Met^{10}) and possible turn structures in N-terminus in the presence of perdeuterated DPC micelles (Chandrashekar, I. R. and S. M. Cowsik 2003).

Membrane charges

The TKs-membrane interactions appear to be rather complex, involving hydrophobic and electrostatic interactions and charge density on the membrane surface (Keire, D. A. and

T. G. Fletcher 1996). To attest to the impact on each of these components for promotion of a stable peptide conformation, we performed experiments in solvents and in two membrane-mimetic environments, liposomes and micelles, varying the head-lipid charge and the concentration of SDS surfactant. TKs are amphipathic peptides, and it is reasonable to assume that the positively charged N-terminal would have a strong impact on the peptide binding through electrostatic interactions with the anionic components of the membrane. Indeed, our experiments support this assumption, demonstrating that the Trp side chain of SPW and NKAW are inserted into the hydrophobic environment of the negatively charged SDS micelles or DMPG liposomes, but it faces the hydrophilic aqueous region in the zwitterionic DMPC liposomes. The red shift of the Trp emission maximum upon an increase of DMPC percentage in mixed DMPG/DMPC liposomes reflects the transfer of Trp to a more hydrophilic environment and its full exposure to water in pure DMPC. These findings are in agreement with NMR data reporting that SP amides are not protected from solvent exchange in zwitterionic dodecylphosphocholine (Auge, S. et al. 2000).

Moreover, increase of the Phe-CN SP fluorescence intensity in this study is consistent with the previous reports indicating increase of Phe-CN intensity upon formation of alpha helix in proteins in TFE.

The mechanism by which neuropeptides bind to micelles has been previously studied by several research groups, however, the findings are contradictory in several cases. Our results, indicating the binding of TKs to zwitterionic and negatively charged lipid membranes-mimetics is in agreement with the experimental data for SP revealed from NMR (Keire, D. A. and M. Kobayashi 1998). Moreover, they proposed the insertion of Phe^7, Phe^8 and Gly^9 into the interfacial region of the SDS micelle headgroups. In contrast, insertion of SP to both zwitterionic and anionic phospholipid bilayers was proposed by neutron diffraction (Bradshaw, J. P. et al. 1998). Nevertheless, it has been indicated that more of the peptide is at the surface compare to the anionic bilayers.

Our data with SDS micelles and LUVs contradict the suggestions that the interaction with a membrane surface does not play an important role in the stabilization of the active conformation. In contrary, as our data show, the electrostatic interactions are essential for

the insertion of the peptide. Keire & Fletcher (1996) studied the conformation of SP in SDS and zwitterionic DPC micelles. Our results are in agreement with Keire & Fletcher (1996) hypothesis that hydrophobic forces play the primary role in determining the conformation of SP at micelle surfaces, and that electrostatic interactions between the positively charged peptide and the different lipid head-groups determine the amount of time SP spends bound in the lipid environment. Based on the observed membrane structures of substance P and compared with pharmacologic and selective binding data taken from the literature, Schwyzer (1986, 1987 and 1995) proposed that when SP and other members of the Tachykinin family interact with a micelle or lipid vesicle they adopt a helical structure as they insert themselves into the hydrophobic core of the micelle or vesicle. The author proposed that SP inserts with its long axis parallel to the long axis of the hydrocarbon tails of the detergent molecules in the micelles. This orientation is very similar to that observed for transmembrane proteins. In contrast, Duplaa and coworkers (1992) performed ^{13}C-NMR experiments and reported that in the interaction between SP and lipid vesicles (phosphatidylcholine or phosphatidylserine) the long axis of the peptide lies parallel to the surface of the vesicle. Though these reports agree that only the hydrophobic side chains of SP are inserted into the hydrophobic core of the vesicle but there is not agreement about the orientation of the peptide. They proposed equilibrium between insertion of the peptide into the lipid layer and adsorption on the lipid surface. Based on monolayer expansion measurements, Seelig & Macdonald (1989) concluded that SP does insert into monolayers containing negatively charged lipids but does not insert into zwitterionic monolayers. In contrast, neutron diffraction studies indicate that SP insert into zwitterionic bilayers, but a larger proportion of the peptide is found at the surface when compared to the anionic bilayers (Bradshaw, J. P. et al. 1998).

Hypothesis about TKs interaction with NK receptors

The structural conformations and molecular bases in which TK ligands are recognized by the NK receptors are important for rational drug design. Thus, it is interesting to interpret our findings in this context. SP is known to act as a ligand for different NK receptors with

different potent activities (Harrison, Selena and Pierangelo Geppetti 2001). On the basis of our data, we hypothesized that the molecular basis for the multiple receptors recognition of TKs may be closely related to formation and stability of two major conformations adopted by the peptides: extended PPII helical and alpha helical structure. It is proposed that PPII is a favorable polypeptide conformation for molecular recognition and binding to proteins (Blanch, E. W. et al. 2000) Formation of PPII structure seems an essential structural feature of the TKs ligand in targeting different receptors, while the alpha helical structure most likely provides the correct conformation of the peptide for receptor signal activation. In the different NK receptors, the segment forming PPII in TKs will address the peptide to different binding pockets, due to PPII flexibility, and consequently, the agonist will attain a new conformation that would activate the receptor. Extended left-handed PPII helical structures have been neglected for years, and only in the last several years growing evidence has accumulated that the PPII conformation is essential for several biological activities, such as molecular recognition, signal transduction, transcription, cell motility, and immune response processes (Kelly, M. A. et al. 2001.Rath, A. et al. 2005.Shi, Zhengshuang. et al. 2006). In general, the PPII conformation forms in polypeptides rich in proline, yet even sequences lacking Pro residue can adopt this structure (Kelly, M. A. et al. 2001). Pro-rich sequences are known as very common recognition sites involved in signal transduction (Chen, Y. and B. A. Wallace 1997.Choo, L. P. et al. 1994.Convert, O. et al. 1991). Furthermore, the ligands are found mostly in an extended conformation, when bound to their receptors, as revealed by X-ray and NMR data. Actually, the N-terminus of SP contains two Pro residues forming two short $(XP)_n$ motifs, known to promote PPII helix formation (Rath, A. et al. 2005). An additional reason to assume the involvement of the PPII structure in the recognition processes of TKs by NK receptors lies in the fact that this regular, periodic structure is very flexible. By adapting the PPII structure TKs may easily behave as an “adaptable glove”, addressing the TKs to the binding pocket in the different NK receptors. Unlike alpha helix secondary structure, the PPII helix precludes formation of intramolecular hydrogen bonds (Bochicchio, B. and A. M. Tamburro 2002), leaving the backbone carbonyl oxygens (and the N-H protons of non-Pro residues) free to participate

in hydrogen bonding with interacting receptors at the interface of the peptide-protein complex. As we have shown here, PPII helix conformation is preformed in the unbound peptide before interacting with the membrane, which presumably guarantees rapid formation of specific peptide-protein complexes.

Based on the modeling, Regoli *et al*., (1994) proposed that NKA adopt an extended structure upon binding to receptor as the N-terminus of NKA is exposed and accessible to the extracellular medium (Zoffmann, S. et al. 2007). Moreover, they proposed that C-terminal parts of NKA and SP do not contribute identically to signaling on their respective receptors. Other report indicates the importance of the NKA folded conformation under hydrophobic conditions in order to bind to the NKA2 receptor .

Considering TKs in aggregation state

Few researches have been studied TKs (mainly SP) aggregation states, especially in a form of morphous-aggregates (fibrils) (Perry, E. K. et al. 1981.Singh, P. K. and S. K. Maji). In these studies, mostly the morphology of the fibrils and the effects of TKs on the fibrillization of β amyloid peptides have been discussed (Flashner, E. et al.).

By performing comprehensive morphological and structural analysis we present here solid evidence that TKs self associate to form fibrillar structures. Formation of TKs fibrils in aqueous solutions is concentration dependent. Moreover we show that higher concentrations may facilitate the nucleation process among fibrilization, as shown for other proteins and peptides (Rochet, J. C. and P. T. Lansbury, Jr. 2000). Side chains hydrogen bonding may also affect generation of TKs fibrils in aqueous solutions. Acceleration effect of aromatic residues on fibrillization is proposed, while some study demonstrated that π-π stacking is not a prerequisite for formation of fibrillar structures (Shtainfeld, A. et al.). On the other hand, our study show that Phe^{8} replaced Trp SP abolishes fibrils formation. Considering the presence of the other Phe residue in the peptide, it suggests different possibilities. Since the fibrils structure is highly organized, any perturbation in the hydrogen binding or orientation provided by the specific patter of stacking may cause disruption of the fibril formation. The second possibility is the

energetic contribution that stems from the stacking itself; such a contribution can thermodynamically drive the self-assembly process (Gazit, E. 2002).

It is claimed that negatively charged lipids make cationic peptides aggregation. Rapid formation of fibrils by negatively charged lipids are discussed for several proteins and peptides (Zhao, H. et al. 2004). Our data show that the interaction of TKs with the negatively charged liposomes is a complex process and depends on the ratio of the peptides and lipids. In ratios of DMPG LUVs:TKs about 100:1, fluorescence quenching of Trp shows the insertion of SPW and NKAW into the membrane, and CD spectroscopy indicates the formation of alpha helical structures in these peptides. Moreover, TEM and HT CD voltages support the absence of TKs aggregations in these conditions. In contrast, in a ratios of DMPG LUVs:TKs about 7:1, the peptides immediately form fibrils.

The main bands of interest in the amide I region for the detection of amyloidogenic protein regions in fibrils are at 1626 and 1632 cm^{-1} for parallel beta sheet structure and at 1690 cm^{-1} for antiparallel beta sheet. The FTIR data of the TKs at mM concentration in DMPG LUVs reveals the presence of 1626 and 1632 cm^{-1} bands assigned to the intermolecular beta sheet conformation (Figure…). In the same conditions TEM data show fibrils, but the lack of ThT test make impossible their assignment to amyloid fibrils.

Using the CD spectroscopy, we showed that a dominant PPII structure is SP transits to beta sheet fibrils. PPII structure may be favorable for beta fibril formation, due to dehydration of extended polypeptide chains (Blanch, E. W. et al. 2000). Subsequently, formation of beta sheet hydrogen bonds in this condition is a highly favorable process entropically (Blanch, E. W. et al. 2000). On the other hand, since strands of PPII helix are close in conformation to beta-strands, they would be expected to readily undergo this type of aggregation with each other and also with established beta sheet (Blanch, E. W. et al. 2000). Based on the Raman optical activity, it is proposed that PPII is relevance for the initial phase of the amyloid plaque formation of various proteins (Eker, F. et al. 2004). Some report indicate the self-association of SP in a concentration range of 5-10 mM, while they did not assigned any fibril formation in this case (Beard, D. J. et al. 2007).

To attempt the role of surfactant on TKs fibrilization, we showed that low concentrations of SP and NKA (80-100 μM) form fibrils in SDS concentrations below CMC. Since the initial nucleation is essential for fibril formation (Gorbenko, G. P. and P. K. Kinnunen 2006), the accelerating effect of SDS on fibril formation may promote the seeded fibril growth in a concentration-dependent manner (Ahmad, M. F. et al. 2006). In contrary, some reports indicate the inhibition effect of SDS on fibrillogenesis (Pertinhez, T. A. et al. 2002).

The toxicity test for the three peptides showed that only NKA in concentrations of 25 and 250 μM is toxic, while in agreement with recent report the fibrils of SP are not toxic. Furthermore, some studies have suggested that oligomers formed in the pathways of amyloid formation are more cytotoxic compared to the mature amyloids. There is a hypothesis indicating that different aggregate sizes can induce different degeneration pathways (Di Carlo, M.). Our CD data show the aggregation state of TKs in the micelle:peptide ratio of about 7:1. Although at the moment, we do not have evident about the structure and toxicity of these aggregates, but reversibility of this aggregations to non-aggregate states and the presence of the intermediate structures in this process, reveals the importance of this sort of aggregation on neurodegenerative diseases in the case of toxic behavior of them.

Ahmad, M. F., T. Ramakrishna, B. Raman and M. Rao Ch. 2006. Fibrillogenic and non-fibrillogenic ensembles of SDS-bound human alpha-synuclein. *J Mol Biol* 364 (5):1061-1072.

Auge, S., B. Bersch, M. Tropis and A. Milon. 2000. Characterization of substance P-membrane interaction by transferred nuclear Overhauser effect. *Biopolymers* 54 (5):297-306.

Beard, D. J., S. A. Perrine, E. Phillips, S. Hoque, S. Conerly, C. Tichenor, M. A. Simmons and J. K. Young. 2007. Conformational comparisons of a series of tachykinin peptide analogs. *J Med Chem* 50 (26):6501-6506.

Blanch, E. W., L. A. Morozova-Roche, D. A. Cochran, A. J. Doig, L. Hecht and L. D. Barron. 2000. Is polyproline II helix the killer conformation? A Raman optical activity study of the amyloidogenic prefibrillar intermediate of human lysozyme. *J Mol Biol* 301 (2):553-563.

Bochicchio, B. and A. M. Tamburro. 2002. Polyproline II structure in proteins: identification by chiroptical spectroscopies, stability, and functions. *Chirality* 14 (10):782-792.

Bordag, N. and S. Keller. Alpha-helical transmembrane peptides: a "divide and conquer" approach to membrane proteins. *Chem Phys Lipids* 163 (1):1-26.

Bradshaw, J. P., S. M. Davies and T. Hauss. 1998. Interaction of substance P with phospholipid bilayers: A neutron diffraction study. *Biophys J* 75 (2):889-895.

Chandrashekar, I. R. and S. M. Cowsik. 2003. Three-dimensional structure of the mammalian tachykinin peptide neurokinin A bound to lipid micelles. *Biophys J* 85 (6):4002-4011.

Chassaing, G., O. Convert and S. Lavielle. 1986. Preferential conformation of substance P in solution. *Eur J Biochem* 154 (1):77-85.

Chen, Y. and B. A. Wallace. 1997. Secondary solvent effects on the circular dichroism spectra of polypeptides in non-aqueous environments: influence of polarisation effects on the far ultraviolet spectra of alamethicin. *Biophys Chem* 65 (1):65-74.

Choo, L. P., M. Jackson and H. H. Mantsch. 1994. Conformation and self-association of the peptide hormone substance P: Fourier-transform infrared spectroscopic study. *Biochem J* 301 (Pt 3):667-670.

Convert, O., H. Duplaa, S. Lavielle and G. Chassaing. 1991. Influence of the replacement of amino acid by its D-enantiomer in the sequence of substance P. 2. Conformational analysis by NMR and energy calculations. *Neuropeptides* 19 (4):259-270.

Di Carlo, M. Beta amyloid peptide: from different aggregation forms to the activation of different biochemical pathways. *Eur Biophys J* 39 (6):877-888.

Dike, A. and S. M. Cowsik. 2005. Membrane-Induced Structure of Scyliorhinin I: A Dual NK1/NK2 Agonist. *Biophys J* 88 (5):3592-3600.

Eker, F., K. Griebenow and R. Schweitzer-Stenner. 2004. Abeta(1-28) fragment of the amyloid peptide predominantly adopts a polyproline II conformation in an acidic solution. *Biochemistry* 43 (22):6893-6898.

Flashner, E., U. Raviv and A. Friedler. The effect of tachykinin neuropeptides on amyloid beta aggregation. *Biochem Biophys Res Commun* 407 (1):13-17.

Gazit, E. 2002. A possible role for pi-stacking in the self-assembly of amyloid fibrils. *Faseb J* 16 (1):77-83.

Gorbenko, G. P. and P. K. Kinnunen. 2006. The role of lipid-protein interactions in amyloid-type protein fibril formation. *Chem Phys Lipids* 141 (1-2):72-82.

Harrison, Selena and Pierangelo Geppetti. 2001. Substance P. *The International Journal of Biochemistry & Cell Biology* 33:555-576.

Keire, D. A. and T. G. Fletcher. 1996. The conformation of substance P in lipid environments. *Biophys J* 70 (4):1716-1727.

Keire, D. A. and M. Kobayashi. 1998. The orientation and dynamics of substance P in lipid environments. *Protein Sci* 7 (11):2438-2450.

Kelly, M. A., B. W. Chellgren, A. L. Rucker, J. M. Troutman, M. G. Fried, A. F. Miller and T. P. Creamer. 2001. Host-guest study of left-handed polyproline II helix formation. *Biochemistry* 40 (48):14376-14383.

Lazarova, T., K. A. Brewin, K. Stoeber and C. R. Robinson. 2004. Characterization of peptides corresponding to the seven transmembrane domains of human adenosine A2a receptor. *Biochemistry* 43 (40):12945-12954.

Perry, E. K., A. E. Oakley, J. M. Candy and R. H. Perry. 1981. Properties and possible significance of substance P and insulin fibrils. *Neurosci Lett* 25 (3):321-325.

Pertinhez, T. A., M. Bouchard, R. A. Smith, C. M. Dobson and L. J. Smith. 2002. Stimulation and inhibition of fibril formation by a peptide in the presence of different concentrations of SDS. *FEBS Lett* 529 (2-3):193-197.

Prabhu, A., A. Malde, E. Coutinho and S. Srivastava. 2005. Solution conformation of Substance P antagonists-[D-Arg1, D-Trp7,9, Leu11]-SP, [D-Arg1, D-Pro2, D-Trp7,9, Leu11]-SP and [D-Pro2, D-Trp7,9]-SP by CD, NMR and MD simulations. *Peptides* 26 (5):875-885.

Qi, X. F., B. S. Zhorov and V. S. Ananthanarayanan. 2000. CD, 1H NMR and molecular modeling studies of the interaction of Ca2+ with substance P and Ala7-substance P in a non-polar solvent. *J Pept Sci* 6 (2):57-83.

Rath, A., A. R. Davidson and C. M. Deber. 2005. The structure of "unstructured" regions in peptides and proteins: role of the polyproline II helix in protein folding and recognition. *Biopolymers* 80 (2-3):179-185.

Rochet, J. C. and P. T. Lansbury, Jr. 2000. Amyloid fibrillogenesis: themes and variations. *Curr Opin Struct Biol* 10 (1):60-68.

Rucker, A. L. and T. P. Creamer. 2002. Polyproline II helical structure in protein unfolded states: lysine peptides revisited. *Protein Sci* 11 (4):980-985.

Seelig, A., T. Alt, S. Lotz and G. Holzemann. 1996. Binding of substance P agonists to lipid membranes and to the neurokinin-1 receptor. *Biochemistry* 35 (14):4365-4374.

Shi, Zhengshuang. et al. . 2006. Conformation of the Backbone in Unfolded Proteins. *Chem. Rev.* 106:1877-1897.

Shtainfeld, A., T. Sheynis and R. Jelinek. Specific mutations alter fibrillation kinetics, fiber morphologies, and membrane interactions of pentapeptides derived from human calcitonin. *Biochemistry* 49 (25):5299-5307.

Singh, P. K. and S. K. Maji. Amyloid-like fibril formation by tachykinin neuropeptides and its relevance to amyloid beta-protein aggregation and toxicity. *Cell Biochem Biophys* 64 (1):29-44.

Whitehead, T. L., S. D. McNair, C. E. Hadden, J. K. Young and R. P. Hicks. 1998. Membrane-induced secondary structures of neuropeptides: a comparison of the solution conformations adopted by agonists and antagonists of the mammalian tachykinin NK1 receptor. *J Med Chem* 41 (9):1497-1506.

Williams, R. W. and J. L. Weaver. 1990. Secondary structure of substance P bound to liposomes in organic solvents and in solution from Raman and CD spectroscopy. *J Biol Chem* 265 (5):2505-2513.

Woolley, G. A. and C. M. Deber. 1987. Peptides in membranes: lipid-induced secondary structure of substance P. *Biopolymers* 26 Suppl:S109-121.

Wu, C. S., A. Hachimori and J. T. Yang. 1982. Lipid-induced ordered conformation of some peptide hormones and bioactive oligopeptides: predominance of helix over beta form. *Biochemistry* 21 (19):4556-4562.

Zhao, H., E. K. Tuominen and P. K. Kinnunen. 2004. Formation of amyloid fibers triggered by phosphatidylserine-containing membranes. *Biochemistry* 43 (32):10302-10307.

Zoffmann, S., S. Bertrand, Q. T. Do, D. Bertrand, D. Rognan, M. Hibert and J. L. Galzi. 2007. Topological analysis of the complex formed between neurokinin A and the NK2 tachykinin receptor. *J Neurochem* 101 (2):506-516.

REFERENCES

Bienkiewicz, E. A., A. Moon Woody and R. W. Woody. 2000. Conformation of the RNA polymerase II C-terminal domain: circular dichroism of long and short fragments. *J Mol Biol* 297 (1):119-133.

Bochicchio, B. and A. M. Tamburro. 2002. Polyproline II structure in proteins: identification by chiroptical spectroscopies, stability, and functions. *Chirality* 14 (10):782-792.

Chen, Y. H., J. T. Yang and H. M. Martinez. 1972. Determination of the secondary structures of proteins by circular dichroism and optical rotatory dispersion. *Biochemistry* 11 (22):4120-4131.

Greenfield, Norma J. 2004. Analysis of circular dichroism data. *METHODS IN ENZYMOLOGY* 383:282-317.

Jacques, D. A. and J. Trewhella. Small-angle scattering for structural biology--expanding the frontier while avoiding the pitfalls. *Protein Sci* 19 (4):642-657.

Jaravine, V. A., A. T. Alexandrescu and S. Grzesiek. 2001. Observation of the closing of individual hydrogen bonds during TFE-induced helix formation in a peptide. *Protein Sci* 10 (5):943-950.

Kelly, M. A., B. W. Chellgren, A. L. Rucker, J. M. Troutman, M. G. Fried, A. F. Miller and T. P. Creamer. 2001. Host-guest study of left-handed polyproline II helix formation. *Biochemistry* 40 (48):14376-14383.

Mertens, H. D. and D. I. Svergun. Structural characterization of proteins and complexes using small-angle X-ray solution scattering. *J Struct Biol* 172 (1):128-141.

Roccatano, D., G. Colombo, M. Fioroni and A. E. Mark. 2002. Mechanism by which 2,2,2-trifluoroethanol/water mixtures stabilize secondary-structure formation in peptides: a molecular dynamics study. *Proc Natl Acad Sci U S A* 99 (19):12179-12184.

Rucker, A. L. and T. P. Creamer. 2002. Polyproline II helical structure in protein unfolded states: lysine peptides revisited. *Protein Sci* 11 (4):980-985.

Shi, Zhengshuang. et al. . 2006. Conformation of the Backbone in Unfolded Proteins. *Chem. Rev.* 106:1877-1897.

Williams, R. W. and J. L. Weaver. 1990. Secondary structure of substance P bound to liposomes in organic solvents and in solution from Raman and CD spectroscopy. *J Biol Chem* 265 (5):2505-2513.

Woody, R. W. 2009. Circular dichroism spectrum of peptides in the poly(Pro)II conformation. *J Am Chem Soc* 131 (23):8234-8245.

Yang, J. T., C. S. Wu and H. M. Martinez. 1986. Calculation of protein conformation from circular dichroism. *Methods Enzymol* 130:208-269.

Bolen, E. J. and P. W. Holloway. 1990. Quenching of tryptophan fluorescence by brominated phospholipid. *Biochemistry* 29 (41):9638-9643.

Bowie, J. U. Membrane protein folding: how important are hydrogen bonds? *Curr Opin Struct Biol* 21 (1):42-49.

Chatterjee, A. et al. . 2001. Thermodynamics of Micelle Formation of Ionic Surfactants: A Critical Assessment for Sodium Dodecyl Sulfate, Cetyl Pyridinium Chloride

and Dioctyl Sulfosuccinate (Na Salt) by Microcalorimetric, Conductometric, and Tensiometric Measurements. *J. Phys. Chem.* 105:12823-12831.

Chen, Y., Barkley, M.D. 1998. Toward understanding tryptophan fluorescence in proteins. *Biochemistry* 37:9976.

Fuguet, Elisabet. et al. . 2005. Critical micelle concentration of surfactants in aqueous buffered and unbuffered systems. *Analytica Chimica Acta* 548:95- 100.

Hassan, P.A, et al. . 2002. Microstructural changes in SDS micelles induced by hydrotropic salt. *Langmuir* 18:2543-2548.

Inayathullah, N. Mohammed. et al. . 2003. Effect of osmolyte on the micellization of SDS at different temperatures. *Langmuir* 19:9545-9547.

Moreno, M. R., J. Guillen, A. J. Perez-Berna, D. Amoros, A. I. Gomez, A. Bernabeu and J. Villalain. 2007. Characterization of the interaction of two peptides from the N terminus of the NHR domain of HIV-1 gp41 with phospholipid membranes. *Biochemistry* 46 (37):10572-10584.

Muino, P. L. and P. R. Callis. 2009. Solvent effects on the fluorescence quenching of tryptophan by amides via electron transfer. Experimental and computational studies. *J Phys Chem B* 113 (9):2572-2577.

Serrano, A. L., T. Troxler, M. J. Tucker and F. Gai. Photophysics of a fluorescent non-natural amino acid: p-Cyanophenylalanine. *Chem Phys Lett* 487 (4-6):303-306.

Taskent-Sezgin, H., J. Chung, V. Patsalo, S. J. Miyake-Stoner, A. M. Miller, S. H. Brewer, R. A. Mehl, D. F. Green, D. P. Raleigh and I. Carrico. 2009. Interpretation of p-cyanophenylalanine fluorescence in proteins in terms of solvent exposure and contribution of side-chain quenchers: a combined fluorescence, IR and molecular dynamics study. *Biochemistry* 48 (38):9040-9046.

Taskent-Sezgin, H., P. Marek, R. Thomas, D. Goldberg, J. Chung, I. Carrico and D. P. Raleigh. Modulation of p-cyanophenylalanine fluorescence by amino acid side chains and rational design of fluorescence probes of alpha-helix formation. *Biochemistry* 49 (29):6290-6295.

Thévenot, Caroline. et al. . 2005. Aggregation number and critical micellar concentration of surfactant determined by time-dependent static light scattering (TDSLS) and conductivity. *Colloids and Surfaces A Physicochemical and Engineering Aspects* 252:105-111.

Zhao, H. and P. K. Kinnunen. 2002. Binding of the antimicrobial peptide temporin L to liposomes assessed by Trp fluorescence. *J Biol Chem* 277 (28):25170-25177.

Barth, Andreas and Christian Zscherp. 2002. What vibrations tell us about the proteins. *Quarterly Reviews of Biophysics* 35 (4):369.

Gorbenko, G. P. and P. K. Kinnunen. 2006. The role of lipid-protein interactions in amyloid-type protein fibril formation. *Chem Phys Lipids* 141 (1-2):72-82.

Juszczyk, P., A. S. Kolodziejczyk and Z. Grzonka. 2009. FTIR spectroscopic studies on aggregation process of the beta-amyloid 11-28 fragment and its variants. *J Pept Sci* 15 (1):23-29.

Ahmad, M. F., T. Ramakrishna, B. Raman and M. Rao Ch. 2006. Fibrillogenic and non-fibrillogenic ensembles of SDS-bound human alpha-synuclein. *J Mol Biol* 364 (5):1061-1072.

Auge, S., B. Bersch, M. Tropis and A. Milon. 2000. Characterization of substance P-membrane interaction by transferred nuclear Overhauser effect. *Biopolymers* 54 (5):297-306.

Beard, D. J., S. A. Perrine, E. Phillips, S. Hoque, S. Conerly, C. Tichenor, M. A. Simmons and J. K. Young. 2007. Conformational comparisons of a series of tachykinin peptide analogs. *J Med Chem* 50 (26):6501-6506.

Blanch, E. W., L. A. Morozova-Roche, D. A. Cochran, A. J. Doig, L. Hecht and L. D. Barron. 2000. Is polyproline II helix the killer conformation? A Raman optical activity study of the amyloidogenic prefibrillar intermediate of human lysozyme. *J Mol Biol* 301 (2):553-563.

Bochicchio, B. and A. M. Tamburro. 2002. Polyproline II structure in proteins: identification by chiroptical spectroscopies, stability, and functions. *Chirality* 14 (10):782-792.

Bordag, N. and S. Keller. Alpha-helical transmembrane peptides: a "divide and conquer" approach to membrane proteins. *Chem Phys Lipids* 163 (1):1-26.

Bradshaw, J. P., S. M. Davies and T. Hauss. 1998. Interaction of substance P with phospholipid bilayers: A neutron diffraction study. *Biophys J* 75 (2):889-895.

Chandrashekar, I. R. and S. M. Cowsik. 2003. Three-dimensional structure of the mammalian tachykinin peptide neurokinin A bound to lipid micelles. *Biophys J* 85 (6):4002-4011.

Chassaing, G., O. Convert and S. Lavielle. 1986. Preferential conformation of substance P in solution. *Eur J Biochem* 154 (1):77-85.

Chen, Y. and B. A. Wallace. 1997. Secondary solvent effects on the circular dichroism spectra of polypeptides in non-aqueous environments: influence of polarisation effects on the far ultraviolet spectra of alamethicin. *Biophys Chem* 65 (1):65-74.

Choo, L. P., M. Jackson and H. H. Mantsch. 1994. Conformation and self-association of the peptide hormone substance P: Fourier-transform infrared spectroscopic study. *Biochem J* 301 (Pt 3):667-670.

Convert, O., H. Duplaa, S. Lavielle and G. Chassaing. 1991. Influence of the replacement of amino acid by its D-enantiomer in the sequence of substance P. 2. Conformational analysis by NMR and energy calculations. *Neuropeptides* 19 (4):259-270.

Di Carlo, M. Beta amyloid peptide: from different aggregation forms to the activation of different biochemical pathways. *Eur Biophys J* 39 (6):877-888.

Dike, A. and S. M. Cowsik. 2005. Membrane-Induced Structure of Scyliorhinin I: A Dual NK1/NK2 Agonist. *Biophys J* 88 (5):3592-3600.

Eker, F., K. Griebenow and R. Schweitzer-Stenner. 2004. Abeta(1-28) fragment of the amyloid peptide predominantly adopts a polyproline II conformation in an acidic solution. *Biochemistry* 43 (22):6893-6898.

Flashner, E., U. Raviv and A. Friedler. The effect of tachykinin neuropeptides on amyloid beta aggregation. *Biochem Biophys Res Commun* 407 (1):13-17.

Gazit, E. 2002. A possible role for pi-stacking in the self-assembly of amyloid fibrils. *Faseb J* 16 (1):77-83.

Gorbenko, G. P. and P. K. Kinnunen. 2006. The role of lipid-protein interactions in amyloid-type protein fibril formation. *Chem Phys Lipids* 141 (1-2):72-82.

Harrison, Selena and Pierangelo Geppetti. 2001. Substance P. *The International Journal of Biochemistry & Cell Biology* 33:555-576.

Keire, D. A. and T. G. Fletcher. 1996. The conformation of substance P in lipid environments. *Biophys J* 70 (4):1716-1727.

Keire, D. A. and M. Kobayashi. 1998. The orientation and dynamics of substance P in lipid environments. *Protein Sci* 7 (11):2438-2450.

Kelly, M. A., B. W. Chellgren, A. L. Rucker, J. M. Troutman, M. G. Fried, A. F. Miller and T. P. Creamer. 2001. Host-guest study of left-handed polyproline II helix formation. *Biochemistry* 40 (48):14376-14383.

Lazarova, T., K. A. Brewin, K. Stoeber and C. R. Robinson. 2004. Characterization of peptides corresponding to the seven transmembrane domains of human adenosine A2a receptor. *Biochemistry* 43 (40):12945-12954.

Perry, E. K., A. E. Oakley, J. M. Candy and R. H. Perry. 1981. Properties and possible significance of substance P and insulin fibrils. *Neurosci Lett* 25 (3):321-325.

Pertinhez, T. A., M. Bouchard, R. A. Smith, C. M. Dobson and L. J. Smith. 2002. Stimulation and inhibition of fibril formation by a peptide in the presence of different concentrations of SDS. *FEBS Lett* 529 (2-3):193-197.

Prabhu, A., A. Malde, E. Coutinho and S. Srivastava. 2005. Solution conformation of Substance P antagonists-[D-Arg1, D-Trp7,9, Leu11]-SP, [D-Arg1, D-Pro2, D-Trp7,9, Leu11]-SP and [D-Pro2, D-Trp7,9]-SP by CD, NMR and MD simulations. *Peptides* 26 (5):875-885.

Qi, X. F., B. S. Zhorov and V. S. Ananthanarayanan. 2000. CD, 1H NMR and molecular modeling studies of the interaction of Ca2+ with substance P and Ala7-substance P in a non-polar solvent. *J Pept Sci* 6 (2):57-83.

Rath, A., A. R. Davidson and C. M. Deber. 2005. The structure of "unstructured" regions in peptides and proteins: role of the polyproline II helix in protein folding and recognition. *Biopolymers* 80 (2-3):179-185.

Rochet, J. C. and P. T. Lansbury, Jr. 2000. Amyloid fibrillogenesis: themes and variations. *Curr Opin Struct Biol* 10 (1):60-68.

Rucker, A. L. and T. P. Creamer. 2002. Polyproline II helical structure in protein unfolded states: lysine peptides revisited. *Protein Sci* 11 (4):980-985.

Seelig, A., T. Alt, S. Lotz and G. Holzemann. 1996. Binding of substance P agonists to lipid membranes and to the neurokinin-1 receptor. *Biochemistry* 35 (14):4365-4374.

Shi, Zhengshuang. et al. . 2006. Conformation of the Backbone in Unfolded Proteins. *Chem. Rev.* 106:1877-1897.

Shtainfeld, A., T. Sheynis and R. Jelinek. Specific mutations alter fibrillation kinetics, fiber morphologies, and membrane interactions of pentapeptides derived from human calcitonin. *Biochemistry* 49 (25):5299-5307.

Singh, P. K. and S. K. Maji. Amyloid-like fibril formation by tachykinin neuropeptides and its relevance to amyloid beta-protein aggregation and toxicity. *Cell Biochem Biophys* 64 (1):29-44.

Whitehead, T. L., S. D. McNair, C. E. Hadden, J. K. Young and R. P. Hicks. 1998. Membrane-induced secondary structures of neuropeptides: a comparison of the solution conformations adopted by agonists and antagonists of the mammalian tachykinin NK1 receptor. *J Med Chem* 41 (9):1497-1506.

Williams, R. W. and J. L. Weaver. 1990. Secondary structure of substance P bound to liposomes in organic solvents and in solution from Raman and CD spectroscopy. *J Biol Chem* 265 (5):2505-2513.

Woolley, G. A. and C. M. Deber. 1987. Peptides in membranes: lipid-induced secondary structure of substance P. *Biopolymers* 26 Suppl:S109-121.

Wu, C. S., A. Hachimori and J. T. Yang. 1982. Lipid-induced ordered conformation of some peptide hormones and bioactive oligopeptides: predominance of helix over beta form. *Biochemistry* 21 (19):4556-4562.

Zhao, H., E. K. Tuominen and P. K. Kinnunen. 2004. Formation of amyloid fibers triggered by phosphatidylserine-containing membranes. *Biochemistry* 43 (32):10302-10307.

Zoffmann, S., S. Bertrand, Q. T. Do, D. Bertrand, D. Rognan, M. Hibert and J. L. Galzi. 2007. Topological analysis of the complex formed between neurokinin A and the NK2 tachykinin receptor. *J Neurochem* 101 (2):506-516.

CONCLUSIONS

1. Substance P (SP), Neurokinin A (NKA) and Scyliorhinin I (ScyI) bind to both zwitterionic DMPC and negatively charged DMPG liposomes. However, binding affinities of the peptides to DMPC liposomes are in the range of 20 to 40 times lower compared to the affinities to DMPG. Moreover, the binding affinities of SP, NKA and ScyI correlate with their net charges when they bind to DMPG, but not when bind to DMPC.
2. An insertion of the C-domain segment of SP, NKA and ScyI peptides into the hydrophobic core was detected only for negatively charged SDS micelles and DMPG liposomes. The negative charge distribution on the membrane surface is indispensible for the insertion process to occur and for peptides to form stable helical segments.
3. In aqueous solutions, sub-micellar concentrations of SDS and in zwitterionic liposomes, SP, NKA and ScyI form dominant polyproline II (PPII) extended helical structure. Formation of PPII structure is non-cooperative, is reversible upon heating and cooling, and may be crucial for the recognition processes of the Tachykinin peptides by neurokinin receptors.
4. In non fibrillar conditions in SDS micelles and DMPG liposomes, SP and ScyI peptides have dominant alpha helical structure, while NKA presents admixed unordered and alpha helical conformations.
5. Under some conditions, mainly at high (mM) concentrations of the peptides, SP, NKA and ScyI self-associate in a form of fibrillar ordered structures.
6. The fibrils present different morphology. SP forms fibrils that are long twisted and straight single filaments, while NKA and ScyI form fibrils that are only single-straight. The widths of the fibrils vary among the peptides. For SP, NKA and ScyI, it was about 15, 9 and 12 nm, respectively.
7. The infrared spectra of the SP, NKA and ScyI in DMPG liposomes and in fibrillar state present bands attributed to helical, β sheets and β turn (only for SP and NKA) conformations.

8. Upon an overnight incubation in SDS under certain conditions, SP undergoes self-association and transit from monomer to a fibrillar structure. During the fibrillization process, the SP conformation show structural transition from dominant PPII (in the monomer state) to β sheet conformation (in the fibrillar sate). Substitution of the Phe^8 residue of SP for Trp^8 abolishes both the formation of fibrils and the conformational changes.

9. Incubation of NKA and its analogue NKAW in sub-micellar concentration of SDS and acid, neutral and alkaline pH causes fibrils formation. At low and neutral pH, during the fibrillization process, NKA undergoes structural changes from PPII to β sheet and β turn conformations. The formed fibrills are amyloid. In the same conditions in NKAW with Phe^8 substituted for Trp amyloid fibrils were detected only in the peptide incubated at acid and alkaline pH. No amyloid fibril formation was detected at pH 7.0.

Acknowledgment

This thesis marks the end of my journey in obtaining my Ph.D. At the end of this journey, it is a pleasant task to express my appreciation to all those who contributed in many ways to the success of this study and made it an unforgettable experience for me. It would not be possible to carry out such a study without the expert knowledge, as well as encouragement and support; the debt I have incurred in the past few years is numerous; my gratitude even greater.

First and foremost, to Esteve I am deeply indebted; who, back in 2008, gave me the opportunity to participate in this project. It has been my good fortune and, indeed, my privilege to come to know him and to have benefited from his vast knowledge and wisdom. I felt motivated and encouraged every time I attended his meetings and without his guidance, insightful ideas and perspective this project would not have materialized.

Greatest thanks to Tzvetana; for her guidance and constant supervision over the past years. I deeply appreciate her knowledge and personal tutoring and I will always be thankful for her solid critical advice. Her invaluable ideas and new insights have also drawn my attention to many sources I should have otherwise missed.

Among friends and labmates, I am, in particular, grateful to Nuria for her remarks while working on……. . which has helped me in developing the project. My thanks go to Rosana, Meritxell, Oliver, Yibin, Ero, Asrar, Danial, Mikhail, Oxana, Fanli, Guillem who have helped me in more ways that I could count. I wish you all the best. I am also indebted to Paco, Victor and Alex, for their wonderful feedbacks, endless observations and remarks.

The patience, trust, supports and confidence of my family is invaluable to me. To my amazing parents, Mohammad and Fahimeh, my debt is incalculable and can only be repaid by constancy and devotion.

And to you, Reyhane, I would like to express my deepest appreciation and affection. You have constantly encouraged me, challenged me, and patiently helped me through this journey; to you goes my eternal gratitude and love for holding my hand and keeping me steady with such grace and understanding. This work would not have been possible without your magical source of strength, your endless patience, and encouragement. I can't thank you enough for your tremendous support and sacrifices. No one walks alone in the journey of life, and I am so lucky to have you by my side. Thanks for everything!

THE JOURNAL OF PHYSICAL CHEMISTRY B

ARTICLE

pubs.acs.org/JPCB

Study of Membrane-Induced Conformations of Substance P: Detection of Extended Polyproline II Helix Conformation

Arash Foroutan,[†] Tzvetana Lazarova,[*,†] and Esteve Padrós[*]

Unitat de Biofísica, Departament de Bioquímica i de Biologia Molecular, and Centre d'Estudis en Biofísica, Facultat de Medicina, Universitat Autònoma de Barcelona, 08193 Bellaterra, Barcelona, Spain

ABSTRACT: We study the conformation of substance P (SP), a ligand of neurokinin 1 receptor, and its analogue [Trp8]SP in membrane-mimetic media to provide further insights into membrane−ligand interactions and the factors determining and modulating the peptide structure. CD data revealed that the neuropeptide attains α-helical fold in negatively charged SDS micelles and DMPG liposomes but not in zwitterionic DMPC. The fluorescence experiments reported that the Trp side chain of [Trp8]SP inserts into the hydrophobic core of the SDS micelles and DMPG liposomes but faces the DMPC hydrophilic region, indicating that electrostatic interactions between membrane and SP are essential for the α-helical fold. Formation of extended polyproline II (PPII) helical structure in aqueous solutions and in submicellar concentrations of SDS and DMPC liposomes was confirmed by comparing CD spectra at increasing temperatures. Moreover, in all conditions where PPII conformation was detected, the Trp was totally exposed to the bulk. The PPII structure may be vital for recognition processes of SP by neurokinin receptors.

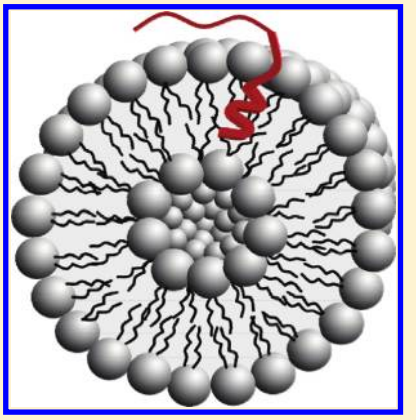

INTRODUCTION

Ligand binding is an essential step for the functioning of the most diverse and largest protein family of G-protein coupled receptors (GPCRs). After agonist binding GPCRs activate, allowing the cytoplasmatic domain of the receptor to interact with a specific G-protein and to transmit the signal.[1] Defects in ligand−GPCR interactions affect inter- and intracellular signaling communications and are considered as one of the main reasons for many human diseases.[2,3] Consequently, the molecular basis of ligand recognition by GPCRs is a topic of primary interest in cellular recognition studies and for understanding how these proteins do work. Despite the biological importance of GPCR proteins, knowledge about the forces and mechanisms governing ligand−receptor interactions is still on the infancy level.[4] Recent determination of the high-resolved structures of three members of the GPCR family including rhodopsin, β2-adrenergic, and adenosine A_{2A} receptors advanced notably our understanding on how these proteins work as signaling molecules.[5,6] However, considering the substantial evidence that GPCR exist in numbers of flexible active conformations, these structures offer only a static view of a single-protein conformation.[1,7] Indeed, for the ligand−receptor studies the high-resolution structure of the ligand bound to the receptor is one of the most desirable. Yet, because of the ligand−receptor complexity, other strategies attempting the structural characterization of the active biological form of the ligand are desirable.

Among the tachykinin family, substance P (SP) is the most potent natural ligand of neurokinin 1 (NK1) GPCR receptor.[8,9] It is a positively charged neuropeptide, composed by 11 amino acids (Arg1-Pro2-Lys3-Pro4-Gln5-Gln6-Phe7-Phe8-Gly9-Leu-10-Met11-NH_2), and is believed to be involved in several physiological processes in the central and peripheral nervous system.[10−12] The implication of SP agonist in stress mechanisms, mood/anxiety regulation, and some neurodegenerative disorders makes it a therapeutically relevant agent. An understanding of how the SP ligand interacts with the NK receptors is essential to permit a rational design of compounds acting selectively at the receptor level.[13]

As suggested by mutagenesis and heterologous expression studies, the binding site of SP is close to the extracellular membrane interface of NK1 receptor, involving residues of the first and second extracellular loop and the second and seventh transmembrane domain.[14−18] Despite the fact that in the several past years SP and NK1 receptor have been extensively studied, the mechanism by which the neuropeptide recognizes its receptor remains elusive. Some authors have proposed that the target cell surface has an important role in the biological activity of SP, either by increasing the ligand concentration at the membrane surface or by inducing and stabilizing its active conformation.[19,20] On the contrary, some other authors believe that lipids may play an important role for the SP storage but most likely are not directly involved in the binding of SP to its receptor.[21] Indeed, membrane-mimetic environments are suitable milieu to obtain insight into the mechanism by which the SP recognizes the receptor. A number of previous reports on the SP structural properties come from molecular dynamics, circular dichroism

Received: October 22, 2010
Revised: February 7, 2011
Published: March 11, 2011

(CD), and nuclear magnetic resonance (NMR) studies. However, most of the molecular dynamics and NMR studies have been performed using methanol, dimethyl sulfoxide, or 2,2,2-trifluoroethanol (TFE) as solvents to mimic the membrane milieu.[22−25] The conformation of SP in micelles and liposomes, two common model systems to mimic the membrane environment, has been more extensively explored by CD, Fourier transform infrared, and recently NMR experiments.[26−30] NMR studies of the micelle-associated structure of SP proposed that the C-terminal tripeptide (Gly-Leu-Met-NH_2) adopts an extended structure while the N-terminal is quite flexible.[31] In the midregion of SP, a conformational equilibrium between α-helical and 3_{10} structures has been proposed,[31,26,32] while other authors have suggested α-helical[33,31] or turn-like structures.[26,34] More recent characterization of SP in phosphatidylcholine vesicles by 2D trNOE NMR spectroscopy reported a well-defined conformation in the last seven C-terminal amino acids consisting of nonstandard turns followed each other in a helix-like manner.[29]

The role of peptide−lipid interactions for the insertion and conformation of SP in the membrane matrix is another area of debate. Using the monolayer technique it was reported that SP inserts into negatively charged 1-palmitoyl-2-oleoyl-*sn*-glycero-3-phosphoglycerol but not into zwitterionic 1-palmitoyl-2-oleoyl-*sn*-glycero-3-phosphocholine.[35,36] The role of the electrostatic interaction for the insertion of SP into bilayer has been questioned by analysis of the binding isotherms, suggesting binding of SP to neutral lipids.[37] CD experiments reported unordered SP structure in phosphatidylcholine but a partially α-helical structure in negatively charged liposomes as well as in sodium dodecyl sulfate (SDS) micelles.[38] Contrary to these reports, an earlier CD work claimed that the conformation of SP is independent of the lipid headgroup type.[33] This view has been lately supported by CD and ^{1}H NMR studies.[26] Although these studies clearly recognize the essentiality of the lipid matrix for insertion, they also reveal that the modes of neuropeptide−receptor interactions and the mechanisms controlling the ligand binding are yet not entirely understood.

In the present work, we study the conformation of SP and its analogue [Trp8]SP (abbreviated SPW) in SDS micelles and liposomes to understand better membrane/neuropeptide interactions and the factors determining and modulating the peptide structure in membrane-mimetic environments. CD experiments were performed to address the questions concerning the SP conformation, while fluorescence spectroscopy was carried out to obtain information about peptide binding and insertion.

MATERIALS AND METHODS

Materials. Monosodium phosphate dihydrate (≥99%), disodium phosphate dehydrate (≥98%), sodium carbonate (≥99%), and sodium hydrogen carbonate (≥99%) were purchased from Merck & Co., Inc. 2,2,2-Trifluoroethanol (TFE) (≥99%), sodium dodecyl sulfate (SDS) (99%), and pyrene (99%) were purchased from Sigma-Aldrich, Inc. 1,2-Dimyristoyl-*sn*-glycero-3-[phospho-rac-(1-glycerol)] (sodium salt) (DMPG) and 1,2-dimyristoyl-*sn*-glycero-3-phosphocholine (DMPC) were purchased from Avanti Polar Lipids, Inc. SP and SPW were purchased from AnaSpec, Inc. The purity of the peptides was >98% as judged by HPLC and further confirmed by mass spectrometry. The lyophilized peptides were stored at −20 °C as solid powders.

Peptides Concentration. The concentration of the peptide solutions was calculated using UV absorption spectroscopy. The molar extinction coefficient (in L $mol^{-1}cm^{-1}$) of the peptides was determined on the basis of the number of aromatic amino acid residues present in the peptides and considering a molar extinction coefficient of Trp and Phe of 5600 (at 280 nm) and 200 M^{-1} cm^{-1} (at 258 nm), respectively.[39] Thus, the molar extinction coefficient calculated for SP and SPW is 400 and 5800 $M^{-1}cm^{-1}$, respectively. The absorption spectra of the peptides were recorded in a 1 cm length quartz cuvette using a UV−vis spectrometer (Varian Cary3 Bio). For all UV spectra an appropriate correction for a nonzero baseline was done. Prior to the measurements, peptide stock solutions (at about 6.7 mg/mL) were dissolved in distilled water.

Evaluation of Critical Micelle Concentration. The critical micelle concentration (CMC) of SDS was evaluated using fluorescence emission spectra of polarity-sensitive dye pyrene, as described previously.[40] The methodology is based on the well-established experimental fact that the fluorescence emission spectrum of monomeric pyrene reflects the polarity experienced by the probe, as smaller values of the intensities ratio of the third and first vibrational (I_3/I_1) peaks correspond to greater polarity of the probe environment and vice versa.[41] Briefly, a stock solution of 1 mM pyrene in ethanol was made and added to the samples to a final concentration of 2 μM. Fluorescence emission spectra of pyrene were measured in the presence of increasing concentrations of SDS micelles (from 50 μM to 10.0 mM) using a 335 nm excitation wavelength. The CMC of the SDS surfactant alone and in the presence of SP was determined by plotting the ratio of fluorescence emission intensities of I_{385}/I_{374} vibronic bands vs surfactant concentration.

Preparation of Large Unilamellar Vesicles (LUVs). First, a thin lipid film was prepared by dissolving an appropriate amount of lipid in chloroform/methanol (2:1 v/v) and drying it by a rotary evaporation system purged continuously with a steam of N_2. To avoid any presence of some residual organic solvents, the lipid film was kept under high vacuum overnight. Further, the dried lipid film was hydrated in 5 mM phosphate buffer (pH 7.0), keeping it above the phase-transition temperature with vigorous vortexing for at least 30 min. The resulting multilamellar vesicles (MLVs) were freeze−thawed in liquid nitrogen for at least seven cycles. To get LUVs, MLVs were extruded repeatedly 10 times through stacked polycarbonate membrane with a pore size of 100 nm using a Mini Extruder (Lipofast, Avestin, Ottawa, Canada). All liposomes were used immediately after preparation. The size distribution of LUVs was evaluated by an Ultrafine Particle Analyzer (UPA) 150 spectrometer (Microtrac, Montgomeryville, PA).

Fluorescence Emission Measurements. The fluorescence emission measurements were performed on a SLM 8000 spectrofluorimeter operating in the photon-counting mode. In the peptide−micelle binding experiments, fluorescence emission spectra of SPW were monitored from 300 to 480 nm using a 280 nm excitation wavelength. All spectra were measured at 22 °C with the following parameters: 10 nm/min scanning speed, 4 and 8 nm bandwidth for excitation and emission slits, respectively, and 1 cm path length quartz cuvette. Typically, to increase the signal-to-noise ratio, at least 6 scans were accumulated and averaged. All spectra were corrected by subtracting blank spectra of the corresponding solutions without peptide and for dilution.

CD Measurements. The far-UV CD spectra (190−260 nm) of the peptides were recorded on a Jasco (Tokyo, Japan) J-715 spectropolarimeter. The instrument was calibrated prior to each measurement. All measurements were carried out at 22 °C using a 1 mm path length quartz cuvette. Each spectrum was obtained after an averaging of at least four scans. Dynode voltage values were simultaneously recorded with CD spectra, and only the CD spectra being in the linear range of the dynode values were further considered for analysis of the data. The usual peptide concentration used in all experiments was 100 μM unless otherwise mentioned. Before final ellipticity calculation, all spectra were corrected by subtraction of the respective spectra obtained from peptide-free samples (containing only membrane mimicking environments). The instrument parameters applied were 2.0 nm bandwidth for all the slits, 10 nm/min scanning speed, 1 data point per nanometer, and 2 s response time. The CD intensity of the peptides is expressed in terms of the mean residue molar ellipticity (MRE) according to the following equation (in deg cm^2 dmol^{-1})

$$[\theta] = \theta_{obs}/10 \times Lcn$$

where θ_{obs} is the observed circular dichroism (in mdeg), L is the optical path length (in cm), c is the peptide concentration (in M), and n is the number of residues.

The percentage of α-helix was calculated according to the method of Chen et al.,[42] assuming that the residue ellipticity at 222 nm is exclusively due to α-helix (in deg cm^2 dmol^{-1})

$$\text{percentage of } \alpha\text{-helix} = [\theta]_{222}/[\theta]_{222}^{max}\left(1 - \frac{k}{n}\right)$$

where $[\theta]_{222}$ is the observed mean residue ellipticity at 222 nm, $[\theta]_{222}^{max}$ is the theoretical mean residue ellipticity for a helix of infinite length (−39 500 at 222 nm), n is the number of residues, and k is a wavelength-dependent constant (2.57 for 222 nm).

Since this method is extremely sensitive to the peptide concentration, complementary estimation of SP secondary structural conformation was done using R1 ($\theta_{195}/\theta_{208}$) and R2 ($\theta_{222}/\theta_{208}$) parameters. These R1 and R2 parameters are independent of peptide concentration and have been shown to be useful in comparing relative helicity for closely related peptides when a two-state α-helix/random-coil equilibrium exists.[43] It has been shown that for a random structure, R1 should be positive and R2 close to zero, while in a highly helical state, R1 should be close to −2 and R2 approach 1.[43,44] The CD spectra of SP and SPW peptides were independent of the peptide concentration (60−100 μM), supporting the idea that the peptides are inserted as monomers into the micelles and liposomes.

RESULTS

SP Conformation in Aqueous Solution. Identification of the Polyproline II (PPII) Conformation. Consistent with earlier reported data, the CD spectrum of SP in water displays a single negative peak at 195 nm, assigned to a random coiled conformation of the peptide.[26] When SP was dissolved in neutral (phosphate pH 7.0) or alkaline (carbonate pH 10.7) buffers, the shape of the spectrum did not change much compared to that in water, presenting a strong negative peak at about 195 nm and a small positive peak at about 222 nm (Figure 1A). The overall features of these spectra and, in particular, the presence of the weak positive band in the near UV range reproduces closely the features of a left-handed helical PPII structure, characterized by a strong negative band around 206 nm (amide $\pi-\pi^*$ transition) and a weak positive band near 225 nm (n$-\pi^*$ transition).[45−47] Because of the spectral similarity of random coil and PPII structures the latter one can be easily mistaken for random coil, and as a result its presence has been often neglected.[47] A typical characteristic of the extended helical PPII structure is its deficiency in intramolecular hydrogen bonds, distinctive for other regular secondary conformations such as α-helix or β-sheets.[48] This makes PPII indistinguishable from an irregular backbone structure using ^{1}H NMR spectroscopy, an otherwise powerful method for conformational analysis.[49] On the other hand, CD spectroscopy so far is widely recognized as the most reliable methodology for identification of this conformation.[46,50] In particular, since PPII helical conformation is more populated at low temperatures, analysis of CD spectra at different temperatures is a relevant approach to discern between unordered and PPII conformations.[46,50] The CD spectra of SP in phosphate buffer, pH 7.0, as a function of the temperature presented in Figure 1B show that the positive band at 208 nm greatly decreases with increasing temperature, thus providing strong evidence for the existence of PPII conformation. Importantly, the changes of both bands are completely reversible upon

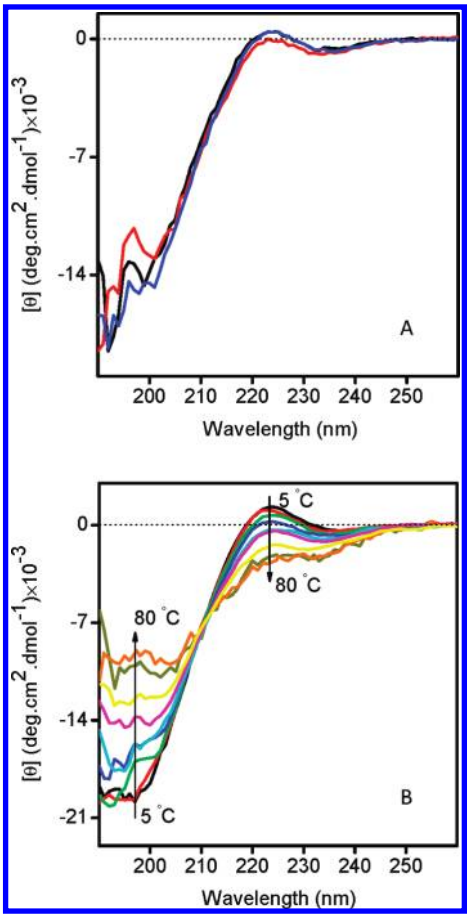

Figure 1. (A) Representative far-UV CD spectra of 100 μM SP in 5 mM Pi buffer pH 7.0 (black line), 3 mM carbonate buffer pH 10.7 (red line), and distilled water (blue line). (B) CD spectra of 100 μM SP in 5 mM Pi buffer pH 7.0 at the following temperatures: 5, 10, 15, 22, 30, 37, 50, 70, and 80 °C.

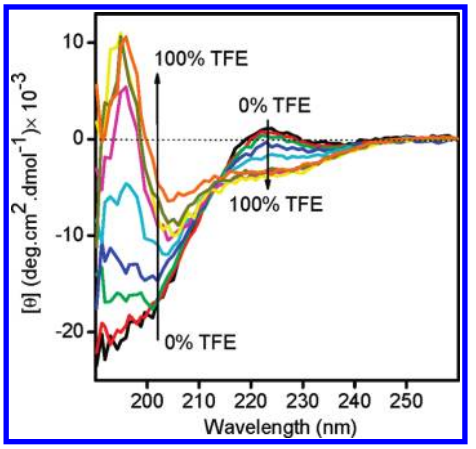

Figure 2. CD spectra of 100 μM SP in TFE/H_2O mixtures of different ratios. The spectra were recorded in distilled water and in 5%, 10%, 15%, 20%, 30%, 40%, 70%, and 100% TFE (v/v). All spectra were collected at 22 °C.

temperature decrease. In addition, the temperature-induced changes in the ellipticity of both bands generate an isoelliptic point at about 211 nm, indicating an equilibrium between unordered and PPII conformations.

Secondary Structure Characterization of SP in the Presence of TFE. To determine the intrinsic helical propensity of SP we carried out experiments in the presence of different concentrations of TFE, known to stabilize α-helical structure in peptides.[51−53] In water and in the presence of less than 15% (v/v) TFE the far-UV CD spectra of SP exhibit a negative peak around 196 nm (Figure 2). Above 30% (v/v) TFE the spectra undergo significant changes and two negative peaks around 208 and 222 nm and a positive peak around 195 nm showed up, indicative of formation of α-helical structure. A further increase of the TFE amount in the mixture results in enhancement of α-helical fold of the peptide, and finally, at concentrations higher than 30% (v/v) TFE it reaches a plateau. The presence of an isodichroic point at about 212 nm implies that the neuropeptide adopts mainly two conformational states. SP follows the same pattern of secondary structural changes with increasing TFE in TFE/phosphate buffer mixtures, pH 7.0. A slightly lower helicity was observed in pure TFE solution than in the TFE/phosphate mixture (data not shown), due to the effect of the salts present in the buffer, as confirmed by comparison with TFE/water experiments.

Secondary Structure Characterization of SP in SDS. To determine the SP conformation(s) in a membrane-mimetic environment, we first analyzed the CD spectra of the neuropeptide in the presence of SDS micelles, a system widely used in structural studies of membrane active peptides.[54,55] In particular, the SDS surfactant was chosen because of 2 reasons: the low turbidity and light scattering of SDS micelles[56,57] and to corroborate our results with previous NMR studies of SP, which generally have been carried out in organic and SDS micelles.[28,31]

In the presence of 10 mM SDS micelles, pH 7.0, highly above the critical micelle concentration (CMC) determined in the buffer (see Figure 4), the CD spectra of SP consist of two negative peaks at 208 and 222 nm, indicating an α-helical conformation (Figure 3A). The structural transition from extended PPII helical structure in aqueous solutions to α-helical in SDS micelles raises the question of how the peptide environment

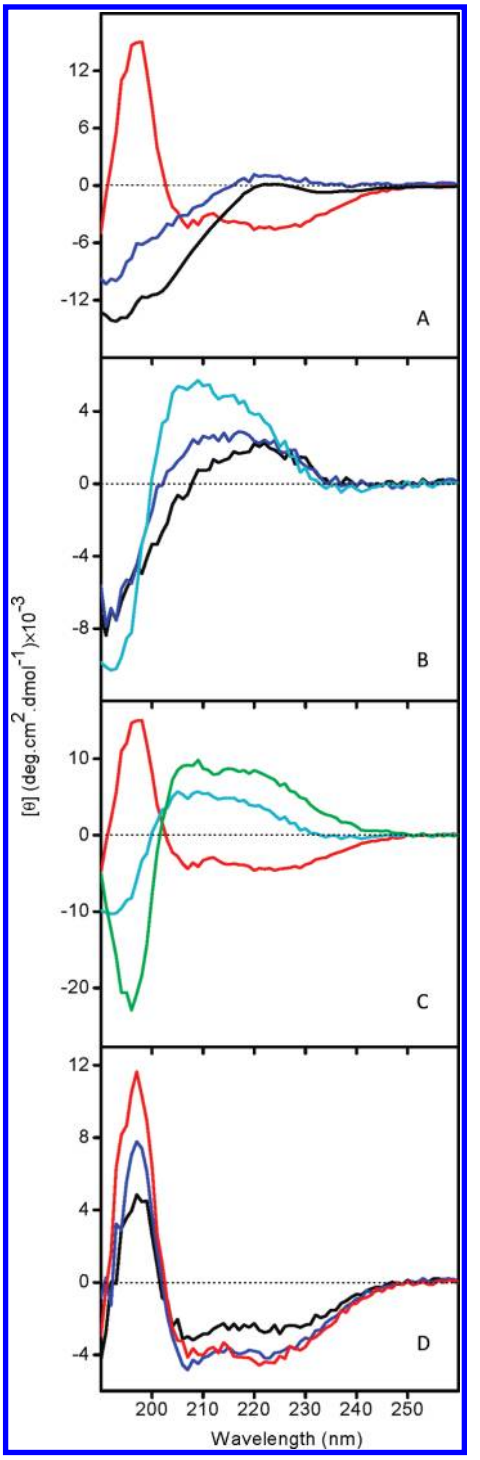

Figure 3. CD spectra of 80 μM SP in (A) 5 mM Pi buffer pH 7.0 (black line) and with 0.2 (blue line) or 10 mM (red line) SDS added. (B) Using 0.4 (black line), 0.6 (blue line), and 0.8 mM (aqua line) SDS. (C) Difference spectrum (green line) calculated by subtraction of the CD spectrum of 80 μM SP in 10 mM SDS (red line) from that in 0.8 mM SDS (aqua line). (D) Using 1.4 (black line), 1.6 (blue line), and 3 mM (red line) SDS. All spectra were collected at 22 °C.

controls and stabilizes these two different conformations. To address this question, we measured CD spectra of SP in SDS solutions below and above the CMC (Figure 3). In the absence

dx.doi.org/10.1021/jp1101253 |J. Phys. Chem. B 2011, 115, 3622–3631

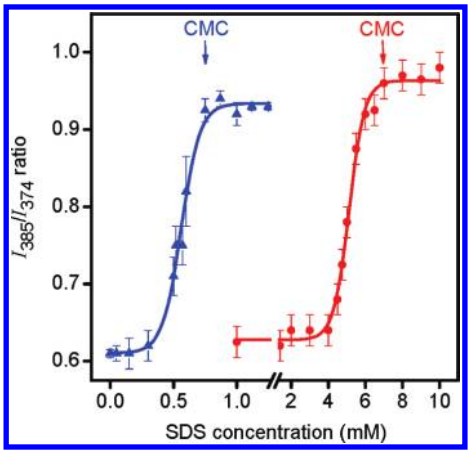

Figure 4. Fluorescence intensity ratio of the third (385 nm) and first (374 nm) vibronic peaks of 2 μM pyrene (I_{385}/I_{374}) in 5 mM Pi buffer pH 7.0, alone (red circles) and in the presence of 25 μM SP (blue triangles) as a function of increasing concentration of SDS from 0 to 10 mM. λ_{exc} was set at 335 nm, and each sample was recorded as an average of 3 emission scans.

and at low (0.2 mM) SDS concentrations the peptide adopts mainly PPII conformation, as judged by the strong negative peak at about 195 nm and a small positive peak at about 222 nm and confirmed by recording the spectra at different temperatures (Figure 1B). A further increase of SDS but still in the submicellar range (between 0.4 and 0.8 mM) results in a decrease and blue shift of the negative peak (of about 5 nm) and appearance of a weak and variable positive peak in the range of 205−208 nm (Figure 3B). A shift of the CD spectral bands to higher or lower wavelengths has been attributed to differences between secondary and tertiary amides of PPII and/or contribution of other secondary structures.[46] To examine the shape diversities of the CD spectra with varying SDS concentrations we calculated the CD difference spectra. In all cases, the difference spectra obtained by subtracting the CD spectra of SP in the presence of 10 mM SDS (highly above CMC) from that measured in SDS concentrations below CMC exhibit a negative band below 200 nm and a positive one at about 217 nm, indicative of formation of PPII structure (Figure 3C). The temperature-dependent intensity of the spectra shown in Figure 3B further confirmed the presence of extended PPII conformation (data not shown). These findings imply that in the presence of SDS, below and near the CMC, SP forms complex secondary conformations of largely PPII admixed with α-helical. Moreover, the enhancement of these bands with an increase of SDS concentration strongly suggests a rise of the fractional population of SP residues involved in PPII structure formation (Figure 3B). At about 1.4 mM SDS the CD spectrum shows α-helical conformation. Further concentration increases results only in a minor changes in the magnitude of the signal, indicating that the SDS-dependent folding of SP is completed (Figure 3D). This SDS concentration roughly corresponds to a peptide/SDS molar ratio of 0.05/1. Assuming 62 molecules of SDS per micelle[58] it seems unlikely that this structure is influenced by possible peptide−peptide interactions. However, the α-helical fold of the peptide observed in SDS at concentrations below the CMC in buffer makes these results somehow unexpected. It is well known that the CMC values of SDS strongly depend on the ionic strength and on the presence of ions.[59] Taking into account the amphipathic character of the

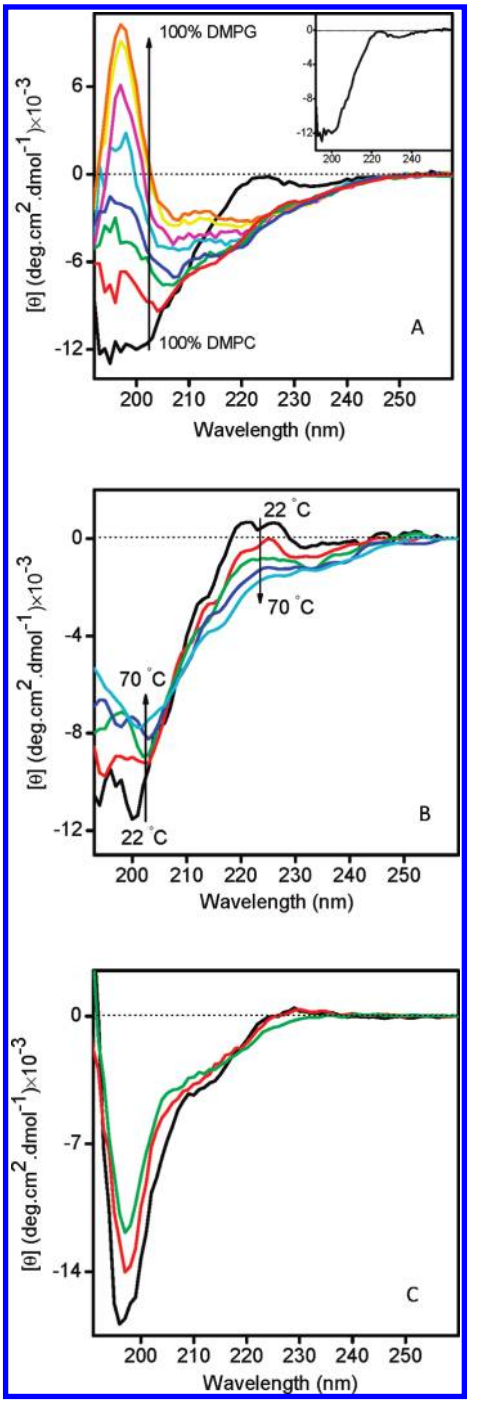

Figure 5. (A) CD spectra of 100 μM SP in phosphate buffer pH 7.0 and 10 mM DMPG/DMPC, prepared at different molar ratios: pure DMPC, 10% DMPG, 15% DMPG, 25% DMPG, 40% DMPG, 50% DMPG, 75% DMPG, and pure DMPG. All spectra were collected at 22 °C. (Inset) CD spectrum of 100 μM SP in 10 mM DMPC. (B) CD spectra of 60 μM SP in DMPC (6 mM) and phosphate buffer pH 7.0, recorded at increasing temperatures: 22, 37, 50, 60, and 70 °C. (C) Difference spectra calculated by subtraction of the CD spectrum of 100 μM SP in 10 mM pure DMPG from that in 10 mM DMPG/DMPC with 10 (black line), 15 (red line), and 25 (green line) mol % of DMPG, pH 7.0.

peptide, we further checked whether the apparent CMC of the surfactant is affected by SP. The plot of the I_{385}/I_{374} ratio of

pyrene bands as a function of SDS concentration (Figure 4) gives an apparent CMC that is about 9-fold lower in the presence of SP, compared to that measured only in buffer. These findings give a rationale for the formation of the α-helical conformation of SP at concentrations above 1.4 mM SDS, as revealed by the CD spectra.

In summary, we conclude that the extended PPII structure is the most populated conformation in SDS monomers. At concentrations near but still below the CMC formation of two fractional conformations, PPII and α-helical, gives rise to distorted CD spectra. Finally, in SDS micelles the α-helical conformation dominates among the other secondary structures.

Lipid-Dependent Folding of SP in Vesicles. Both DMPC and DMPG are structurally similar to the lipid composition in the postsynaptic membranes where NK1 receptor and SP ligand are expressed and functioning.[60] Therefore, LUVs prepared with these lipids mimic most closely phospholipids bilayer in vivo and were used to monitor the membrane-bound conformations of SP.

In zwitterionic DMPC vesicles, the CD spectrum of SP shows the same features as in aqueous solutions, displaying a negative peak around 195 nm and a small shoulder at about 222 nm, suggesting formation of PPII structure (Figure 5A, inset). The temperature-induced changes in the CD spectra of SP in DMPC vesicles unambiguously confirm our assignment to PPII (Figure 5B). Unlikely in DMPC, the CD spectrum of SP in the presence of negatively charged DMPG liposomes exhibits two negative bands at 208 and 222 nm, diagnostic of a dominant α-helical conformation of SP (Figure 5A). Both DMPC and DMPG lipids share a similar length of the acyl chains but differ in their lipid headgroups. To explore the effect of the electrostatic interactions on peptide conformation we measured the spectra of SP in DMPG/DMPC liposomes, prepared with different molar ratios of both lipids (Figure 5A). The presence of DMPG up to 25 mol % in mixed DMPG/DMPC liposomes causes a decrease of the 196 nm band intensity and its shift to 205−208 nm. These alterations are most likely caused by the superposition of CD spectra from different conformations (Figure 5A). Moreover, the small positive shoulder at about 222 nm, seen in pure DMPC, disappears. In the search to identify the structural origin of these spectral changes, we calculated the difference spectra by subtracting the CD spectra of SP in pure DMPG from those in DMPG/DMPC vesicles (Figure 5C). The difference spectra display a strong negative peak at about 195 nm and a small positive peak at about 222 nm, suggesting the presence of PPII conformation. In addition, the intensities of the negative and positive bands illustrate a decrease of PPII content as the DMPG percentage increases. At above 40% (mol/mol) DMPG in DMPG/DMPC liposomes, the CD spectra show α-helical structure, as visualized by the positive band at 196 nm and two negative bands at 208 and 22 nm (Figure 5A). These data demonstrate clearly that the α-helical fold of SP strongly depends on the relative amount of anionic DMPG in the vesicles, since zwitterionic DMPC alone did not induce any α-helix formation, as shown above. Moreover, conformational preference for the α-helical structure in mixed DMPG/DMPC liposomes reflects the favorable electrostatic interaction of the SP with the headgroups of the lipid matrix.

Characterization of the SP Interaction with the Membrane-Mimetic Systems by Fluorescence Spectroscopy. The CD spectra of peptides/membrane-mimetic systems reflect primarily the secondary structural conformation adopted by the peptide, rather than their interactions with the membrane. To seek SP−membrane interactions, we used Trp intrinsic fluorescence, which is highly sensitive to the solvent environment and can serve as a probe to monitor these interactions.[54] In all fluorescence experiments we used SPW, an analogue of SP, in which Phe8 was substituted by Trp. Before using SPW, we tested whether Phe8 substitution for Trp affects the secondary structure of the peptide. Comparison of the CD spectra of SP with those of SPW shows very similar spectral features for both peptides in SDS micelles and DMPG liposomes, except for some subtle differences (Figures 5A, 3A, and 6). Importantly, we found also that SDS in concentrations below the CMC and DMPC above 85% (mol/mol) in DMPG/DMPC vesicles induce conformational changes in SPW similar to those observed in SP, namely, formation of PPII (data not shown). The same structural conformations adopted by SPW and SP allowed us to use the former peptide as a probe for assessing SP−membrane interactions.

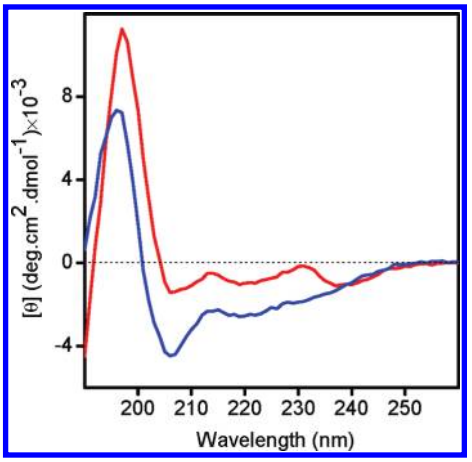

Figure 6. CD spectra of 100 μM SPW in 10 mM SDS (blue line) and in 10 mM DMPG (red line), in phosphate buffer pH 7.0. Spectra were collected at 22 °C.

Figure 7A shows the fluorescence emission spectra of SPW in four different media: aqueous solutions, SDS micelles, and DMPC and DMPG vesicles. In aqueous solutions and DMPC vesicles the fluorescence maximum is located at about 350 nm, indicating that the Trp is totally exposed to the media solution. A significantly blue-shifted maximum to 342 and 337 nm in SDS micelles and DMPG vesicles, respectively, point out the insertion of SPW into the hydrophobic core of these membrane mimetics. Moreover, a larger blue shift and higher Trp intensity of SPW in DMPG liposomes compared to that in SDS micelles suggest a more rigid, hydrophobic environment of Trp side chain in the former environment. The interaction of SPW with SDS surfactant below and above the CMC was monitored by Trp flores-cence emission measurements (Figure 7B). The plot of the titration experiments shows a highly hydrophilic environment of the Trp (with a maximum around 350 nm) in the absence and low SDS concentration range, where the CD spectra revealed an extended PPII-like conformation (Figure 3B). At above 1.2 mM SDS the Trp maximum undergoes a significant blue shift (up to 10 nm), implying insertion of the peptide into the hydrophobic core, which strongly correlates with induction of the α-helical fold observed by CD (Figure 3D).

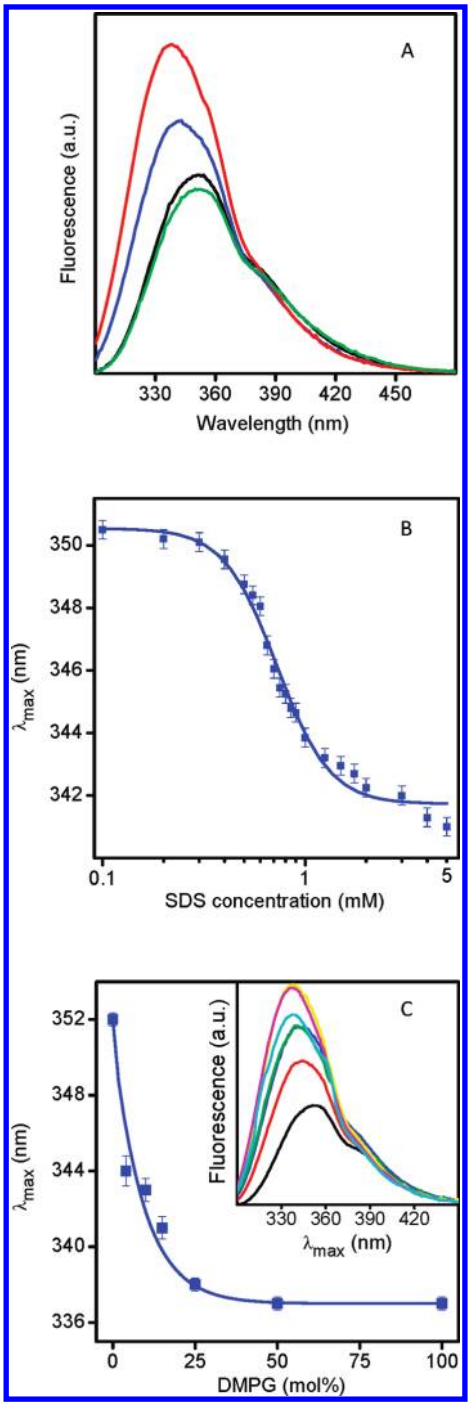

Figure 7. (A) Fluorescence emission spectra of 5 μM SPW in 5 mM Pi buffer (black line) pH 7.0, 10 mM SDS (blue line), 0.5 mM DMPG (red line), and 0.5 mM DMPC (green line). (B) Fluorescence emission λ_{max} of SPW (5 μM) as a function of SDS concentration (pH 7.0). (C) Fluorescence emission λ_{max} of SPW (10 μM) in 1 mM DMPG/DMPC mixtures as a function of different percentages of DMPG: 0%, 4%, 10%, 15%, 25%, 50%, and 100% (mol/mol). (Inset) Fluorescence emission spectra of SPW (10 μM) in DMPG/DMPC mixtures (1 mM) as a function of different molar percentages of DMPG: 0% (black line), 4% (red line), 10% (blue line), 15% (green line), 25% (yellow line), 50% (purple line), and 100% (aqua line). In all cases, λ_{exc} was set at 280 nm.

To evaluate the binding affinity of SPW for the lipid, we measured the Trp fluorescence maximum in liposomes, formed at different DMPG and DMPC molar ratios (Figure 7C). Addition of DMPG up to 15% (mol/mol) results in conformational changes of the peptide segment, involving the Trp residue, as revealed by the blue-shifted Trp maximum (about 10 nm). These data suggest transfer of Trp side chain from a highly hydrophilic in pure DMPC to a more hydrophobic environment in the presence of the anionic DMPG lipid. Above 40% DMPG, the neuropeptide is inserted into the hydrophobic core of the liposomes, as judged by the intensity increase (Figure 7C inset) and strongly blue-shifted Trp maximum (about 15 nm). Therefore, the fluorescence data correlate nicely with formation of the α-helical structure due to the increase of DMPG, as observed by CD measurements (Figure 5A).

It is worth mentioning that in all conditions where CD spectra reported a dominant PPII conformation in the neuropeptide, the fluorescence experiments demonstrated that Trp side chain faces the hydrophilic environment, thus ruling out SPW partition into the hydrophobic core of the micelle or the lipid bilayer. These data are consistent with previous data reporting that peptide segments forming PPII conformation were well exposed to the solvent.[61]

Analysis of the Secondary Structures of SP, Evaluated by CD Experiments. The method of Chen's and co-workers[42] has been widely used for quantitative evaluation of the α-helical content of peptides, and in particular, it has been employed in previous CD studies of SP.[23,26,36] The CD spectra of SP recorded in TFE solvent (Figure 2), SDS micelles (Figure 3), or DMPG and mixed DMPG/DMPC liposomes (Figure 5) are distinct from the spectral signatures for unordered or β-sheet conformations. They represent clearly α-helical conformation, and applying Chen's equation,[42] we calculated the α-helical content of the peptide in these membrane mimetics (Table 1). The α-helical content varies depending on the environment, suggesting genuine differences in the intrinsic helical propensity of SP in different media. The calculated MRE values are in good agreement with a 10−30% α-helical content of SP, previously estimated by CD and Raman spectroscopy measurements.[23,26] From the other side, however, the relatively low MRE values obtained by us and others stress the presence of other conformations being overlooked by Chen's method. We should keep in mind that in any CD spectrum the signal from the α-helical structure usually predominates over the β-turn and unordered ones,[62] resulting in an inability to distinguish between very short helical segments and β-turns.[23] Additionally, any inaccuracy in the determination of peptide concentration could also add some error in estimation of the mean residue ellipticity.[63] Altogether, these considerations reinforce our assumption that the CD spectra of SP most likely represent a superposition of different local conformations, dominated by the most visible and best predicted by CD spectroscopy, the α-helical conformation.

In an attempt to provide further insight into conformations of SP in different membrane-mimetic environments, we calculated R1 ($\theta_{195}/\theta_{208}$) and R2 ($\theta_{222}/\theta_{208}$) parameters, known to be independent of the peptide concentration (Table 1). It is readily seen that R1 is negative in all cases, while R2 is near 1 or >1 in SDS micelles and in DMPG and DMPG/DMPC liposomes. Furthermore, at any TFE concentration in TFE/water mixtures, R2 values are much less than 1. R2 $\ll$ 1 is believed to be diagnostic for short helical segments,[64] the so-called 3_{10}-helical structure, commonly found in short peptides. Thus, we can speculate that the peptide adopts some 3_{10}-helical conformation in the TFE. 3_{10}-Helical structure has been proposed as an

Table 1. Evaluation of α helical content of SP in different membrane-mimetic environments

		DMPG liposomes		SDS micelles		
	70% TFE/water (v/v)	pH 7.0	pH 10.7	pH 7.0	pH 10.7	40% mol DMPG/60% mol DMPC
α-helix %	10.50 ± 1.4	11.5 ± 1.0	13.5 ± 1.5	13.3 ± 0.8	15.3 ± 0.02	16.7 ± 1.4
R1[a]	−1.05 ± 0.12	−1.8 ± 1.0	−2.84 ± 0.4	−4.09 ± 0.8	−4.50 ± 0.02	−0.56 ± 0.04
R2[a]	0.41 ± 0.02	0.90 ± 0.2	1.00 ± 0.02	1.15 ± 0.2	1.20 ± 0.02	0.86 ± 0.04

[a] Definitions of R1 and R2 parameters are given in the experimental section.

intermediate in α-helical formation,[65] though some authors argued that the CD appearance of a 3_{10}-helix is very close to that of an α-helix[66,67] and that the R method to differentiate between both does not work always.[68] Thus, discrimination between 3_{10} and α-helical and quantitative evaluation of extended PPII conformation and β-turn types structures in SP remains a question to be further tested by more sensitive Fourier transform infrared spectroscopy (work in progress in our lab).

DISCUSSION AND CONCLUSIONS

To date, random coil and α-helical conformations have been proposed as the two major types of secondary structures of the neuropeptide SP.[23,36,69,70] In the present work we present CD evidence that α-helical and extended PPII helical structures are the predominant conformations adopted by SP.

On the basis of our CD and fluorescence data we found that the interaction between SP and the membrane mimetics and formation of stable secondary conformations depends strongly on peptide environment. The SP−membrane interactions appear to be rather complex, involving hydrophobic and electrostatic interactions and charge density on the membrane surface.[26] To attest to the impact on each of these components for promotion of a stable peptide conformation we performed experiments in solvents and in two membrane-mimetic environments, liposomes and micelles, varying the head−lipid charge and the concentration of SDS surfactant.

SP is an amphipathic peptide, and it is reasonable to assume that the positively charged N-terminal (involving Arg1 and Lys3) would have a strong impact on the peptide binding through electrostatic interactions with the anionic components of the membrane. Indeed, our experiments support this assumption, demonstrating that the Trp side chain of SPW is inserted into the hydrophobic environment of the negatively charged SDS micelles or DMPG liposomes, but it faces the hydrophilic aqueous region in the zwitterionic DMPC liposomes (Figure 7). The red shift of the Trp emission maximum upon an increase of DMPC percentage in mixed DMPG/DMPC liposomes reflects the transfer of Trp to a more hydrophilic environment and its full exposure to water in pure DMPC. These findings are in agreement with NMR data reporting that SP amides are not protected from solvent exchange in zwitterionic dodecylphosphocholine.[29]

It is worth comparing the fluorescence results with CD data, reporting the conformation of SP in these conditions. As CD data demonstrate, an increase of DMPC percentage in DMPG/DMPC liposomes leads to a decrease of α helicity of SP and in pure DMPC liposomes the extended PPII helical structure appears to be the most preferred and dominant conformation. This indicates that hydrophobic interactions between the peptide and the zwitterionic DMPC liposomes are not sufficient to promote α-helical conformation even though DMPC has the same hydrophobic potential, 12-carbon hydrophobic tail, as DMPG. On the contrary, the negatively charged SDS micelles and DMPG liposomes are able to induce α-helical folding of SP. CD spectra of SP in SDS surfactant below the CMC represent mainly the extended PPII helical conformation (Figure 3). Submicellar SDS is a mixed solvent system, providing a partially organic (low dielectric) and a partially aqueous environment. With increases of SDS concentration the dominant presence of PPII conformation is lost, and when SDS concentration reaches the CMC, the secondary structure of SP is dominated by the α-helical conformation (Figure 3). These findings point out that electrostatic interactions between membrane-mimetic and the charged residues of SP are essential prerequisites for efficient α-helical fold. The electrostatic interactions between peptides and negatively charged lipids have been proposed as driving forces for binding of some peptides to membranes.[54,55] Most likely, the electrostatic interactions are needed to anchor the basic SP to micelle and vesicle interfaces and promote its insertion into the hydrophobic core, thus enabling the hydrophobic interactions required for initiation of the helical formation and stabilization of the α-helix hydrogen-bond network.

Another question addressed in this work was the formation of the extended PPII helix conformation in SP and its biological relevance. CD spectral features of SP in aqueous solutions, submicellar SDS concentrations, and DMPC liposomes definitely show formation of PPII structure, as confirmed by plotting CD spectra over a temperature range (Figures 1B, 3B, and 5B). Actually, CD spectra of SP in aqueous solutions and in zwitterionic lysophosphatidylcholine micelles published previously show spectral features very similar to those reported here, but the authors assigned them to the random coil structures.[22,23,26,33,36,38] Importantly, in all conditions where the CD spectra reported formation of the PPII conformation, the florescence experiments indicate that the Trp side chain has a hydrophilic environment, thus excluding SP partition into the hydrophobic core of the micelles or the lipid bilayer. These results are in accordance with the recognized tendency of PPII helix to form on the surfaces of proteins.[49]

Previously, based on the CD data of SP interaction with SDS and zwitterionic lysophosphatidylcholine micelles, it was claimed that the charge has a pronounced effect on the strength of binding interactions but did not affect the induced conformation of SP.[33] However, the CD spectra presented in Figure 2 of ref 33 clearly show two different peptide conformations, namely, the α-helical structure in SDS micelles and PPII helix in lysophosphatidylcholine micelles. Therefore, a clear influence of the electrical charge can be assumed. On the other hand, NMR experiments reported in the same work show a strong binding of SP with SDS (with some residues inserted) and a weaker binding with the neutral lysophosphatidylcholine (with unaffected Lys NH resonance by the lipid and C-terminal involved in a specific

interaction). These data strongly suggest that the positively charged N-terminal assures a particular spatial topology of the peptide needed for the consequent proper α-helical fold. Therefore, reinterpreting the CD assignments reported in that work,[33] both CD and NMR data strongly support our proposal that electrostatic interactions between the membrane and SP are essential for promoting the α-helical fold. Furthermore, contrary to the α-helical conformation, induction of PPII structure does not need the interaction of the peptide with the membrane, pointing out that PPII formation presumably is dictated by the specific amino acid sequence of SP.

Finally, it is interesting to interpret our findings in the context of SP ligand−NK1 receptor interactions. SP is known to act as a ligand for different NK receptors with different potent activities.[71] On the basis of our data, we hypothesized that the molecular basis for the multiple receptors recognition of SP may be closely related to formation and stability of two major conformations adopted by the peptide: extended PPII helical and α-helical structure. Formation of PPII structure seems an essential structural feature of the SP ligand in targeting different receptors, while the α-helical structure most likely provides the correct conformation of the peptide for receptor signal activation. In the different NK receptors, the segment forming PPII in SP will address the peptide to different binding pockets, due to PPII flexibility, and consequently, the agonist will attain a new conformation that would activate the receptor.

Extended left-handed PPII helical structures have been neglected for years, and only in the last several years growing evidence has accumulated that the PPII conformation is essential for several biological activities, such as molecular recognition, signal transduction, transcription, cell motility, and immune response processes.[47,49] In general, the PPII conformation forms in polypeptides rich in proline, yet even sequences lacking Pro residue can adopt this structure.[61] Pro-rich sequences are known as very common recognition sites involved in signal transduction.[48,72−74] Furthermore, the ligands are found mostly in an extended conformation, when bound to their receptors, as revealed by X-ray and NMR data. Actually, the N-terminus of SP contains two Pro residues forming two short $(XP)_n$ motifs, known to promote PPII helix formation.[49] An additional reason to assume the involvement of the PPII structure in the recognition processes of SP by NK receptors lies in the fact that this regular, periodic structure is very flexible. By adapting the PPII structure SP may easily behave as an "adaptable glove", addressing the SP to the binding pocket in the different NK receptors. Unlike α-helix secondary structure, the PPII helix precludes formation of intramolecular hydrogen bonds,[50] leaving the backbone carbonyl oxygens (and the N−H protons of non-Pro residues) free to participate in hydrogen bonding with interacting receptors at the interface of the peptide−protein complex. As we show here, PPII helix conformation is preformed in the unbound peptide before interacting with the membrane, which presumably guarantees rapid formation of specific peptide−protein complexes.

AUTHOR INFORMATION

Corresponding Author

*T.L.: phone, +34935814504; e-mail, tzvetana.lazarova@uab.cat. E.P.: phone, +34935811870; e-mail, esteve.padros@uab.cat.

Author Contributions

†These authors contributed equally to this work.

ACKNOWLEDGMENT

The authors are grateful to Drs. Víctor Lórenz-Fonfría and Josep Cladera for critical reading of the manuscript and helpful suggestions. This work was supported by a Ministerio de Ciencia e Innovación grant BFU2009-08758/BMC. A.F. is grateful to Ravis Sustainable Development Consulting Engineers Co. (Tehran, Iran) for a fellowship.

ABBREVIATIONS

CD, circular dichroism; CMC, critical micelle concentration; DMPC, 1,2-dimyristoyl-*sn*-glycero-3-phosphocholine; DMPG, 1,2-dimyristoyl-*sn*-glycero-3-[phospho-rac-(1-glycerol)]; GPCR, G-protein coupled receptor; LUV, large unilamellar vesicle; MLV, multilamellar vesicle; MRE, mean residue molar ellipticity; NK, neurokinin; NMR, nuclear magnetic resonance; PPII, polyproline II; SDS, sodium dodecyl sulfate; SP, substance P; SPW or [Trp8]SP, [Trp8]-substance P; TFE, 2,2,2-trifluoroethanol.

REFERENCES

(1) Kobilka, B. K.; Deupi, X. *Trends Pharmacol. Sci.* **2007**, *28*, 397–406.
(2) Shenker, A. *Baillieres Clin. Endocrinol. Metab.* **1995**, *9*, 427–451.
(3) Conn, P. M.; Ulloa-Aguirre, A.; Ito, J.; Janovick, J. A. *Pharmacol. Rev.* **2007**, *59*, 225–250.
(4) Vilardaga, J. P.; Bunemann, M.; Feinstein, T. N.; Lambert, N.; Nikolaev, V. O.; Engelhardt, S.; Lohse, M. J.; Hoffmann, C. *Mol. Endocrinol.* **2009**, *23*, 590–599.
(5) Rosenbaum, D. M.; Rasmussen, S. G.; Kobilka, B. K. *Nature* **2009**, *459*, 356–363.
(6) Costanzi, S.; Siegel, J.; Tikhonova, I. G.; Jacobson, K. A. *Curr. Pharm. Des.* **2009**, *15*, 3994–4002.
(7) Kobilka, B.; Schertler, G. F. *Trends Pharmacol. Sci.* **2008**, *29*, 79–83.
(8) Shimizu, Y.; Matsuyama, H.; Shiina, T.; Takewaki, T.; Furness, J. B. *Cell. Mol. Life Sci.* **2008**, *65*, 295–311.
(9) Van Loy, T.; Vandersmissen, H. P.; Poels, J.; Van Hiel, M. B.; Verlinden, H.; Vanden Broeck, J. *Peptides* **2010**, *31*, 520–524.
(10) Longmore, J.; Hill, R. G.; Hargreaves, R. J. *Can. J. Physiol. Pharmacol.* **1997**, *75*, 612–621.
(11) Murtra, P.; Sheasby, A. M.; Hunt, S. P.; De Felipe, C. *Nature* **2000**, *405*, 180–183.
(12) Covenas, R.; Martin, F.; Belda, M.; Smith, V.; Salinas, P.; Rivada, E.; Diaz-Cabiale, Z.; Narvaez, J. A.; Marcos, P.; Tramu, G.; Gonzalez-Baron, S. *BMC Neurosci.* **2003**, *4*, 3.
(13) Ebner, K.; Sartori, S. B.; Singewald, N. *Curr. Pharm. Des.* **2009**, *15*, 1647–1674.
(14) Fong, T. M.; Huang, R. R.; Strader, C. D. *J. Biol. Chem.* **1992**, *267*, 25664–25667.
(15) Gether, U.; Johansen, T. E.; Schwartz, T. W. *J. Biol. Chem.* **1993**, *268*, 7893–7898.
(16) Huang, R. R.; Yu, H.; Strader, C. D.; Fong, T. M. *Biochemistry* **1994**, *33*, 3007–3013.
(17) Boyd, N. D.; Kage, R.; Dumas, J. J.; Krause, J. E.; Leeman, S. E. *Proc. Natl. Acad. Sci. U.S.A.* **1996**, *93*, 433–437.
(18) Lequin, O.; Bolbach, G.; Frank, F.; Convert, O.; Girault-Lagrange, S.; Chassaing, G.; Lavielle, S.; Sagan, S. *J. Biol. Chem.* **2002**, *277*, 22386–22394.
(19) Schwyzer, R. *EMBO J.* **1987**, *6*, 2255–2259.
(20) Sankararamakrishnan, R. *Biosci. Rep.* **2006**, *26*, 131–158.
(21) Holzemann, G.; Greiner, H. E.; Harting, J.; Barnickel, G.; Seelig, A. *Regul. Pept.* **1993**, *46*, 453–454.
(22) Chassaing, G.; Convert, O.; Lavielle, S. *Eur. J. Biochem.* **1986**, *154*, 77–85.

(23) Williams, R. W.; Weaver, J. L. *J. Biol. Chem.* **1990**, *265*, 2505–2513.
(24) Corcho, F. J.; Salvatella, X.; Canto, J.; Giralt, E.; Perez, J. J. *J. Pept. Sci.* **2007**, *13*, 728–741.
(25) Wymore, T.; Wong, T. C. *Biophys. J.* **1999**, *76*, 1199–1212.
(26) Keire, D. A.; Fletcher, T. G. *Biophys. J.* **1996**, *70*, 1716–1727.
(27) Keire, D. A.; Kobayashi, M. *Protein Sci.* **1998**, *7*, 2438–2450.
(28) Gao, X.; Wong, T. C. *Biopolymers* **1999**, *50*, 555–568.
(29) Auge, S.; Bersch, B.; Tropis, M.; Milon, A. *Biopolymers* **2000**, *54*, 297–306.
(30) Beard, D. J.; Perrine, S. A.; Phillips, E.; Hoque, S.; Conerly, S.; Tichenor, C.; Simmons, M. A.; Young, J. K. *J. Med. Chem.* **2007**, *50*, 6501–6506.
(31) Young, J. K.; Anklin, C.; Hicks, R. P. *Biopolymers* **1994**, *34*, 1449–1462.
(32) Cowsik, S. M.; Lucke, C.; Ruterjans, H. *J. Biomol. Struct. Dyn.* **1997**, *15*, 27–36.
(33) Woolley, G. A.; Deber, C. M. *Biopolymers* **1987**, *26* (Suppl.), S109–121.
(34) Koziej, P.; Mutter, M.; Gremlich, H. U.; Holzemann, G. *Z. Naturforsch. B* **1985**, *40*, 1570–1574.
(35) Seelig, A.; Macdonald, P. M. *Biochemistry* **1989**, *28*, 2490–2496.
(36) Seelig, A.; Alt, T.; Lotz, S.; Holzemann, G. *Biochemistry* **1996**, *35*, 4365–4374.
(37) Pérez-Paya, E.; Porcar, I.; Gómez, C. M.; Pedrós, J.; Campos, A.; Abad, C. *Biopolymers* **1997**, *42*, 169–181.
(38) Wu, C. S.; Hachimori, A.; Yang, J. T. *Biochemistry* **1982**, *21*, 4556–4562.
(39) Campbell, I. D.; Dwek, R. A. *Biological Spectroscopy*; Benjamin-Cummings Publishing Co.: Menlo Park, CA, 1984, pp 61−90.
(40) Domínguez, A.; Fernández, A.; González, N.; Iglesias, E.; Montenegro, L. *J. Chem. Educ.* **1997**, *74*, 1227–1231.
(41) Kalyanasundaram, K.; Thomas, J. K. *J. Am. Chem. Soc.* **1977**, *99*, 2039–2044.
(42) Chen, Y. H.; Yang, J. T.; Martínez, H. M. *Biochemistry* **1972**, *11*, 4120–4131.
(43) Bruch, M. D.; Dhingra, M. M.; Gierasch, L. M. *Proteins* **1991**, *10*, 130–139.
(44) Rizo, J.; Blanco, F. J.; Kobe, B.; Bruch, M. D.; Gierasch, L. M. *Biochemistry* **1993**, *32*, 4881–4894.
(45) Miles, A. J.; Wallace, B. A. *Chem. Soc. Rev.* **2006**, *35*, 39–51.
(46) Woody, R. W. *J. Am. Chem. Soc.* **2009**, *131*, 8234–8245.
(47) Shi, Z.; Chen, K.; Liu, Z.; Kallenbach, N. R. *Chem. Rev.* **2006**, *106*, 1877–1897.
(48) Sreerama, N.; Woody, R. W. *Proteins* **1999**, *36*, 400–406.
(49) Rath, A.; Davidson, A. R.; Deber, C. M. *Biopolymers* **2005**, *80*, 179–185.
(50) Bochicchio, B.; Tamburro, A. M. *Chirality* **2002**, *14*, 782–792.
(51) Nelson, J. W.; Kallenbach, N. R. *Proteins* **1986**, *1*, 211–217.
(52) Nelson, J. W.; Kallenbach, N. R. *Biochemistry* **1989**, *28*, 5256–5261.
(53) Merutka, G.; Stellwagen, E. *Biochemistry* **1989**, *28*, 352–357.
(54) Lazarova, T.; Brewin, K. A.; Stoeber, K.; Robinson, C. R. *Biochemistry* **2004**, *43*, 12945–12954.
(55) Bordag, N.; Keller, S. *Chem. Phys. Lipids* **2010**, *163*, 1–26.
(56) Hoyt, D. W.; Gierasch, L. M. *Biochemistry* **1991**, *30*, 10155–10163.
(57) Garavito, R. M.; Ferguson-Miller, S. *J. Biol. Chem.* **2001**, *276*, 32403–32406.
(58) Thévenot, C.; Grassl, B.; Bastiat, G.; Binana, W. *Colloid Surf. A* **2005**, *252*, 105–111.
(59) le Maire, M.; Champeil, P.; Moller, J. V. *Biochim. Biophys. Acta* **2000**, *1508*, 86–111.
(60) O'Brien, J. S.; Sampson, E. L. *J. Lipid Res.* **1965**, *6*, 537–544.
(61) Rucker, A. L.; Creamer, T. P. *Protein Sci.* **2002**, *11*, 980–985.
(62) Yang, J. T.; Wu, C. S.; Martínez, H. M. *Methods Enzymol.* **1986**, *130*, 208–269.
(63) Greenfield, N. J. *Methods Enzymol.* **2004**, *383*, 282–317.
(64) Silva, R. A.; Yasui, S. C.; Kubelka, J.; Formaggio, F.; Crisma, M.; Toniolo, C.; Keiderling, T. A. *Biopolymers* **2002**, *65*, 229–243.
(65) Millhauser, G. L. *Biochemistry* **1995**, *34*, 3873–3877.
(66) Miick, S. M.; Martínez, G. V.; Fiori, W. R.; Todd, A. P.; Millhauser, G. L. *Nature* **1992**, *359*, 653–655.
(67) Andersen, N. H.; Liu, Z.; Prickett, K. S. *FEBS Lett.* **1996**, *399*, 47–52.
(68) Sudha, T. S.; Vijayakumar, E. K.; Balaram, P. *Int. J. Pept. Protein Res.* **1983**, *22*, 464–468.
(69) Qi, X. F.; Zhorov, B. S.; Ananthanarayanan, V. S. *J. Pept. Sci.* **2000**, *6*, 57–83.
(70) Prabhu, A.; Malde, A.; Coutinho, E.; Srivastava, S. *Peptides* **2005**, *26*, 875–885.
(71) Harrison, S.; Geppetti, P.; Substance, P. *Int. J. Biochem. Cell Biol.* **2001**, *33*, 555–576.
(72) Chen, Y.; Wallace, B. A. *Biophys. Chem.* **1997**, *65*, 65–74.
(73) Choo, L. P.; Jackson, M.; Mantsch, H. H. *Biochem. J.* **1994**, *301*, 667–670.
(74) Convert, O.; Duplaa, H.; Lavielle, S.; Chassaing, G. *Neuropeptides* **1991**, *19*, 259–270.